Title
Redox Characterization of Proteins Involved in the Mitochondrial Intermembrane Space Pathway

Author
Neal, Sonya Elina

Publication Date
2013

Peer reviewed|Thesis/dissertation

UNIVERSITY OF CALIFORNIA

Los Angeles

Redox Characterization of Proteins Involved in the Mitochondrial Intermembrane Space Import Pathway

A dissertation submitted in partial satisfaction of the

requirements for the degree Doctor of Philosophy

in Molecular Biology

by

Sonya Elina Neal

2013

ABSTRACT OF THE DISSERTATION

Redox Characterization of Proteins Involved in the Mitochondrial Intermembrane Space Import Pathway

by

Sonya Elina Neal

Doctor of Philosophy in Molecular Biology

University of California, Los Angeles, 2013

Professor Carla M. Koehler, Chair

A redox-regulated import pathway consisting of Mia40 and Erv1 was identified to mediate the import of cysteine-rich proteins into the mitochondrial intermembrane space. Mia40 mediates the import and oxidative folding of substrates and Erv1 is a putative oxidant for Mia40. The mechanism involved in the oxidation of substrates and subsequent release from Mia40 is not clear. In this study, we have reconstituted the disulfide exchange reaction in vitro using Tim13 as the substrate. By reconstituting the Mia40-Erv1 import pathway with cysteine mutants of Tim13, we were able to determine that C57, C61 and C73 are required for oxidative folding by Mia40. Moreover, we show that Tim13 is able to induce a conformational change and reduce 6 cysteines in Mia40. Finally, *in organello* studies confirmed that in yeast strains deficient in

Erv1, Mia40 remains in a reduced state. In all, these experiments suggest that Mia40 is able to act as an electron sink in which it accumulates electrons in the presence of Tim13.

Subsequently, the Mia40-Erv1 import pathway has electron acceptors to continue the process of disulfide bond formation. The aerobic electron acceptors include oxygen and cytochrome *c*, but an anaerobic acceptor has not been identified. Here we show that the fumarate reductase Osm1, which transfers electrons from fumarate to generate succinate, fills this gap as a new electron acceptor. In addition to microsomes, Osm1 localizes to the IMS and assembles with Erv1 in a complex. In reconstitution studies, Erv1 transfers electrons to Osm1 in the oxidation of Tim13. Comparative assays support that Osm1 accepts electrons with similar efficiency as cytochrome *c* and that the cell has strategies to coordinate expression of the terminal electron acceptors. Thus, Osm1 is a new terminal electron acceptor in the IMS that may also have a similar function in the endoplasmic reticulum.

The dissertation of Sonya Elina Neal is approved.

Alexander M. van der Bliek

Mike A. Teitell

Catherine F. Clarke

Carla M. Koehler, Committee Chair

University of California, Los Angeles

2013

DEDICATION

I dedicate this to my daughter Elina, whose love and support has kept me motivated everyday, and her breadth of unconditional love has made my "why" much more apparent to me. I also dedicate this to my parents, Jerome and Yumiko Neal. They have always supported me in every endeavor. They are the reason why I'm here at all, and made me who I am today.

TABLE OF CONTENTS

LIST OF FIGURES

LIST OF TABLES

APPENDICES

LIST OF ABBREVIATIONS

AMS	4-acetamido-4-maleimidylstilbene-2,2-disulfonic acid
ATP	Adenine triphosphate
βME	Beta-mercaptoethanol
Dsb	Disulfide bond
DMSO	Dimethyl sulfoxide
DTT	Dithiothreitol
E_m	Midpoint potential
ER	Endoplasmic reticulum
ERO1	ER oxidoreductin 1
ETS	Electron transport chain
F	Fluorescence intensity
FAD	Flavin adenine dinucleotide
IAA	Iodoacetamide
IM	Inner Membrane
IMS	Intermembrane space
Kda	kiloDaltons
M	Molar
mBBr	Monobromobimane
mg	Milligrams
µg	Micrograms
µl	Microliters
µmol	Micromole
ml	Milliters
mM	Millimolar
µM	Micromolar
mV	Milivolts
NAD	Nicotinamide Adenine dinucleotide
NADP	Nicotinamide Adenine dinucleotide phosphate
OM	Outer membrane
PAGE	Polyacrylamide gel electrophoresis
PDI	Protein disulfide isomerase
SDS	Sodium dodecyl sulfate
Trx	Thioredoxin
TOM	Translocon of the Outer Membrane
TIM	Translocon of the Inner Membrane
TM	Transmembrane

ACKNOWLEDGEMENTS

The past five years have been demanding and rewarding, and there are many people for whom I am appreciative for contributing to my graduate school career. I would first like to thank my professor, Dr. Carla Koehler, who saw more potential in me than I did, and challenged me to push myself far beyond limits that I didn't think I was capable of even reaching. I would like to thank Dr. Deepa Dabir for mentoring and assisting me during my first couple of years in graduate school. Her insights and mentorship shaped me into the scientist that I came to be today. I would also like to thank my committee members, Dr. Mike Teitell, Dr. Cathy Clarke, Dr. Alex Van Der Bliek and Dr. Sabeeha Merchant for their support and advice over the years. I was privileged to be the head "yeast clan leader" and mentor a number of gifted and hardworking students: Holly Dickinson, Kathrin Glaser, Jonathan Gonzalez and Cennyana Boon. I am extremely grateful for their assistance and dedication over the years. I am grateful for my former and current labmates who inspired great scientific discussions and friendship over the years.

I would like to thank my graduate student friends who commiserated and celebrated every event that happened in and out of lab over the past 5 years: Esther, who is a great listener and provided me with a Kleenex several times, Miss Boon Boon, who has been a great friend and shared my love for shopping and playing with Elina, Fern who constantly made me laugh during our daily morning coffee breaks, Kathrin, who is always uplifting and positive, J-dub who was my fitness partner in crime and was always down for anything, and Matt and Tanya , the gang who were always up for great and "interesting" conversations during the morning coffee breaks. I am grateful for my close friends Laurencia, Jenny, Wendy and Nina who have been my

proverbial rocks, and without whom I couldn't have made it through high school and college, let alone grad school.

I am indebted to my family, especially my parents and brother, and Alvaro's family. I will always treasure the fact that every time I thought I couldn't do this, one or all of you managed to convince me that I was more than capable of finishing my PhD.

I have been privileged to have a father who served in the Marine Corp for 30 years and is a veteran of the Vietnam and Desert Storm War. You have and will always serve as my inspiration to achieve everything that is within my grasp. Dad, you are my mentor in life, both in and out of the lab, and I will never be able to thank you enough for all of the love and support.

Lastly, I need to thank Alvaro and Elina. Alvaro, you supported me throughout all the hardships I was faced with. I have (as most people who know me are aware of) a hard shell and it is difficult for me to open up at times. I somehow found the one person who is uncannily able to get through to me and show me how to open up and enjoy and appreciate life to the fullest. You are my heart, and I couldn't love anything more than I love you. My pumpkin Lin Lin, you are the very reason why I have been motivated throughout life; both in and out of graduate school. You have given me the best and most rewarding job in the world; and that is to be a mother. By having you, I have been able to balance both graduate life and motherhood and I don't regret a single day of it. Mommy loves you so much pumpkin and I hope to serve as your inspiration just as "Ojiisan" is an inspiration to me.

The introduction is a version of a review in preparation coauthored by myself and Koehler CM. We thank Tanya Hioe for the illustrations of the DsbA-DsbB pathway, Pdi-Ero1 pathway and the Mia40-Erv1 pathway.

Chapter 1 is a reprint of the journal article Tienson HL, Dabir DV, Neal S, Loo J, Hasson SA, Boontheung P, Kim SK, Loo J, Koehler CM; Reconstitution of the Mia40-Erv1 oxidative folding pathway for the small Tims proteins; Molecular Biology of the Cell. My contribution to this publication was determining the midpoint potential of Mia40 by thiol-trapping with AMS, mBBr titration, and intrinsic tryptophan fluorescence of Mia40, which is seen in Figure 2 and Supplemental Figure 2.

Chapter 2 is a version of a manuscript in preparation to be authored by myself, Tienson HL, Glaser K, Loo R, and Koehler CM; Mia40 serves as an electron sink in the Mia40-Erv1 import pathway. The cysteine mutants of Tim13 were generated by Heather Tienson. The cysteine mutants of recombinant Erv1 and *erv1-101* yeast strain were generated by Fred Tsai and Edward Leverich respectively. The mixed-disulfide trapping assay was performed by Kathrin Glaser. We thank Rachel Loo for assistance with MALDI-MS analysis and calculations. We also thank Heather Tienson for helpful discussions.

Chapter 3 is a version of a manuscript in preparation to be authored by myself, Dabir DV, Boon C, Wijaya J and Koehler CM; Osm1 is a new electron acceptor for Erv1 in the mitochondrial intermembrane space. Osm1 import assays were performed by Deepa Dabir. MPP cleavage assays were performed by Juwina Wijaya. Carbonate extraction experiments were performed by Cennyana Boon. Jonathan Gonzales assisted with generating the Osm1 fusion constructs, $Osm1^{1-32}$-DHFR-myc and $Osm1^{1-60}$-DHFR-myc. The Osm1-His yeast strain

was generated by Cennyana Boon. The *erv-101* temperature-sensitive yeast strain was generated by Edward Leverich. We thank Tanya Hioe and Justin Hotter for technical assistance and Deepa Dabir and Steven Claypool for helpful discussions.

Robert Damoiseaux and Sam Hasson made significant contributions to my training for SGA analysis in Chapter 4. I would like to thank Sam Hasson and Robert Damoiseaux for training me in high throughput screening at the Molecular Screening Shared Resource (MSSR) facility. I would like to thank Jong Lee and Winnie Hwong for assistance with setting up the screening platform and hit characterization. The *osm*1::LEU2 strain was generated by Kathrin Glaser.

All of the work was supported by grants from the NIH (Ruth L. Kirschstein National Research Service Award (GM871082) to S.E.N and (IR01GM61721) to C.M.K and the American Heart Association (0640076N to C.M.K.).

VITA

2004-2007	UC LEADS Scholar University of California, San Diego
2005-2007	Warren Provost Honor University of California, San Diego
2007	B.S. in Chemistry-Biochemistry University of California, San Diego
2007	National Science Foundation (NSF) Alliance for Graduate Education and the Professoriate (AGEP) Fellow University of California, Los Angeles
2007-2012	Graduate Student Researcher Molecular Biology Interdepartmental Ph.D. program University of California, Los Angeles
2007-2008	Eugene V. Cota Robles Fellowship University of California, Los Angeles
2008-2011	Cellular and Molecular Biology Trainee Adjunct University of California, Los Angeles
2010-2012	Teaching Assistant Department of Chemistry and Biochemistry University of California, Los Angeles
2008-2013	Ruth L. Kirschstein National Research Service Award University of California, Los Angeles

PRESENTATIONS AND PUBLICATIONS

Tienson, H. L., D. V. Dabir, **S. E. Neal**, R. Loo, S. A. Hasson, P. Boontheung, S.-K. Kim, J. A. Loo, and C. M. Koehler. 2009. Reconstitution of the Mia40-Erv1 oxidative folding pathway for the small Tim proteins. Mol Biol Cell.

S.E. Neal C.M. Koehler. 2012. Osm1 is a new electron acceptor for Erv1 in the mitochondrial intermembrane space. Poster presentation at the Gordon Research Conference, Galveston, Texas.

S.E. Neal and C.M. Koehler. 2011. The Redox Properties of Mia40 and Erv1 in the Mitochondrial Intermembrane Space. Oral presentation at the 3rd year CMB Seminar Series, UCLA.

S.E. Neal and C.M. Koehler. 2011. The Mia40-Erv1 disulfide relay system for protein import into the mitochondrial intermambrane space. Poster presentation at the EMBO Conference, Sardegna, Italy.

S.E. Neal and C.M. Koehler. 2010. Characterization of the redox properties of proteins in the mitochondrial intermembrane space. Oral presentation at the mitochondrial group meeting, UCLA

S.E. Neal and C.M. Koehler. 2010. Characterization of the redox properties of proteins in the mitochondrial intermembrane space. Oral presentation at the 3rd year MBIDP Seminar, UCLA

S.E. Neal and C.M. Koehler. 2010. Characterization of the redox properties of proteins in the mitochondrial intermembrane space. Oral presentation at the 2nd year CMB Seminar Series, UCLA

S.E. Neal, D.V. Dabir and C.M. Koehler. 2009. Investigation of the redox properties of Mia40 and Erv1. Poster presentation at the FASEB conference, Carefree, Arizaona

S.E. Neal, D.V. Dabir, and C.M. Koehler. 2009. Osm1 is an electron acceptor of Erv1. Oral presentation at UCLA mitochondrial group meeting, UCLA.

S.E. Neal, H.L. Tienson, D.V. Dabir, and C.M. Koehler. 2008. Investigation of the redox properties of Mia40 and Erv1. Poster presentation at the Seaborg Symposium, UCLA

S.E. Neal, H.L. Tienson, D.V. Dabir, and C.M. Koehler. 2008. Investigation of the redox properties of Mia40 and Erv1. Poster presentation at the GRC Mitochondria and Chloroplasts Gordon-Kenan Research Seminar, Biddeford, ME

S. E. Neal, H. L. Tienson, D. V. Dabir, and C. M. Koehler. 2008. Investigation of the redox properties of Mia40 and Erv1. Poster presentation at the GRC Thiol-based Redox Regulation and Signaling Conference, Lucca (Barga), Italy

S. E. Neal, D. V. Dabir, and C. M. Koehler, 2007. Redox pathways of the mitochondrion. Oral presentation at UCLA mitochondrial group meeting, UCLA.

S. E. Neal, D. V. Dabir, and C. M. Koehler. 2007. Characterization of the redox properties of Erv1. Oral presentation at the NSF UCLA Competitive Edge: Graduate Summer Research Program Symposium, UCLA.

S.E. Neal, H. Tienson, and C.M. Koehler. 2007. The role of redox chemistry in protein import into the mitochondrial intermembrane space. Oral presentation at the UC Leads Symposium. UCLA.

S.E. Neal, H. Tienson, and C.M. Koehler. 2006. The role of redox chemistry in protein import into the mitochondrial intermembrane space. Poster presentation at the Society for Advancement of Chicanos and Native Americans in Science(SACNAS) National Conference, Tampa Bay, Florida.

S.E. Neal, T. Duong, and E. Theodorakis. 2006. Synthesis of Fluoro-butenolide. Oral Presentation at the Faculty Mentor Program Research Symposium, UCSD.

S.E. Neal, T. Duong, and E. Theodorakis. 2006. Synthesis of Butenolide Diels-Alder Adduct. Poster Presentation at the UC LEADS Symposium, UCSC.

S.E. Neal, T. Duong, and E. Theodorakis. 2005. Synthesis of Butenolide Diels-Alder Adduct. Oral Presentation at the STARS Symposium, UCSD.

Introduction: Oxidative Protein Folding in Bacteria and Eukaryotes

1. Introduction

Major advances have been made in studying disulfide bond formation in prokaryotes and eukaryotes. Disulfide bonds are essential for the proper folding, and stability, of proteins (Bardwell, 1994; Collet and Bardwell, 2002; Depuydt et al., 2011). Although disulfide bonds form spontaneously, cysteines oxidize slowly in the presence of oxygen (Bardwell, 1994, 2002). Organisms have developed an intricate system for inserting disulfide bonds. The enzymes responsible for inserting disulfide bonds are thiol-disulfide oxidoreductases. Thiol-disulfide oxidoreductases function in the periplasm of prokaryotes and the endoplasmic reticulum and mitochondria of eukaryotes(Kadokura et al., 2003a; Depuydt et al., 2011; Gennaris and Collet; Koehler and Tienson, 2009). There is a redox active cysteine pair in the active site that catalyzes the oxidation of two cysteines in the substrate (Depuydt et al., 2011). Two electrons are released and shuttled through multiple electron carriers (Ito and Inaba, 2008a; Depuydt et al., 2011) until finally, the electrons are donated to the final terminal electron acceptor; which is characterized as the oxidizing source of the pathway (Dabir et al., 2007; Bardwell, 2002; Kadokura et al., 2000; Bihlmaier et al., 2007).

Prokaryotes and eukaryotes use a diverse array of terminal electron acceptors to ensure the proper folding of proteins. For example, in aerobic conditions, bacteria and eukaryotes use oxygen via the respiratory pathway. In anaerobic conditions, bacteria and yeast use small metabolites such as fumarate or nitrate as the terminal electron acceptor. Thus, organisms from bacteria to humans have developed a backup system of electron acceptors to continue oxidative

folding. Also, the functional redundancy of electron acceptors confirms the importance of disulfide bond formation.

Reviewed here is the wide array of terminal electron acceptors of the DsbA-DsbB folding pathway in bacteria and the PDI-Ero1 and Mia40-Erv1 folding pathway in the endoplasmic reticulum and mitochondria of eukaroyotes, respectively. The major questions that remain to be answered are also highlighted.

2. Oxidative Folding Pathway of the DsbA-DsbB System

In *E. coli*, hundreds of soluble and membrane proteins with cysteines are secreted into the periplasm. Upon entering the periplasm, proteins are oxidized by the disulfide bond protein (Dsb) oxidation machinery(Inaba, 2009). The oxidative folding pathway has two major players, DsbA and DsbB (Heras et al., 2007; Kadokura et al., 2003b; Ito and Inaba, 2008a)(Figure 1). This is observed by the decrease in the oxidation of secreted proteins in dsbA and dsbB single mutants. Thus, DsbA and DsbB are central components of the folding pathway(Bardwell et al., 1991; Kamitani et al., 1992).

2.1. Mechanism of the DsbA-DsbB System in Bacterial Periplasm

DsbA, a 21-kDa soluble protein, introduces disulfide bonds into newly secreted proteins (Depuydt et al., 2011; Bardwell, 1994). DsbA has a thioredoxin-like (Trx) fold and a CXXC motif (Cys30 and Cys33) in its active site. The redox-active cysteine pair directly oxidizes unfolded proteins (Bardwell, 1994; Collet and Bardwell, 2002; Depuydt et al., 2011; Heras et al., 2007). The alpha helical domain embedded in the Trx fold mediates the binding of substrates (Inaba, 2009; Ito and Inaba, 2008b; Guddat et al., 1997). Genetic and biochemical studies have elucidated the mechanism of DsbA-mediated oxidation. Initially, an intermolecular disulfide intermediate is formed between DsbA and the target protein (Wunderlich et al., 1995). The low

pKa of DsbA Cys30 (pKa~3) thermodynamically drives the transfer of electrons from the target protein to DsbA (Nelson and Creighton, 1994).

DsbB, a 20 kDa membrane protein, plays a major role in reoxidizing DsbA (Collet and Bardwell, 2002; Inaba, 2009). This allows DsbA to initiate another round of oxidation for newly secreted proteins. DsbB has four transmembrane domains and two periplasmic loops facing the cytoplasm. The N-terminal periplasmic loop has a redox-active cysteine pair (Cys41 and Cys44) and the C-terminal periplasmic loop has another redox-active cysteine pair (Cys104 and Cys130) (Inaba, 2009; Inaba et al., 2006). Initially, DsbB binds to the hydrophobic groove of DsbA; followed by the oxidation of DsbA (Cys30 and Cys33) by DsbB (Cys104-Cys130). Finally, the electrons are shuttled to (Cys41 and Cys44) followed by concomitant electron release to a variety of terminal electron acceptors (Inaba et al., 2006, 2009; Kadokura, 2002).

2.3. Terminal Electron Acceptors in Aerobic Conditions

The discovery of DsbB initially raised the idea of the DsbA-DsbB pathway being coupled to the electron transport chain (Dailey and Berg, 1993). DsbA and DsbB are not efficiently oxidized in *E. coli* containing defective components from the respiratory pathway. For instance, defects in heme and quinone biosynthesis leads to an accumulation of reduced DsbA and DsbB (Kobayashi et al., 1997a). Also, DsbB is sensitive to reducing agents when membranes are depleted of heme and quinones (Kobayashi et al., 1997a). Furthermore, the oxidation of the DsbA and DsbB machinery is dependent on oxygen (Bader et al., 1999). In all, these studies show a strong connection between the DsbA-DsbB oxidative pathway and the respiratory chain.

Recent works have complemented previous findings on the DsbA-DsbB pathway done *in vivo*. *In vitro* reconstitution with purified components of DsbB and ubiquinone variants (ubiquinone-5 and decyl-ubiquinone), shows the transfer of electrons from DsbB to ubiquinone

(Bader et al., 1999). Structural analysis confirmed a quinone binding site in DsbB. Also, the binding of quinone is mediated by a conserved arginine residue and a C-terminal segment of DsbB (Kadokura et al., 2000; Kobayashi et al., 2001). Indeed, DsbB is reoxidized by ubiquinone.

In *E. coli*, DsbB shuttles electrons to ubiquinone and ubiquinone is reoxidized by major terminal oxidases, either cytochrome *bd* oxidase or cytochrome *bo* oxidase. The main function of terminal oxidases is to transport electrons from the ubiquinone pool to oxygen. Cytochrome *bo* oxidase is abundant in aerobic conditions whereas cytochrome *bd* oxidase is abundant in limited aerobic conditions (Ingledew and Poole, 1984). Thus, ubiquinone mediates electron transfer from the DsbA-DsbB pathway to either cytochrome *bo* or cytochrome *bd* oxidase. *In vitro* reconstitution with purified components of DsbA, DsbB, ubiquinone, and either cytochrome *bo* oxidase or cytochrome *bd* oxidase shows the oxidation rate of DsbA is 49 μmol DsbA/umol DsbB/ min and 82 μmol DsbA/umol DsbB/min, respectively (Bader et al., 1999). This suggests electrons transport to cytochrome *bd* oxidase in aerobic conditions, while electrons transport to cytochrome *bo* oxidase in limited oxygen conditions. Taken together, the DsbA-DsbB pathway shuttles electrons to the terminal oxidases of the respiratory chain, and the driving force of the pathway is oxygen.

2.4. Terminal Electron Acceptors in Anaerobic conditions

There is evidence showing the DsbA-DsbB oxidative folding pathway has alternative electron acceptors in anaerobic conditions. For example, DsbA-DsbB machinery continues to insert disulfide bonds into phosphatase under anaerobiosis (Kamitani et al., 1992). In addition, disulfide bonds are correctly inserted into components of the flagellum under conditions deprived of oxygen (Dailey and Berg, 1993). Based on these observations, Bader et al., looked at

disulfide bond formation under anaerobic conditions. Under oxygen-deprived conditions, the DsbA-DsbB machinery inserts disulfide bonds into TEM B-lactamase (Bader et al., 1999). Taken together, there are, most likely, additional terminal electron acceptors in the DsbA-DsbB pathway. Thus, the hunt for alternative electrons acceptors became imminent.

Menaquinone became a strong candidate for DsbB oxidation. Menaquinone is the major quinone in the cell during anaerobic growth (Universio, 1977). Moreover, menaquinone shuttles electrons to terminal electrons acceptors such as fumarate via fumarate reductase, DMSO via DMSO reductase, or nitrate via nitrate reductase (Unden and Bongaerts, 1997). In anaerobic conditions, menaquinone most likely substitutes for ubiquinone in the reoxidation of DsbB. Several studies show that menaquinone is able to substitute for ubiquinone in oxidizing DsbB. In vitro reconstitution with purified components of the DsbA-DsbB machinery with menaquinone shows the ability of menaquinone to reoxidize DsbB (Bader et al., 1999). There is also a strong defect in disulfide bond formation in *E. coli* strains lacking ubiquinone, menaquinone and fumarate reductase (Kobayashi et al., 1997b; Bader et al., 1999). These studies confirmed that menaquinone is oxidized by DsbB in anaerobic conditions.

E.coli have successfully adapted a backup system of alternative electron acceptors to ensure that the essential process of disulfide bond formation continues. Aerobically, the DsbA-DsbB pathway is able to shuttle electrons to ubiquinone, which is shuttled to either cytochrome *bo* or cytochrome *bd* terminal oxidases. Anerobically, the DsbA-DsbB pathway shuttles electrons to menaquinone, which is shuttled to a variety of terminal electron acceptors including fumarate, nitrate, and DMSO. This reiterates the importance of having a wide array of terminal electron acceptors in disulfide bond formation pathways.

3. Oxidative Folding Pathway of the PDI-Ero1 system

It is critical that proteins destined to the secretory pathway are properly oxidized and folded. Initially, proteins destined to this pathway are co-translationally inserted into the Endoplasmic Reticulum (ER) (Depuydt et al., 2011; Feige and Hendershot, 2011). Studies in yeast and humans reveal *de novo* disulfide bond formation is catalyzed by the PDI-Ero1 oxidative folding pathway (Frand and Kaiser, 1999; Tu and Weissman, 2004)(Figure 2). It is important to note the current contradiction in this field; which is whether or not the PDI-Ero1 oxidative folding pathway is responsible for protein oxidation in the ER. This contradiction stems from new studies in higher eukaryotes in which they display a minor phenotype when either Ero1 or PDI is disrupted (Zito et al., 2010; Hatahet and Ruddock, 2009). For the purpose of this review, only the terminal electron acceptors of the PDI-Ero1 pathway focused on in the past two decades will be discussed.

3.1. Mechanism of the PDI-Ero1 System in the Endoplasmic Reticulum of Eukaryotes

PDI, discovered a half century ago, is a major component of the ER oxidative folding pathway (Venetianer and Straub, 1963; Service, 1963). Yeast Pdip is essential and is present in high concentrations in the ER (Lambert and Freedman, 1985; Tu and Weissman, 2004). PDI is a multifunctional enzyme with a role in substrate oxidation, disulfide bond reduction, and isomerization (Depuydt et al., 2011; Kulp et al., 2006). It is characterized by four thioredoxin domains: a catalytically active a and a' domains, inactive b and b' domains, and a c segment at the C-terminus containing the ER retention sequence (Edman et al.; Inaba and Araki, 2011). In both the a and a' active domains, there is a redox-active cysteine pair catalyzing the thiol-disulfide exchange reactions with incoming substrates(Hawkins and Freedman, 1991; Karala et al., 2010; Darby et al., 1996). Structural analysis of Pdip shows substrate binding is mediated by

the hydrophobic surface comprised of all four domains (Karala et al., 2010)(Karala et al., 2010)(Tian et al., 2006). When PDI is functioning as an oxidase, the PDI CXXC motif inserts disulfide bonds into the substrate (Depudyt, 2011).

Ero1 is responsible for *de novo* disulfide bond formation via the oxidation of PDI (Pagani et al., 2000; Cabibbo et al., 2000). Ero1 is a sulfhydryl oxidase; which are a class of enzymes known for using Flavin Adenine Nucleotide (FAD) as a cofactor to transfer electrons from the substrate to molecular oxygen, producing hydrogen peroxide(Gross et al., 2006; Frand and Kaiser, 1999). Ero1 has four highly conserved cysteines participating in PDI oxidation: the CXXC motif adjacent to the FAD moiety and another CXXC motif located on the flexible loop (Gross et al., 2004). Once Ero1 binds to PDI, electrons are shuttled from the CXXC in PDI to the CXXC in Ero1 located on the flexible shuttle loop (Inaba and Araki, 2011). This is followed by electron transfer to the CXXC adjacent to FAD.

Erv2, identified in yeast, plays the same role as Ero1in the ER oxidative folding pathway. Although Erv2 is able to substitute for Ero1, ERV2 delete in yeast partially compromises disulfide bond formation (Tu and Weissman, 2002). This suggests that Ero1p is the major flavoenzyme in the ER.

3.2. Terminal Electron Acceptors in Aerobic Conditions

Unlike the DsbA-DsbB pathway, the PDI-Ero1 pathway is independent of the electron transport chain. Genetic studies by (Tu, 2000) show that depletion of heme, ubiquinone and ER-associated cytochrome does not compromise disulfide bond formation in the ER. This confirms that oxidative folding machinery is independent of components from the electron transport system.

Until recently, FAD was suggested to be the oxidizing source of the pathway. The first observation of Ero1 oxidation by FAD came from the isolation of Ero1p in which FAD was found bound to it (Tu, 2000). Further support came from genetic studies showing *ero1-1* and *fad1-1* mutants are synthetically lethal, and that over-expression of FAD rescues the temperature-sensitive phenotype of *ero1-1* (Tu and Weissman, 2002; Tu, 2000). Lastly, Ero1p's activity is dependent on increasing concentrations of FAD (Tu and Weissman, 2002; Tu, 2000). Altogether, genetic and biochemical analyses suggest a shuttling of electrons from the CXXC motif of Ero1 (adjacent to FAD) to its cofactor, FAD.

The FAD cofactor of Ero1 shuttles electrons directly to molecular oxygen. In comparison to FAD, oxygen is a strong oxidant, making it a strong candidate for Ero1-mediated oxidation. *In vitro* reconstitution comprised of reduced RNaseA, Pdip and Ero1p with increasing concentrations of FAD under anaerobic conditions, shows only a fraction of RNaseA is oxidized (Tu and Weissman, 2002). This suggests FAD is unable to serve as the oxidizing source of the pathway. However, Ero1p is directly oxidized by oxygen (Tu and Weissman, 2002). The K_m value of Ero1 for oxygen is reported to be 4 μM(Gross et al., 2006). The low K_m value implies that Ero1 is able to bind oxygen efficiently. There is also compromised growth in the *ero1-1* yeast mutant under anaerobic conditions (Tu and Weissman, 2002). In all, this suggests that molecular oxygen is the oxidizing source of the PDI-ERO1 oxidative pathway in aerobic conditions.

3.3. Terminal Electron Acceptors in Anaerobic Conditions

There is considerable evidence that Ero1 has alternative electron acceptors. For example, the majority of PDI is oxidized in yeast grown anaerobically (Tu and Weissman, 2002). Also, *ero1-2* yeast is sensitive to the reducing agent DTT in the absence of oxygen (Tu and Weissman,

2002). Indeed, Ero1 is still functional in anaerobic conditions suggesting the presence of alternative terminal acceptors in the oxidative folding pathway.

Gross et al. analyzed Ero1p's ability to transfer electrons to a diverse array of redox-active molecules including free FAD, cytochrome *c*, cytochrome and bacterial azurin. Interestingly, Ero1 shuttles electrons to a diverse set of redox-active molecules (Gross et al., 2006). Unfortunately, the majority of these redox active molecules is not localized in the ER and is not physiologically relevant for Ero1 oxidation. However, this study unveils Ero1's potential in transferring electrons to a number of electron acceptors; thus the hunt for potential electron acceptors in the ER came into the forefront of the field.

Ascorbate potentially acts as an Ero1 alternative acceptor in oxidizing PDI. The properties of ascorbate make it the perfect candidate for PDI oxidation. Firstly, it is found in high concentrations in the ER. Additionally, it is able to accept one electron at a time, making it suitable as an electron acceptor of PDI (Hatahet and Ruddock, 2009). Ascorbate-mediated oxidation of proteins was initially observed in rat liver microsomes (Szarka et al., 2002). There are several reports indicating oxidation in the ER is coupled to PDI oxidation by ascorbate. For example, the addition of ascorbate to rat, guinea pig, and human liver microsomes correlated with a decrease in reduced thiol concentration (Margittai et al., 2009). In addition, the rate of ascorbate oxidation was directly proportional to the activity of PDI in microsomes from different organs (Nardai et al., 2001). Unfortunately, most of these findings were largely neglected in the field. This was due to the rising view of Ero1-mediated oxidation of PDI. However, the characteristics of ascorbate make it an excellent candidate for thiol-mediated oxidation in the ER. Additional studies are needed to further address the role of ascorbate in the oxidation of PDI.

Vitamin K epoxide reductase (VICOR) is postulated to function as an alternative electron acceptor for PDI. In the ER, VICOR subsequently transfers electrons to Vitamin K (Hatahet and

Ruddock, 2009). PDI was recently found to be in a complex with VICOR (Wajih et al., 2007). Additionally, VICOR is able to functionally replace DsbB (which is the bacterial homologue of Ero1) (Hatahet and Ruddock, 2009; Dutton et al., 2008). Although it is tempting to speculate that VICOR may play a role in the oxidation of PDI, future studies are necessary to elucidate the role of VICOR in disulfide bond formation in the ER.

We recently discovered a novel oxidoreductase in yeast, Osm1, is dual localized to the mitochondria and microsome. Interestingly, there is a synthetic lethal interaction in yeast strains harboring *ero1-1* and Δ*osm1*, suggesting Ero1 and Osm1 function in the same pathway (Costanzo et al., 2010). This suggests Osm1 potentially functions as an anaerobic electron acceptor of Ero1. Future studies in yeast will be necessary to elucidate Osm1's role in disulfide bond formation in the ER.

Similar to bacteria, eukaryotes have developed a wide array of alternative electron acceptors in the ER; and so far, the majority of these studies were done in yeast. Additional experiments are needed to address if these alternative electron acceptors extend into higher eukaryotes. Finally, the findings on VICOR and ascorbate have hinted at the possibility of higher eukaryotes having alternative electron acceptors in the ER.

4. Oxidative Folding Pathway of the Mia40-Erv1 System

An endiosymbiotic event gave rise to a mitochondrion; one of few organelles that contain its own genome(McCutcheon and Moran, 2012). Although the mitochondrion has a small genome, the majority of mitochondrial proteins is transcribed and translated in the cytosol (Koehler, 2004; Bauer et al., 2002; Pfanner and Wiedemann, 2002). These polypeptides contain an important targeting and sorting sequence that allows for import into the various compartments within mitochondria (Koehler, 2004). A new pathway emerged involving the import of

reduced-cysteine rich proteins into the mitochondrial intermembrane space (IMS). The pathway is mediated by redox chemistry and requires disulfide bond formation of newly imported substrates via the Mia40-Erv1 oxidative folding machinery (Chacinska and Rehling, 2004; Mesecke et al., 2005; Tokatlidis, 2005; Rissler et al., 2005; Koehler and Tienson, 2009)(Figure 3).

4.1. Mechanism of Mia40-Erv1 System in the IMS of Mitochondria

Mia40, an essential protein, functions as an import receptor in the IMS and introduces disulfide bonds into cysteine-rich polypeptides. Mia40 has three highly conserved cysteine pairs. Two pairs are in a twin CX_9C motif and are postulated to stabilize the protein, and one redox-active cysteine pair is in a CPC motif; playing a role in accepting electrons from incoming substrates (Grumbt et al., 2007). Upon translocation through the TOM complex, oxidized Mia40 interacts with the unfolded polypeptides. This is mediated by the binding of the targeting signal of the substrate to the hydrophobic pocket of Mia40 (Banci et al., 2009; Sideris et al., 2009). A mixed disulfide intermediate is formed between a cysteine from the substrate, and cysteine from the CPC motif of Mia40 (Sideris and Tokatlidis, 2010). The CPC motif accepts electrons from its substrate, resulting in the concomitant release of its substrate in an oxidized, and folded, state.

Erv1 is an essential sulhydryl oxidase and has a major role in oxidizing Mia40 (Lisowsky, 1992; Mesecke et al., 2005). Erv1 functions as a homodimer where each subunit contains two sets of highly conserved redox-active cysteine pairs. A CXXC motif is located on the flexible loop of the N-terminus, and another CXXC motif is adjacent to the FAD cofactor (Farrell and Thorpe, 2005; Bien et al., 2010). Once Erv1 binds to Mia40, a mixed disulfide intermediate is formed between the second cysteine of the Mia40 CPC motif and a cysteine from the N-terminal domain of Erv1(Sideris and Tokatlidis, 2010). This initiates a cascade of electron

transfer in which electrons are shuttled from the N-domain of Erv1 to the CXXC motif of the FAD domain. Finally, the electrons are passed onto the FAD cofactor, leaving Mia40 reoxidized (Bien et al., 2010).

4.2. Terminal Electron Acceptors in Aerobic Conditions

Recent works identified electron acceptors of Erv1 to be either cyt *c* or O_2. In vitro reconstitution with components of the Mia40-Erv1 pathway clearly show Erv1 donating electrons to oxygen to produce hydrogen peroxide (Dabir et al., 2007). Also, a fraction of cyt *c* binds to Erv1 and Erv1 shuttles electrons to cyt *c* (Bihlmaier et al., 2007; Dabir et al., 2007). In comparison to oxygen, cyt *c* is the preferred substrate for Erv1. *In vitro* reconstitution using yeast Erv1 and human Alr shows cyt *c* is a better electron acceptor than oxygen by 100-fold. The K_m values for oxygen and cyt *c* were reported to be 240 μM and 10 μM, respectively (Farrell and Thorpe, 2005). In the oxygen consumption assay, addition of cyt *c* causes a delay in Erv1-mediated oxygen consumption. Interestingly, addition of both cyt *c* and Ccp1 causes a drastic delay in Erv-mediated oxygen consumption, suggesting cyt *c* and Ccp1 cooperate together to oxidize Erv1 (Dabir et al., 2007). Taken together, Erv1 shuttles electrons to either oxygen or cyt *c,* and cyt *c* shuttles electrons Ccp1.

Previous findings on cyt *c* oxidation of Erv1 led to the postulation of the Mia40-Erv1 pathway being coupled to the electron transport chain. The redox state of Mia40 is dependent on oxygen concentration and the activity of the electron transport chain. Moreover, the majority of Mia40 is in a reduced state in yeast strains harboring mutations in cyt *c* or cyt *c* oxidase (Bihlmaier et al., 2007). This suggests the IMS import pathway is connected to the electron transport chain via cytochrome *c* and cytochrome *c* oxidase. Therefore, Erv1 donates electrons to cyt *c,* and cyt *c* donates electrons to either Ccp1 or the respiratory chain.

4.3. Terminal Electron Acceptors in Anaerobic Conditions

Analogous to the DsbA-DsbB and PDI-Ero1 pathways, the Mia40-Erv1 pathway most likely has alternative electron acceptors. For instance, yeasts are known to grow anaerobically. Also, *erv1* mutants grow anaerobically in the absence of the mitochondrial genome (Dabir et al., 2007). Different pathways must be present to oxidize Erv1. As such, there must be additional oxidizing sources of the Mia40-Erv1 pathway that have yet to be identified.

Genetic studies propose a role for cyt *c* in oxidizing Erv1 in anaerobic conditions. Yeast Δ*cyc3erv1* and Δ*cyc1* mutants fail to grow anaerobically (Allen et al., 2005; Dabir et al., 2007; Bihlmaier et al., 2007). In anaerobic conditions, yeast Δ*cyc1cyc7* mutants are sensitive to reducing agent (DTT) and the majority of Mia40 is in a reduced state (Bihlmaier et al., 2007). Cyt *c* is clearly needed for the oxidation of Erv1 under anaerobiosis. Interestingly, yeast express two isoforms of cyt *c*; Cyc1 and Cyc7 are expressed in oxygen-saturated conditions, and oxygen limiting conditions, respectively. The isoforms most likely interchange as Erv1 electron acceptors in different oxygen concentrations. Although it is clear that cyt *c* is needed for Erv1 oxidation, it is not clear how cyt *c* is oxidized. Future studies are needed to determine the oxidizing source of cyt *c* in oxygen-depleted conditions.

Recently, fumarate reductases Osm1 and Frds1 came to the forefront of the field and are postulated to be electron acceptors of Erv1. In general, fumarate reductases non-covalently attach $FADH_2$, and reduce fumarate, to succinate. Frd1s localizes to the cytosol, whereas Osm1's enzymatic activity has been enriched in the mitochondria (Muratsubaki and Enomoto, 1998). Intriguingly, Δ*osm1frds1* mutants fail to grow anaerobically, suggesting the two genes are essential in anaerobic conditions (Arikawa et al., 1998). Moreover, both fumarate reductases are proposed to have a role in maintaining a redox balance within yeast by oxidizing $FADH_2$ in

anaerobic conditions (Camarasa et al., 2007). Osm1, or Frds1, may play a role in oxidizing the FAD of Erv1 in the IMS. In all, Frds1 and Osm1 are strong candidates for being alternative electrons acceptors in the Mia40-Erv1 import pathway.

We demonstrated that Erv1 shuttles electrons to Osm1. Fractionation and biochemical studies confirmed Osm1 is a peripheral protein dual-localized to the microsome and the IMS of mitochondria. Since Frds1 is localized to the cytosol, we pursued Osm1 instead. Intriguingly, Δ*erv1osm1* mutant failed to grow anaerobically, suggesting Osm1 and Erv1 function in a similar pathway. *In organello* studies confirmed a fraction of Osm1 is bound to Erv1; and *in vitro* reconstitution assays for Tim13 oxidation showed electrons are transferred from Erv1 to Osm1. Interestingly, cyt *c* steady-state levels are upregulated in yeasts lacking Osm1. It seems that yeasts regulate the levels of its terminal electron acceptors. Further studies are required to elucidate the mechanism for the regulation of electron acceptors in yeast. Based on our studies, we have identified a new oxidoreductase, Osm1,that accepts electrons from Erv1.
There may be additional electron acceptors that have not been identified in the Mia40-Erv1 import pathway. For example, we did not observe growth defects in Δ*osm1* yeasts grown anaerobically. This observation may be explained by cyt *c* substituting for Osm1 in yeast absent for Osm1 or the presence of another electron acceptor that has not been identified. Also, cytosolic Frds1 may functionally replace Osm1 as described by (Camarasa et al., 2007); however, it is not known whether the mitochondria are able to shuttle FAD/FADH2 to the cytosol. Additional experiments are needed to explain the observation of no defect in strains lacking Osm1. Thus, there may be alternative oxidizing sources associated with the oxidative folding pathway.

It is unclear if similar terminal electron acceptors exist in higher eukaryotes. To date, no fumarate reductases have been identified in higher eukaryotes. The closest homology to Osm1

has been identified in trypanosomes. Mammals may not need anaerobic electron acceptors since cells are hardly anaerobic; however, it is known that low oxygen levels exist in certain tissues of mammals. Also, there are certain cases in which embryonic stem cells and tumor cells are surrounded by a hypoxic microenvironment (Thomson et al., 1998). It will be interesting to determine the minimum level of oxygen needed to carry out oxidative folding of proteins. Interestingly, a recent study showed that human cancer cells undergo a reverse in complex II activity and exhibit fumarate respiration(Sakai et al., 2011). It is plausible that cells in hypoxic conditions are able to perform fumarate respiration, just like Osm1 in yeast. Moreover, GSSH/GSH may potentially be the driving force for the oxidative folding of the IMS import pathway in higher eukaryotes. Higher eukaryotes most likely developed a backup system to ensure the continuation of inserting disulfide bonds.

Conclusion

We are just beginning to dissect and identify a range of terminal electrons that exist in the disulfide bond formation pathways mentioned above. Proper folding of proteins via disulfide bonds is essential for all organisms. In addition, terminal electron acceptors ensure the continuation of the oxidative folding pathways. Thus, identifying these oxidizing sources will help us understand their contribution to disulfide formation.

Figures

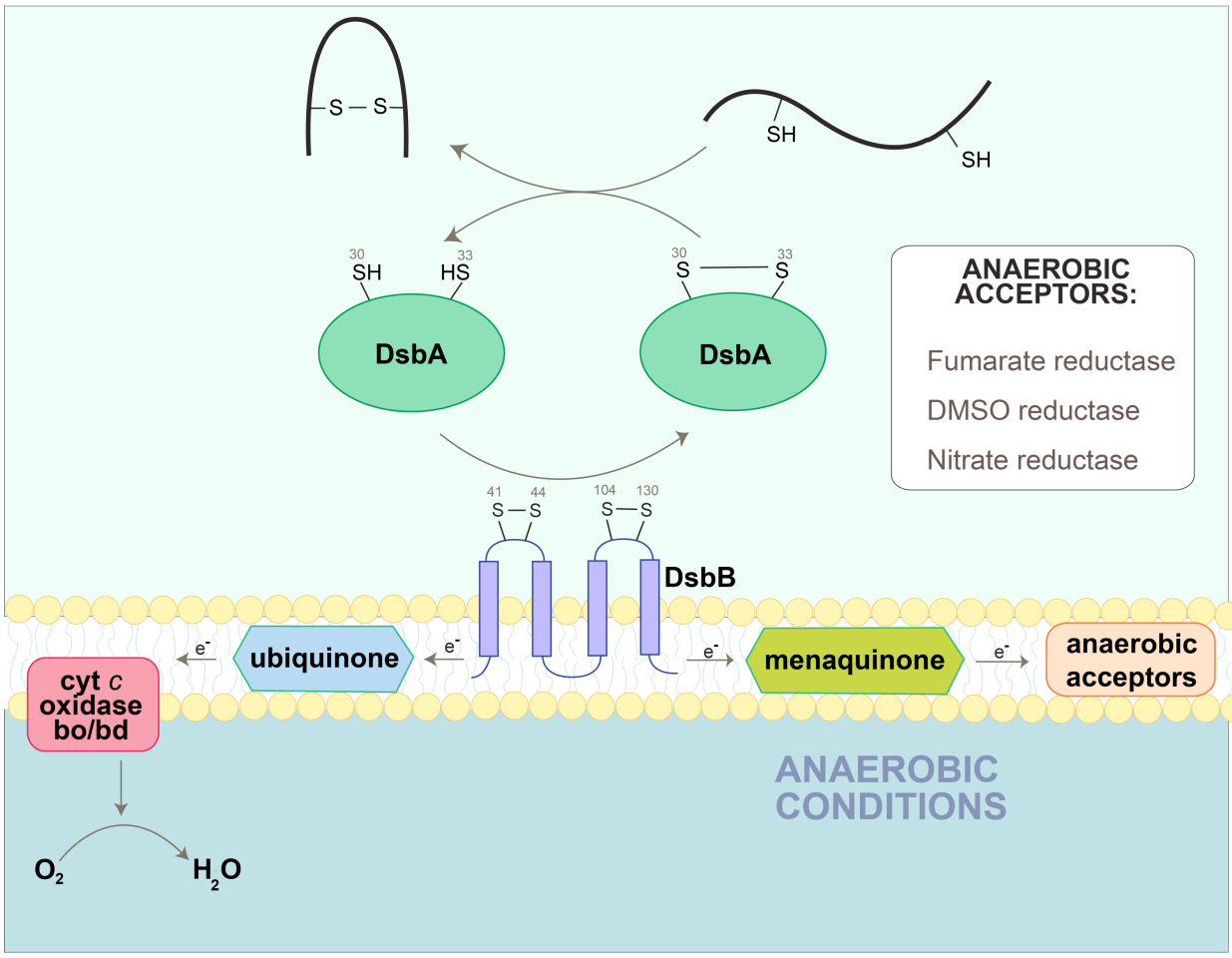

Figure 1. **Disulfide bond formation in bacterial periplasm.** Proteins synthesized in the cytoplasm are secreted into the periplasm as unfolded polypeptides. Disulfide bonds are then introduced by DsbA, which is recycled by the inner membrane protein DsbB. Finally, e- are shuttled from DsbB to cyt c oxidase bo/bd via ubiquinone in aerobic conditions or to the various anaerobic acceptors via menaquinone in anaerobic conditions.

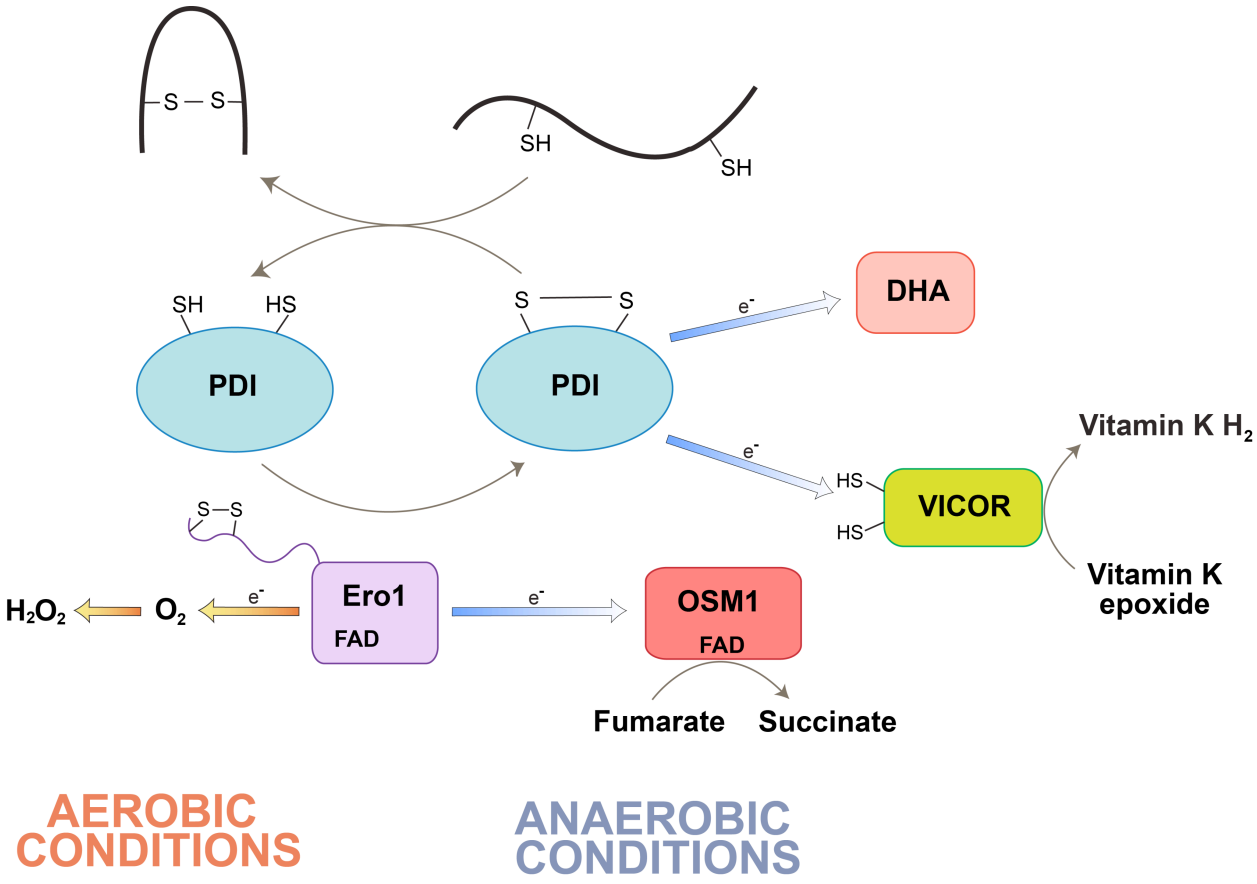

Figure 2. **The Pdi-Ero1 pathway of the ER.** In the ER, disulfide bonds are introduced by PDI. PDI subsequently shuttle electrons to the flavoprotein Ero1, which transfers the e- to molecular oxygen, generating hydrogen peroxide or to Osm1 to convert fumarate into succinate. In an alternative pathway, PDI is also able to pass electrons to DHA (Dehydroascorbic acid; oxidized form of ascorbic acid) or to VICOR(Vitamin K epoxide reductase) to convert Vitamin K epoxide to Vitamin K.

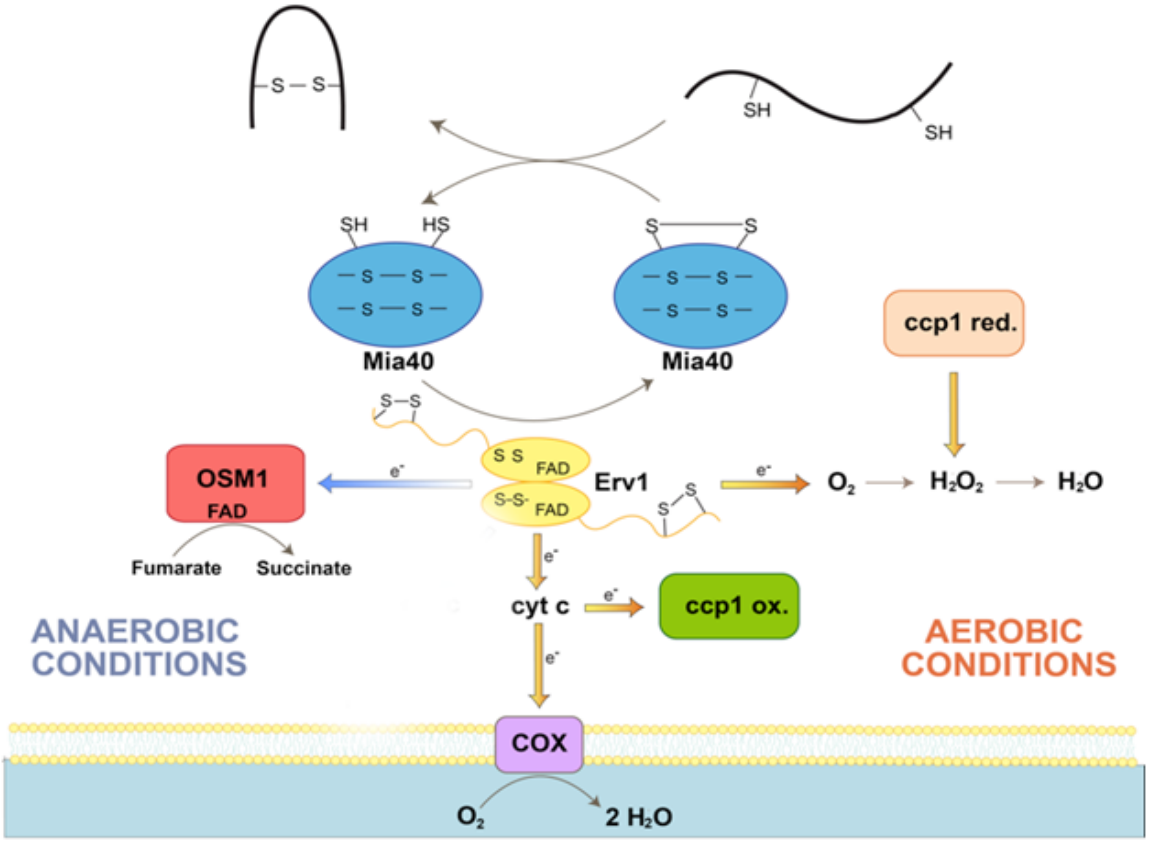

Figure 3. **The Mia40-Erv1 pathway in the mitochondrial IMS.** Proteins targeted to the intermembrane space of mitochondria have their disulfide bonds formed by Mia40. Mia40 is regenerated by the dimeric flavoenzyme Erv1. e- is subsequently transferred directly to O_2 to produce H_2O_2, to Cyt c which can be shuttled to cytochrome c oxidase of the electron transport chain or to Ccp1. In addition, Erv1 can shuttle electrons to Osm1 to convert fumarate to succinate.

References

Allen, S., V. Balabanidou, D.P. Sideris, T. Lisowsky, and K. Tokatlidis. 2005. Erv1 mediates the Mia40-dependent protein import pathway and provides a functional link to the respiratory chain by shuttling electrons to cytochrome c. *Journal of molecular biology*. 353:937-44.

Arikawa, Y., K. Enomoto, H. Muratsubaki, and M. Okazaki. 1998. Soluble fumarate reductase isoenzymes from Saccharomyces cerevisiae are required for anaerobic growth. *FEMS microbiology letters*. 165:111-6.

Bader, M., W. Muse, D.P. Ballou, C. Gassner, and J.C. Bardwell. 1999. Oxidative protein folding is driven by the electron transport system. *Cell*. 98:217-27.

Banci, L., I. Bertini, C. Cefaro, S. Ciofi-Baffoni, A. Gallo, M. Martinelli, D.P. Sideris, N. Katrakili, and K. Tokatlidis. 2009. MIA40 is an oxidoreductase that catalyzes oxidative protein folding in mitochondria. *Nature structural & molecular biology*. 16:198-206.

Bardwell, J.C. a. 2002. Disulfide bond formation, a race between FAD and oxygen. *Developmental cell*. 3:758-60.

Bardwell, J.C., K. McGovern, and J. Beckwith. 1991. Identification of a protein required for disulfide bond formation in vivo. *Cell*. 67:581-9.

Bardwell, J.C.A. 1994. MicroReview Building bridges : disulphide bond formation in the cell. 14.

Bauer, M.F., S. Hofmann, and W. Neupert. 2002. Import of mitochondrial proteins. *International review of neurobiology*. 53:57-90.

Bien, M., S. Longen, N. Wagener, I. Chwalla, J.M. Herrmann, and J. Riemer. 2010. Mitochondrial disulfide bond formation is driven by intersubunit electron transfer in Erv1 and proofread by glutathione. *Molecular cell*. 37:516-28.

Bihlmaier, K., N. Mesecke, N. Terziyska, M. Bien, K. Hell, and J.M. Herrmann. 2007. The disulfide relay system of mitochondria is connected to the respiratory chain. *The Journal of cell biology*. 179:389-95.

Cabibbo, a, M. Pagani, M. Fabbri, M. Rocchi, M.R. Farmery, N.J. Bulleid, and R. Sitia. 2000. ERO1-L, a human protein that favors disulfide bond formation in the endoplasmic reticulum. *The Journal of biological chemistry*. 275:4827-33.

Camarasa, C., V. Faucet, and S. Dequin. 2007. Role in anaerobiosis of the isoenzymes for Saccharomyces cerevisiae fumarate reductase encoded by OSM1 and FRDS1. *Yeast*. 391-401.

Chacinska, A., and P. Rehling. 2004. Moving proteins from the cytosol into mitochondria. *Biochemical Society transactions*. 32:774-6.

Collet, J.-francois, and J.C.A. Bardwell. 2002. MicroReview Oxidative protein folding in bacteria. *Molecular Microbiology*. 44:1-8.

Dabir, D.V., E.P. Leverich, S.-K. Kim, F.D. Tsai, M. Hirasawa, D.B. Knaff, and C.M. Koehler. 2007. A role for cytochrome c and cytochrome c peroxidase in electron shuttling from Erv1. *The EMBO journal*. 26:4801-11.

Dailey, F.E., and H.C. Berg. 1993. Mutants in disulfide bond formation that disrupt flagellar assembly in Escherichia coli. *Proceedings of the National Academy of Sciences of the United States of America*. 90:1043-7.

Darby, N.J., J. Kemmink, and T.E. Creighton. 1996. Identifying and characterizing a structural domain of protein disulfide isomerase. *Biochemistry*. 35:10517-28.

Depuydt, M., J. Messens, and J.-F. Collet. 2011. How proteins form disulfide bonds. *Antioxidants & redox signaling*. 15:49-66.

Dutton, R.J., D. Boyd, M. Berkmen, and J. Beckwith. 2008. Bacterial species exhibit diversity in their mechanisms and capacity for protein disulfide bond formation. *Proceedings of the National Academy of Sciences of the United States of America*. 105:11933-8.

Edman, J.C., L. Ellis, R.W. Blacher, R.A. Roth, and W.J. Rutter. Sequence of protein disulphide isomerase and implications of its relationship to thioredoxin. *Nature*. 317:267-70.

Farrell, S.R., and C. Thorpe. 2005. Augmenter of liver regeneration: a flavin-dependent sulfhydryl oxidase with cytochrome c reductase activity. *Biochemistry*. 44:1532-41.

Feige, M.J., and L.M. Hendershot. 2011. Disulfide bonds in ER protein folding and homeostasis. *Current opinion in cell biology*. 23:167-75.

Frand, a R., and C. a Kaiser. 1999. Ero1p oxidizes protein disulfide isomerase in a pathway for disulfide bond formation in the endoplasmic reticulum. *Molecular cell*. 4:469-77.

Gennaris, A., and J. Collet. Oxidative Protein Folding.

Gross, E., D.B. Kastner, C. a Kaiser, and D. Fass. 2004. Structure of Ero1p, source of disulfide bonds for oxidative protein folding in the cell. *Cell*. 117:601-10.

Gross, E., C.S. Sevier, N. Heldman, E. Vitu, M. Bentzur, C. a Kaiser, C. Thorpe, and D. Fass. 2006. Generating disulfides enzymatically: reaction products and electron acceptors of the endoplasmic reticulum thiol oxidase Ero1p. *Proceedings of the National Academy of Sciences of the United States of America*. 103:299-304.

Grumbt, B., V. Stroobant, N. Terziyska, L. Israel, and K. Hell. 2007. Functional characterization of Mia40p, the central component of the disulfide relay system of the mitochondrial intermembrane space. *The Journal of biological chemistry*. 282:37461-70.

Guddat, L.W., J.C. Bardwell, T. Zander, and J.L. Martin. 1997. The uncharged surface features surrounding the active site of Escherichia coli DsbA are conserved and are implicated in peptide binding. *Protein science : a publication of the Protein Society*. 6:1148-56.

Hatahet, F., and L.W. Ruddock. 2009. Protein disulfide isomerase: a critical evaluation of its function in disulfide bond formation. *Antioxidants & redox signaling*. 11:2807-50.

Hawkins, H.C., and R.B. Freedman. 1991. The reactivities and ionization properties of the active-site dithiol groups of mammalian protein disulphide-isomerase. *The Biochemical journal*. 275 (Pt 2:335-9.

Heras, B., M. Kurz, S.R. Shouldice, and J.L. Martin. 2007. The name's bond.....disulfide bond. *Current opinion in structural biology*. 17:691-8.

Inaba, K. 2009. Disulfide bond formation system in Escherichia coli. *Journal of biochemistry*. 146:591-7.

Inaba, K., S. Murakami, A. Nakagawa, H. Iida, M. Kinjo, K. Ito, and M. Suzuki. 2009. Dynamic nature of disulphide bond formation catalysts revealed by crystal structures of DsbB. *The EMBO journal*. 28:779-91.

Inaba, K., S. Murakami, M. Suzuki, A. Nakagawa, E. Yamashita, K. Okada, and K. Ito. 2006. Crystal structure of the DsbB-DsbA complex reveals a mechanism of disulfide bond generation. *Cell*. 127:789-801.

Inaba, K., and K. Araki. 2011. Structure, mechanism and evolution of Ero1 family enzymes. *Antioxidants & redox signaling*. 16.

Ingledew, W.J., and R.K. Poole. 1984. The respiratory chains of Escherichia coli. *Microbiological reviews*. 48:222-71.

Ito, K., and K. Inaba. 2008a. The disulfide bond formation (Dsb) system. *Current opinion in structural biology*. 18:450-8.

Ito, K., and K. Inaba. 2008b. The disulfide bond formation (Dsb) system. *Current opinion in structural biology*. 18:450-8.

Kadokura, H. 2002. Four cysteines of the membrane protein DsbB act in concert to oxidize its substrate DsbA. *The EMBO Journal*. 21:2354-2363.

Kadokura, H., M. Bader, H. Tian, J.C. Bardwell, and J. Beckwith. 2000. Roles of a conserved arginine residue of DsbB in linking protein disulfide-bond-formation pathway to the respiratory chain of Escherichia coli. *Proceedings of the National Academy of Sciences of the United States of America*. 97:10884-9.

Kadokura, H., F. Katzen, and J. Beckwith. 2003a. Protein disulfide bond formation in prokaryotes. *Annual review of biochemistry*. 72:111-35.

Kadokura, H., F. Katzen, and J. Beckwith. 2003b. Protein disulfide bond formation in prokaryotes. *Annual review of biochemistry*. 72:111-35.

Kamitani, S., Y. Akiyama, and K. Ito. 1992. Identification and characterization of an Escherichia coli gene required for the formation of correctly folded alkaline phosphatase, a periplasmic enzyme. *The EMBO journal*. 11:57-62.

Karala, A.-R., A.-K. Lappi, and L.W. Ruddock. 2010. Modulation of an active-site cysteine pKa allows PDI to act as a catalyst of both disulfide bond formation and isomerization. *Journal of molecular biology*. 396:883-92.

Kobayashi, T., S. Kishigami, M. Sone, H. Inokuchi, T. Mogi, and K. Ito. 1997a. Respiratory chain is required to maintain oxidized states of the DsbA-DsbB disulfide bond formation system in aerobically growing Escherichia coli cells. *Proceedings of the National Academy of Sciences of the United States of America*. 94:11857-62.

Kobayashi, T., S. Kishigami, M. Sone, H. Inokuchi, T. Mogi, and K. Ito. 1997b. Respiratory chain is required to maintain oxidized states of the DsbA-DsbB disulfide bond formation

system in aerobically growing Escherichia coli cells. *Proceedings of the National Academy of Sciences of the United States of America*. 94:11857-62.

Kobayashi, T., Y. Takahashi, and K. Ito. 2001. Identification of a segment of DsbB essential for its respiration-coupled oxidation. *Molecular microbiology*. 39:158-65.

Koehler, C.M. 2004. New developments in mitochondrial assembly. *Annual review of cell and developmental biology*. 20:309-35.

Koehler, C.M., and H.L. Tienson. 2009. Redox regulation of protein folding in the mitochondrial intermembrane space. *Biochimica et biophysica acta*. 1793:139-45.

Kulp, M.S., E.-M. Frickel, L. Ellgaard, and J.S. Weissman. 2006. Domain architecture of protein-disulfide isomerase facilitates its dual role as an oxidase and an isomerase in Ero1p-mediated disulfide formation. *The Journal of biological chemistry*. 281:876-84.

Lambert, N., and R.B. Freedman. 1985. The latency of rat liver microsomal protein disulphide-isomerase. *The Biochemical journal*. 228:635-45.

Lisowsky, T. 1992. Dual function of a new nuclear gene for oxidative phosphorylation and vegetative growth in yeast. *Molecular & general genetics : MGG*. 232:58-64.

Margittai, E., M. Csala, J. Mandl, and G. Bánhegyi. 2009. Participation of low molecular weight electron carriers in oxidative protein folding. *International journal of molecular sciences*. 10:1346-59.

McCutcheon, J.P., and N.A. Moran. 2012. Extreme genome reduction in symbiotic bacteria. *Nature reviews. Microbiology*. 10:13-26.

Mesecke, N., N. Terziyska, C. Kozany, F. Baumann, W. Neupert, K. Hell, and J.M. Herrmann. 2005. A disulfide relay system in the intermembrane space of mitochondria that mediates protein import. *Cell*. 121:1059-69.

Muratsubaki, H., and K. Enomoto. 1998. One of the fumarate reductase isoenzymes from Saccharomyces cerevisiae is encoded by the OSM1 gene. *Archives of biochemistry and biophysics*. 352:175-81.

Nardai, G., L. Braun, M. Csala, V. Mile, P. Csermely, a Benedetti, J. Mandl, and G. Banhegyi. 2001. Protein-disulfide isomerase- and protein thiol-dependent dehydroascorbate reduction and ascorbate accumulation in the lumen of the endoplasmic reticulum. *The Journal of biological chemistry*. 276:8825-8.

Nelson, J.W., and T.E. Creighton. 1994. Reactivity and ionization of the active site cysteine residues of DsbA, a protein required for disulfide bond formation in vivo. *Biochemistry*. 33:5974-83.

Pagani, M., M. Fabbri, C. Benedetti, a Fassio, S. Pilati, N.J. Bulleid, a Cabibbo, and R. Sitia. 2000. Endoplasmic reticulum oxidoreductin 1-lbeta (ERO1-Lbeta), a human gene induced in the course of the unfolded protein response. *The Journal of biological chemistry*. 275:23685-92.

Pfanner, N., and N. Wiedemann. 2002. Mitochondrial protein import: two membranes, three translocases. *Current opinion in cell biology*. 14:400-11.

Rissler, M., N. Wiedemann, S. Pfannschmidt, K. Gabriel, B. Guiard, N. Pfanner, and A. Chacinska. 2005. The essential mitochondrial protein Erv1 cooperates with Mia40 in biogenesis of intermembrane space proteins. *Journal of molecular biology*. 353:485-92.

Sakai, C., E. Tomitsuka, H. Esumi, S. Harada, and K. Kita. 2011. Mitochondrial fumarate reductase as a target of chemotherapy: From parasites to cancer cells. *Biochimica et biophysica acta*.

Service, H. 1963. Acceleration of Reactivation of Reduced Ribonuclease by a Microsomal System Bovine Pancreatic from Rat Liver. *System*. 238.

Sideris, D.P., N. Petrakis, N. Katrakili, D. Mikropoulou, A. Gallo, S. Ciofi-Baffoni, L. Banci, I. Bertini, and K. Tokatlidis. 2009. A novel intermembrane space-targeting signal docks cysteines onto Mia40 during mitochondrial oxidative folding. *The Journal of cell biology*. 187:1007-22.

Sideris, D.P., and K. Tokatlidis. 2010. Oxidative protein folding in the mitochondrial intermembrane space. *Antioxidants & redox signaling*. 13:1189-204.

Szarka, A., K. Stadler, V. Jenei, E. Margittai, M. Csala, J. Jakus, J. Mandl, and G. Bánhegyi. 2002. Ascorbyl free radical and dehydroascorbate formation in rat liver endoplasmic reticulum. *Journal of bioenergetics and biomembranes*. 34:317-23.

Thomson, J.A., J. Itskovitz-Eldor, S.S. Shapiro, M.A. Waknitz, J.J. Swiergiel, V.S. Marshall, and J.M. Jones. 1998. Embryonic stem cell lines derived from human blastocysts. *Science (New York, N.Y.)*. 282:1145-7.

Tian, G., S. Xiang, R. Noiva, W.J. Lennarz, and H. Schindelin. 2006. The Crystal Structure of Yeast Protein Disulfide Isomerase Suggests Cooperativity between Its Active Sites. *Cell*. 61-73.

Tokatlidis, K. 2005. A disulfide relay system in mitochondria. *Cell*. 121:965-7.

Tu, B.P. 2000. Biochemical Basis of Oxidative Protein Folding in the Endoplasmic Reticulum. *Science*. 290:1571-1574.

Tu, B.P., and J.S. Weissman. 2002. The FAD- and O(2)-dependent reaction cycle of Ero1-mediated oxidative protein folding in the endoplasmic reticulum. *Molecular cell*. 10:983-94.

Tu, B.P., and J.S. Weissman. 2004. Oxidative protein folding in eukaryotes: mechanisms and consequences. *The Journal of cell biology*. 164:341-6.

Unden, G., and J. Bongaerts. 1997. Alternative respiratory pathways of Escherichia coli: energetics and transcriptional regulation in response to electron acceptors. *Biochimica et biophysica acta*. 1320:217-34.

Universio, A.N. 1977. 461 (1977) 84-100 Elsevier/North-Holland Biomedical Press. *Measurement*. 461:84-100.

Venetianer, P., and F.B. Straub. 1963. The enzymic reactivation of reduced ribonuclease. *Biochimica et biophysica acta*. 67:166-8.

Wajih, N., S.M. Hutson, and R. Wallin. 2007. Disulfide-dependent protein folding is linked to operation of the vitamin K cycle in the endoplasmic reticulum. A protein disulfide

isomerase-VKORC1 redox enzyme complex appears to be responsible for vitamin K1 2,3-epoxide reduction. *The Journal of biological chemistry*. 282:2626-35.

Wunderlich, M., A. Otto, K. Maskos, M. Mücke, R. Seckler, and R. Glockshuber. 1995. Efficient catalysis of disulfide formation during protein folding with a single active-site cysteine. *Journal of molecular biology*. 247:28-33.

Zito, E., E.P. Melo, Y. Yang, Å. Wahlander, T. a Neubert, and D. Ron. 2010. Oxidative protein folding by an endoplasmic reticulum-localized peroxiredoxin. *Molecular cell*. 40:787-97.

Chapter 1: Reconstitution of the Mia40-Erv1 Oxidative Folding Pathway for the Small Tim Proteins

Molecular Biology of the Cell
Vol. 20, 3481–3490, August 1, 2009

Reconstitution of the Mia40-Erv1 Oxidative Folding Pathway for the Small Tim Proteins

Heather L. Tienson,* Deepa V. Dabir,* Sonya E. Neal,† Rachel Loo,†‡ Samuel A. Hasson,* Pinmanee Boontheung,* Sung-Kun Kim,§ Joseph A. Loo,*†‡‖¶ and Carla M. Koehler*†‖

*Department of Chemistry and Biochemistry, †Molecular Biology Institute, ‖Jonsson Comprehensive Cancer Center, and ¶Department of Biological Chemistry, ‡David Geffen School of Medicine, UCLA, Los Angeles, CA 90095; and §Department of Chemistry and Biochemistry, Baylor University, Waco, TX 76798

Submitted October 23, 2008; Revised May 8, 2009; Accepted May 20, 2009
Monitoring Editor: Thomas D. Fox

Mia40 and Erv1 execute a disulfide relay to import the small Tim proteins into the mitochondrial intermembrane space. Here, we have reconstituted the oxidative folding pathway in vitro with Tim13 as a substrate and determined the midpoint potentials of Mia40 and Tim13. Specifically, Mia40 served as a direct oxidant of Tim13, and Erv1 was required to reoxidize Mia40. During oxidation, four electrons were transferred from Tim13 with the insertion of two disulfide bonds in succession. The extent of Tim13 oxidation was directly dependent on Mia40 concentration and independent of Erv1 concentration. Characterization of the midpoint potentials showed that electrons flowed from Tim13 with a more negative midpoint potential of −310 mV via Mia40 with an intermediate midpoint potential of −290 mV to the C130-C133 pair of Erv1 with a positive midpoint potential of −150 mV. Intermediary complexes between Tim13-Mia40 and Mia40-Erv1 were trapped. Last, mutating C133 of the catalytic C130-C133 pair or C30 of the shuttle C30-C33 pair in Erv1 abolished oxidation of Tim13, whereas mutating the cysteines in the redox-active CPC motif, but not the structural disulfide linkages of the CX_9C motif of Mia40, prevented Tim13 oxidation. Thus, we demonstrate that Mia40, Erv1, and oxygen are the minimal machinery for Tim13 oxidation.

INTRODUCTION

To import proteins from the cytosol, the mitochondrion contains translocons of the outer membrane (TOM) and inner membrane (TIM). Proteins with a typical N-terminal targeting sequence are imported via the TIM23 pathway, whereas polytopic inner membrane proteins use the TIM22 import pathway (Milenkovic *et al.*, 2007; Neupert and Herrmann, 2007). In contrast, proteins imported into the intermembrane space use a variety of import pathways (Herrmann and Hell, 2005). Notably, a class of proteins that have conserved cysteine motifs, including the small Tim proteins with the twin CX_3C motif and proteins with a twin CX_9C motif, such as Cox17 and Cox19, use Mia40 and Erv1 (Chacinska *et al.*, 2004; Allen *et al.*, 2005; Mesecke *et al.*, 2005; Rissler *et al.*, 2005). The Mia40-Erv1 pathway represents the oxidative folding pathway of the intermembrane space (Koehler *et al.*, 2006; Herrmann and Kohl, 2007; Hell, 2008; Stojanovski *et al.*, 2008).

This article was published online ahead of print in *MBC in Press* (http://www.molbiolcell.org/cgi/doi/10.1091/mbc.E08–10–1062) on May 28, 2009.

Address correspondence to: Carla Koehler (koehler@chem.ucla.edu).

Abbreviations used: AMS, 4-acetamido-4-maleimidylstilbene-2,2-disulfonic acid; CD, circular dichroism; E_m, midpoint potential; IAA, iodoacetamide; Mal-PEG, maleimide-PEG-2K; mBBr, monobromobimane; TIM, translocase of inner membrane; TOM, translocase of inner membrane.

Substrates of the oxidative folding pathway consist of a subset of intermembrane space residents that contain disulfide bonds. These include the small Tim proteins Tim8, Tim9, Tim10, Tim12, and Tim13 that form juxtapositional disulfide bonds (Curran *et al.*, 2002; Allen *et al.*, 2003; Webb *et al.*, 2006). A large set of CX_9C proteins, including Mia40, Cox17, Cox19, and several of uncharacterized function, also possess thiol bonds (Nobrega *et al.*, 2002; Arnesano *et al.*, 2005; Gabriel *et al.*, 2007; Banci *et al.*, 2008; Hell, 2008). In addition, the proteins Sco1 and Sco2, which mediate cytochrome oxidase assembly, contain disulfide linkages in a single CX_3C motif (Williams *et al.*, 2005; Banci *et al.*, 2007). The machinery responsible for mediating the oxidative folding of these substrates consists of the receptor Mia40 and the sulfhydryl oxidase Erv1 (Tokatlidis, 2005; Hell, 2008; Stojanovski *et al.*, 2008). Electrons are shuttled from Erv1 to a variety of electron acceptors, including oxygen and cytochrome *c* (Bihlmaier *et al.*, 2007; Dabir *et al.*, 2007). Thus, the mitochondrial intermembrane space supports the assembly of disulfide bonds in proteins like the bacterial periplasm and the endoplasmic reticulum.

Mia40 acts as a receptor for the import of these cysteine-rich proteins and forms a transient disulfide bond with the substrate (Chacinska *et al.*, 2004; Mesecke *et al.*, 2005; Terziyska *et al.*, 2005; Grumbt *et al.*, 2007). Mia40 contains three disulfide bonds. Specifically, two disulfide bonds are formed by cysteines in the twin CX_9C motif, which may function in a structural role; the third disulfide bond is formed by the CPC motif near the N terminus, which participates in the thiol exchange reaction (Grumbt *et al.*, 2007). After binding, the substrate is released from Mia40 in a folded state, and the sulfhydryl oxidase Erv1 reoxidizes

Mia40 (Allen *et al.*, 2005; Mesecke *et al.*, 2005; Rissler *et al.*, 2005).

Erv1 has three redox-active centers (Coppock and Thorpe, 2006; Dabir *et al.*, 2007). There are two pairs of redox-active cysteines at C30-C33 and C130-C133 that are separated by two amino acids (CX_2C motif). The C130-C133 is located near the active site flavin and transfers electrons to FAD, whereas the C30-C33 pair, referred to as the "shuttle" disulfide motif for its role in mediating electron transfer from substrates to the active site, is located distal to the active site (Fass, 2008). Electrons are transferred from the substrate through the C30-C33 pair to C130-C133 and then to FAD (Fass, 2008). Subsequently, electrons from Erv1 are transferred via the flavin to a combination of electron acceptors that function synergistically (Farrell and Thorpe, 2005; Bihlmaier *et al.*, 2007; Dabir *et al.*, 2007). Erv1 forms a complex with cytochrome *c* (cyt *c*) and thus can transfer electrons directly to cyt *c* (Bihlmaier *et al.*, 2007; Dabir *et al.*, 2007). From cyt *c*, electrons are donated to the electron transport chain or to cytochrome *c* peroxidase (Ccp1) (Dabir *et al.*, 2007). In addition, molecular oxygen accepts electrons from Erv1 to generate H_2O_2, which is in turn converted to water by Ccp1 (Farrell and Thorpe, 2005; Dabir *et al.*, 2007). This oxidative folding pathway is therefore versatile at donating electrons to several terminal electron acceptors like the oxidative folding pathways in the bacterial periplasm (Bader *et al.*, 1999).

That electrons can flow from a substrate to oxygen suggests that the midpoint potentials (E_m) of the individual components are arranged from more negative to more positive values. The E_m of a subset of the components has been determined. Specifically, the E_m of substrates Tim9, Tim10, and Cox17 are −310, −320, and −340 mV, respectively (Lu and Woodburn, 2005; Voronova *et al.*, 2007; Morgan and Lu, 2008). For the sulfhydryl oxidase Erv1, the E_m for the active site C130-C133 pair, the shuttle C30-C33 pair, and the FAD are −150, −320, and −215 mV, respectively (Dabir *et al.*, 2007). Electron acceptors cyt *c* and oxygen have an E_m of +250 and +820 mV, respectively (Wallace, 1984).

Portions of this pathway have been reconstituted in vitro. For example, using the nonphysiological substrate dithiothreitol (DTT), electron transfer through Erv1 to oxygen and cyt *c* has been reconstituted (Farrell and Thorpe, 2005; Bihlmaier *et al.*, 2007; Dabir *et al.*, 2007). In addition, the transfer of disulfide bonds from Erv1 to Mia40 has been demonstrated previously (Grumbt *et al.*, 2007). Here, we report in vitro reconstitution of the entire pathway from reduced Tim13 via Mia40 and Erv1 to oxygen with the subsequent generation of oxidized Tim13 and H_2O_2. The E_m values of these components are generally aligned from more negative to more positive, supporting that this pathway is thermodynamically favorable for electron transfer. Thus, the oxidative folding of Tim13 can be modeled in vitro.

MATERIALS AND METHODS

Plasmids and Strains

Recombinant Erv1 was expressed and purified under native conditions as described previously (Dabir *et al.*, 2007). The C-terminal region of Mia40 starting at amino acid 251 was amplified by PCR (primer pair 5′-GGAATTCTTAAGGTTTGGATTCCTC-3′ and 5′-CGGGATCCCGCTAAGCAATCTGAATCT-3′) from yeast stain GA74 and cloned into pET28a with an N-terminal 6xHIS-tag by using BamHI and EcoRI restriction sites. Mia40 was purified under native conditions using a similar protocol to that of Erv1 purification (Dabir *et al.*, 2007). Cysteine point mutants of Mia40 and Erv1 were generated by site-directed mutagenesis using overlap extension and confirmed by nucleotide sequencing (Ho *et al.*, 1989). Recombinant Tim13 was purified under denaturing conditions as described previously (Beverly *et al.*, 2008) and was dialyzed into 20 mM Tris, pH 7.0, 150 mM KCl, and 1 mM EDTA. Proteins Tim13, Mia40, and Erv1 were detected with polyclonal antibodies and immunoblot analysis.

Table 1. Midpoint potential measurements of Mia40

Method	Status	Midpoint potential (mV)
mBBr titration	Anaerobic	−277 ± 7.5
mBBr titration	Aerobic	−322 ± 2.5
Intrinsic tryptophan fluorescence	Anaerobic	−289 ± 2.5
Intrinsic tryptophan fluorescence	Aerobic	−289 ± 4.8

Redox Titrations

Redox titrations of disulfide/dithiol redox couples were performed as described previously (Krimm *et al.*, 1998; Masuda *et al.*, 2002; Dabir *et al.*, 2007) by using either thiol labeling with monobromobimane (mBBr) or intrinsic tryptophan fluorescence. Redox equilibration was achieved in redox buffers consisting of defined mixtures of either reduced and oxidized dithiothreitol (DTT/DTT_{ox}) or glutathione (GSH/GSSG). DTT/DTT_{ox} was used for ambient redox potential (E_h) values from −230 to −400 mV, and GSH/GSSG for values more positive than −230 mV (Hirasawa *et al.*, 2000).

More specifically, 100 μg of Tim13 was equilibrated in buffer containing 0.1 M HEPES, pH 7.0, and a DTT/DTT_{ox} ratio (total concentration of 2.0 or 5.0 mM) to generate ambient redox potentials of −240 to −400 mV. The samples were incubated for 2 h under aerobic conditions before incubation with mBBr for 30 min at 25°C. The protein was then precipitated by the addition of 10% trichloroacetic acid (TCA) and resuspended in 0.1 M Tris, pH 8.0, and 0.1% SDS. The fluorescence of the sample was measured on a Quant Master QM-4 spectrofluorometer from Photon Technology International (Lawrenceville, NJ), with an excitation wavelength of 380 nm and emission monitored at 475 nm.

Redox equilibrations for all Mia40 titrations were performed in the same manner. Thirty micrograms of Mia40 was equilibrated for 2 or 4 h in 0.1 M HEPES, pH 7.0, containing DTT or glutathione redox couples at a total concentration of 2.0 or 5.0 mM, generating ambient redox potentials of −100 to −400 mV under both aerobic and anaerobic conditions. E_m values for Mia40 were independent of the redox equilibrium time and the total DTT or total GSH concentrations present in the redox equilibrium buffer (Setterdahl *et al.*, 2003). Measurement of the midpoint potential using mBBr was performed as for Tim13 described above. To monitor the changes in the intrinsic tryptophan fluorescence after redox equilibration the fluorescence of the protein at 280 nm was immediately monitored by the spectrofluorimeter. For Mia40, differing results were obtained under ambient oxygen concentrations or under nitrogen atmosphere in the glove box, so the midpoint potential was based on the most reproducible method, which was intrinsic tryptophan fluorescence (Table 1). All E_m values reported represent the average from at least three replicate titrations. The experimental errors in E_m values estimated from the average deviations are all less than the inherent experimental uncertainties in redox titrations of approximately ±10 mV.

The raw data were normalized such that the fluorescent measurement at the most reducing redox potential was assigned a value of 100% reduced, and the fluorescent measurement at the most oxidizing redox potential was assigned a value of 0% reduced. A theoretical curve calculated from the Nernst equation at the respective reduction potentials was fit to the titration data for Mia40 and Tim13. The Mia40 data gave an excellent fit for a two-electron transfer, whereas the curve fit to the Tim13 data was solved for a four-electron transition. For titration of Tim13, curves for n = 2 (R^2 = 0.9644) and n = 4 (R^2 = 0.9923) electrons were included. The probability was higher (99.99%) that the data fit a curve for n = 4 electrons than n = 2 electrons (0.01%) as calculated using the informational theory approach Akaike's criterion using Prism (GraphPad Software, San Diego, CA; Akaike, 1974). If the difference in likelihood was not very large (i.e., 40 vs. 60%), either curve could have been likely.

Thiol Trapping Studies

For Tim13 samples after circular dichroism (CD) analysis, 1 μg of protein was modified by 20 mM maleimide-polyethylene glycol (PEG) 2K (Mal-PEG) (Figure 1C); addition of Mal-PEG increases the molecular mass by 5 kDa (Wu *et al.*, 2000). Samples were resolved on 15% SDS gels and visualized by SYPRO Ruby stain using an FX ProPlus imager (Bio-Rad Laboratories, Hercules, CA).

Mia40 was incubated in different redox buffers for 2 h at the indicated redox potentials (Figure 2C). Subsequently, Mia40 was precipitated using 10% TCA and then resuspended in sample buffer containing 20 mM 4-acetamido-4-maleimidylstilbene-2,2-disulfonic acid (AMS). The samples were resolved on

a 6–16% Tris-Tricine gel under nonreducing conditions followed by SYPRO Ruby staining.

Reconstitution Studies and Analysis of Trapped Mixed Disulfides

For the reconstitution assays, Tim13 was reduced in the presence of 5 mM DTT for 2 h. The DTT was removed by gel filtration using an NAP5 column, and Tim13 was eluted in 20 mM Tris-HCl, pH 7.0, 150 mM KCl, and 1 mM EDTA. In the reconstitution experiments, 15 μM reduced Tim13 was incubated with 0.5 μM Mia40 and/or Erv1, Erv1C133S, or Erv1C30S as indicated, for 4 h at 25°C in 20 mM Tris-HCl, pH 7.0, 150 mM KCl, and 1 mM EDTA. Concentrations of Mia40 and Erv1 and the length of incubation were varied per experiment as indicated. The redox state of Mia40 and Tim13 were determined by thiol trapping with AMS. For Tim13, 1 μg of sample was incubated with 20 mM AMS for 1 h at 37°C and then resolved by nonreducing SDS-polyacrylamide gel electrophoresis (PAGE). Tim13 was detected by immunoblot analysis. Quantitation was performed on a VersaDoc Imaging System model 5000 (Bio-Rad Laboratories) using Quantity One software (Bio-Rad Laboratories) and expressed as the fraction of monomeric Tim13 that is oxidized.

To detect the presence of mixed disulfide, 10 μM Mia40, Erv1, and reduced Tim13 were incubated at 30°C for 10 min. The reaction was halted by addition of 50 mM iodoacetimide (IAA). The proteins were then resolved on reducing and nonreducing SDS gels and detected by immunoblot analysis. As a control, similar amounts of each protein alone also were resolved on the same gel.

Analysis of Hydrogen Peroxide Levels

H_2O_2 levels in the reconstitution assays were measured using the Amplex Red Hydrogen Peroxide/Peroxidase Assay kit according to the manufacturer's protocol (Dabir *et al.*, 2007; Invitrogen, Carlsbad, CA). In brief, Erv1 and Mia40 were mixed at the indicated concentrations with the Amplex Red/horseradish peroxidase reaction mix. The reaction was initiated by the addition of reduced Tim13. The Erv1-catalyzed reduction of O_2 to H_2O_2 was measured by a FlexStation plate reader (Molecular Devices, Sunnyvale, CA) controlled via the SoftMax Pro software package (Molecular Devices) for data acquisition. Statistical analysis was performed using Prism software (GraphPad Software). The reaction was performed at a shorter time period than the reconstitution assays because the Amplex Red assay was very sensitive. Some background activity was detected in the assay, perhaps due to low levels of reductant from Tim13 purification. Therefore, we used the Amplex Red assay to verify that hydrogen peroxide was being produced in proportion to the oxidation of Tim13.

CD Studies

The redox equilibrations were performed in 20 mM Tris, pH 7.0, 150 mM KCl, and 1 mM EDTA. Tim13 (0.2 mg/ml) was equilibrated under anaerobic conditions for 20 h at the indicated redox potentials (Figure 1). The secondary structure content of recombinant proteins was detected using circular dichroism on a J-715 spectropolarimeter (Jasco, Tokyo, Japan) at 25°C. Each sample was analyzed with a scan speed of 50 nm/min, a bandwidth of 1.0 nm, and a wavelength interval of 0.5 nm. Four scans were averaged for each spectrum. The baseline correction option was used to subtract a buffer baseline. Spectra were recorded from 260 to 200 nm in a 1-mm pathlength cell, with protein concentrations of 0.1–0.2 mg/ml. Spectra were analyzed for secondary structure content by using a self-consistent method, the convex constraint algorithm for secondary structure prediction (Perczel *et al.*, 1992; Sreerama and Woody, 1993; Greenfield, 2006), or both. For the folding studies in Figure 1A, control spectra in which Tim13 was reduced by incubation in 2 mM DTT, oxidized by incubation in 2 mM oxidized DTT, and untreated controls were included. Samples were equilibrated for 20 h. The change in the CD spectra at 208 nm was used to calculate the fraction of Tim13 reduced using the following equation:

$$\textit{Fraction reduced} = \frac{(\theta_{ox} - \theta_{exp})}{(\theta_{ox} - \theta_{red})}$$

where θ_{ox} is the molar ellipticity of the oxidized sample, θ_{red} is the molar ellipticity of the reduced sample, and θ_{exp} is the molar ellipticity of the experimental sample that is being calculated for each redox potential. We could not fit the Nernst equation to these data because it is an indirect measurement of electron transfer and a direct measure of changes in secondary structure content. Instead, nonlinear regression analysis was performed using Prism software (GraphPad Software). The midpoint from the generated curve is reported as the reduction potential for Tim13, which agrees with the midpoint potential calculated from mBBr redox titrations.

RESULTS

Tim13 Has a Midpoint Potential of −310 mV

Dissection of the specific steps in import of cysteine-rich proteins into the mitochondrial intermembrane space is difficult because Mia40 and Erv1 are essential proteins and mutations in key cysteine residues lead to inviability. However, mechanistic studies in the endoplasmic reticulum and bacterial periplasm have been completed by reconstitution experiments with excess amounts of substrate and catalytic amounts of oxidative folding components (Bader *et al.*, 1998; Tu *et al.*, 2000). With a similar goal of in vitro reconstitution of the oxidative folding pathway in the mitochondrion, the midpoint potentials of the individual components that were not characterized previously were determined. We measured the E_m of Tim13 at equilibrium over a range of redox potentials by using mBBr titration (Dabir *et al.*, 2007), CD studies (Curran *et al.*, 2002), and thiol trapping (Curran *et al.*, 2002; Dabir *et al.*, 2007) in both anaerobic and aerobic conditions. Recombinant Tim13 was equilibrated in DTT/DTT_{ox} redox buffers to poise samples at E_h values ranging from −240 to −380 mV (Hirasawa *et al.*, 1999; Dabir *et al.*, 2007) and then incubated with mBBr to form a thiol-specific fluorescent covalent adduct (Dabir *et al.*, 2007). The titration results were independent of the equilibration time and the anaerobic/aerobic state, indicating the likelihood of good redox equilibration between Tim13 and the ambient potential imposed by the redox buffers. The titration results were fit to curves for a two-electron and four-electron couple calculated from the Nernst equation. The titration gave an excellent fit to the Nernst equation for a four-electron redox couple and not a two-electron redox couple, suggesting that the two disulfide bonds formed simultaneously. A midpoint potential of −315 mV was calculated (Supplemental Figure S1).

When Tim13 was subject to CD studies, the recombinant protein displayed secondary structure content with α-helical properties (Figure 1A), as reported previously (Curran *et al.*, 2002; Beverly *et al.*, 2008). In the presence of oxidant (oxidized DTT), the secondary structure content of Tim13 was similar to that displayed by the untreated protein. When Tim13 was reduced by DTT treatment, the structure sustained conformational changes. This suggested that CD analysis could be used to determine the specific E_m for Tim13. The critical midpoint potential was −310 mV; in reduction potentials more negative than −310 mV, Tim13 showed secondary structural content similar to Tim13 in the presence of oxidant; and in reduction potentials more positive than −310 mV, Tim13 showed secondary structural content similar to Tim13 in the presence of reductant (Figure 1A). The changes in CD spectra were used to calculate the fraction of Tim13 that was reduced. A nonlinear regression analysis on the resulting curve confirmed that the transition point was −310 mV (Figure 1B). Last, thiol-trapping with Mal-PEG was performed to confirm that the cysteine residues transitioned at this midpoint from a reduced to disulfide bonded state (Figure 1C). The addition of Mal-PEG to free cysteine residues increases the molecule weight by 5 kDa (Makmura *et al.*, 2001). Tim13 was equilibrated at the indicated redox potentials and treated with Mal-PEG, followed by separation on nonreducing SDS-PAGE and detection with SYPRO Ruby staining. Indeed, at redox potentials more negative than −310 mV, approximately four Mal-PEG additions (designated Tim13-MP4) were detected, whereas at redox potentials more positive than −310 mV, the number of Mal-PEG additions decreased markedly to zero (Figure 1C). Together, Tim13 has one midpoint potential of −310 mV and four electrons were removed simultaneously in these equilibrium titration assays.

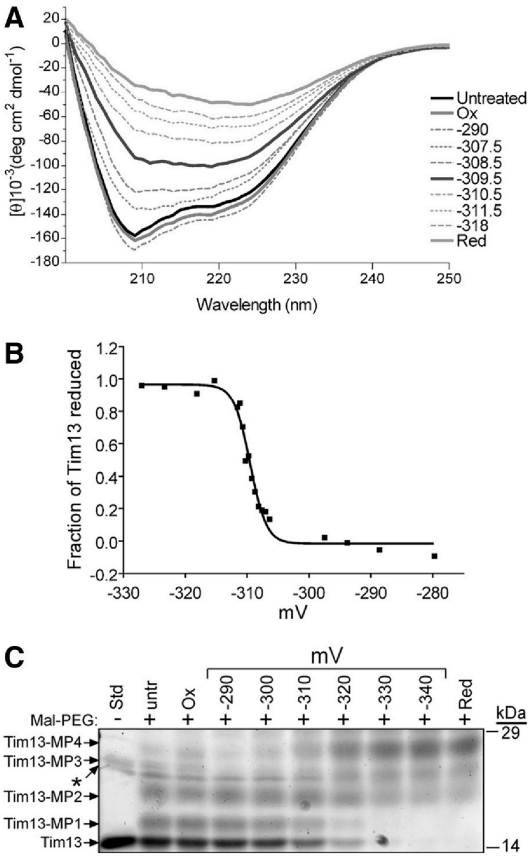

Figure 1. The midpoint potential of Tim13 is −310 mV. The redox titration of the Tim13 dithiol/disulfide couple was performed in a DTT redox buffer at pH 7.0 under anaerobic conditions with a 20-h equilibration time. (A) The secondary structure of each sample was monitored by CD analysis at the indicated redox potentials. Control spectra for untreated, oxidized (Ox), and reduced (Red) Tim13 were included. (B) The fraction of reduced Tim13 in each sample from A was calculated from the differences in the CD spectra at 208 nm and plotted versus the midpoint potential of the sample. Data in all titrations were analyzed using nonlinear curve regression analysis, which yielded a sigmoidal curve. (C) Tim13 samples were incubated at the indicated redox potentials for 20 h followed by addition of Mal-PEG, analyzed by nonreducing SDS-PAGE, and detected by SYPRO Ruby staining. Up to four Mal-PEG equivalents attached to the four cysteine residues in Tim13, which is indicated by Tim13-MP1 through Tim13-MP4 (n = 5).

Mia40 Has a Midpoint Potential of Approximately −290 mV

We also determined the E_m of Mia40 using mBBr titration and intrinsic tryptophan fluorescence titration under aerobic and anaerobic conditions. Mia40 has two CX_9C motifs that assemble in structural disulfide bonds and one CPC motif that is seemingly redox active (Grumbt *et al.*, 2007). With titration using mBBr or intrinsic tryptophan fluorescence in anaerobic or aerobic conditions, the analysis showed the presence of a single two-electron component (Figure 2, A and B). The average values for the E_m were −277 and −289 mV for mBBr and intrinsic tryptophan fluorescence, respectively, as calculated by the Nernst equation. In contrast, when the E_m was calculated in aerobic conditions, values of −322 and −289 mV were measured using titration methods with mBBr and intrinsic tryptophan fluorescence, respectively (Supplemental Figure S2). To confirm the redox potential titrations, the thiol status at the indicated redox potentials was monitored with the use of AMS, each AMS modification increases the molecular mass by 0.5 kDa) (Figure 2C). Mia40-AMS adducts were separated by nonreducing SDS-PAGE followed by detection with SYPRO Ruby staining. In control reactions, two AMS molecules were added when Mia40 was incubated in the presence of 20 mM DTT and six AMS molecules were added in the presence of 20 mM DTT and incubation at 95°C. Thus, full addition of AMS to the six cysteines was achieved only when the protein was completely unfolded by thermal denaturation (Grumbt *et al.*, 2007). When Mia40 was incubated at redox potentials more reducing than −260 mV, two AMS equivalents were added; AMS addition was not detected at redox potentials more positive than −260 mV. Thus, the sum of several methods specify that the E_m of Mia40 is approximately −290 mV (Table 1), placing it between that of Tim13 and the C130-C133 pair in the active site of Erv1. And of the six cysteine residues in Mia40, only two seem to be redox active.

The Combination of Erv1 and Mia40 Mediates Tim13 Oxidation In Vitro

To reconstitute the oxidative folding pathway with the minimal components, we expressed recombinant Erv1 and mutants C30S and C133S and characterized their sulfhydryl oxidase activity with the nonphysiologic substrate DTT (Supplemental Figure S3). Erv1 and the mutants C30S and C133S showed the same secondary structure content when analyzed by circular dichroism (Supplemental Figure S4). To generate a kinetic profile for Erv1 and C30S Erv1 mutant, both enzymes (1 μM) were incubated with DTT ranging from 0 to 400 μM. Enzymatic activity was measured using an Amplex Red substrate that is converted to fluorescently active resorufin in the presence of H_2O_2 (Dabir *et al.*, 2007). The negative control for the H_2O_2 production assay was the enzymatically inactive C133S Erv1 mutant (1 μM) (Hofhaus *et al.*, 2003). The velocity of H_2O_2 that was produced by the C133S Erv1 mutant was essentially zero, confirming that the mutation inactivates the enzyme. Erv1 and the C30S Erv1 mutant displayed a V_{max} value of 1.18 and 0.68 pmol/s, respectively. In addition, the turnover numbers of 65 and 38 for Erv1 and the C30S Erv1 mutant were on par with the reported turnover numbers of 53 and 17 for Erv1 and the C30S Erv1 mutant (Hofhaus *et al.*, 2003). Thus, the C30S Erv1 mutant showed some redox activity, indicating that the active site C130-C133 pair can partially oxidize the small substrate DTT and bypass the C30-C33 pair. Importantly, the recombinant Erv1 is an active sulfhydryl oxidase.

We reconstituted the oxidation of Tim13 by incubating 15 μM reduced Tim13 with 0.5 μM Mia40 and 0.5 μM Erv1 in an aerobic environment (Figure 3, A and B). At these concentrations, the substrate Tim13 is in excess and Mia40 and Erv1 are in catalytic concentrations, similar to systems reconstituted in the endoplasmic reticulum (Tu *et al.*, 2000). Oxidation was monitored over a 4-h time course by the addition of AMS followed by nonreducing SDS-PAGE and immunoblot analysis with anti-Tim13; the absence of AMS addition indicated that Tim13 was oxidized. Tim13 was first reduced by treatment with DTT followed by gel filtration to remove the reductant. In a set of control reactions, AMS addition to the four cysteine residues of Tim13 occurred only after pretreatment of Tim13 with reductant (Figure 3A, lanes 1–4), confirming that the Tim13 thiols were reduced at the start of the assay. When Tim13 was incubated for 4 h

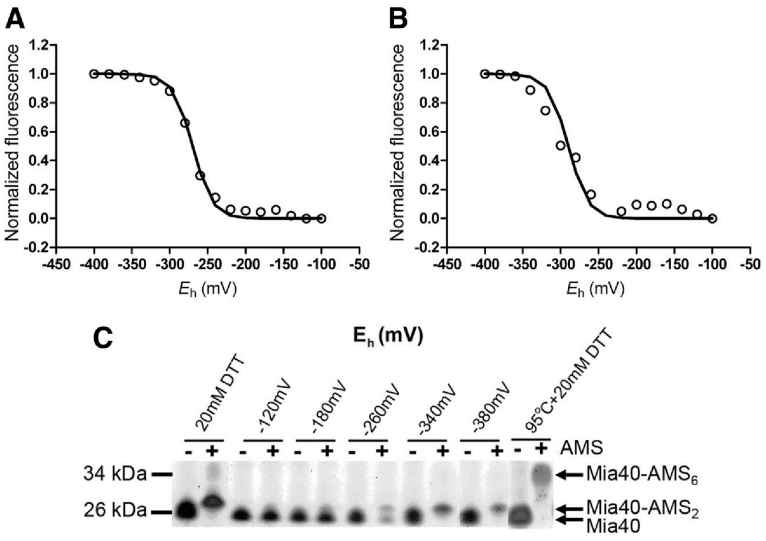

Figure 2. The midpoint potential of Mia40 is approximately −290 mV. Redox titration of the dithiol/disulfide couple of Mia40 was performed in a DTT or glutathione redox buffer. Equilibration was achieved at 2 h at pH 7.0 under anaerobic conditions. Data in all titrations were fit to the Nernst equation for a two-electron carrier. (A) Redox titrations were performed with mBBr. The best fit to the mBBr fluorescence magnitude versus E_h value was obtained with an E_m of −277 mV (n = 3). (B) Redox titrations were performed as in A and intrinsic tryptophan fluorescence was used to monitor the redox state of Mia40. The best fit to the data were for a single n = 2 component with E_m = −289 mV (n = 3). (C) Mia40 samples were incubated in aerobic conditions at the indicated redox (E_h) values. Samples were treated with AMS, which adds a molecular mass of 0.5 kDa. As controls, reduced (20 mM DTT) and reduced-denatured (95°C + 20 mM DTT) samples were included, demonstrating the addition of two and six equivalents of AMS, respectively (n = 3).

alone or in the presence of Mia40 or Erv1, minor amounts of Tim13 were oxidized because AMS added to the majority of the Tim13 pool (Figure 3A, lanes 5–7, and B). This confirms that Tim13 did not oxidize spontaneously during the assay nor did Mia40 or Erv1 alone result in substantial oxidation of Tim13. However, when incubated with Erv1 and Mia40 together, Tim13 was oxidized as shown by the decreased AMS addition to the Tim13 pool over time (Figure 3A, lanes 8–11, and B). The amount of oxidized Tim13 was determined by quantitation using densitometry and the fraction of oxidized Tim13 (unmodified by AMS) was expressed as the percentage of total Tim13 (Figure 3B). Specifically, oxidized Tim13 was detected within 30 min after addition of both Mia40 and Erv1; and the fraction of oxidized Tim13 increased with the incubation time. Interestingly, an intermediate state with two AMS additions was not detected, indicating that all four cysteines were oxidized at once in this assay. Importantly, active Erv1 was required, because mutation of the shuttle (C30S) or active site (C133S) cysteine pair impaired Tim13 oxidation (Figure 3A, lanes 12–19). Therefore, the combination of both Erv1 and Mia40 is required for Tim13 oxidation.

As Tim13 was oxidized, H_2O_2 was produced concomitantly with oxygen consumption by Erv1. We measured H_2O_2 production using the fluorometric assay (Figure 3C) (Dabir *et al.*, 2007). As predicted, H_2O_2 production was minimal when Tim13 was incubated alone or in the presence of Mia40. The combination of Mia40 and Erv1 in the absence of Tim13 also led to negligible H_2O_2 production. Only when Tim13 was oxidized in the presence of both Mia40 and Erv1 did H_2O_2 production increase by 400%. Although the combination of Tim13 and Erv1 resulted in an increase in H_2O_2 production, oxidation of Tim13 was not detected by thiol-trapping (Figure 3A, lane 7). Finally, active Erv1 was required because the reactions with Erv1 mutants C30S and C133S produced negligible amounts of H_2O_2. Thus, the Amplex Red fluorometric assay is a reliable method to monitor the flow of electrons from Tim13 through Erv1.

We also measured the oxidation state of Mia40 in the reconstitution assay (Figure 3D). In the control reaction, Mia40 was oxidized at the start of the reaction (Figure 3D, lanes 1 and 2) and remained oxidized after incubating for 2 h (Figure 3D, lane 3), because AMS addition was not detected. When Mia40 was incubated with Erv1 (Figure 3D, lanes 4–7), Mia40 remained oxidized. However, Mia40 became reduced when incubated with reduced Tim13 alone (Figure 3D, lanes 8–11), as indicated by the addition of two AMS molecules. The addition of Erv1 to the combination of Tim13 and Mia40 resulted in reoxidation of Mia40 (Figure 3D, lanes 12–15). Thus, Mia40 oxidizes Tim13 directly and then Erv1 functions to reoxidize Mia40, completing the disulfide relay system.

To test the requirement for the key cysteine residues of Mia40 in Tim13 oxidation, we sequentially mutated the first and second cysteines of the CPC motif to serine, generating SPC and CPS mutants, and the first cysteine of the CX_9C motif, designated SX_9C. From CD studies, the SPC and CPS mutants were folded similar to wild-type (wt) Mia40 (Supplemental Figure S4). In contrast, the SX_9C mutant displayed less alpha-helical content than wt Mia40 as shown by the spectral differences at 222 nm (Supplemental Figure S4). These mutants were used in the oxidation assay as described in Figure 3A (Figure 4A). Whereas wt Mia40 in the presence of Erv1 oxidized Tim13, Mia40 mutants SPC and CPS in combination with Erv1 failed to oxidize Tim13. In contrast, the Mia40 mutant SX_9C with Erv1 oxidized Tim13 but less efficiently compared with wt Mia40. The amount of H_2O_2 produced was significantly higher ($p < 0.001$) for the combination of Mia40 and Erv1 than the combination of Erv1 and the Mia40 mutants (Figure 4B). The cysteine residues in the CPC motif site are therefore redox active and essential for Tim13 oxidation.

Dependence of Tim13 Oxidation on Mia40 Concentration

To pinpoint the dependence of the disulfide relay on Mia40 and Erv1, we tested whether Tim13 oxidation was dependent on Erv1 or Mia40 concentration. Specifically, the concentration of Tim13 (15 μM) and Erv1 (0.1 μM) was fixed, and the Mia40 concentration was varied over a range of 0–1 μM. The oxidation of Tim13 and the amount of H_2O_2 production was measured after a fixed period of time (Figure 5, A and B). As the concentration of Mia40 increased, the amount of Tim13 oxidation and of H_2O_2 production escalated. If the concentration of Erv1 was fixed in the assay at concentrations of 0.5 μM with varying Mia40 (0–1 μM), the oxidation curve for Tim13 was similar (data not shown). In

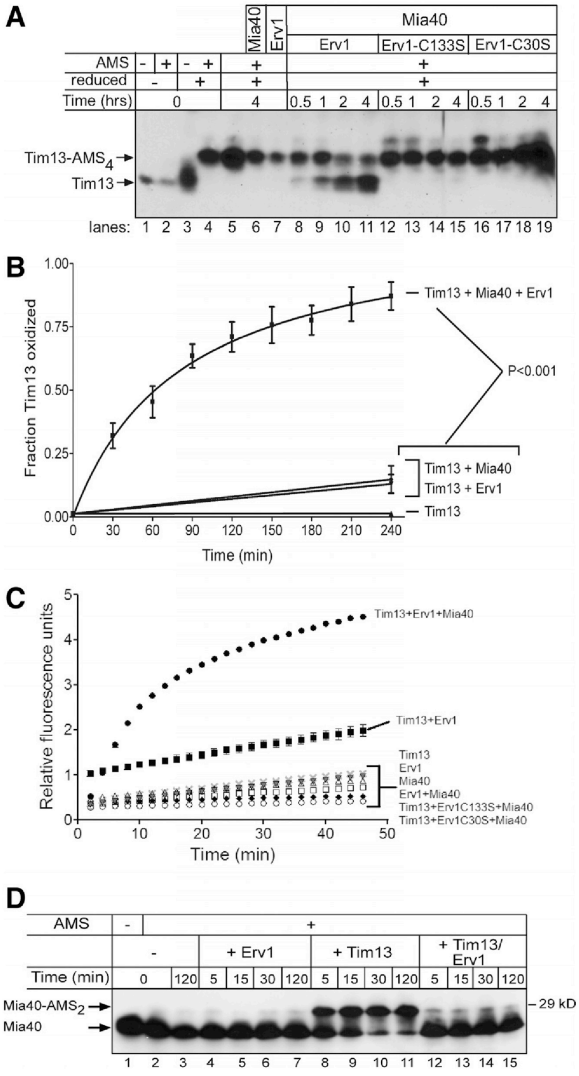

Figure 3. The combination of Mia40 and Erv1 directly oxidize Tim13 in vitro. (A) Reduced Tim13 (15 μM) was incubated with combinations of Mia40 (0.5 μM), Erv1 (0.5 μM), and mutant Erv1 (C133S or C30S, 0.5 μM) in a time course assay as indicated. Aliquots were removed at the indicated times and free thiols on Tim13 were blocked with AMS. Oxidized and reduced (Tim13-AMS_4) Tim13 were detected by nonreducing SDS-PAGE followed by immunoblotting with antibodies against Tim13. (B) The amount of oxidized Tim13 was quantitated using VersaDoc and associated Quantity One software (Bio-Rad Laboratories) ($p < 0.001$; n = 4). (C) H_2O_2 production was monitored over a 50-min time period during Tim13 oxidation. H_2O_2 production was detected with the indicator Amplex Red and displayed as relative fluorescence units (n = 3). (D) As in A, Mia40 was incubated with Erv1, reduced Tim13, and the combination of reduced Tim13 and Erv1. Aliquots were removed at 5, 15, 30, and 120 min, and the Mia40 oxidation state was monitored by thiol trapping with AMS and immunoblotting with an antibody against Mia40. Note that the addition of two AMS molecules was detected (Mia40-AMS_2; n = 3).

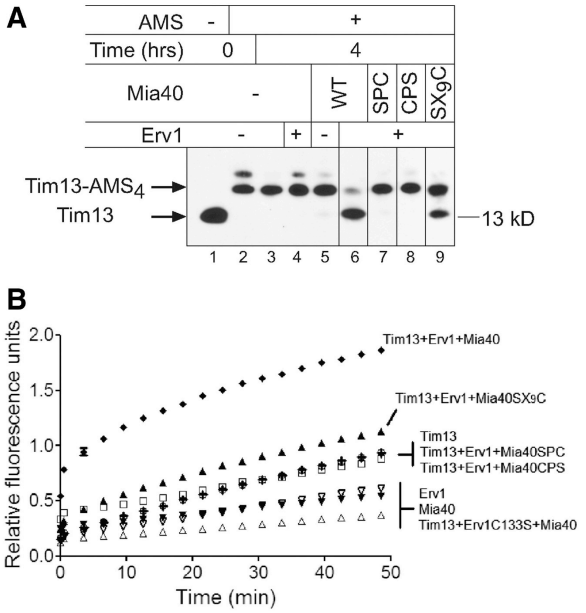

Figure 4. Mia40 is required for Tim13 oxidation in vitro. (A) As in Figure 3A, a time course of Tim13 oxidation was investigated at 4 h with Mia40 mutants (SPC, CPS, and SX_9C). (B) As in Figure 3C, H_2O_2 production was monitored over a 50-min time period during Tim13 oxidation.

reciprocal experiments in which Tim13 (15 μM) and Mia40 (1.0 μM) concentrations were fixed with varied Erv1 concentrations (0–1 μM), both the amount of Tim13 oxidized and H_2O_2 production remained constant (Figure 5, C and D). Based on the hypothesis of the disulfide relay, Mia40 seemingly oxidizes a small fraction of Tim13, presumably until Mia40 is completely reduced. Then, a catalytic amount of Erv1 subsequently reoxidizes Mia40 to allow further cycles of Tim13 oxidation. Therefore, the amount of Tim13 that becomes oxidized depends on the concentration of Mia40.

Tim13-Mia40 and Mia40-Erv1 Intermediates Are Formed during Tim13 Oxidation

Oxidation of Tim13 requires the generation of disulfide-bonded intermediates among Tim13, Mia40, and Erv1. To trap intermediates, equal concentrations of reduced Tim13 was incubated with Mia40 and Erv1, treated with IAA to block free thiols and subjected to nonreducing SDS-PAGE followed by immunoblotting for Tim13, Mia40, and Erv1 (Figure 6). As a control, the proteins were separated in the presence of β-mercaptoethanol (Figure 6A). A small fraction of the Tim13 formed multimers (indicated with the asterisk) that were not reduced by the presence of reductant. Mia40 and Erv1, however, were reduced and migrated as monomers.

In the absence of reductant, intermediates between Tim13-Mia40 and Mia40-Erv1 were detected by immunoblot analysis (Figure 6B). Again, nonspecific multimers of Tim13 (indicated by the asterisk) were formed. In addition, a dimer of Mia40 (indicated by ◆) and a dimer of Erv1 (indicated by ■) were identified. The intermediate between Mia40-Erv1 was difficult to detect because it migrates at a similar molecular mass as the Mia40 dimer, but given that the same band is detected with antibodies against Mia40 and Erv1 in the lanes where all three proteins were mixed, we interpret this as a Mia40-Erv1 intermediate. Neither a Tim13-Erv1 dimer nor a Tim13-Mia40-Erv1 trimer was identified. Together, this re-

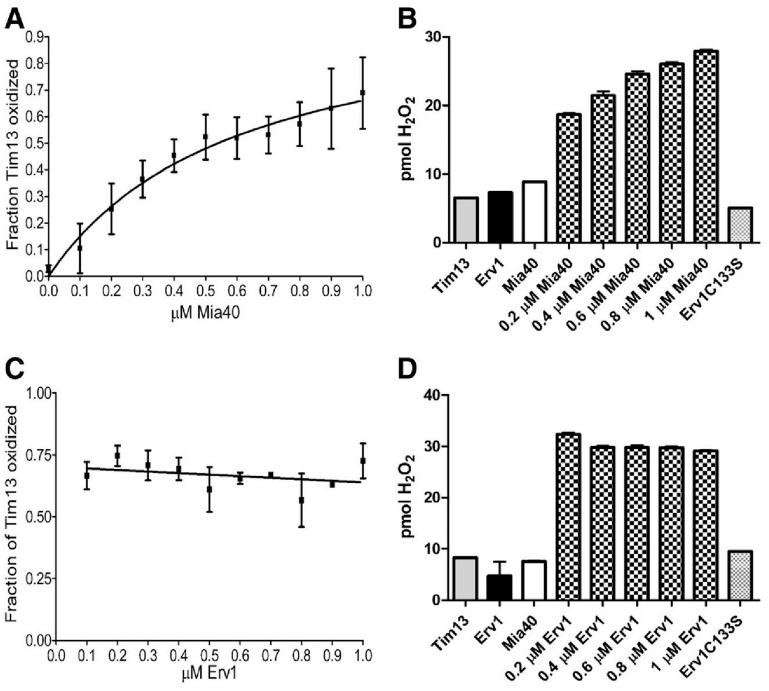

Figure 5. Tim13 oxidation is dependent on Mia40 concentration. (A) The oxidation of 15 μM Tim13 was monitored as described in Figure 3, A and B, after 90 min in the presence of 0.1 μM Erv1 and 0–1.0 μM Mia40. (B) H_2O_2 production was monitored as in Figure 3C, after 35 minutes, in the presence of 15 μM Tim13, 1.0 μM Erv1, and 0–1.0 μM Mia40. (C) Tim13 oxidation was monitored as described in Figure 3, A and B, after 90 min in the presence of 1.0 μM Mia40 and 0.1–1.0 μM Erv1. (D) H_2O_2 production of was monitored as in Figure 3C, after 35 minutes, in the presence of 15 μM Tim13, 1.0 μM Mia40, and 0.2–1.0 μM Erv1 (n = 3).

lay seems to consist of specific thiol linkages between Tim13-Mia40 and Mia40-Erv1.

DISCUSSION

The Midpoint Potentials of Tim13 and Mia40 Are Poised to Shuttle Electrons to Erv1

In this study, we present a detailed characterization of the redox behavior of Tim13 and Mia40, building on the previous study in which we examined the redox behavior of Erv1 (Dabir *et al.*, 2007). Thus, we have filled in the gaps in the E_m of the players of the disulfide relay and verified the direction of electron shuttling in this pathway. Like Tim9, Tim10, and Cox17 (Lu and Woodburn, 2005; Voronova *et al.*, 2007; Banci *et al.*, 2008; Morgan and Lu, 2008), the E_m of Tim13 is very reducing at −310 mV (Figure 7). Interestingly, the equilibrium analysis (Figure 1) shows the presence of one transition of four electrons, indicating that Tim13 is either reduced or oxidized at once. This phenomena is shared by other substrates of this pathway as well such as Tim10 and Cox17 (Voronova *et al.*, 2007; Banci *et al.*, 2008). The CD analysis supports that this transition is accompanied by a structural change of "less structured" in the reduced state to "more structured" in the oxidized state. Unexpectedly, no evidence of a two electron transition for Tim13 was detected in our reconstitution experiments. Because the redox-active CPC motif of Mia40 is poised to receive only two electrons, two molecules of Mia40 may simultaneously bind to the substrate Tim13 or a combination of both Erv1 and Mia40 may directly oxidize Tim13 simultaneously. Alternatively, molecular oxygen could remove the second set of electrons from Tim13, but this does not seem likely, particularly in an anaerobic environment. Future studies will be required to analyze the coordinated removal of four electrons from Tim13.

In contrast, the E_m of Mia40 was slightly more oxidizing at −290 mV. We used mBBr titration, intrinsic tryptophan fluorescence, and thiol trapping in anaerobic and aerobic conditions to investigate the redox status of Mia40. Although the measurements varied slightly (Table 1), the E_m determined under anaerobic conditions seemed consistent (Figure 2). Given that Mia40 has six cysteine residues, up to three different E_m were expected from the titration analysis. However, all methods consistently showed that only one inflection occurred that was accompanied by a two-electron transition when fit to the Nernst equation. This was specifically supported by the thiol trapping experiments with Mia40 (Figure 2C) in which two AMS molecules were added to Mia40 at potentials of −340 and −380 mV. Only when the protein was completely denatured by heat in the presence of reductant were six AMS molecules added. This suggests that the twin CX_9C motif likely serves a structural role and that the CPC motif is involved in redox chemistry (Grumbt *et al.*, 2007). It was interesting that the midpoint potential of human Mia40 was more oxidizing (−200 mV) (Banci *et al.*, 2009), which might reflect a difference between mammalian and yeast proteins. Alternatively, the differing midpoint potentials may reflect differences in experimental conditions, especially as our study suggests that the observed midpoint potential can vary depending on experimental approach. Similarly, the redox titrations by Banci *et al.* (2009) were conducted with the glutathione redox couple that is poised for redox titrations more oxidizing than −230 mV (Hirasawa *et al.*, 2000); midpoint potentials more reducing than −230 mV may not be measured as accurately with glutathione compared with DTT. Nevertheless, both studies place the midpoint potential of Mia40 between the substrates and Erv1.

From a previous study, we have determined the E_m of Erv1 (Dabir *et al.*, 2007). The C30-C33 pair has an E_m of −320 mV and functions to shuttle electrons to the active site

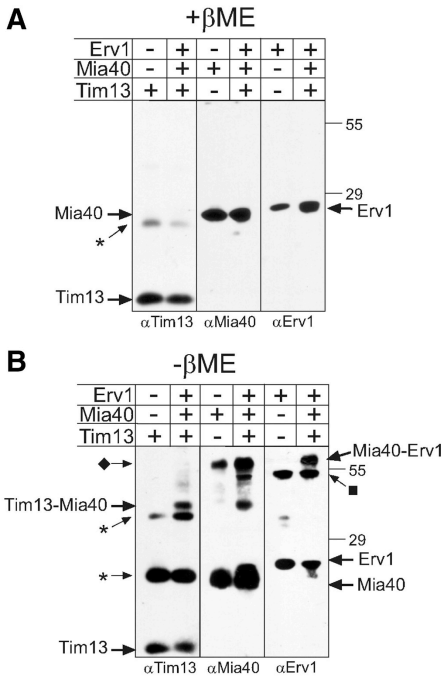

Figure 6. Mixed disulfides of Tim13-Mia40 and Mia40-Erv1 were detected in the presence of Tim13, Mia40, and Erv1. Equimolar amounts of recombinant Mia40, Erv1 and reduced Tim13 were incubated together for 10 min followed by treatment with IAA. The mix was separated on reducing (A) and nonreducing (B) SDS gels. Proteins were detected by immunoblotting with specific antibodies. As a control, a lane with the single protein is included. The asterisk denotes multimers of Tim13, the diamond marks a dimer of Mia40, and the square marks a dimer of Erv1.

C130-C133 pair (Fass, 2008). The C130-C133 pair has an E_m of −150 mV, whereas the FAD has a E_m of −215 mV. Electron acceptors of Erv1, oxygen and cyt *c*, have more oxidative E_m (Figure 7).

The E_m are roughly sorted from more reducing for substrates to more oxidizing for Erv1 and cyt *c*, suggesting that shuttling of electrons from substrates to terminal electron acceptors is thermodynamically favored. Obviously, the E_m of the C30-C33 pair of Erv1 suggests that it may be difficult to shuttle electrons from Mia40 (−290 mV) to the C30-C33 pair (−320 mV) and then to the active site cysteines (−150 mV) and FAD (−215 mV). However, the E_m measurements are determined at thermodynamic equilibrium, and the E_m of individual components within the context of the intermembrane space may vary, particularly in a kinetic scope when proteins are being imported and electrons are being transferred efficiently. Finally, the most positive E_m of cyt *c* and oxygen may serve as a sink to draw electrons. Indeed, a hydrophobic oxygen channel in the related Erv2 sulfhydryl oxidase of the ER facilitates electron shuttling (Vitu *et al.*, 2006).

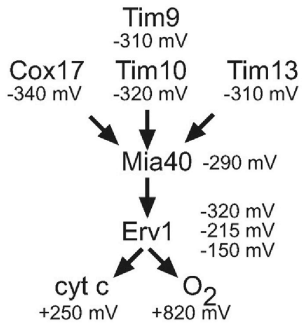

Figure 7. Schematic of electron flow during import of small Tim proteins in the mitochondrial intermembrane space. Electrons are transferred from substrates such as Tim10, Tim13, and Cox17 to Erv1 via Mia40. Electrons are then shuttled to cyt *c* and oxygen. See text for details.

Reconstitution of the Mia40-Erv1 Disulfide Relay

Although not as efficient as in organello import assays, the reconstitution assay with purified proteins allows us to investigate the details of this pathway and demonstrates clearly that catalytic amounts of Mia40 and Erv1 together are required to oxidize Tim13 efficiently. As shown in Figure 3D, Mia40 can directly oxidize Tim13, but Erv1 is needed to reoxidize Mia40. Our studies suggest that electrons flow from the substrate Tim13 through Mia40 to Erv1 and finally oxygen (Figure 7). To this end, intermediates between Tim13-Mia40 and Mia40-Erv1 were trapped, indicating that electrons likely flow through Mia40 to Erv1. Although Erv1 is seemingly not covalently bound to the Tim13-Mia40 intermediate, Erv1 dictates the redox state of Mia40 (Figure 3D). Also, the concentration of Mia40 determines the extent of Tim13 oxidation in the reconstitution assay. However, Erv1 is required for further rounds of import, because in its absence, Mia40 accumulates predominantly in the reduced form (Figure 3D) (Grumbt *et al.*, 2007).

The CPC pair of Mia40 and both CX_2C sites in Erv1 are critical for oxidation of Tim13. For Mia40, mutation of the first cysteine (SX_9C) in the Mia40 twin CX_9C motif slows, but does not abrogate, oxidation of Tim13. Because the SX_9C mutation impairs folding of Mia40, the structure of the Mia40 core seems important for mediating thiol exchange reactions. For Erv1, both CX_2C sites are essential for oxidation of Tim13, via recycling of Mia40, indicating that both sites are important in the disulfide relay. Based on the structure of Erv2, electrons most likely are shuttled through the distal C30-C33 pair to the active site C130-C133 and then the FAD (Fass, 2008). Even though the measured E_m do not favor such a flow of electrons, our studies confirm that electrons most likely follow this pathway.

This work shows the reconstitution of the Mia40-Erv1 oxidative folding pathway in the mitochondrial intermembrane space. We have addressed specifically how the electrons are shuttled from substrate through components in this redox pathway. The in vitro reconstitution system is a novel approach particularly because the studies with Erv1 and Mia40 cysteine mutants cannot be done in vivo because the mutants are not viable. Establishing this assay also provides a framework to probe additional questions. Specifically, Mia40 has been the only substrate identified for Erv1. Given that Erv1 also may function in FeS cluster (Lange *et al.*, 2001) and heme export (Dabir *et al.*, 2007), it may have other substrates. In addition, it is not apparent how four electrons are removed simultaneously from Tim13 to Mia40, because an intermediate in which two electrons were first removed was not identified. It may be that such an intermediate is short-lived or an alternative mechanism may be used to remove the second set of electrons, with potential candidates including a second molecule of Mia40, Erv1, or mo-

lecular oxygen. Additional studies, designed to elucidate these pathways in greater detail, will be required.

ACKNOWLEDGMENTS

Establishment and equipment in the UCLA Mass Spectrometry and Proteomics Technology Center were supplied by a generous gift from the W. M. Keck Foundation. We thank F. Tsai for technical assistance and K. Beverly and M. Phillips for helpful discussions. This work was supported by U.S. Public Health Service National Research Service Award grant GM-07185 (to H.L.T.), U.S. Public Health Service National Research Service Award grant GM-008296 (to S.A.H.), United Mitochondrial Disease Foundation (to D.V.D.), UCLA Cota-Robles Fellowship (to S.A.N.), National Institutes of Health grant R01-GM-061721 (to C.M.K.), Muscular Dystrophy Association grant 022398 (to C.M.K.), and the American Heart Association grant 0640076N (to C.M.K.). C.M.K. is an Established Investigator of the American Heart Association.

REFERENCES

Akaike. (1974). A new look at the statistical model identification. IEEE Trans. Automat. Control *19*, 716–723.

Allen, S., Balabanidou, V., Sideris, D. P., Lisowsky, T., and Tokatlidis, K. (2005). Erv1 mediates the Mia40-dependent protein import pathway and provides a functional link to the respiratory chain by shuttling electrons to cytochrome *c*. J. Mol. Biol. *353*, 937–944.

Allen, S., Lu, H., Thornton, D., and Tokatlidis, K. (2003). Juxtaposition of the two distal "CX3C" motifs via intrachain disulfide bonding is essential for the folding of Tim10. J. Biol. Chem. *278*, 38505–38513.

Arnesano, F., Balatri, E., Banci, L., Bertini, I., and Winge, D. R. (2005). Folding studies of Cox17 reveal an important interplay of cysteine oxidation and copper binding. Structure *13*, 713–722.

Bader, M., Muse, W., Ballou, D. P., Gassner, C., and Bardwell, J. C. (1999). Oxidative protein folding is driven by the electron transport system. Cell *98*, 217–227.

Bader, M., Muse, W., Zander, T., and Bardwell, J. (1998). Reconstitution of a protein disulfide catalytic system. J. Biol. Chem. *273*, 10302–10307.

Banci, L., Bertini, I., Cefaro, C., Ciofi-Baffoni, S., Gallo, A., Martinelli, M., Sideris, D. P., Katrakili, N., and Tokatlidis, K. (2009). MIA40 is an oxidoreductase that catalyzes oxidative protein folding in mitochondria. Nat. Struct. Mol. Biol. *16*, 198–206.

Banci, L., Bertini, I., Ciofi-Baffoni, S., Gerothanassis, I. P., Leontari, I., Martinelli, M., and Wang, S. (2007). A structural characterization of human SCO2. Structure *15*, 1132–1140.

Banci, L., Bertini, I., Ciofi-Baffoni, S., Janicka, A., Martinelli, M., Kozlowski, H., and Palumaa, P. (2008). A structural-dynamical characterization of human Cox17. J. Biol. Chem. *283*, 7912–7920.

Beverly, K. N., Sawaya, M. R., Schmid, E., and Koehler, C. M. (2008). The Tim8-Tim13 complex has multiple substrate binding sites and binds cooperatively to Tim23. J. Mol. Biol. *382*, 1144–1156.

Bihlmaier, K., Mesecke, N., Terziyska, N., Bien, M., Hell, K., and Herrmann, J. M. (2007). The disulfide relay system of mitochondria is connected to the respiratory chain. J. Cell Biol. *179*, 389–395.

Chacinska, A., Pfannschmidt, S., Wiedemann, N., Kozjak, V., Sanjuan Szklarz, L. K., Schulze-Specking, A., Truscott, K. N., Guiard, B., Meisinger, C., and Pfanner, N. (2004). Essential role of Mia40 in import and assembly of mitochondrial intermembrane space proteins. EMBO J. *23*, 3735–3746.

Coppock, D. L., and Thorpe, C. (2006). Multidomain flavin-dependent sulfhydryl oxidases. Antioxid. Redox. Signal. *8*, 300–311.

Curran, S. P., Leuenberger, D., Schmidt, E., and Koehler, C. M. (2002). The role of the Tim8p-Tim13p complex in a conserved import pathway for mitochondrial polytopic inner membrane proteins. J. Cell Biol. *158*, 1017–1027.

Dabir, D. V., Leverich, E. P., Kim, S. K., Tsai, F. D., Hirasawa, M., Knaff, D. B., and Koehler, C. M. (2007). A role for cytochrome c and cytochrome c peroxidase in electron shuttling from Erv1. EMBO J. *26*, 4801–4811.

Farrell, S. R., and Thorpe, C. (2005). Augmenter of liver regeneration: a flavin-dependent sulfhydryl oxidase with cytochrome c reductase activity. Biochemistry *44*, 1532–1541.

Fass, D. (2008). The Erv family of sulfhydryl oxidases. Biochim. Biophys. Acta *1783*, 557–566.

Gabriel, K., Milenkovic, D., Chacinska, A., Muller, J., Guiard, B., Pfanner, N., and Meisinger, C. (2007). Novel mitochondrial intermembrane space proteins as substrates of the MIA import pathway. J. Mol. Biol. *365*, 612–620.

Greenfield, N. J. (2006). Using circular dichroism collected as a function of temperature to determine the thermodynamics of protein unfolding and binding interactions. Nat. Protoc. *1*, 2527–2535.

Grumbt, B., Stroobant, V., Terziyska, N., Israel, L., and Hell, K. (2007). Functional characterization of Mia40p, the central component of the disulfide relay system of the mitochondrial intermembrane space. J. Biol. Chem. *282*, 37461–37470.

Hell, K. (2008). The Erv1-Mia40 disulfide relay system in the intermembrane space of mitochondria. Biochim. Biophys. Acta *1783*, 601–609.

Herrmann, J. M., and Hell, K. (2005). Chopped, trapped or tacked–protein translocation into the IMS of mitochondria. Trends Biochem. Sci. *30*, 205–211.

Herrmann, J. M., and Kohl, R. (2007). Catch me if you can! Oxidative protein trapping in the intermembrane space of mitochondria. J. Cell Biol. *176*, 559–563.

Hirasawa, M., Ruelland, E., Schepens, I., Issakidis-Bourguet, E., Miginiac-Maslow, M., and Knaff, D. B. (2000). Oxidation-reduction properties of the regulatory disulfides of sorghum chloroplast nicotinamide adenine dinucleotide phosphate-malate dehydrogenase. Biochemistry *39*, 3344–3350.

Hirasawa, M., Schurmann, P., Jacquot, J. P., Manieri, W., Jacquot, P., Keryer, E., Hartman, F. C., and Knaff, D. B. (1999). Oxidation-reduction properties of chloroplast thioredoxins, ferredoxin:thioredoxin reductase, and thioredoxin f-regulated enzymes. Biochemistry *38*, 5200–5205.

Ho, S. N., Hunt, H. D., Horton, R. M., Pullen, J. K., and Pease, L. R. (1989). Site-directed mutagenesis by overlap extension using the polymerase chain reaction. Gene *77*, 51–59.

Hofhaus, G., Lee, J. E., Tews, I., Rosenberg, B., and Lisowsky, T. (2003). The N-terminal cysteine pair of yeast sulfhydryl oxidase Erv1p is essential for in vivo activity and interacts with the primary redox centre. Eur. J. Biochem. *270*, 1528–1535.

Koehler, C. M., Beverly, K. N., and Leverich, E. P. (2006). Redox pathways of the mitochondrion. Antioxid. Redox. Signal. *8*, 813–822.

Krimm, I., Lemaire, S., Ruelland, E., Miginiac-Maslow, M., Jaquot, J. P., Hirasawa, M., Knaff, D. B., and Lancelin, J. M. (1998). The single mutation Trp35–>Ala in the 35–40 redox site of *Chlamydomonas reinhardtii* thioredoxin h affects its biochemical activity and the pH dependence of C36–C39 1H–13C NMR. Eur. J. Biochem. *255*, 185–195.

Lange, H., Lisowsky, T., Gerber, J., Muhlenhoff, U., Kispal, G., and Lill, R. (2001). An essential function of the mitochondrial sulfhydryl oxidase Erv1p/ALR in the maturation of cytosolic Fe/S proteins. EMBO Rep. *2*, 715–720.

Lu, H., and Woodburn, J. (2005). Zinc binding stabilizes mitochondrial Tim10 in a reduced and import-competent state kinetically. J. Mol. Biol. *353*, 897–910.

Makmura, L., Hamann, M., Areopagita, A., Furuta, S., Munoz, A., and Momand, J. (2001). Development of a sensitive assay to detect reversibly oxidized protein cysteine sulfhydryl groups. Antioxid. Redox. Signal. *3*, 1105–1118.

Masuda, S., Dong, C., Swem, D., Setterdahl, A. T., Knaff, D. B., and Bauer, C. E. (2002). Repression of photosynthesis gene expression by formation of a disulfide bond in CrtJ. Proc. Natl. Acad. Sci. USA *99*, 7078–7083.

Mesecke, N., Terziyska, N., Kozany, C., Baumann, F., Neupert, W., Hell, K., and Herrmann, J. M. (2005). A disulfide relay system in the intermembrane space of mitochondria that mediates protein import. Cell *121*, 1059–1069.

Milenkovic, D., Muller, J., Stojanovski, D., Pfanner, N., and Chacinska, A. (2007). Diverse mechanisms and machineries for import of mitochondrial proteins. Biol. Chem. *388*, 891–897.

Morgan, B., and Lu, H. (2008). Oxidative folding competes with mitochondrial import of the small Tim proteins. Biochem. J. *411*, 115–122.

Neupert, W., and Herrmann, J. M. (2007). Translocation of proteins into mitochondria. Annu. Rev. Biochem. *76*, 723–749.

Nobrega, M. P., Bandeira, S. C., Beers, J., and Tzagoloff, A. (2002). Characterization of COX19, a widely distributed gene required for expression of mitochondrial cytochrome oxidase. J. Biol. Chem. *277*, 40206–40211.

Perczel, A., Park, K., and Fasman, G. D. (1992). Analysis of the circular dichroism spectrum of proteins using the convex constraint algorithm: a practical guide. Anal. Biochem. *203*, 83–93.

Rissler, M., Wiedemann, N., Pfannschmidt, S., Gabriel, K., Guiard, B., Pfanner, N., and Chacinska, A. (2005). The essential mitochondrial protein Erv1 cooperates with Mia40 in biogenesis of intermembrane space proteins. J. Mol. Biol. *353*, 485–492.

Setterdahl, A. T., *et al.* (2003). Effect of pH on the oxidation-reduction properties of thioredoxins. Biochemistry *42*, 14877–14884.

Sreerama, N., and Woody, R. W. (1993). A self-consistent method for the analysis of protein secondary structure from circular dichroism. Anal. Biochem. *209*, 32–44.

Stojanovski, D., Muller, J. M., Milenkovic, D., Guiard, B., Pfanner, N., and Chacinska, A. (2008). The MIA system for protein import into the mitochondrial intermembrane space. Biochim. Biophys. Acta *1783*, 610–617.

Terziyska, N., Lutz, T., Kozany, C., Mokranjac, D., Mesecke, N., Neupert, W., Herrmann, J. M., and Hell, K. (2005). Mia40, a novel factor for protein import into the intermembrane space of mitochondria is able to bind metal ions. FEBS Lett. *579*, 179–184.

Tokatlidis, K. (2005). A disulfide relay system in mitochondria. Cell *121*, 965–967.

Tu, B. P., Ho-Schleyer, S. C., Travers, K. J., and Weissman, J. S. (2000). Biochemical basis of oxidative protein folding in the endoplasmic reticulum. Science *290*, 1571–1574.

Vitu, E., Bentzur, M., Lisowsky, T., Kaiser, C. A., and Fass, D. (2006). Gain of function in an ERV/ALR sulfhydryl oxidase by molecular engineering of the shuttle disulfide. J. Mol. Biol. *362*, 89–101.

Voronova, A., Meyer-Klaucke, W., Meyer, T., Rompel, A., Krebs, B., Kazantseva, J., Sillard, R., and Palumaa, P. (2007). Oxidative switches in functioning of mammalian copper chaperone Cox17. Biochem. J. *408*, 139–148.

Wallace, C. J. (1984). The effect of complete or specific partial acetimidylation on the biological properties of cytochrome c and cytochrome c-T. Biochem. J. *217*, 595–599.

Webb, C. T., Gorman, M. A., Lazarou, M., Ryan, M. T., and Gulbis, J. M. (2006). Crystal structure of the mitochondrial chaperone TIM9.10 reveals a six-bladed alpha-propeller. Mol. Cell *21*, 123–133.

Williams, J. C., Sue, C., Banting, G. S., Yang, H., Glerum, D. M., Hendrickson, W. A., and Schon, E. A. (2005). Crystal structure of human SCO 1, implications for redox signaling by a mitochondrial cytochrome c oxidase "assembly" protein. J. Biol. Chem. *280*, 15202–15211.

Wu, H. H., Thomas, J. A., and Momand, J. (2000). p53 protein oxidation in cultured cells in response to pyrrolidine dithiocarbamate: a novel method for relating the amount of p53 oxidation in vivo to the regulation of p53-responsive genes. Biochem. J. *351*, 87–93.

Supplementary Figures
Reconstitution of the Mia40-Erv1 oxidative folding pathway for the small Tim proteins

Heather L. Tienson[1], Deepa V. Dabir[1], Sonya Neal[1], Rachel Loo[2,4] , Samuel A. Hasson[1], Pinmanee Boontheung[1], Sung-Kung Kim[5], Joseph A. Loo[1,2,4], and Carla M. Koehler[1,2,3]*

Department of Chemistry and Biochemistry,[1] Molecular Biology Institute,[2] Jonsson Comprehensive Cancer Center,[3] Department of Biological Chemistry, David Geffen School of Medicine,[4] UCLA, Los Angeles, California 90095 and Department of Chemistry and Biochemistry, Baylor University, Waco, Texas 76798[5]

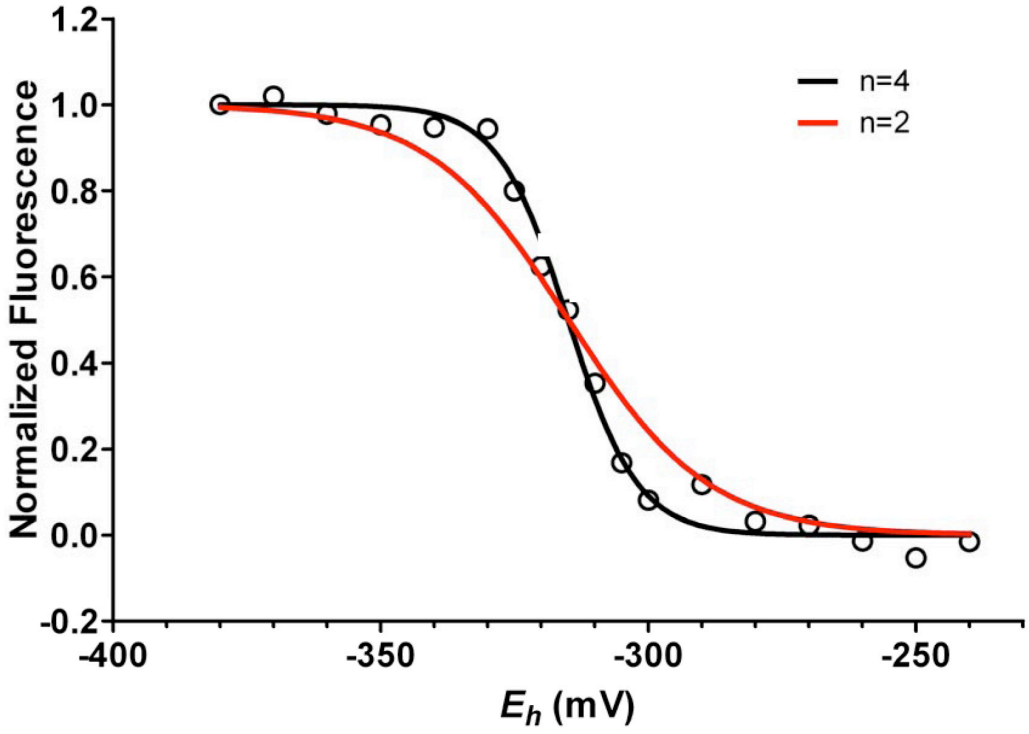

Supplementary Figure 1 mBBr titrations for Tim13 yield a similar E_m as CD studies. As in Fig. 1, redox titrations of dithiol/disulfide couples in Tim13 were carried out using DTT redox buffers. Redox equilibration was performed for 2.0 h at pH 7.0 with total redox buffer concentrations of 2.0 mM under anaerobic conditions. Data in all titrations were fit to the Nernst equation for a four-electron carrier (black line) and two-electron carrier (red line). The likelihood of the data to fit a curve for a four electron carrier vs. a two electron carrier was calculated using the informational theory approach Akaike's criterion with Prism (Akaike, 1974). The probability was higher (98 %) that the data fit a curve for $n = 4$ electrons than $n = 2$ electrons (2 %) ($n = 4$)

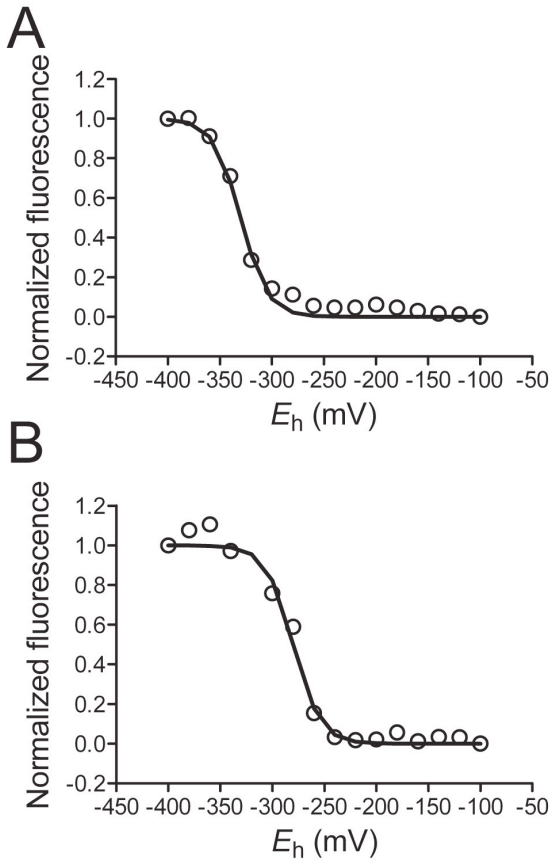

Supplementary Figure 2 Oxidation-reduction titrations of Mia40 under aerobic conditions give a similar E_m as those under anaerobic conditions. As in Figure 2, Mia40 was incubated over a range of redox potentials in aerobic conditions and the midpoint potential was measured with (A) mBBr titration and (B) intrinsic tryptophan fluorescence. Values of -322 mV and -289 mV were obtained, respectively. ($n = 4$)

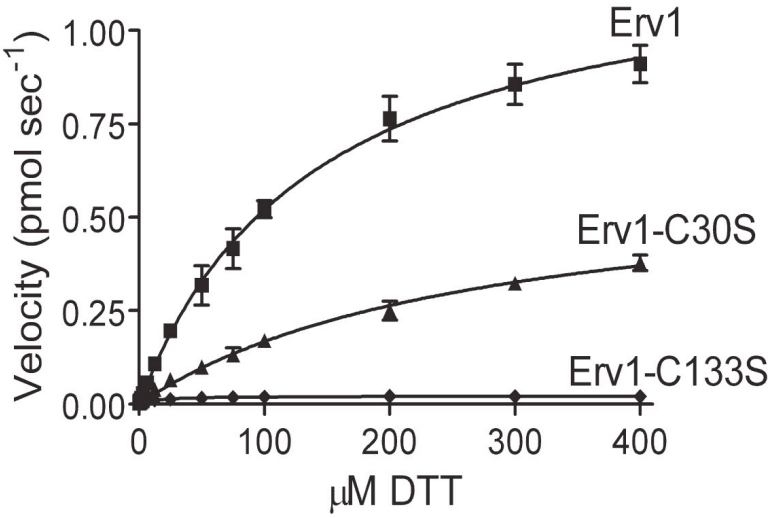

Supplementary Figure S3 Erv1 and the C30S Erv1 mutant oxidize the nonphysiologic substrate DTT. 1 μM Erv1, C30S Erv1, and C133S Erv1 were incubated with 0-400 μM DTT over a 50 min time course. Aliquots were removed during the time course and the concentration of H_2O_2 was measured. The velocity (pmol/sec) of H_2O_2 produced was plotted vs. the concentration of DTT in the assay.

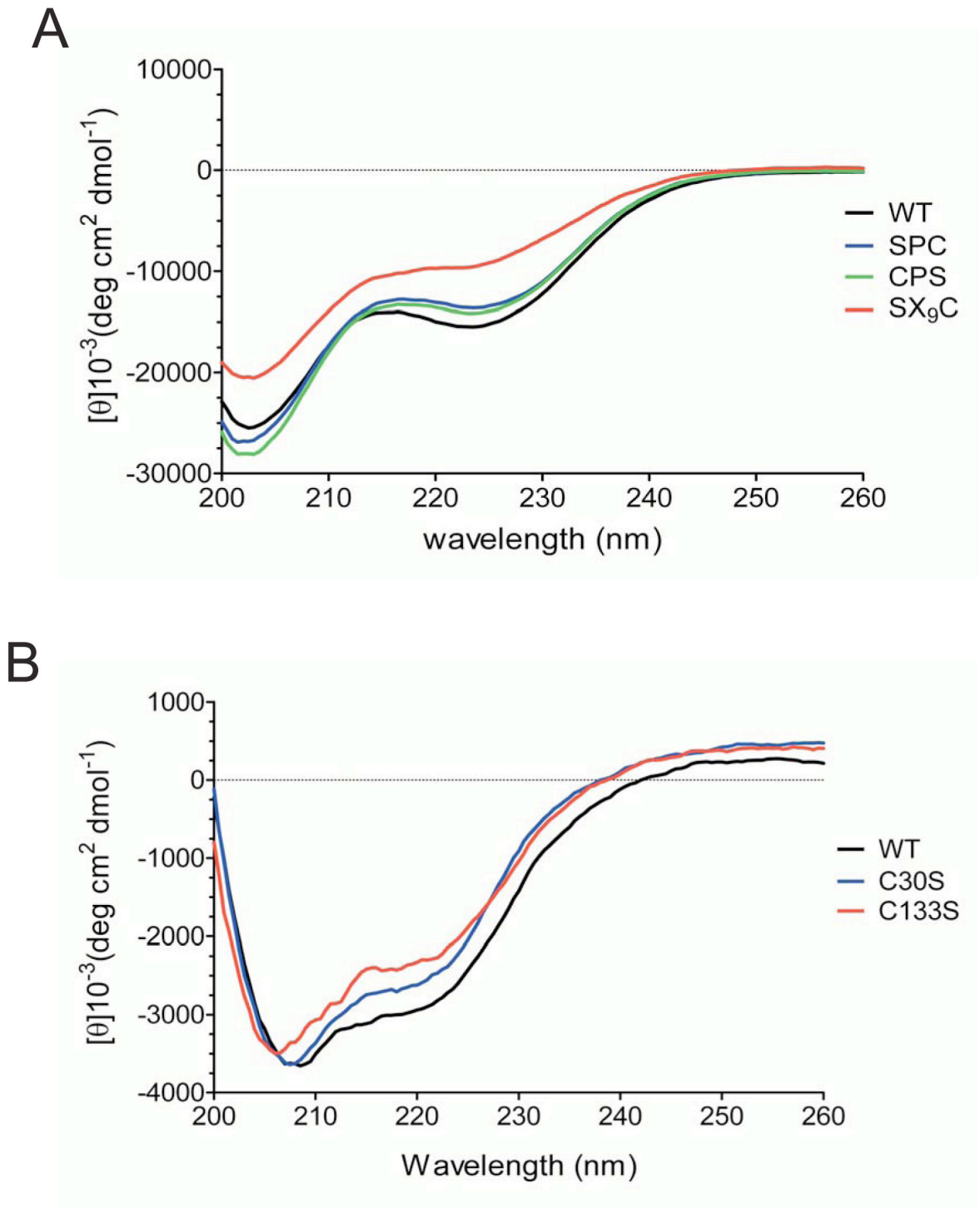

Supplementary Figure S4. CD analysis of the secondary structure content for the Mia40 and Erv1 mutants. (A) CD analyses of the Mia40 mutants SPC and CPS show similar spectra to WT, while analyses of the SX_9C mutant shows a slight decrease in alpha-helical content, as shown by the shallow peak at 225 nm. (B) CD analyses of the Erv1 mutants C30S and C133S indicate that the structures do not differ markedly from the WT protein.

Chapter 2: Mia40 serves as an electron sink in the Mia40-Erv1 import pathway

Introduction

Import pathways of the mitochondria

Endosymbiosis of an α proteobacteria gave rise to a mitochondria with only a small portion of proteins encoded in the mitochondrial genome (McCutcheon and Moran, 2012). The vast majority of mitochondrial proteins are transcribed and translated in the cytosol and imported into the correct mitochondrial compartment (Koehler, 2004; Bauer et al., 2002; Pfanner and Wiedemann, 2002). Newly synthesized polypeptides contain important targeting and sorting sequence which directs them to the matrix and inner membrane via the Translocase of Outer Membrane (TOM) complex and Translocase of the Inner Membrane (TIM) complexes (Koehler, 2004). Proteins directed into the inner membrane space (IMS) utilizes a variety of import pathways (Herrmann and Hell, 2005).

Mia40-Erv1 import pathway of the mitochondrial IMS

A Mia40 oxidative-folding import pathway for IMS cysteine-rich proteins has been identified that utilizes the two essential mitochondrial proteins Erv1 and Mia40 (Chacinska and Rehling, 2004; Mesecke et al., 2005; Tokatlidis, 2005; Rissler et al., 2005; Koehler and Tienson, 2009). Several substrates of this import pathway include the small Tims (Tim8, Tim9, Tim10, Tim13) with a conserved CX_3C motif and proteins involved in cytochrome oxidase assembly (Cox17 and Cmc1) with a conserved CX_9C motif.

Mechanism of the Mia40-Erv1 import pathway

The mechanism of the oxidative folding import pathway involves translocation of reduced and unfolded intermembrane space proteins via the TOM complex(Lu et al., 2004; Lutz et al., 2003). In the intermembrane space, the reduced substrates interact with oxidized Mia40 by formation of an intermolecular disulfide bond. The substrate is oxidized and released by Mia40. To allow for further rounds of import, reduced Mia40 is reoxidized by Erv1 (Fig. 1). This suggests that electrons are transferred from the imported proteins to Erv1 via Mia40. Erv1 transfers the electrons through its flavin cofactor to a variety of electron acceptors, including cytochrome *c* and oxygen/cytochrome *c* peroxidase (Ccp1)(Dabir et al., 2007; Bihlmaier et al., 2007).

Mia40 has 3 conserved cysteine pairs; two pairs has a twin CX_9C motif and are postulated to stabilize the protein and one redox-active cysteine pair containing an N-terminal CPC motif which is involved in the thiol exchange reactions with substrates and Erv1(Grumbt et al., 2007)(Fig. 2).

Recent works have been dedicated to elucidating the mechanisms involved in substrate oxidation by Mia40. The N-terminus IMS-targeting signal of newly imported substrates covalently binds to the hydrophobic pocket of Mia40 (Banci et al., 2009; Sideris et al., 2009). The amino terminus cysteine of the small Tims forms an intermolecular disulfide bond with the second cysteine in the CPC motif of Mia40. Moreover, the formation of the inner disulfide bond pair is prerequisite to the formation of the outer disulfide bond which breaks the intermolecular disulfide intermediate with Mia40 and releases the oxidized substrate(Sideris and Tokatlidis, 2010)(Fig. 3).

It remains unclear how the second disulfide bond is introduced into substrates. Since Mia40 has one redox-active cysteine pair, it can only insert one disulfide bond into substrates per cycle of Mia40 oxidation. There are several possible mechanisms suggesting the formation of

the inner disulfide bond. The first possibility is the formation of a stable complex containing substrate, Mia40 and Erv1 in which Erv1 inserts a second disulfide bond into the substrate(Stojanovski et al., 2008). Despite this important observation; in vitro reconstitution was unable to detect thiol linkages of Tim13-Mia40-Erv1 trimer or Tim13-Erv1 dimer(Tienson et al., 2009). An alternative possibility is that oxidized glutathione or O_2 directly inserts the second disulfide bond to substrates bound to Mia40 (Sideris and Tokatlidis, 2010). However, there is no data supporting oxidized glutathione's role in oxidation of substrates. In addition, substrate oxidation by O_2 is inconceivable since the oxidative folding pathway functions in yeast under anaerobic conditions. The third possibility is that reduced glutathione assists Mia40 in the disulfide bond formation(Bien et al., 2010a). In contrast, our studies were unable to demonstrate reduced glutathione's role in the rapid oxidation of substrates. In all, oxidative folding of substrates by Mia40 remains unclear despite increased effort for unraveling the mechanistic details of the pathway.

To gain further understanding of the mechanistic detail of the Mia40 oxidative folding pathway, we reconstituted the import pathway in vitro using Tim13 as a substrate. *In vitro* reconstitution provided evidence that the first three cysteines of Tim13 are essential for oxidative folding by Mia40 and that Tim13 is able to reduce six cysteines of Mia40. Also, limited proteolysis experiment revealed that Tim13 is able to induce conformational changes of Mia40. In all, these experiments is able to elucidate the mechanistic details in the oxidation of Tim13 by Mia40.

Results

Glutathione decreases the rate of Tim13 oxidation

A primary question that has not been resolved for a typical reduced substrate with two disulfide bonds is how four electrons are transferred to acquire two disulfide bonds during import. Mia40 inserts one disulfide bond through a disulfide exchange reaction, but acquiring the second disulfide bond is still an unanswered question. Potential mechanisms include different small oxidants such as glutathione (GSH), oxygen or metals or possibly Mia40 under anaerobic conditions (Banci et al., 2010; Bien et al., 2010b). We therefore investigated how electrons might be handled in oxidation of substrates. As a first approach, we considered whether the reductant glutathione might be required, based on the studies by Bien et al., (2010). The oxidation of reduced Tim13 was tested in the presence of 5 mM GSH, Erv1, and Mia40 (Fig. 4A, B). The oxidation state of Tim13 was monitored by addition of AMS, which covalently binds to reduced cysteines and causes an increase in molecular mass of 500 daltons per addition. Based on no addition of 4 AMS moieties simultaneously, Tim13 is oxidized in one step; a partially oxidized intermediate was not observed. However, GSH addition slowed Tim13 oxidation, with only 50% being oxidized over the time course (Fig. 4B,D). We tested if the general reductant ascorbate acted similarly. Addition of 5 mM ascorbate inhibited Tim13 oxidation by 95% (Fig. 4C, D). Under these in vitro condition, the addition of reductants impaired Tim13 oxidation in the presence of Mia40, Erv1, and oxygen.

Glutathione decreases the import of Cmc1

We subsequently tested the effect of reductants on import of Tim13 and the CX_9C substrate Cmc1 into isolated mitochondria. Mitochondria were incubated with 2 mM and 5 mM GSH or ascorbate for 10 min followed by the addition of the substrate (Fig. 5A, B). Again, the addition of reductants strongly inhibited Tim13 and Cmc1 import. In contrast, GSH addition did

not interfere with the import of TIM23 substrate Su9-DHFR (Fig. 5C). Thus, GSH and ascorbate impair both the in vitro oxidation and *in organello* import of Mia40 substrates.

Tim13-Mia40 and Mia40-Erv1 intermediates are formed via disulfide bonds

Another mechanism for oxidation of Mia40-dependent substrates is through the formation ternary complex of substrate, Mia40 and Erv1 in which the components cooperatively work together to insert two disulfide bonds into Mia40 (Stojanovski et al., 2008). Previous work from our laboratory failed to identify a ternary complex that was linked by disulfide bonds in the reconstitution assay with purified components, but instead showed the formation of Tim13-Mia40 and Mia40-Erv1 intermediates during Tim13 oxidation (Tienson et al., 2009). We expanded this analysis by investigating interactions with all combinations of reduced Tim13 with Mia40 and Erv1 followed by immunoblotting with antibodies against Tim13, Mia40, and Erv1. Disulfide-linked intermediates were trapped by treatment with IAA to stabilize the mix-disulfides, followed by SDS-PAGE on nonreducing gels (Fig. 6A). In the absence of reductant, an intermediate between Tim13 and Mia40 was detected (Fig. 6A, lanes, 2, 6, 10, 12). This intermediate was mediated by free thiols in Tim13 because pretreatment of Tim13 with IAA prevented formation of the Tim13-Mia40 mixed disulfide (Fig. 6A, lanes 3, 7, 11, 13). Mia40 showed an unexpectedly large shift upward when treated with IAA (Fig. 6A, lane 6), suggesting that IAA might be adding to several reduced thiols; this shift was subsequently eliminated when Erv1 was added (Fig. 6A, lane 12). Intermediates between Tim13-Erv1 [Fig. 6A, lane 4-7, 16-19 (obscured by an Erv1 dimer, indicated by ■)] and Mia40-Erv1 [Fig. 6A, lane 9,12,13 (obscured by a Mia40 dimer, indicated by ♦) and lanes 15, 18-19] were also detected. Non-specific multimers of Tim13 (indicated by the asterisks) also formed. A stable ternary complex with

Mia40, Erv1, and Tim13 above the molecular mass of 72 kDa was not detected (data not shown); as described by Chacinska and colleagues, this complex may be short lived. As a control, resolving the intermediates on a reducing gel resulted in migration of the proteins at their native molecular mass (Fig. 3B). This analysis suggests that Mia40 may be completely reduced by Tim13.

C1, C2 and C3 of Tim13 is required for oxidative folding by Mia40

Previously, we set up an in vitro reconstitution assay for monitoring the oxidation of Tim13 over time with purified proteins of the Mia40-Erv1 pathway(Tienson et al., 2009). We adapted this system to assess the cysteines of Tim13 that are required for oxidation by Mia40 and Erv1. The Tim13 mutants were incubated with catalytic amounts of Mia40 and Erv1 (1 uM) and oxidation of Tim13 was monitored over 4 hours. As a control, the Tim13 mutants alone or in the presence of Mia40 or Erv1 were not oxidized in four hours as shown by majority of Tim13 being modified by 4 AMS (Fig. 7A,B,C,D Lanes 3-6). Interestingly, Tim13 C1S, C1S, and C3S were not oxidized in the presence of both Mia40 and Erv1 since no oxidized species of Tim13 was detected in four hours (Fig. 7A, B, C Lanes 7,8). For C3S, we observed a minor oxidized species (Tim13-AMS_1) (Fig. 7C Lanes 5-8). However, this species were already present when incubated with Mia40 or Erv1 alone (Fig. 7C Lanes 4-6). Notably, C4S was oxidized over time with Mia40 and Erv1 together as shown by an increase in the oxidized form which corresponds to 1 AMS addition (Fig. 7D, Lane 8). By monitoring the redox state of Mia40 over time in the presence of the Tim13 mutants, Mia40 was not reduced by 4 hours whereas C4S was able to partially reducing Mia40 (Fig. 8A Lanes 7, 10, 13,16). Based on the reconstitution assay, the first three cysteines of Tim13 are required for oxidation by Mia40 and Erv1.

C1, C2 and C3 of Tim13 are required to pass electrons through Mia40 and Erv1

An Amplex Red flourometric assay was employed to monitor the electron flow from Tim13 through Erv1. Erv1 is a sulfhydryl oxidase, which accepts electrons from its FAD moiety and converts oxygen to hydrogen peroxide (Dabir et al., 2007). Thus, in the presence of hydrogen peroxide, Amplex Red substrate is converted to a fluorescently active resorufin. Tim13 mutants were incubated with catalytic amounts of Mia40 and Erv1 and hydrogen peroxide production was measured over 30 minutes. As expected, WT and Tim13 mutants alone or in the presence of either Mia40 or Erv1 led to minimal amount of fluorescence via hydrogen peroxide production. When WT Tim13 was incubated with both Mia40 and Erv1, there was an increase in fluorescence relative to the negative controls indicating electron flow from Tim13 to Mia40 and from Mia40 to Erv1. However, Tim13 C1S, C2S, or C3S incubated with both Mia40 and Erv1 did not result in an increase of fluorescence suggesting these mutants were unable to pass electrons through Mia40 and Erv1. Interestingly, Tim13 C4S in the presence of both Mia40 and Erv1 resulted in an increase in fluorescence, although not as high as WT Tim13 (Fig. 7E). This suggests that C4S is capable of passing electrons onto Mia40 and Erv1. In all, C1, C2 and C3 of Tim13 are required to shuttle electrons onto Mia40 and Erv1.

Tim13 reduces six cysteines of Mia40

Using the vitro reconstitution system developed in our laboratory, we determined the specific redox state of Mia40 in the presence of excess reduced Tim13 or Tim13 mutants in which each cysteine residue was individually replaced with serine (Fig. 8A). The Tim13 mutants have been designated C1S (C57S), C2S (C61S), C3S (C73S), and C4S (C77S). Reduced Tim13 (15 μM) was incubated with Mia40 (1 μM) or both Mia40 (1 μM) and Erv1 (1 μM); the

redox state of Mia40 was monitored at 1 and 4 hours by the addition of AMS time course followed by nonreducing SDS-PAGE and immunoblot analysis with anti-Mia40. In a control reaction, Mia40 was treated with 20 mM DTT at 25^{o}C for 1 hr and 2 AMS added to Mia40 (Grumbt et al., 2007) (Fig. 8A, lane 3), indicating complete reduction. Incubation of excess WT Tim13 with Mia40 resulted in an addition of 6 AMS molecules, demonstrating Mia40 was completely reduced (Fig. 8A, lane 4). Subsequent Erv1 addition oxidized Mia40 (Fig. 8A, lane 5,6). With the Tim13 C4S mutant, 2 and 6 AMS added to a subset of the Mia40 pool (Fig. 8A, lane 7), which was mostly oxidized by the addition of Erv1 (Fig. 8A, lanes 8,9). However, the additional Tim13 mutants C1S, C2S, and C3S failed to oxidize Mia40 (Fig. 8A, lanes 10, 13, 16).

We refined the analysis of Mia40 reduction and oxidation using a time course assay. As in Fig. 4A, excess Tim13 was incubated with Mia40. During the first 90 minutes (Fig. 8B, lanes 1-3), a progression of 2 and 6 AMS modifications was detected, until 120 minutes when the majority of the Mia40 pool was reduced (Fig. 8B, lane 4). The addition of Erv1 resulted in partial oxidation of Mia40 at 15 min (Fig. 8B, lane 5) followed by full oxidation at 120 min (Fig. 8B, lane 6-8). Thus, Mia40 can be fully reduced by Tim13, but the reduction was not immediate. We adjusted the ratio of Tim13 to Mia40 to estimate the amount of Tim13 that was required to reduce Mia40 (Fig. 8C). In a control reaction, we incubated the buffer, excluding Tim13, with Mia40 for 2 hrs; Mia40 remained oxidized (Fig 8C, lanes 1-6). Addition of the reduced Tim13 with Mia40 resulted in partial Mia40 reduction when the ratio of thiols was equal (6:6) to two-fold higher (12:6) at 2 hrs (Fig. 8C, lanes 9-10). When the thiols were in excess of 4- and 8-fold, Mia40 became reduced (Fig. 8C, lanes 11-12).

To verify that the Mia40 thiols are specifically blocked by AMS, we used the complementary method of mass spectrometry (MALDI-MS) analysis. Because AMS did not

work well in the analysis, we switched to the thiol-modifying reagent NEM (Table 2). Mia40 was reduced with 20 mM DTT for 1 hour at 25°C and incubated at 25°C or 95°C for 5 minutes followed by incubation in the presence of 20 mM NEM at 25°C for 1 hr. Intact proteins were separated by MALDI and the mass of the peptides was analyzed. At 25°C, 85% of the reduced Mia40 pool had two NEM modifications, based on the increased molecular mass. When Mia40 was incubated at 95°C, the number of NEM additions increased to 5-6, demonstrating that Mia40 was mostly reduced. An increased ratio of Tim13:Mia40 (4:1 → 12:1) in the mass spec analysis correlated with an increased reduction in Tim13. In sum, the in vitro analysis supports that Mia40 can accept up to six electrons from substrate Tim13. Also, Mia40 reduction by Tim13 requires the presence of the 1st, 2nd and 3rd cysteines in Tim13.

Tim13 induces conformational changes upon reduction Mia40

Because Mia40 can accept up to 6 electrons from Tim13 in vitro, we tested the stability of Mia40 in limited proteolysis experiments to determine whether the transfer of electrons to Mia40 corresponded with conformational changes. Recombinant reduced Tim13 and Mia40 were incubated together for 2 hours at 25°C and treated with 5 μg/ml trypsin at 37°C. Aliquots were removed at the indicated time points, stopped with the addition of soybean trypsin inhibitor, and analyzed by SDS-PAGE and immunoblot analysis with anti-Mia40. As a control, Mia40 was reduced and denatured with 20 mM DTT and incubation at 95°C for 5 minutes followed by treatment with trypsin; Mia40 was rapidly degraded within 5 minutes (Fig. 9A). Untreated Mia40 was less sensitive to trypsin, because fragments were resistant to trypsin after 20 min (Fig. 9B). In the presence of 12 μM Tim13 after 2 hours, 1 μM Mia40 was degraded in 2-5 minutes and resistant products were not detected (Fig. 9C). Thus, the protease sensitivity of Mia40 in the presence of excess Tim13 is similar to that of reduced/heated Mia40.

Mia40 is completely reduced in the *erv1-101* mutant

The requirement for functional Erv1 in the oxidation of Mia40 was tested. Recombinant Tim13 and Mia40 were incubated with WT or Erv1 mutants C30S or C133S (Fig. 6A). Aliquots were removed at 4 hours and the redox state of Mia40 was analyzed with AMS. The presence of WT Erv1 resulted in the oxidation of Mia40, because AMS addition was not observed (Fig. 10A, lane 2). In contrast, the control reaction of Tim13 and Mia40 without Erv1 showed reduction of Mia40 (Fig. 6A, lane 1). The Erv1 mutants C30S or C133S failed to oxidize Mia40 (Fig. 10A, lane 3, 4).

We also performed *in organello* thiol-trapping to assess the redox state of Mia40 in mitochondria from the *erv1-101* temperature-sensitive yeast strain. As a control to confirm that differences in Mia40 migration corresponding with the addition of 2 and 6 AMS molecules could be separated in the gel system, we synthesized full-length Mia40 or mutant Mia40 that lacked the four cysteine residues in the core region (Mia40-CPC-SX_9S-SX_9S) in the reticulocyte lysate system, followed by AMS treatment and separation by SDS-PAGE (Fig. 10B). Whereas the addition of two AMS moieties caused a small shift, six AMS additions increased the mobility of Mia40. Thus the gel system is adequate for detecting differences in the addition of 2 and 6 AMS molecules.

We purified mitochondria from WT or *erv1-101* yeast strains and TCA-precipitated solubilized mitochondrial proteins followed by treatment with AMS and SDS-PAGE analysis with anti-Mia40. In WT mitochondria, AMS did not add to untreated Mia40, indicating that Mia40 was oxidized. In contrast, both reduced and reduced/heated it was As a control to verify that Mia40 could be reduced that being reduced and reduced/denatured, WT purified

mitochondria were treated with 20 mM DTT or both 20 mM DTT and incubation at 95^{o}C respectively. Under these conditions, there was a same shift of Mia40 with AMS addition. Unfortunately, with both controls having the same shift, we were unable to distinguish if the reduced/denatured control resulted in addition of 6 AMS or 2 AMS addition (Fig. 10B Lanes 4, 6). Also, AMS addition to untreated WT mitochondria resulted in majority of Mia40 being oxidized since there was no shift in Mia40 (Fig. 10B Lane 2). In purified mitochondria in which *erv1-101* yeast strain was grown in the permissive temperature at 25^{o}C, majority of Mia40 remained oxidized (Fig. 10B, Lane 8). In *erv1-101* yeast strain grown in the nonpermissive temperature at 37^{o}C, Mia40 was reduced (Fig.10B, Lane 10). Because the shift of Mia40 with AMS addition corresponded to the same shift in the reduced/denatured and reduced control of WT mitochondria, we were unable to determine the number of cysteines of Mia40 that were reduced. Taken together, we provided in vitro evidence that six cysteines of Mia40 play a role in shuttling electrons to Erv1.

DISCUSSION

The role of GSH in the Mia40-Erv1 import pathway

Previous studies reported that GSH stimulates the import and oxidation of Cox19 in the Mia40-Erv1 import pathway via the removal of off-pathway intermediates, which consists of incorrect disulfide bond arrangements within Cox19. This was shown through an increase in import and oxidation of Cox19. In the contrary, we showed in vitro reconstitution of the Mia40-Erv1 pathway in the presence of GSH decreased the rate of Tim13 oxidation. Also, *in organello* import studies showed a decrease in the rate of Cmc1 import in the presence of GSH. Recently,

Bien et al. detected Cox 19 off-pathway intermediates in oxygen-depleted conditions (2010). However, Mia40 in excess is capable of fully oxidizing its substrates in the absence of oxygen. Recent data on Tim10, further supports Mia40's role in inserting disulfide bonds correctly into its substrates in a GSH independent manner. Taken together, it seems that the current model of substrate oxidation via Mia40 occurs independently of an isomerase or additional small oxidants such as GSH.

Dissecting the Mia40-dependent import pathway

Reconstituting the pathway with individual cysteine mutants of Tim13 allowed us to identify the cysteine residues of Tim13 important for oxidation via Mia40. Based on the in vitro reconstitution and fluorometric assay, we were able to show a requirement of the first three cysteines for Tim13 oxidation and reduction of Mia40. This is supported from structure data of the Cox17-Mia40 intermediate in which the first cysteine is essential for the formation of the initial disulfide linkage with Mia40 (Banci et al., 2010). Also, the requirement for the second and third cysteine in Tim13 oxidation is supported from studies by Sideris et al. in which the inner disulfide bond formation of Tim10 is an essential process (Sideris and Tokatlidis, 2007). We were able to complement these findings using the C61S,C73S double mutant of Tim13 (CX_3**C-C**X_3C), which solely forms the outer disulfide bond. As expected, C61S,C73S was not able to pass electrons through Mia40 and Erv1 further indicating the inner cysteines of Tim13 are essential in the oxidation process by Mia40(Fig.11 (S1)). Also, mixed disulfide trapping revealed that all cysteines of Tim13 are able to form a mixed disulfide intermediate with Mia40. This finding helps explain how both the inner and outer cysteines of Tim13 are able to shuttle electrons directly to Mia04. This finding was further verified by blocking all cysteine residues of Tim13 with IAA, which abolished the Tim13-Mia40 intermediate. In all, the in vitro

reconstitution system and fluorometric assay allowed us to determine the cysteine residues of Tim13 that are essential for oxidation by the Mia40-Erv1 pathway.

Mia40 is fully reduced by Tim13

We were interested in following the redox state of Mia40 during the in vitro reconstitution with Tim13 as our model substrate. In this study, we showed that six cysteines of Mia40 potentially play a role in accepting electrons from Tim13, which was confirmed in our mass spectrometry results. We analyzed the kinetics of Mia40 reduction and showed that in the presence of Tim13 in 12-fold excess of Mia40, Mia40 was fully reduced in two hours. This is the first evidence that all cysteines of Mia40 are able to accept electrons from its substrates. Based on the NMR structure of the Cox17-Mia40 intermediate, the cysteine pairs are not in proximity to accommodate electron transfer between the cysteine-pairs within Mia40 (Banci et al., 2010). However, we showed that Tim13 induces a conformational change in Mia40, which most likely facilitates the electron transfer within Mia40.

To date, the most accurate depiction of substrate binding to Mia40 came from NMR structure study on the Cox17-Mia40 intermediate in which there are no significant changes in the conformation of Mia40 upon binding to Cox17. However, a Mia40 cysteine mutant at the CPC motif was used in this study to stabilize the Cox17-Mia40 intermediate which blocks electron accumulation in Mia40 (Banci et al., 2010). This most likely explains why no change in the conformation of Mia40 is observed upon binding to Cox17. Whereas the full reduction of Mia40 occurred in the presence of reduced Tim13 in 12-fold excess, the Cox17-Mia40 intermediate was established with Cox17 in only 2-fold excess of Mia40. Although the NMR structure accurately showed the folding of the ITS signal is Mia40-dependent, it is still an open question as to how substrates are fully oxidized.

Mia40 has been characterized to have one redox active cysteine pair (CPC motif), which is poised to only accept 2 e- from its substrates (Terziyska et al., 2009). There are numerous postulations as to how the second disulfide bond is formed in substrates containing either the twin CX_3C or twin CX_9C motif. However, no studies to date have analyzed the redox state of Mia40 in the presence of substrate. Herein, we provided the first evidence *in vitro* in which all six cysteines of Mia40 were reduced in the presence of Tim13. This process may explain how 4 electrons are simultaneously removed from substrates containing two disulfide bonds. However, the *in vitro* approach used in this study is limiting since the physiological levels of substrates that Mia40 encounters are not known *in vivo*. Thus, future studies are needed *in vivo* in order to assess if all cysteines of Mia40 are able to accept electrons from cysteine-rich substrates.

Materials and Methods

Plasmids and Strains

Cysteine point mutants of Tim13 were generated by site-directed mutagenesis using the QuikChange II Site-Directed Mutagenesis kit(Stratagene). Tim13 C57S, C61S, C73S and C77S were generated by primers containing the desired mutation. Cysteine point mutants of Erv1 were generated by site-directed mutagenesis using overlap extension (Ho *et al*., 1989). General genetic techniques were used to generate precursors for imports. To generate Su9-DHFR, the first 69 amino acids of ATPase subunit 9 from *Neurospora* was fused to DHFR and cloned into the SmaI site of pGEM3. For Cmc1, the open reading frame was cloned into BamHI and SalI restriction sites of pSP65. The temperature-sensitive *erv1* yeast strain (*erv1-101)* was generated as previously described (Dabir *et al*., 2007).

Protein Expression and Purification

Recombinant Mia40 and Erv1 was expressed and purified under native conditions as previously described (Dabir *et al*., 2007; Tienson *et al*., 2009). In addition, recombinant Tim13 was purified under denaturing conditions and reduced with DTT as previously described (Tienson *et al*., 2009).

Reconstitution Studies

In the reconstitution assays, reduced Tim13 or Tim13 cysteine mutants were incubated with Mia40 and/or Erv1 or Erv1 mutants. Length of incubation varied as indicated and the redox state of Mia40 and Tim13 was determined by thiol trapping with AMS as previously described (Tienson et al., 2009). All proteins were separated by nonreducing SDS-PAGE followed by immunoblot analysis with antibodies against Tim13p or Mia40p.

Mixed disulfide trapping

Wild type or cysteine mutants of Tim13 either pretreated or not pretreated with 60 mM Iodoacetamide (IAA) were incubated with equimolar amounts of Mia40 and Erv1. The reaction was quenched with addition of IAA as previously described (Tienson *et al*., 2009). All proteins were resolved on reducing and nonreducing SDS-PAGE gels and detected by immunoblot analysis.

Amplex Red Reconstitution Studies

In the reconstitution assay, reduced Tim13 of Tim13 cysteine mutants were incubated with different combinations of Mia40 and/or Erv1 and the production of hydrogen peroxide was measured overtime using the Amplex Red/horseradish peroxidase reaction mix as previously described (Tienson *et al*., 2009).

In Organello Thiol-trapping

Mitochondria was isolated from yeast strains, GA74a and temperature-sensitive *erv1-101,* as previously described. Mitochondria was solubilized in 100 µL lysis buffer(1% digitonin, 50 mM Tris pH 7.0, 150 mM KCL, and 1 mM EDTA supplemented with protease inhibitors: 200 mM PMSF, 10 mM Leupeptin, 1 mM Chymostatin and 1 mM Pepstatin) for 1 hour at 4^{o}C followed by centrifugation at 14,000 rpm for 30 minutes at 4^{o}C. For control reactions, mitochondrial extracts were reduced with 20 mM DTT or reduced and denatured with 20 mM DTT and 2% SDS. After 1 hour of incubation at room temperature, mitochondrial proteins were precipitated by the addition of 125 µL of 100% (w/v) TCA. After 30 minutes of incubation on ice, the protein pellet was centrifuged at 14,000 rpm for 30 minutes, and the pellet was washed with 1 mL of acetone. This was followed by a final spin at 14,000 rpm for 2 minutes at 4^{o}C. To determine the redox state of Mia40, the pellet was resuspended in 20 uL of 20 mM AMS and incubated for 1 hour at 37 ^{o}C.

Protease Sensitivity Assay

1 µM of Mia40 was incubated in the presence or absence of 15 µM reduced Tim13 in a buffer containing 20 mM Tris, pH 7.0, 150 mM KCL, and 1mM EDTA. 5 ug/ml of trypsin was added to the samples at 37^{o}C. At the indicated time points, 5 uL of the sample was removed and the reaction was halted with the addition of 200 mM of soybean trypsin inhibitor. For controls, 1 µM of recombinant Mia40 was denatured at 95^{o}C and/or reduced with 20 mM DTT. Proteins were resolved on nonreducing SDS-PAGE followed by immunoblot analysis with antibodies against Mia40.

Miscellaneous Recombinant proteins were analyzed by SDS-PAGE using a 12 or 15% polyacrylamide gel and a Tricine-based running buffer. Proteins were detected by immunoblotting using nitrocellulose membranes.

Figures and Tables

Table 1. Strains used in this study

Strain	Genotype	Source
GA74-1A	**MATa** *his3-11,15 leu2 ura3 trp1 ade8 rho+ mit+*	(Koehler et al., 1998)
erv1-101	**MATα** *his3-11,15 leu2 ura3 trp1 ade8 erv1::HIS3 [perv1- 101:TRP1* CEN]	(Dabir et al., 2007)

Table 2. **MALDI-MS analysis of NEM-treated Mia40 samples**

		Percentage of NEM addition					
# of NEM modification	**0**	**1**	**2**	**3**	**4**	**5**	**6**
untreated Mia40			34	38	28		
reduced Mia40	5	10	85				
reduced/denatured Mia40				5	20	35	40
4:1 Tim13:Mia40			30	35	35		
12:1 Tim13:Mia40						10	90

The number of NEM addition has been expressed as a percentage that was calculated from peak height measurements on 1+ and 2+ ions to the extent permitted by spectral resolution.

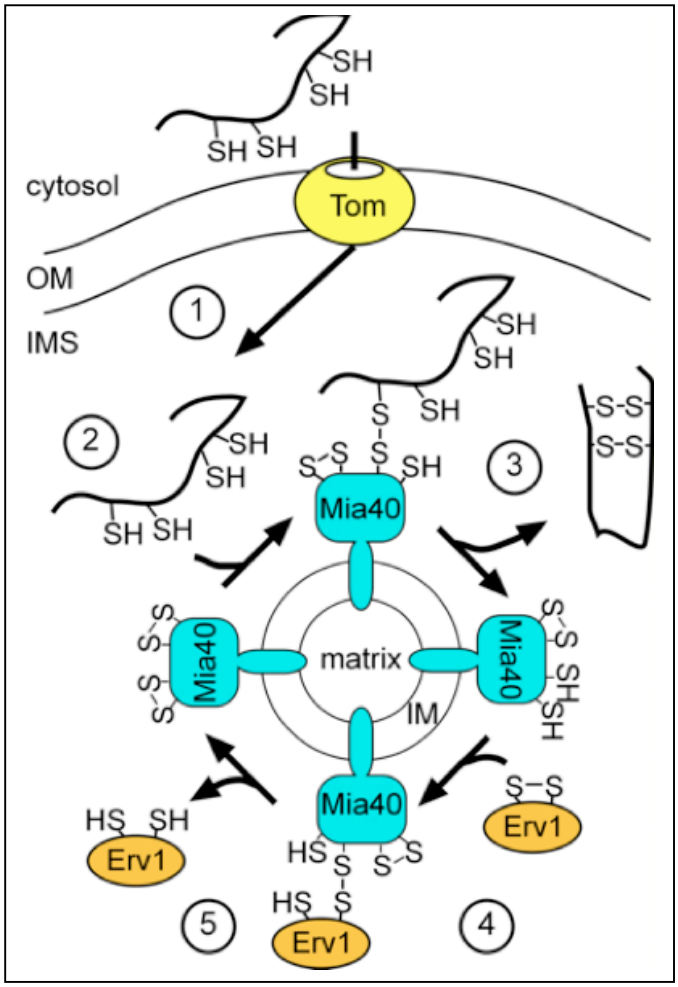

Figure 1. **The Mia40-Erv1 import pathway for CX_3C and CX_9C proteins.** The substrates (model substrate is a small Tim protein) are imported in an unfolded, reduced state across the outer membrane (OM). Oxidized Mia40 serves as the import receptor and forms a transient disulfide with the substrate.

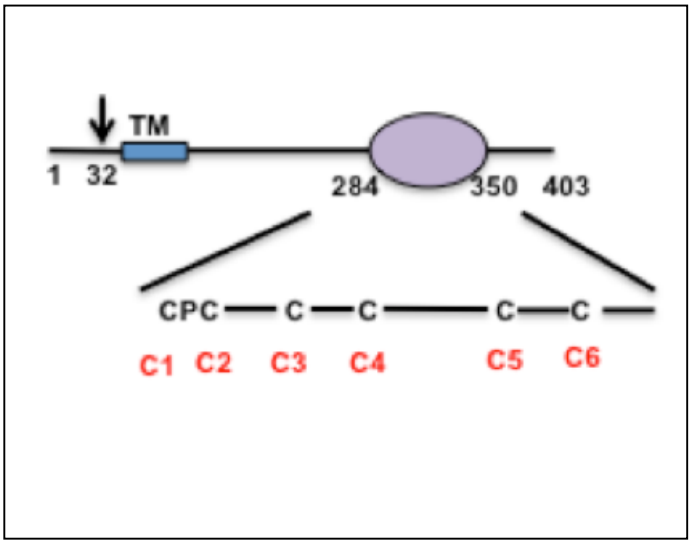

Figure 2. **Structure of Mia40**. (A) The C-terminal fragment comprising residues 284–403, Mia40C, contains a highly conserved domain (*oval*, residues 284–350). Mia40p has six cysteine residues that are all present in the conserved domain. These cysteine residues and their amino acid residue positions in the protein are indicated. The CPC motif comprises the first and the second cysteine residue of Mia40, referred to as C1 and C2. The cysteine residues of the two CX_9C segments are referred to as C3 to C6. The presequence of Mia40p is cleaved off by the matrix processing peptidase, indicated by an *arrow*.

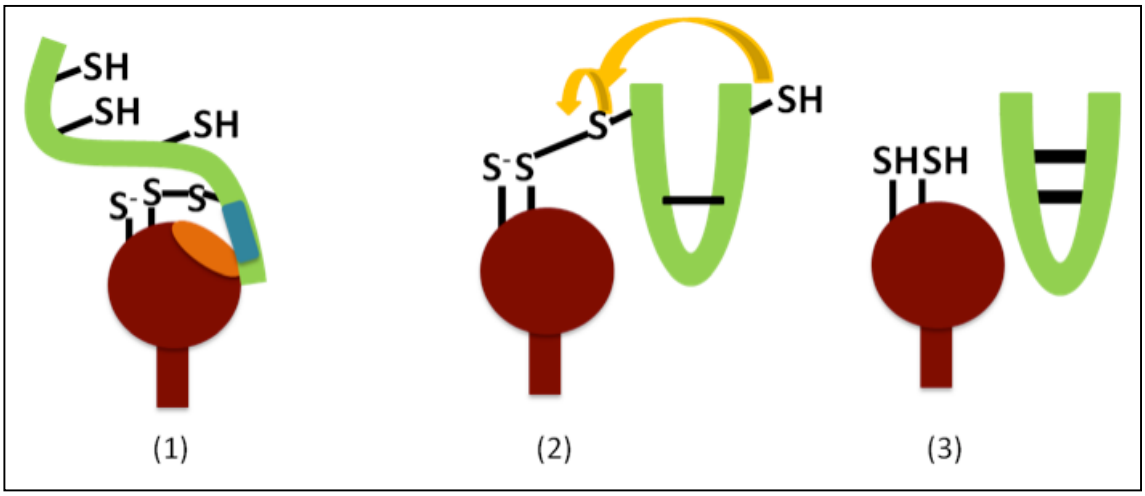

Figure 3. **Substrate oxidation by the MIA40 pathway** (1)Substrate recognition and docking. The recognition step can be split in two steps. Step 1 (sliding): the reduced substrate slides onto the Mia40 hydrophobic cleft (*orange circle*). Step 2 (docking): Hydrophobic interactions driven by the ITS/MISS of the substrate (*blue rectangle*) stabilize the substrate onto Mia40 and orient it in a way that the docking cysteine (in this case the amino terminus cysteine C1 of the substrate will perform a nucleophilic attack on the catalytic disulfide bond of Mia40. A mixed disulfide intermediate between the two docks the substrate onto Mia40. This recognition cascade reactions are Erv1 independent. (2) Substrate oxidation and release. The inner disulfide bridge of the substrate is formed, while it is still docked onto Mia40 via the amino terminal cysteine C1. This reaction occurs by an unidentified mechanism, although Erv1, metal or another small oxidizing molecule have been speculated to be involved. The formation of the inner disulfide bridge brings the carboxy-terminus cysteine C4 in proximity to the docking cysteine C1 which results in an intramolecular nucleophilic attack to the mixed disulfide bond between Mia40 and the substrate. The fully oxidized substrate is released from Mia40 with the concomitant reduction of the active site of Mia40.

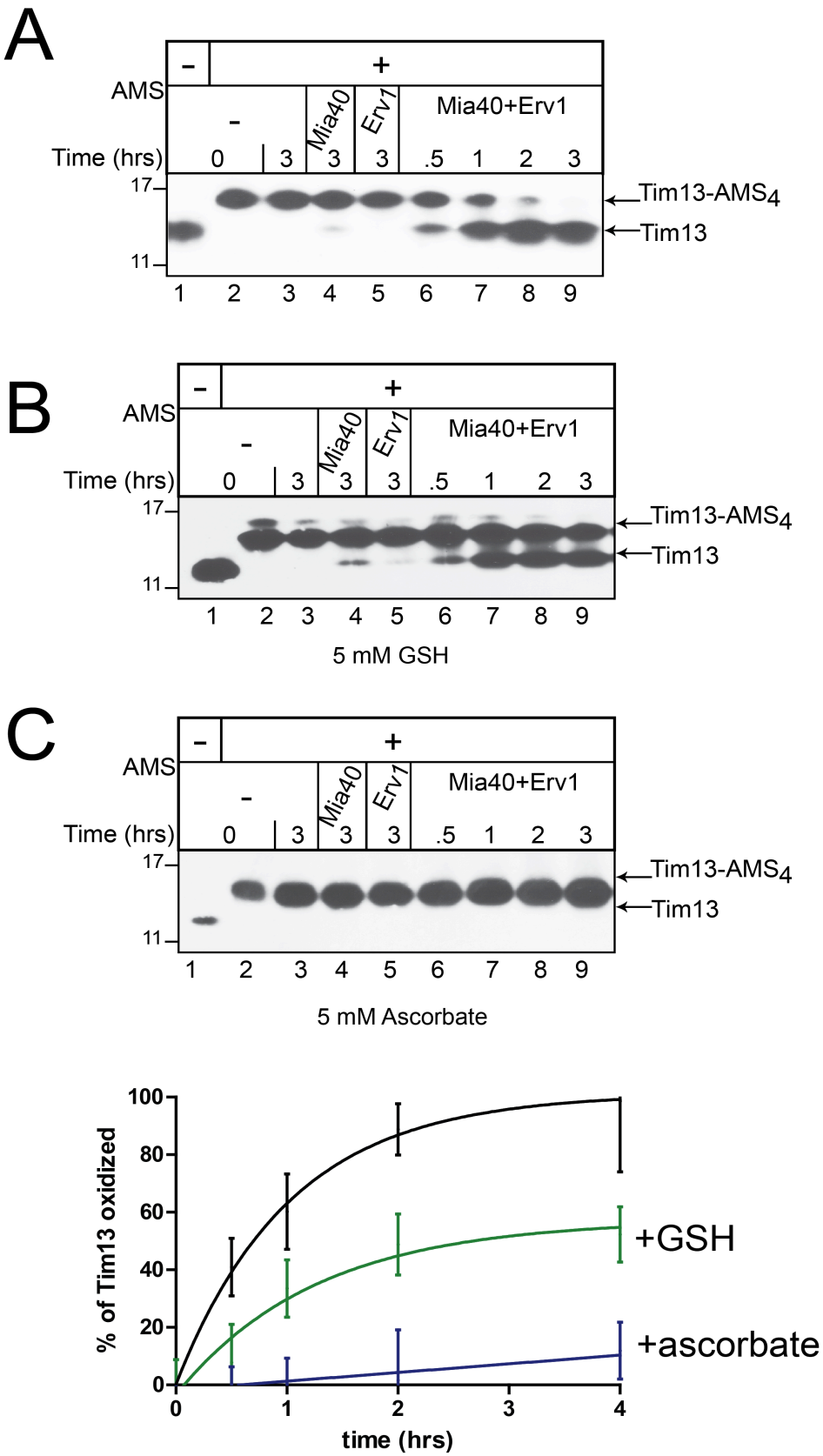
A
AMS
–
+
–
Mia40
Erv1
Mia40+Erv1
Time (hrs)
0
3
3
3
.5
1
2
3
17
11
Tim13-AMS4
Tim13
1 2 3 4 5 6 7 8 9
B
AMS
–
+
–
Mia40
Erv1
Mia40+Erv1
Time (hrs)
0
3
3
3
.5
1
2
3
17
11
Tim13-AMS4
Tim13
1 2 3 4 5 6 7 8 9
5 mM GSH
C
AMS
–
+
–
Mia40
Erv1
Mia40+Erv1
Time (hrs)
0
3
3
3
.5
1
2
3
17
11
Tim13-AMS4
Tim13
1 2 3 4 5 6 7 8 9
5 mM Ascorbate
% of Tim13 oxidized
100
80
60
40
20
0
0
1
2
3
4
time (hrs)
+GSH
+ascorbate

Figure 4. **Glutathione inhibits the oxidation of Tim13.** Treatment with reductant decreases the rate of Tim13 oxidation with Mia40 and Erv1. (A) Reduced Tim13 (15 μM) was incubated with combinations of Mia40 (1 μM) and Erv1 (1 μM) in a time course assay as indicated. Aliquots were removed at the indicated times and free thiols were blocked with AMS. Oxidized and reduced (Tim13-AMS_4) Tim13 were detected by nonreducing SDS-PAGE followed by immunoblotting with antibodies against Tim13. (B) As indicated in (A) except 5 mM of reduced glutathione was added. (C) As indicated in (A) except 5 mM of ascorbate was added.

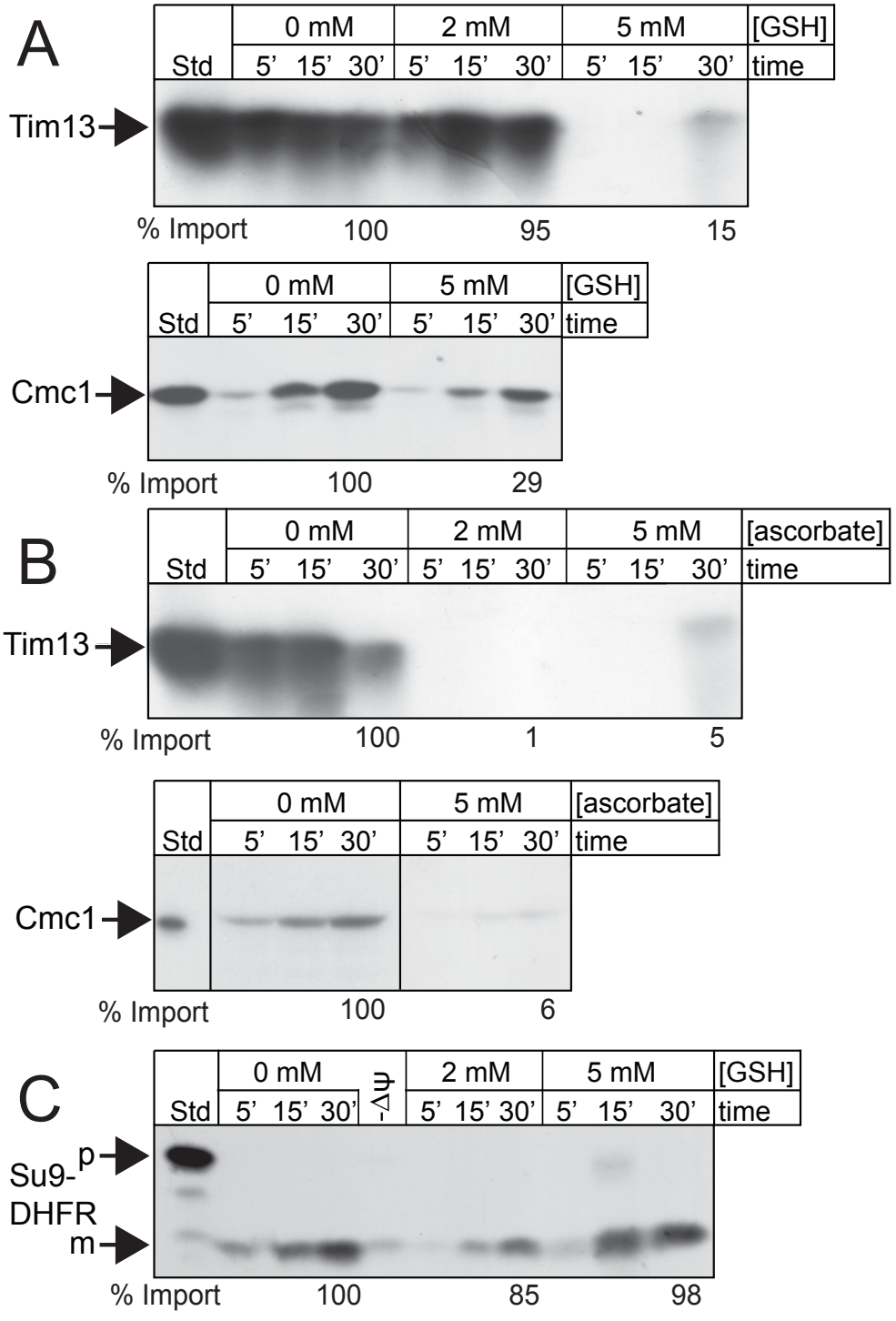
A
0 mM
2 mM
5 mM
[GSH]
Std
5' 15' 30'
5' 15' 30'
5' 15' 30'
time
Tim13
% Import
100
95
15
0 mM
5 mM
[GSH]
Std
5' 15' 30'
5' 15' 30'
time
Cmc1
% Import
100
29
B
0 mM
2 mM
5 mM
[ascorbate]
Std
5' 15' 30'
5' 15' 30'
5' 15' 30'
time
Tim13
% Import
100
1
5
0 mM
5 mM
[ascorbate]
Std
5' 15' 30'
5' 15' 30'
time
Cmc1
% Import
100
6
C
0 mM
-Δψ
2 mM
5 mM
[GSH]
Std
5' 15' 30'
5' 15' 30'
5' 15' 30'
time
Su9-DHFR
p
m
% Import
100
85
98

Figure 5. **Glutathione decreases the import of Cmc1.** (A) Cmc1 was incubated with mitochondria in the presence of varying concentrations of glutathione. Non imported protein was removed by protease and imported protein was analyzed by reducing SDS-PAGE and autoradiography. (B) As indicated in 'A' except that ascorbate was added to mitochondria. (C) As in 'A', except Su9-DHFR was imported in the presence of glutathione

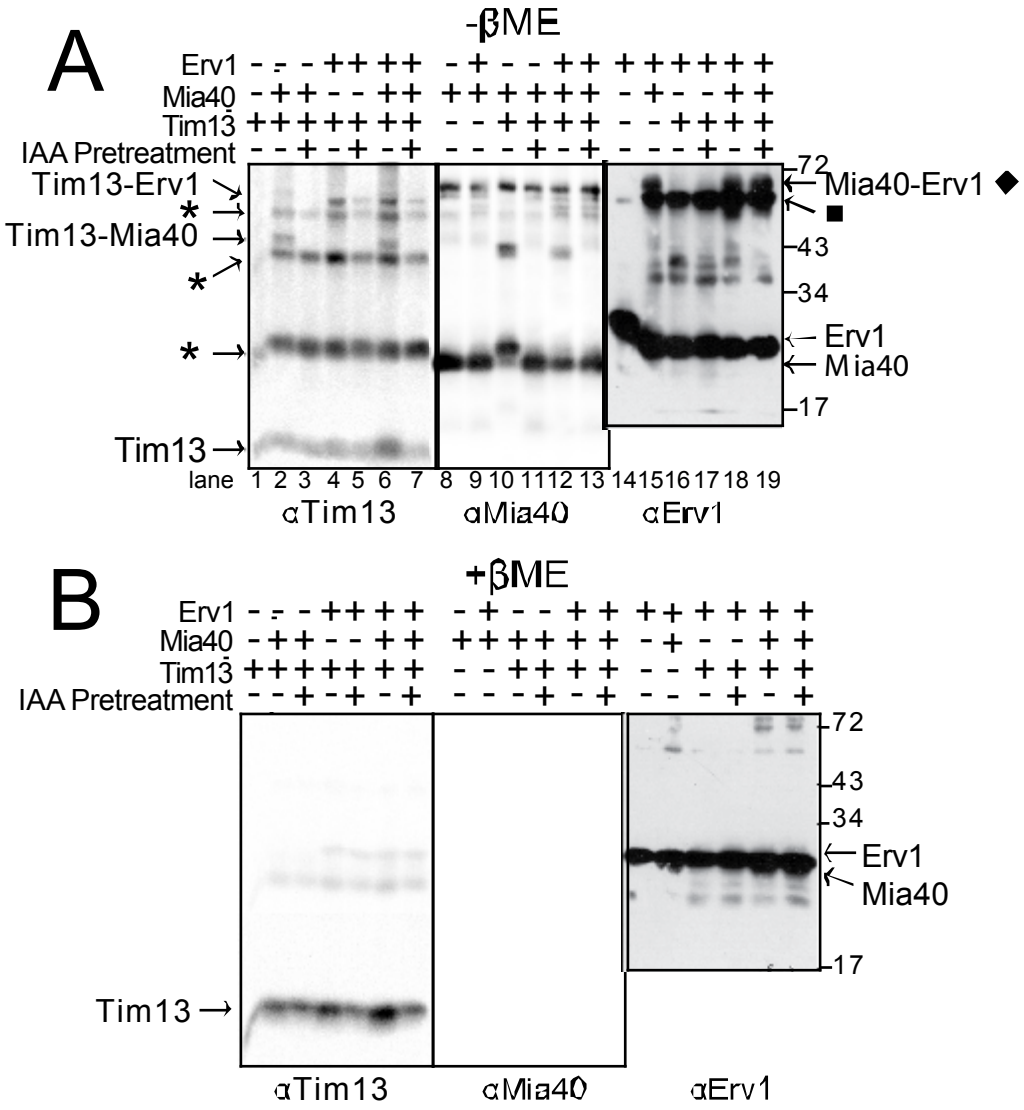

Figure 6. **Mixed disulfides of Tim13-Mia40 and Mia40-Erv1 were detected** (A) Mixed disulfides of Tim13-Mia40 and Mia40-Erv1 were detected in the presence of Tim13 (either pretreated or not pretreated with IAA), Mia40, and Erv1. Equimolar amounts of recombinant Mia40, Erv1 and reduced Tim13 were incubated together for 10 min followed by treatment with IAA. The mixture was separated on nonreducing (A) and reducing (B) SDS gels. Proteins were detected by immunoblotting with specific antibodies. As a control, lanes with the single proteins are included.

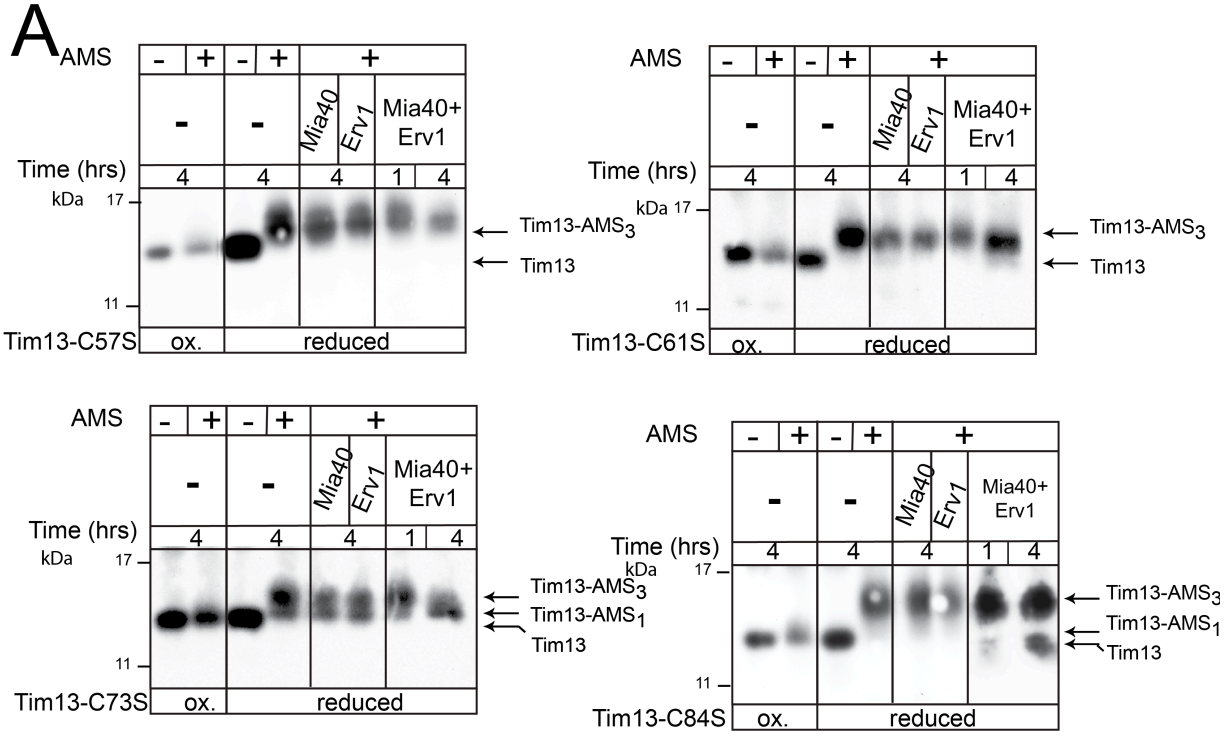
A
AMS
- + - + +
- - Mia40 Erv1 Mia40+ Erv1
Time (hrs)
4 4 4 1 4
kDa 17
11
Tim13-C57S
ox. reduced
Tim13-AMS3
Tim13
Tim13-C61S
Tim13-C73S
Tim13-AMS1
Tim13-C84S

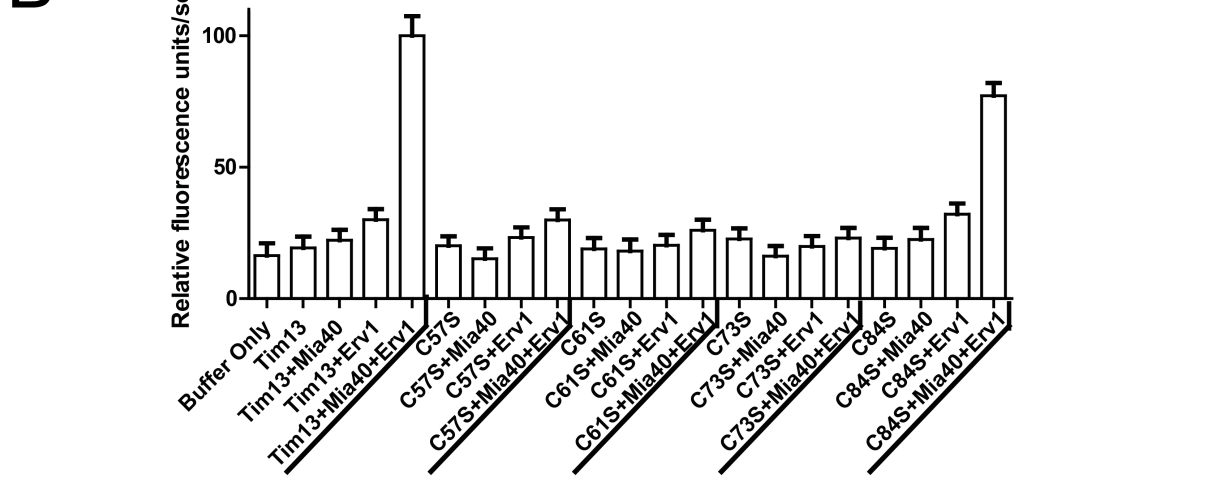
B
Relative fluorescence units/sec
100
50
0
Buffer Only
Tim13
Tim13+Mia40
Tim13+Erv1
Tim13+Mia40+Erv1
C57S
C57S+Mia40
C57S+Erv1
C57S+Mia40+Erv1
C61S
C61S+Mia40
C61S+Erv1
C61S+Mia40+Erv1
C73S
C73S+Mia40
C73S+Erv1
C73S+Mia40+Erv1
C84S
C84S+Mia40
C84S+Erv1
C84S+Mia40+Erv1

Figure 7. **C57, C61, C73 and C77 of Tim13 are required for oxidative folding by Mia40.** (A), (B), (C), and (D) Reduced mutants of Tim13 (C57S, C61S, C73S or C77S) were incubated with combinations of Mia40 (1μM) and Erv1 (1μM) in a time course assay as indicated. Aliquots were removed at the indicated times and free thiols on Tim13 mutants were blocked with AMS. Oxidized and reduced Tim13 (Tim13-AMS_3) were detected by nonreducing SDS-PAGE followed by immunoblotting with antibodies against Tim13. (D) As in (A) except H_2O_2 levels in the reconstitution assays were measured using the Amplex Red Hydrogen Peroxide/Peroxidase Assay kit. The Erv1-catalyzed reduction of O_2 to H_2O_2 was measured by a FlexStation plate reader via the SoftMax Pro software package.

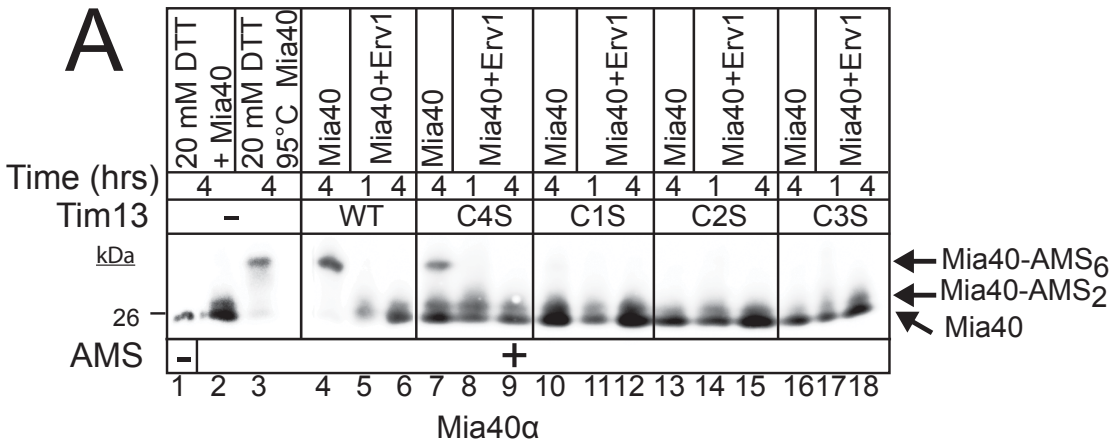
A
20 mM DTT + Mia40
20 mM DTT 95°C Mia40
Mia40
Mia40+Erv1
Time (hrs)
Tim13
WT
C4S
C1S
C2S
C3S
kDa
26
AMS
Mia40-AMS6
Mia40-AMS2
Mia40
1 2 3 4 5 6 7 8 9 10 11 12 13 14 15 16 17 18
Mia40α

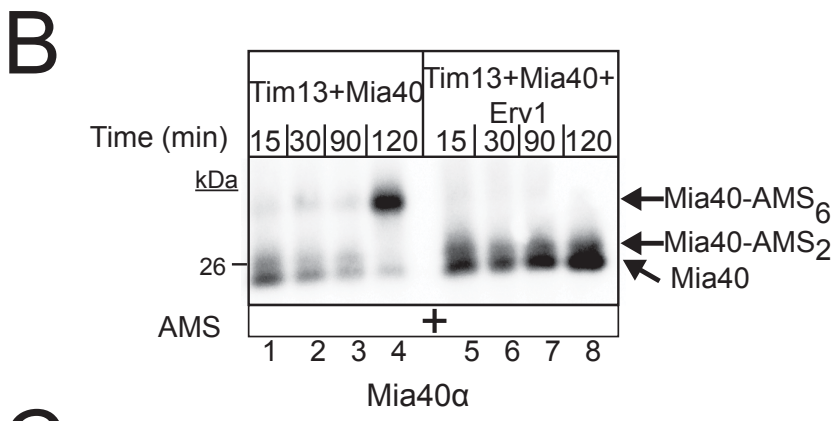
B
Tim13+Mia40
Tim13+Mia40+ Erv1
Time (min)
15 30 90 120
kDa
26
AMS
Mia40-AMS6
Mia40-AMS2
Mia40
1 2 3 4 5 6 7 8
Mia40α

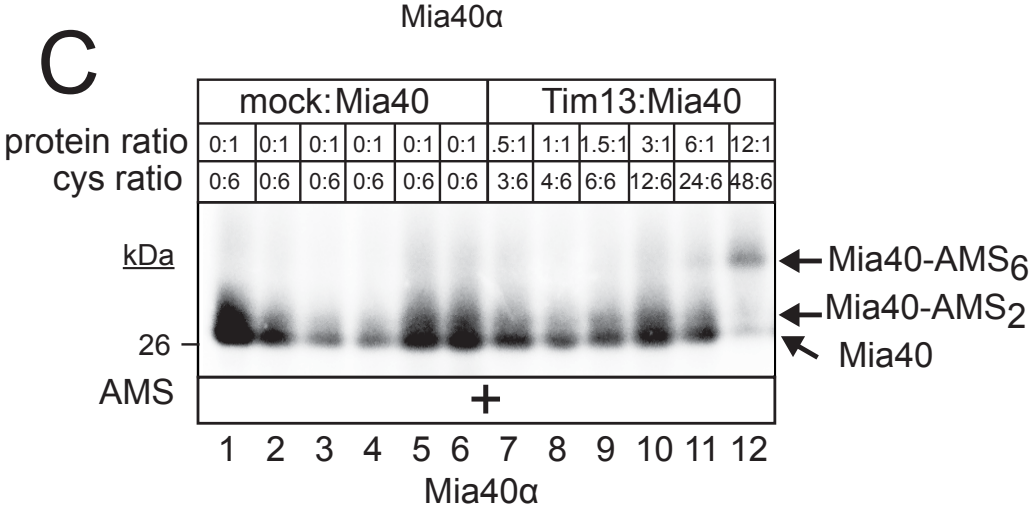
C
mock:Mia40
Tim13:Mia40
protein ratio
cys ratio
0:1 0:1 0:1 0:1 0:1 0:1 .5:1 1:1 1.5:1 3:1 6:1 12:1
0:6 0:6 0:6 0:6 0:6 0:6 3:6 4:6 6:6 12:6 24:6 48:6
kDa
26
AMS
Mia40-AMS6
Mia40-AMS2
Mia40
1 2 3 4 5 6 7 8 9 10 11 12
Mia40α

Figure 8. **Tim13 reduces six cysteines of Mia40.** (A) The redox state of Mia40 was determined by incubation of 15 μM reduced wild type or mutant Tim13 (C57S, C61S, C73S or C77S) with either 1 μM Mia40 alone or both 1 μM Mia40 and Erv1 followed by addition of AMS to free thiols of Mia40. The samples were resolved on nonreducing SDS-PAGE and immunoblotted with anti-Mia40. In control reactions, two AMS molecules were added to Mia40 samples reduced with 20 mM DTT and six AMS molecules were added for Mia40 samples reduced with 20 mM DTT and denatured at 95 ^{o}C. (B) As in (A) except reduced wild type Tim13(15 μM) was incubated with combinations of 1 μM Mia40 and 1 μM Erv1 in a time course assay as indicated. Aliquots were removed at the indicated times and free thiols on Mia40 were blocked with AMS. (C) As in (A) except the redox state of Mia40 was determined by titrating increasing amounts of reduced Tim13 in the presence of 1 μM Mia40 followed by addition of AMS to free thiols of Mia40. Protein ratios (Tim13:Mia40) and cysteine ratios (Tim13 cysteines:Mia40 cysteines) were listed as indicated.

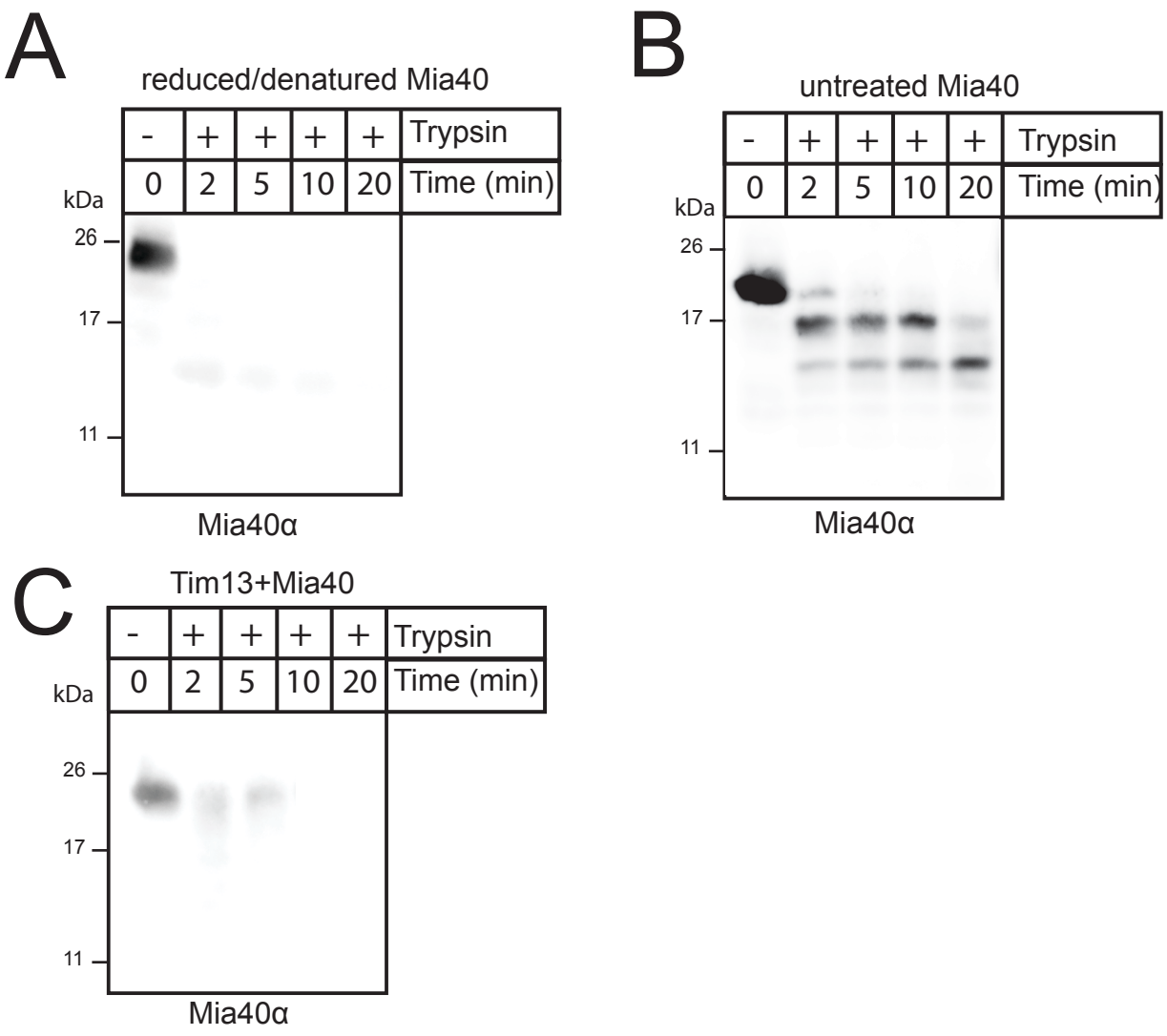

Figure 9. **Tim13 induces conformational changes of Mia40**. (A) Reduced Tim13 (15 μM) was incubated with Mia40 (1 μM) followed by addition of 5 μg/ml trypsin at 37°C. At the indicated period, aliquots were removed and soybean trypsin inhibitor was added. Samples were separated by SDS-PAGE followed by immunoblot analysis with antibodies against Mia40.

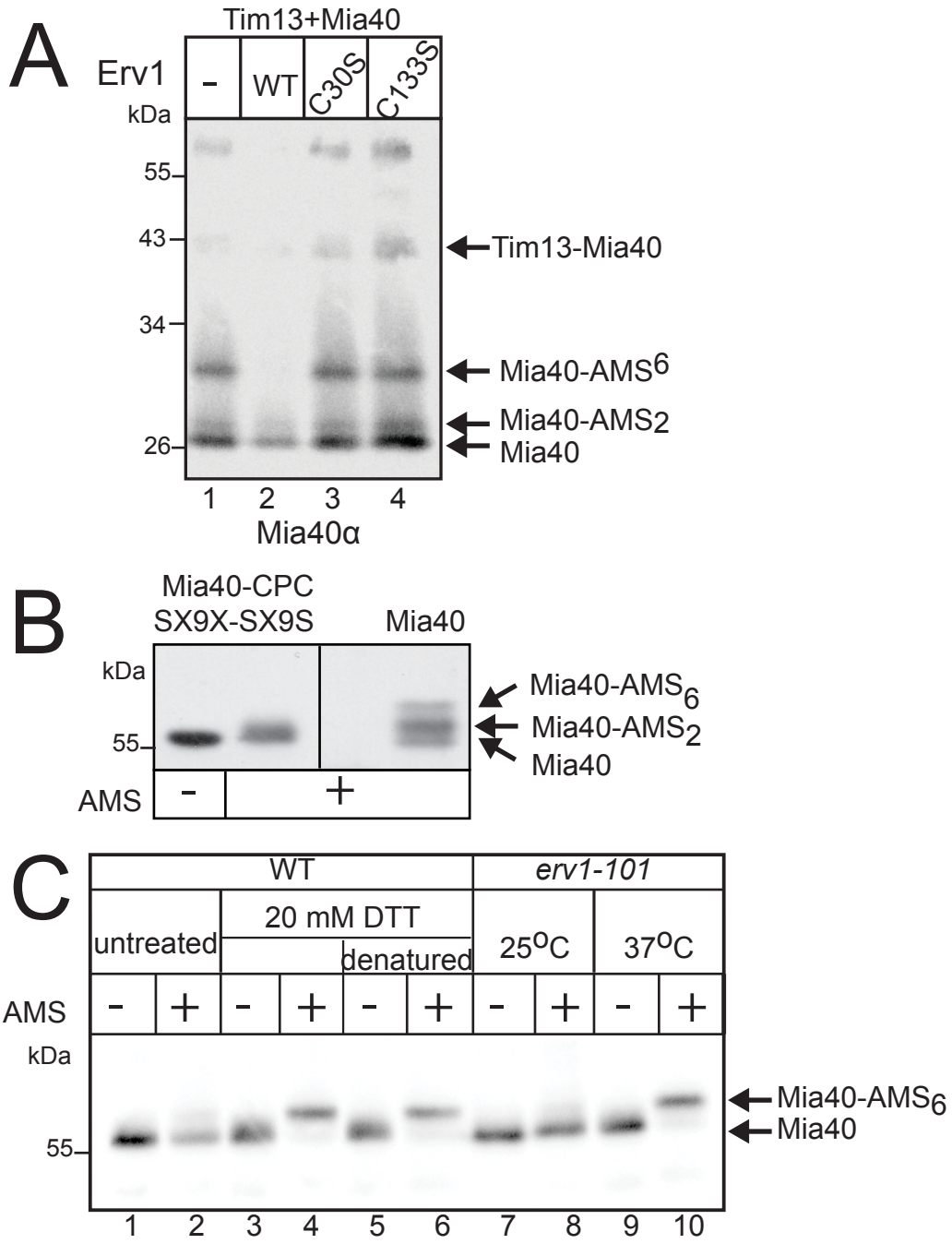
A
Tim13+Mia40
Erv1
-
WT
C30S
C133S
kDa
55
43
34
26
Tim13-Mia40
Mia40-AMS6
Mia40-AMS2
Mia40
1 2 3 4
Mia40α
B
Mia40-CPC
SX9X-SX9S
Mia40
kDa
55
Mia40-AMS6
Mia40-AMS2
Mia40
AMS
-
+
C
WT
erv1-101
untreated
20 mM DTT
denatured
25°C
37°C
AMS
- + - + - + - + - +
kDa
55
Mia40-AMS6
Mia40
1 2 3 4 5 6 7 8 9 10

Figure 10. **Mia40 remains in a reduced state with nonfunctional Erv**1. (A) The redox state of Mia40 was analyzed in the presence of wild type and Erv1 mutants (C30S or C133S) Reduced Tim13 (15 μM) was incubated with combinations of Mia40 (1 μM), Erv1 (1 μM), and mutant Erv1 (C133S or C30S, 1 μM). Aliquots were removed by 4 hours and free thiols on Mia40 were blocked with AMS. Oxidized and reduced Mia40 were detected by nonreducing SDS-PAGE followed by immunoblotting with antibodies against Mia40. (B) The redox state of Mia40 was investigated in mitochondria isolated from wild type and *erv1-101* yeast strains grown in permissive temperature (25^{o}C) or non-permissive temperature (37^{o}C). This was followed by an addition of AMS to the free thiols of Mia40. In control reactions, proteins in isolated wild type mitochondria were reduced with 20 mM DTT and/or denatured with .5% SDS and 8 M Urea. Mitochondrial proteins were resolved on nonreducing SDS-PAGE and immuno-blotted with anti-Mia40.

Supplemental Figures

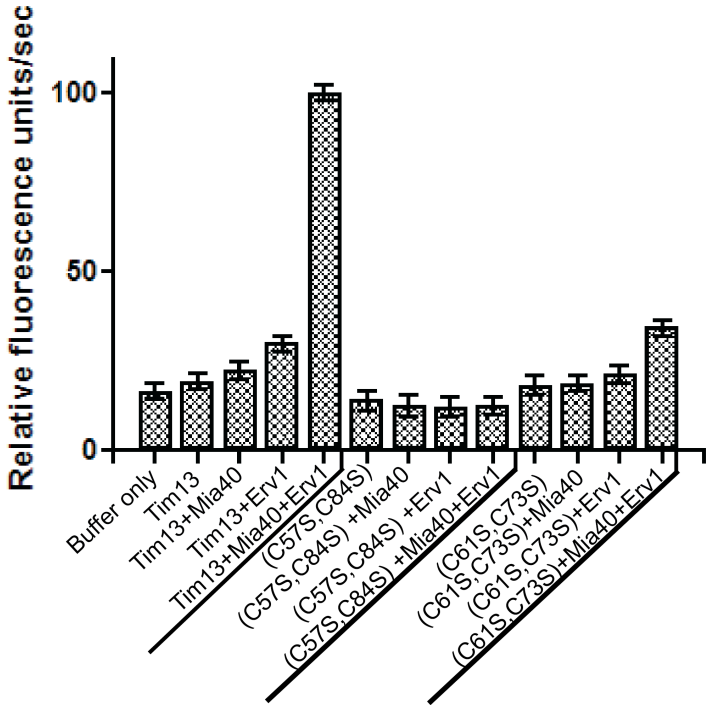

Figure 11 (S1). **In vitro reconstitution of Tim13 double mutants via Amplex Red assay.** As in Figure (4E) except Tim13 double mutants (C57S, C84S) and (C61S, C73S) were used.

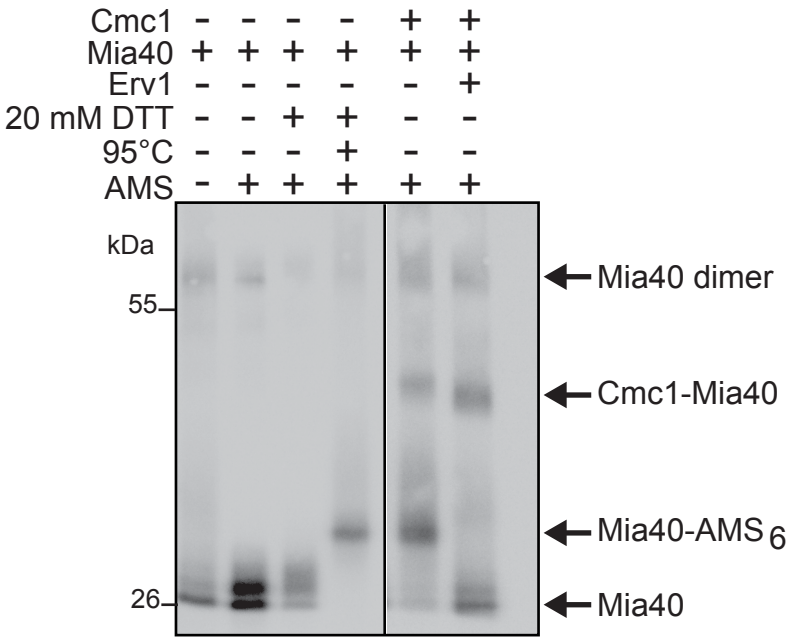

Figure 12 (S2) **Cmc1 reduces six cysteines of Mia40.** (A) The redox state of Mia40 was determined as in Fig. 8A except 15 µM of reduced Cmc1 was incubated with either 1 µM Mia40 alone or both 1 µM Mia40 and Erv1 followed by addition of AMS to free thiols of Mia40.

Appendix A: MALDI-Mass Spectrometry Data

untreated Mia40 (-NEM)

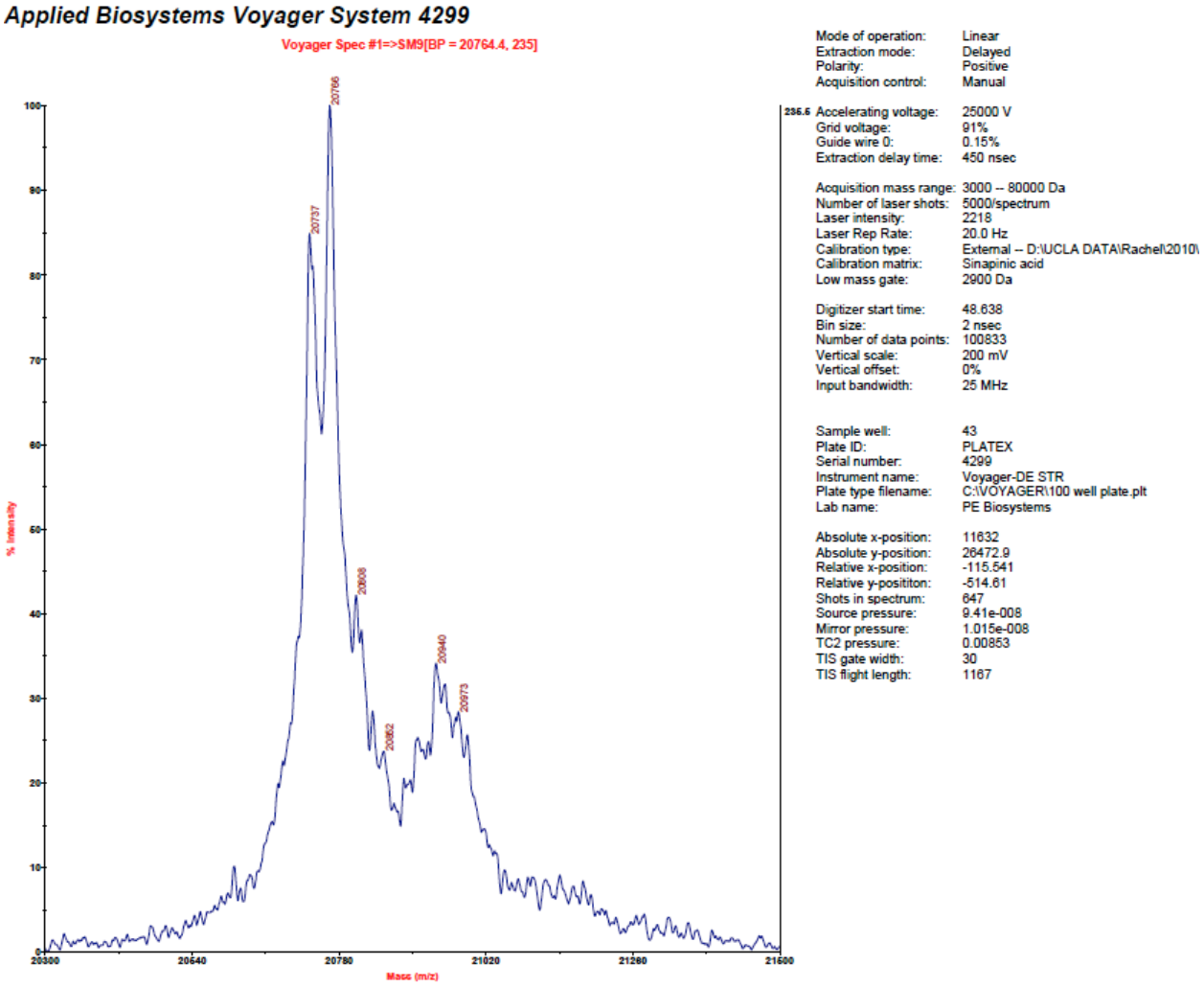

untreated Mia40 (+NEM)

Applied Biosystems Voyager System 4299

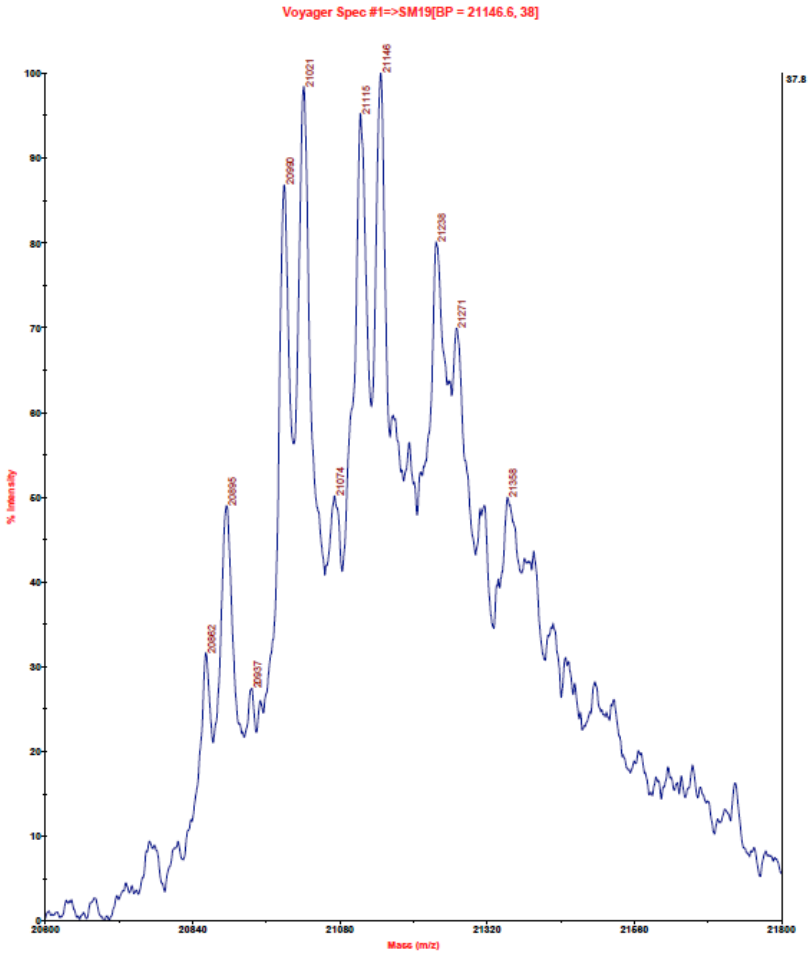

Mode of operation:	Linear
Extraction mode:	Delayed
Polarity:	Positive
Acquisition control:	Manual
Accelerating voltage:	25000 V
Grid voltage:	91%
Guide wire 0:	0.15%
Extraction delay time:	400 nsec
Acquisition mass range:	5200 -- 80000 Da
Number of laser shots:	5000/spectrum
Laser intensity:	1816
Laser Rep Rate:	20.0 Hz
Calibration type:	External -- D:\UCLA DATA\Rachel\2010\Koehler\
Calibration matrix:	Sinapinic acid
Low mass gate:	5000 Da
Digitizer start time:	64
Bin size:	2 nsec
Number of data points:	93130
Vertical scale:	200 mV
Vertical offset:	0%
Input bandwidth:	25 MHz
Sample well:	45
Plate ID:	PLATEX
Serial number:	4299
Instrument name:	Voyager-DE STR
Plate type filename:	C:\VOYAGER\100 well plate.plt
Lab name:	PE Biosystems
Absolute x-position:	21701.8
Absolute y-position:	27280.7
Relative x-position:	-205.671
Relative y-posititon:	293.242
Shots in spectrum:	1359
Source pressure:	4.74e-008
Mirror pressure:	6.817e-009
TC2 pressure:	0.00763
TIS gate width:	30
TIS flight length:	1167

reduced Mia40 (-NEM)

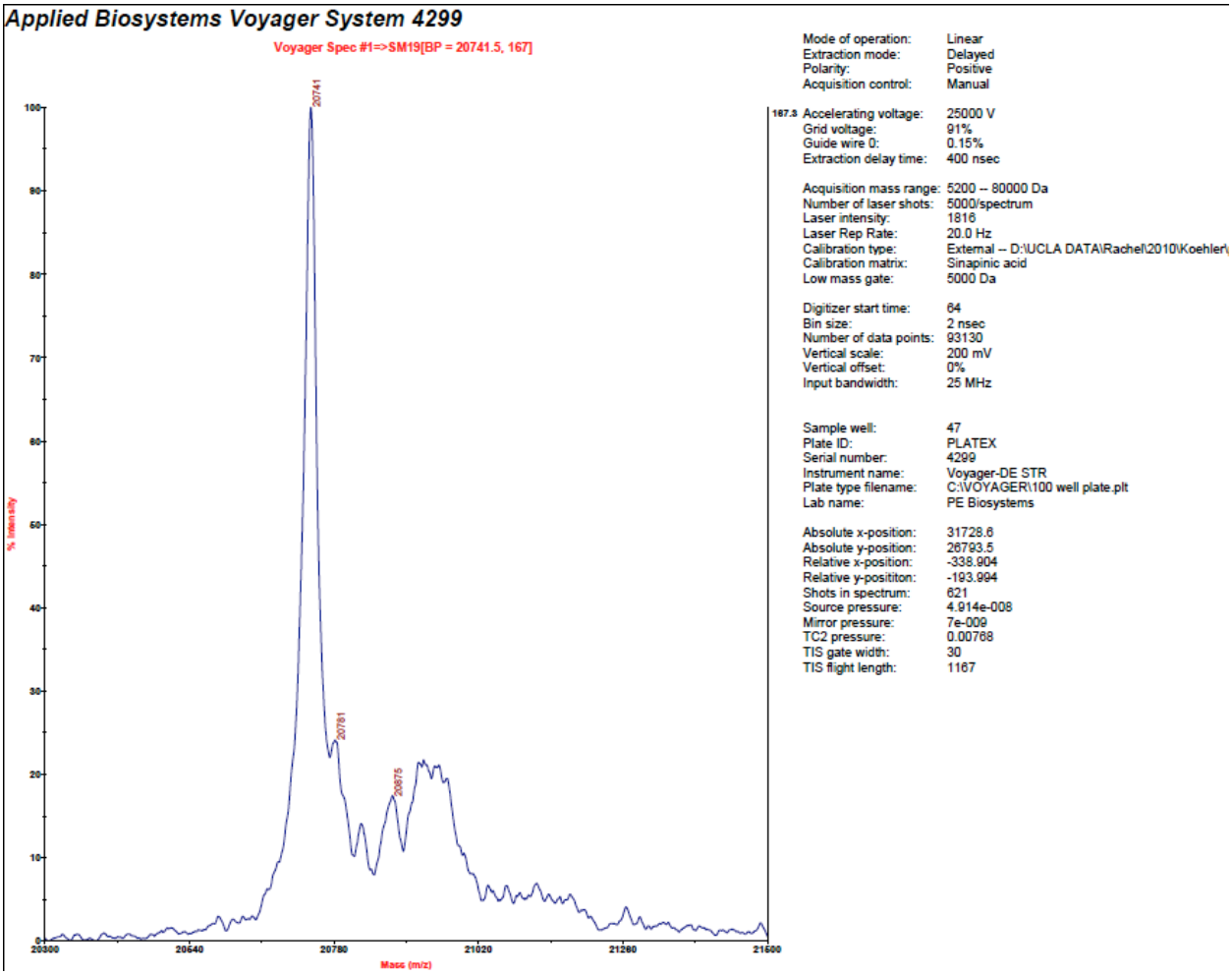

reduced Mia40 (+NEM)

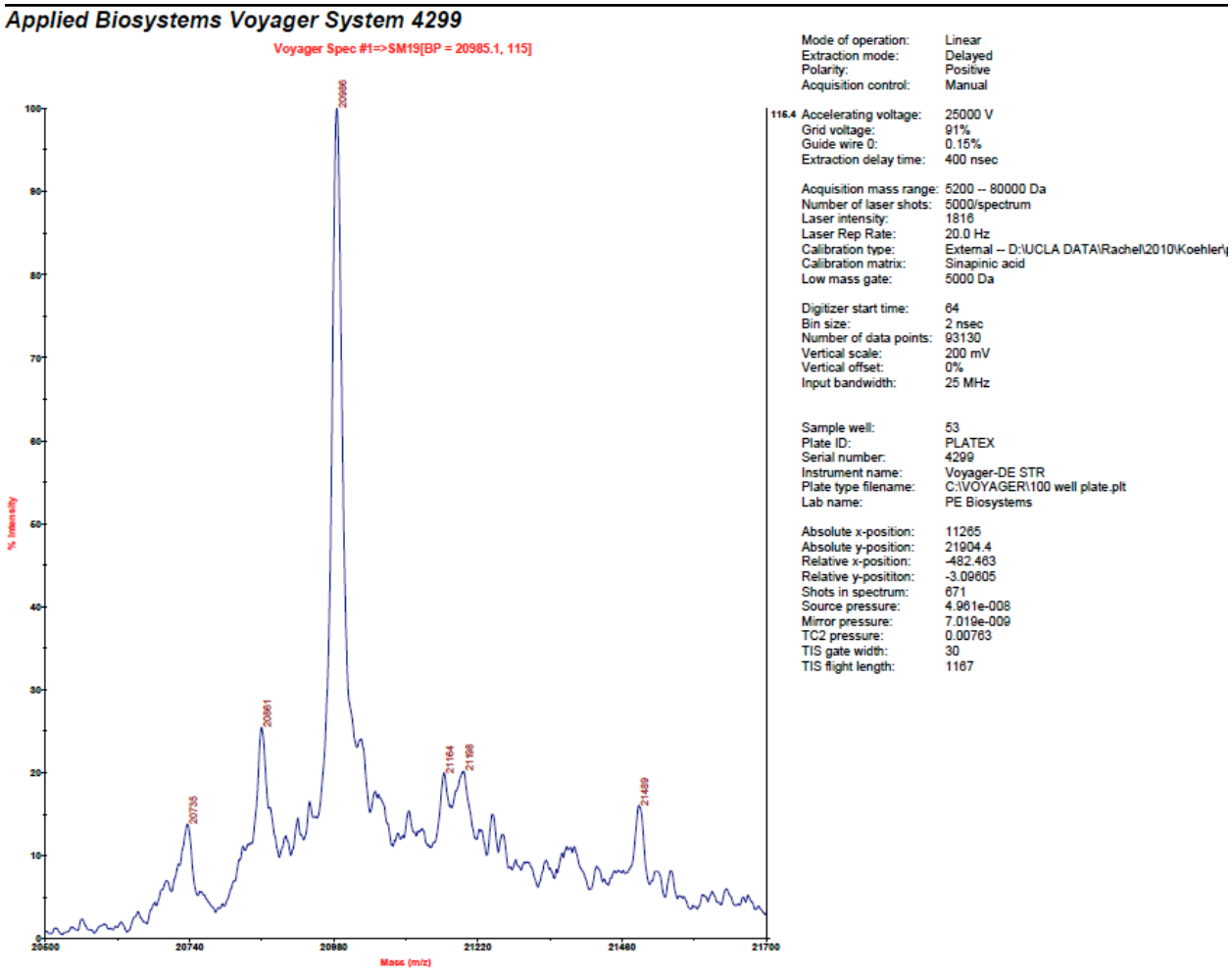

reduced & denatured Mia40 (-NEM)

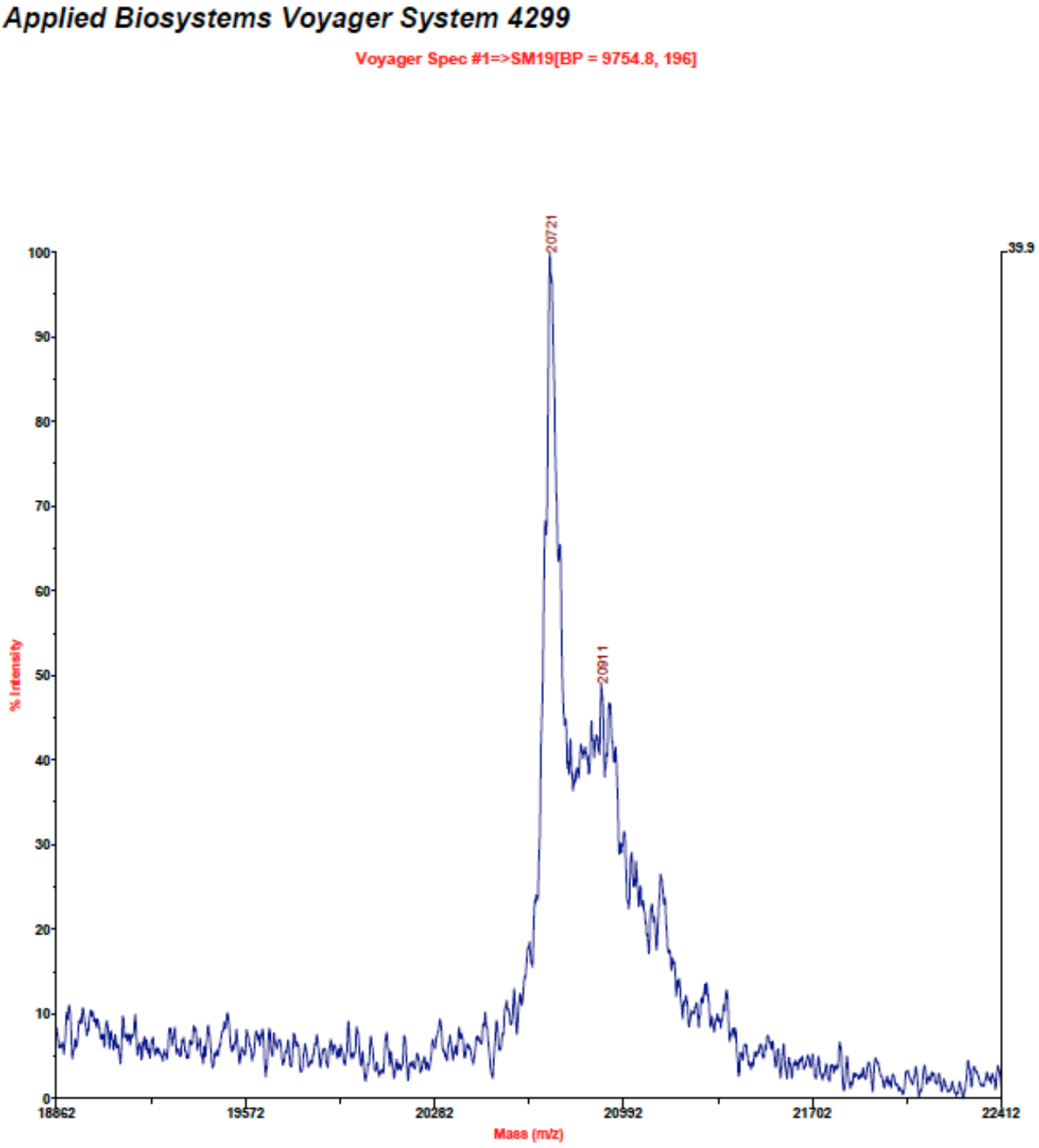

reduced & denatured Mia40 (+NEM)

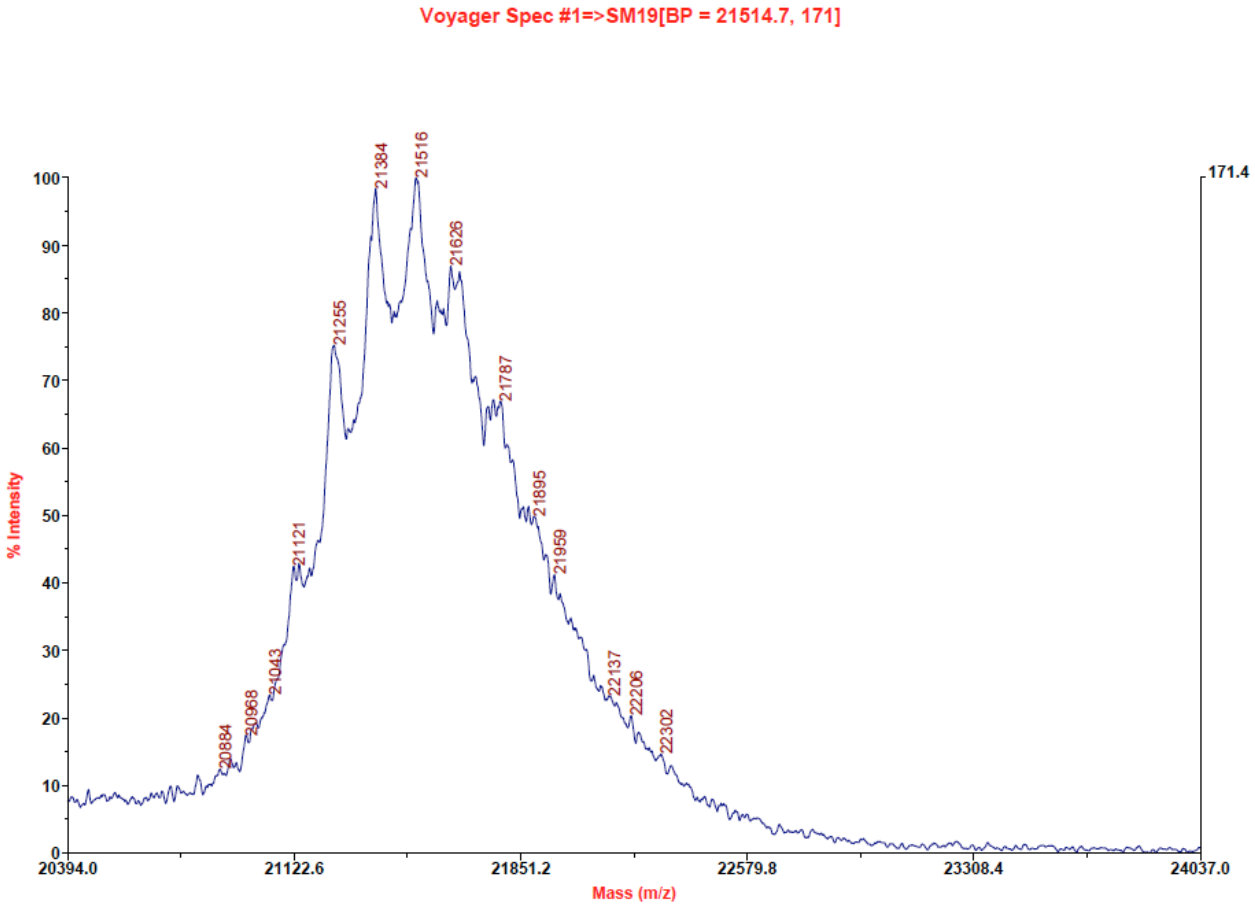

Tim13+Mia40 4:1 (-NEM)

Applied Biosystems Voyager System 4299

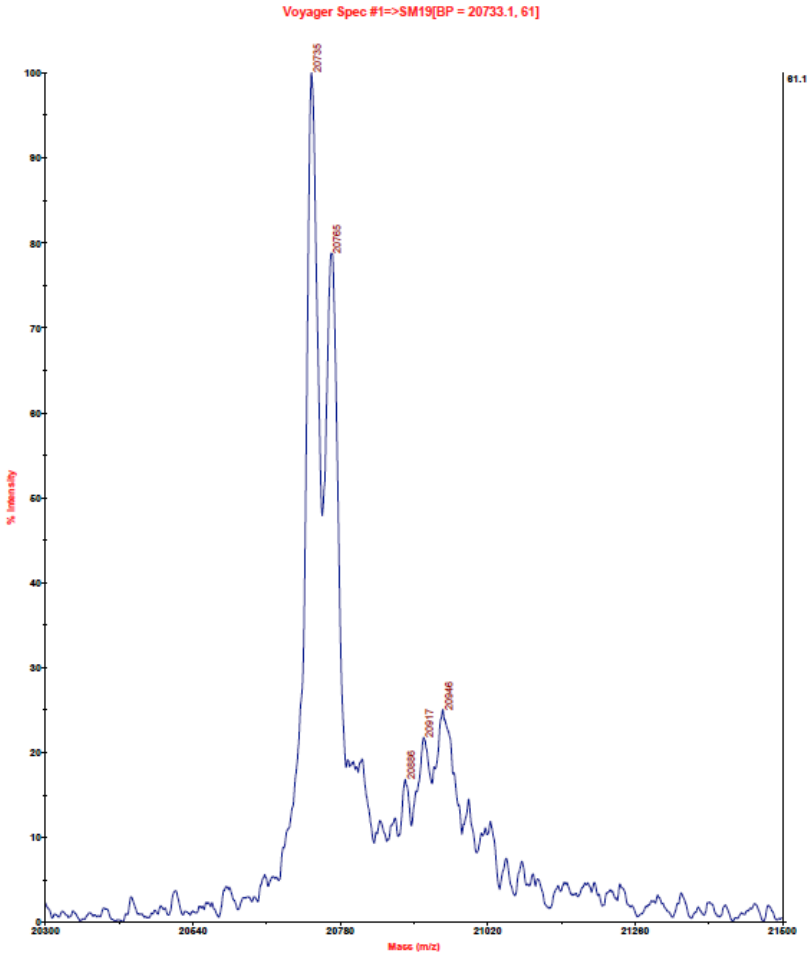

61.1

Mode of operation:	Linear
Extraction mode:	Delayed
Polarity:	Positive
Acquisition control:	Manual
Accelerating voltage:	25000 V
Grid voltage:	91%
Guide wire 0:	0.15%
Extraction delay time:	400 nsec
Acquisition mass range:	5200 -- 80000 Da
Number of laser shots:	5000/spectrum
Laser intensity:	1818
Laser Rep Rate:	20.0 Hz
Calibration type:	External -- D:\UCLA DATA\Rachel\2010\Koehler\
Calibration matrix:	Sinapinic acid
Low mass gate:	5000 Da
Digitizer start time:	64
Bin size:	2 nsec
Number of data points:	93130
Vertical scale:	200 mV
Vertical offset:	0%
Input bandwidth:	25 MHz
Sample well:	63
Plate ID:	PLATEX
Serial number:	4299
Instrument name:	Voyager-DE STR
Plate type filename:	C:\VOYAGER\100 well plate.plt
Lab name:	PE Biosystems
Absolute x-position:	11029.7
Absolute y-position:	16828.8
Relative x-position:	-717.773
Relative y-posititon:	1.27344
Shots in spectrum:	552
Source pressure:	6.037e-008
Mirror pressure:	7.709e-009
TC2 pressure:	0.00787
TIS gate width:	30
TIS flight length:	1167

Tim13+Mia40 4:1 (+NEM)

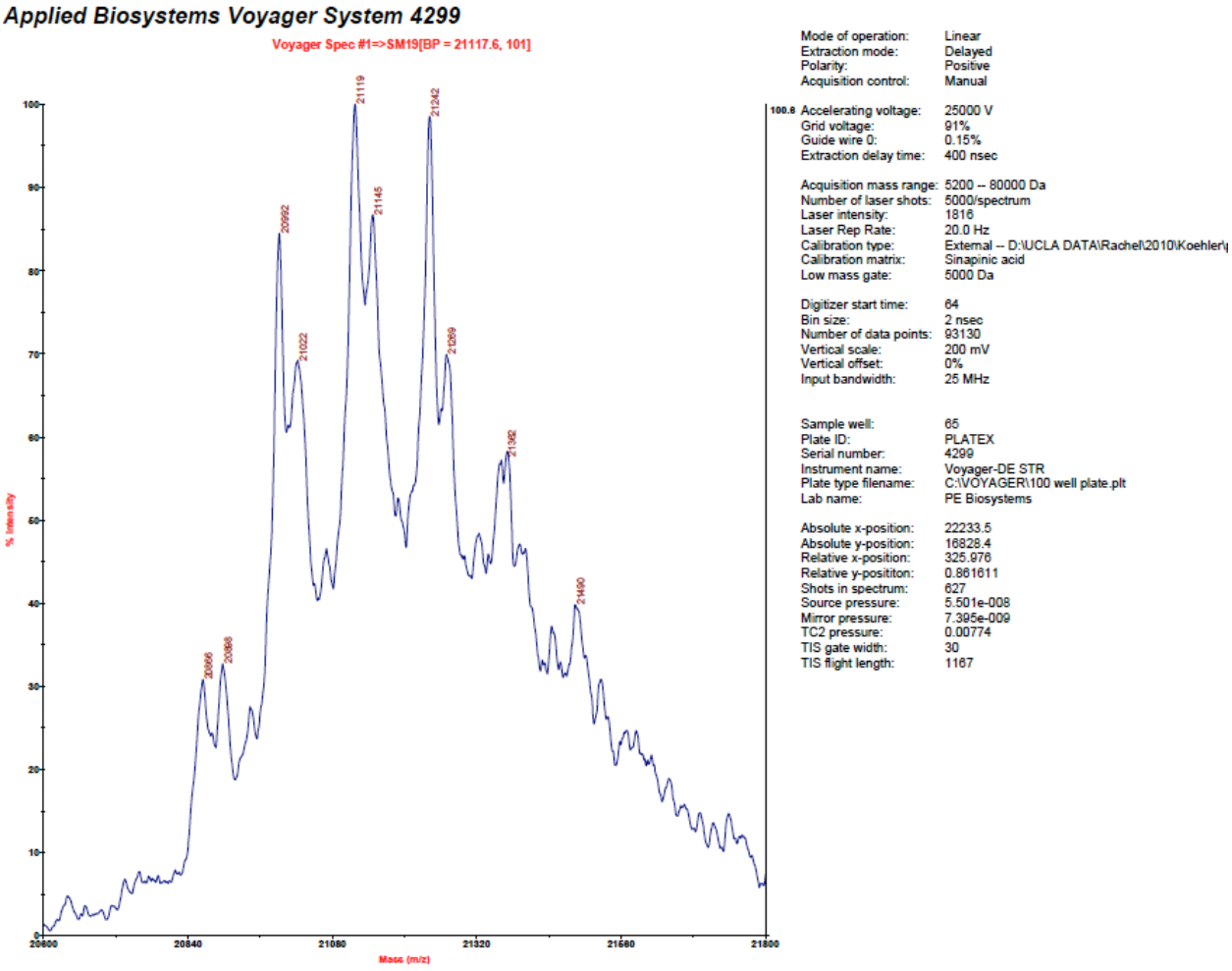

Tim13+Mia40 12:1 (-NEM)

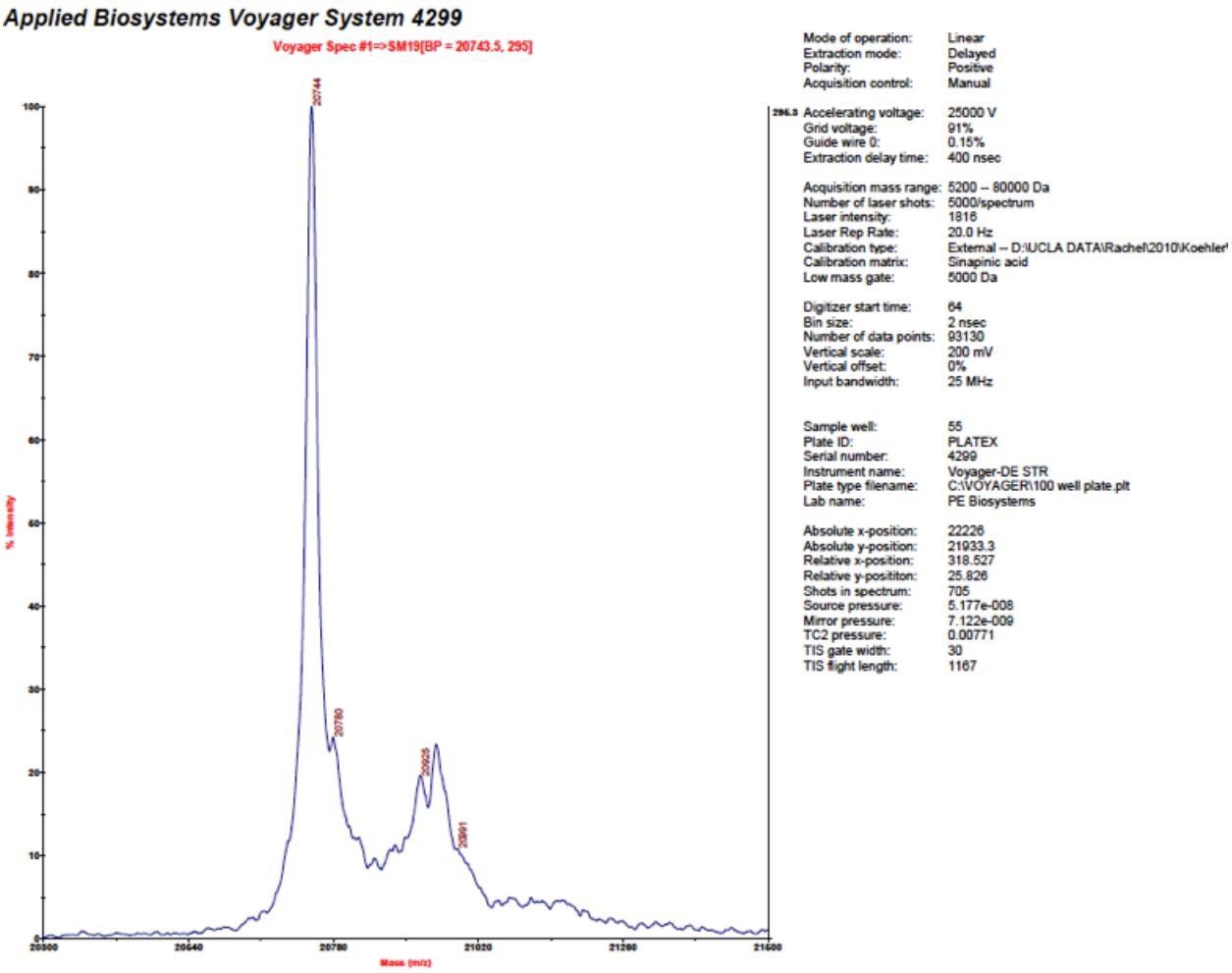

Tim13+Mia40 12:1 (+NEM)

Applied Biosystems Voyager System 4299

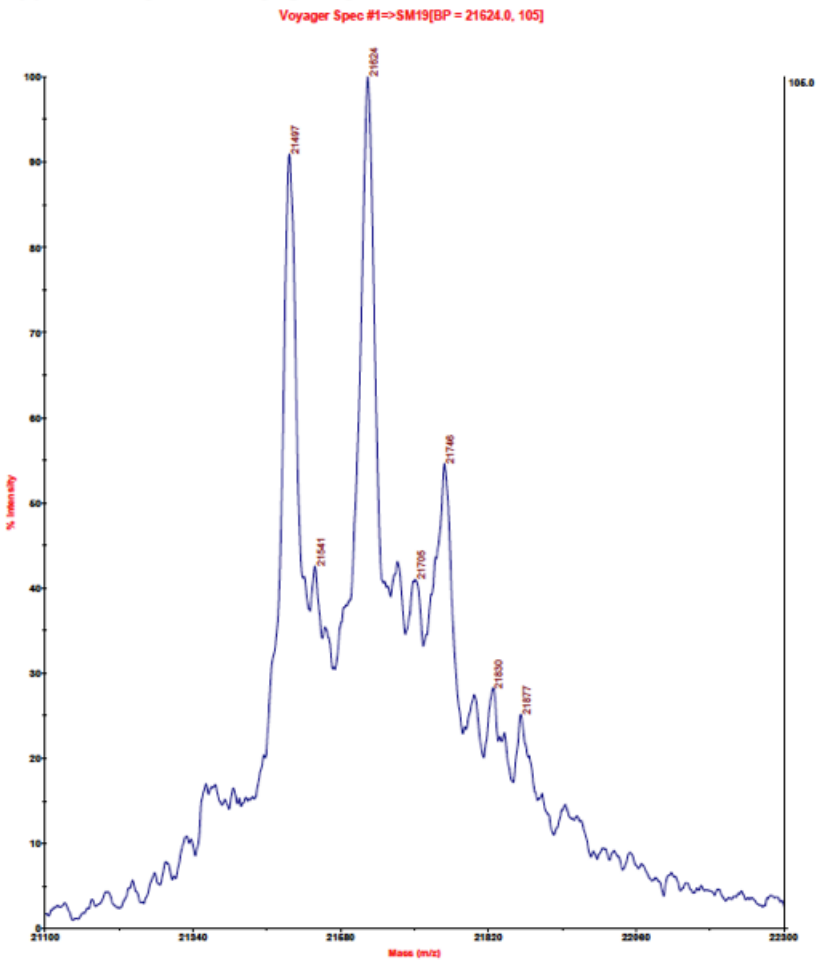

Mode of operation:	Linear
Extraction mode:	Delayed
Polarity:	Positive
Acquisition control:	Manual
105.0 Accelerating voltage:	25000 V
Grid voltage:	91%
Guide wire 0:	0.15%
Extraction delay time:	400 nsec
Acquisition mass range:	5200 -- 80000 Da
Number of laser shots:	5000/spectrum
Laser intensity:	1916
Laser Rep Rate:	20.0 Hz
Calibration type:	External -- D:\UCLA DATA\Rachel\2010\Koehler
Calibration matrix:	Sinapinic acid
Low mass gate:	5000 Da
Digitizer start time:	64
Bin size:	2 nsec
Number of data points:	93130
Vertical scale:	200 mV
Vertical offset:	0%
Input bandwidth:	25 MHz
Sample well:	57
Plate ID:	PLATEX
Serial number:	4299
Instrument name:	Voyager-DE STR
Plate type filename:	C:\VOYAGER\100 well plate.plt
Lab name:	PE Biosystems
Absolute x-position:	31947.4
Absolute y-position:	21732.2
Relative x-position:	-120.112
Relative y-posititon:	-175.348
Shots in spectrum:	760
Source pressure:	5.224e-008
Mirror pressure:	7.207e-009
TC2 pressure:	0.00779
TIS gate width:	30
TIS flight length:	1167

References

Banci, L., I. Bertini, C. Cefaro, L. Cenacchi, S. Ciofi-Baffoni, I.C. Felli, A. Gallo, L. Gonnelli, E. Luchinat, D. Sideris, and K. Tokatlidis. 2010. Molecular chaperone function of Mia40 triggers consecutive induced folding steps of the substrate in mitochondrial protein import. *Proceedings of the National Academy of Sciences of the United States of America*. 107:20190-5.

Banci, L., I. Bertini, C. Cefaro, S. Ciofi-Baffoni, A. Gallo, M. Martinelli, D.P. Sideris, N. Katrakili, and K. Tokatlidis. 2009. MIA40 is an oxidoreductase that catalyzes oxidative protein folding in mitochondria. *Nature structural & molecular biology*. 16:198-206.

Bauer, M.F., S. Hofmann, and W. Neupert. 2002. Import of mitochondrial proteins. *International review of neurobiology*. 53:57-90.

Bien, M., S. Longen, N. Wagener, I. Chwalla, J.M. Herrmann, and J. Riemer. 2010a. Mitochondrial disulfide bond formation is driven by intersubunit electron transfer in Erv1 and proofread by glutathione. *Molecular cell*. 37:516-28.

Bihlmaier, K., N. Mesecke, N. Terziyska, M. Bien, K. Hell, and J.M. Herrmann. 2007. The disulfide relay system of mitochondria is connected to the respiratory chain. *The Journal of cell biology*. 179:389-95.

Chacinska, A., and P. Rehling. 2004. Moving proteins from the cytosol into mitochondria. *Biochemical Society transactions*. 32:774-6.

Dabir, D.V., E.P. Leverich, S.-K. Kim, F.D. Tsai, M. Hirasawa, D.B. Knaff, and C.M. Koehler. 2007. A role for cytochrome c and cytochrome c peroxidase in electron shuttling from Erv1. *The EMBO journal*. 26:4801-11.

Grumbt, B., V. Stroobant, N. Terziyska, L. Israel, and K. Hell. 2007. Functional characterization of Mia40p, the central component of the disulfide relay system of the mitochondrial intermembrane space. *The Journal of biological chemistry*. 282:37461-70.

Herrmann, J.M., and K. Hell. 2005. Chopped, trapped or tacked--protein translocation into the IMS of mitochondria. *Trends in biochemical sciences*. 30:205-11.

Koehler, C.M. 2004. New developments in mitochondrial assembly. *Annual review of cell and developmental biology*. 20:309-35.

Koehler, C.M., and H.L. Tienson. 2009. Redox regulation of protein folding in the mitochondrial intermembrane space. *Biochimica et biophysica acta*. 1793:139-45.

Lu, H., S. Allen, L. Wardleworth, P. Savory, and K. Tokatlidis. 2004. Functional TIM10 chaperone assembly is redox-regulated in vivo. *The Journal of biological chemistry*. 279:18952-8.

Lutz, T., W. Neupert, and J.M. Herrmann. 2003. Import of small Tim proteins into the mitochondrial intermembrane space. *The EMBO journal*. 22:4400-8.

McCutcheon, J.P., and N.A. Moran. 2012. Extreme genome reduction in symbiotic bacteria. *Nature reviews. Microbiology*. 10:13-26.

Mesecke, N., N. Terziyska, C. Kozany, F. Baumann, W. Neupert, K. Hell, and J.M. Herrmann. 2005. A disulfide relay system in the intermembrane space of mitochondria that mediates protein import. *Cell*. 121:1059-69.

Pfanner, N., and N. Wiedemann. 2002. Mitochondrial protein import: two membranes, three translocases. *Current opinion in cell biology*. 14:400-11.

Rissler, M., N. Wiedemann, S. Pfannschmidt, K. Gabriel, B. Guiard, N. Pfanner, and A. Chacinska. 2005. The essential mitochondrial protein Erv1 cooperates with Mia40 in biogenesis of intermembrane space proteins. *Journal of molecular biology*. 353:485-92.

Sideris, D.P., N. Petrakis, N. Katrakili, D. Mikropoulou, A. Gallo, S. Ciofi-Baffoni, L. Banci, I. Bertini, and K. Tokatlidis. 2009. A novel intermembrane space-targeting signal docks cysteines onto Mia40 during mitochondrial oxidative folding. *The Journal of cell biology*. 187:1007-22.

Sideris, D.P., and K. Tokatlidis. 2007. Oxidative folding of small Tims is mediated by site-specific docking onto Mia40 in the mitochondrial intermembrane space. *Molecular microbiology*. 65:1360-73.

Sideris, D.P., and K. Tokatlidis. 2010. Oxidative protein folding in the mitochondrial intermembrane space. *Antioxidants & redox signaling*. 13:1189-204.

Stojanovski, D., D. Milenkovic, J.M. Müller, K. Gabriel, A. Schulze-Specking, M.J. Baker, M.T. Ryan, B. Guiard, N. Pfanner, and A. Chacinska. 2008. Mitochondrial protein import: precursor oxidation in a ternary complex with disulfide carrier and sulfhydryl oxidase. *The Journal of cell biology*. 183:195-202.

Terziyska, N., B. Grumbt, C. Kozany, and K. Hell. 2009. Structural and functional roles of the conserved cysteine residues of the redox-regulated import receptor Mia40 in the intermembrane space of mitochondria. *The Journal of biological chemistry*. 284:1353-63.

Tienson, H.L., D.V. Dabir, S.E. Neal, R. Loo, S.A. Hasson, P. Boontheung, S.-K. Kim, J.A. Loo, and C.M. Koehler. 2009. Reconstitution of the mia40-erv1 oxidative folding pathway for the small tim proteins. *Molecular Biology of the Cell*. 20:3481-3490.

Tokatlidis, K. 2005. A disulfide relay system in mitochondria. *Cell*. 121:965-7.

Chapter 3: Osm1 is a new electron acceptor for Erv1 in the mitochondrial intermembrane space

Introduction

Disulfide bonds are required for the correct folding of many proteins, particularly those that are secreted (Dutton et al., 2008; Mamathambika and Bardwell, 2008). Oxidative folding pathways are present in the periplasmic space of prokaryotes and the endoplasmic reticulum (ER) and mitochondrial intermembrane space (IMS) in eukaryotes (Depuydt et al., 2011). Whereas the components lack conservation at the sequence level, hallmarks of the pathway are similar across these systems.

The prokaryotic oxidative folding pathway has insertion and editing elements. Disulfide bonds are introduced by DsbA in the well characterized system of Gram-negative bacteria and DsbA is recycled by DsbB (Mamathambika and Bardwell, 2008). Electrons are then shuttled from DsbB to different aerobic and anaerobic electron acceptors via ubiquinone (Q) and menaquinone (MQ) (Bader et al., 1999; Takahashi et al., 2004). In aerobic conditions, Q passes electrons to cytochrome oxidase and oxygen (O_2), whereas in anaerobic conditions, MQ transfers electrons to fumarate or nitrate reductases. DsbC proofreads DsbA activity by removing non-native disulfide bonds (Rietsch et al., 1996). DsbC is maintained in a reduced state by membrane protein DsbD and electrons are provided by the thioredoxin system in the cytosol (Katzen and Beckwith, 2000). Finally, secreted glutathione (GSH) and cysteine contribute to the global redox equilibrium in the periplasm (Messens et al., 2007; Ohtsu et al., 2010).

The ER has the oxidoreductase, protein disulfide isomerase (PDI), that both inserts and edits disulfide bonds in imported ER proteins (Sevier and Kaiser, 2006). PDI is then maintained in an oxidized state by the sulfhydryl oxidase Ero1 and electrons are subsequently donated to O_2, generating hydrogen peroxide (Tu et al., 2000). Yeast also have a second sulfhydryl oxidase Erv2 that has an auxiliary role in oxidizing ER proteins (Sevier, 2012). In contrast, studies suggest that mammals may use vitamin K epoxide reductase, quiescin sulfhydryl oxidase, and/or peroxiredoxin IV as Ero1 alternatives (Mairet-Coello et al., 2004; Wajih et al., 2007; Zito et al., 2010). The redox environment, which supports the oxidation of cysteines, is -190 mV and is maintained with a ratio of reduced GSH to oxidized glutathione (GSSG) of 3:1 (Sevier et al., 2007). However, an anaerobic electron acceptor for the ER has not been specifically identified, although yeast can grow anaerobically; potential acceptors that have been suggested include free flavins, which can be reduced in vitro, or other small molecules (Gross et al., 2006).

The mitochondrial system consists of the oxidoreductase Mia40 and the sulfhydryl oxidase Erv1 (Allen et al., 2005; Chacinska et al., 2004; Koehler and Tienson, 2009; Mesecke et al., 2005; Naoe et al., 2004). Both proteins are essential for viability (Becher et al., 1999; Chacinska et al., 2004). Mia40 acts as a receptor in the IMS and inserts disulfide bonds into IMS substrates as they are imported (Grumbt et al., 2007). Substrates include proteins with the CX_3C motif (the small Tim proteins) and the CX_9C motif (a subset function in cytochrome oxidase assembly) (Gabriel et al., 2007; Longen et al., 2009). Electrons are passed from Mia40 to Erv1, and a ternary complex with substrate transiently assembles (Stojanovski et al., 2008). Erv1 shuttles electrons to either O_2 or cytochrome (cyt *c*) (Bihlmaier et al., 2007; Dabir et al., 2007). O_2 subsequently forms hydrogen peroxide and cyt *c* donates electrons to the electron transport system or to Ccp1. Whereas the two terminal electron acceptors function in aerobic conditions, a

potential anaerobic electron acceptor has not been identified (Dabir et al., 2007; Herrmann and Riemer, 2012).

Considering anaerobic electron acceptors, two candidates in *Saccharomyces cerevisiae* are the fumarate reductases Frd1 and Osm1 that use a non-covalently bound $FADH_2$ to reduce fumarate to succinate (Enomoto et al., 2002; Muratsubaki and Enomoto, 1998). Frd1 is a soluble cytosolic enzyme, whereas the Osm1 enzymatic activity has been localized to mitochondria and Osm1 has a putative mitochondrial targeting sequence (Enomoto et al., 2002; Muratsubaki and Enomoto, 1998). Expression of Frd1 is induced in anaerobic conditions, but Osm1 is expressed constitutively; Frd1 provides the most fumarate reductase activity under anaerobic conditions. Nevertheless, a *Δfrd1Δosm1* strain fails to grow under anaerobic conditions whereas the single mutants grow (Arikawa et al., 1998; Camarasa et al., 2007). Frd1 and Osm1 likely play an overall role in controlling redox balance, potentially through the reoxidation of NADH or $FADH_2$ for the regeneration of the FAD-prosthetic group of essential flavoprotein enzymes (Arikawa et al., 1998; Camarasa et al., 2007).

Given that Osm1 was localized to mitochondria, we considered a potential role as a terminal electron acceptor for Erv1, playing a crucial role in anaerobic conditions. Here we report that Osm1 showed dual localization to microsomes and the mitochondrial IMS. Moreover, Osm1 accepted electrons from Erv1 using in vitro reconstitution assays in which reduced Tim13 was oxidized. Both Osm1 and cyt *c* functioned equally well in accepting electrons from Erv1 and cyt *c* expression was induced in cells lacking *osm1*. Thus, Osm1 is a new terminal electron acceptor that may be coordinately regulated with cyt *c*.

Results

osm1 and *erv1* are synthetic lethal in anaerobic conditions

Under aerobic conditions, Erv1 donates electrons to O_2 or cyt *c*. However, the *erv1* mutant is viable under anaerobic conditions (Dabir et al., 2007), suggesting that an acceptor for anaerobiosis is required. We used a candidate approach and considered the fumarate reductase Osm1 as a potential anaerobic electron receptor, because it is reported to have a location within the mitochondrion (Muratsubaki and Enomoto, 1998). It was reported that a *Δosm1* strain grew slowly under anaerobic conditions, whereas the double *Δfrd1Δosm1* mutant failed to grow (Enomoto et al., 2002). Deletion of *osm1* in our parental strain did not display any marked growth defects in aerobic or anaerobic conditions (Fig. 1A). We predicted that Osm1 would display synthetic lethality with a temperature-sensitive *erv1* mutant under anaerobic conditions. We therefore crossed *Δosm1* and *erv1-101* and analyzed growth of the tetrads under anaerobic conditions (Fig. 1B). The *Δtim54* strain was included as a control because it is petite-negative and does not grow anaerobically (Hwang et al., 2007). In aerobic conditions, all strains including the mutants grew, although strains with the *erv1-101* allele showed compromised growth. In anaerobic conditions all strains, with the exception of *Δtim54* and the double mutant *erv1-101Δosm1*, grew. Thus, the *erv1-101Δosm1* displayed synthetic lethality, suggesting that Osm1 and Erv1 genetically interacts in anaerobic conditions.

Osm1 localizes to microsomes and the mitochondrial IMS

Frd1 is likely cytosolic, but the location of Osm1 within mitochondria has not been reported (Muratsubaki and Enomoto, 1998). We localized Frd1 and Osm1 in spheroplasts (Fig. 2A,B). Tagged constructs were generated in which Frd1 and Osm1 contained a C-terminal myc

tag. Lysates from spheroplasts were subject to differential centrifugation and analyzed by SDS-PAGE and immunoblotting. Analyzed fractions included the pellet from the 13K spin (mitochondria) and the supernatant (cytosol) and pellet (microsomes) from the 40K spin. Immunoblotting with appropriate markers, Erv1 for mitochondria, Hsp70 for cytosol, and protein disulfide isomerase (PDI) for ER, verified integrity of the fractionation. Frd1 localized to the cytosol, as expected (Fig. 2B). However, Osm1 was detected in both the microsomal and mitochondrial fractions (Fig. 2A). The mitochondrial form migrated at a lower molecular mass, likely because the targeting sequence was cleaved by a processing protease (Muratsubaki and Enomoto, 1998). An identical localization pattern for Osm1 was also detected in WT cells using a polyclonal antibody against Osm1 (Fig. S1A, indicating that the myc tag does not interfere with localization. In addition, Osm1 translocation into isolated mitochondria was tested (Fig. 2C). Osm1 import into WT mitochondria was dependent on a membrane potential ($\Delta\Psi$). In addition, Osm1 was imported into *erv1-101* mitochondria with decreased efficiency.

The dual localization of Osm1 to mitochondria and microsomes is atypical (Karniely and Pines, 2005). However, Osm1 may function with Ero1 or the homolog Erv2 that resides in the ER (Gerber et al., 2001; Sevier et al., 2001). Indeed, a synthetic lethal interaction was reported for *ero1-1* and Δ*osm1* (Costanzo et al., 2010). A likely strategy to attain dual localization is that the N-terminus may contain a mitochondrial targeting sequence followed by a hydrophobic region that may traffick Osm1 to the ER, as has been reported for cytochrome P4502B1 (Anandatheerthavarada et al., 1999). Analysis of the Osm1 N-terminus indicated that amino acids 1-32 have properties of a typical mitochondrial targeting sequence (Omura, 1998), including clustering of the positive residues as well as clustering of hydrophobic residues (Fig. S1B,C). In addition, a hydrophobic patch was identified from region 32-60 that could direct Osm1 to the ER (Fig S1B) (Walter and Johnson, 1994). We appended DHFR to Osm1 amino

acids 1-32 (Osm1$^{1-32}$-DHFR-myc) and 1-60 Osm1 (Osm1$^{1-60}$-DHFR-myc) and localized the resulting fusion proteins when expressed in WT yeast (Fig. 2D,E). Amino acids 1-32 targeted DHFR exclusively to the mitochondria, whereas amino acids 1-60 targeted DHFR to both ER and mitochondria. Thus, the 32 N-terminal residues directed Osm1 to the mitochondria and the following hydrophobic region conferred targeting to the ER. Osm1 is another example of a protein that functions in more than one compartment.

Osm1 localization with the mitochondria was investigated in detail (Fig. 3A). Mitochondria from the WT strain were subjected to osmotic shock to disrupt the outer membrane; mitoplasts that contain the matrix and intact inner membrane were separated from the soluble IMS contents by centrifugation and protease treatment verified localization to the IMS. Osm1 and IMS control Mia40 associated with the mitoplast pellet, but were sensitive to protease in the mitoplast fraction, indicating a location facing the IMS. In contrast, matrix controls Tim44 and aconitase were protected from protease and recovered in the mitoplast pellet fraction. Mitoplast analysis was also coupled with the in vitro import assay (Fig. S2). Imported Osm1 and Mia40 were sensitive to protease, confirming residency in the IMS. However, Su9-DHFR was protected from protease, because of localization to the matrix. Osm1 association with the membrane was also tested using carbonate extraction over pH range 10.5 to 12.5 (Fig. 4B) (Fujiki et al., 1982); integral membrane proteins are recovered in the pellet fraction vs. peripheral and soluble proteins that are recovered in the supernatant. Osm1 was released to the supernatant at pH 10.5 to 11, in contrast to integral membrane proteins Mia40 and Tim23 that were released at a pH of 12 to 12.5. Taken together, Osm1 is a peripheral membrane protein of the IMS.

Osm1 is a peripheral protein in the ER and is able to accept electrons from Erv2

Osm1's localization to the microsome suggests that it is able to accept electrons from Erv2, a homolog of Erv1. Osm1's association with the ER membrane was tested using carbonate extraction. Osm1 was readily released to the supernatant at pH 11.5, in contrast to the soluble protein, PDI, which was recovered in the supernatant fraction in all the pH range tested(Fig.3A). Just like the mitochondria, Osm1 is a peripheral protein in the ER. Next, we tested if Erv2 is able to shuttle electrons directly to Osm1. The O_2 electrode was used to determine if Osm1/fumarate could compete with O_2 during the oxidation of the nonphysiological substrate DTT (Fig. 3B). Using a Hansatech O_2 electrode, fumarate, Osm1, and Erv2 were added to the buffer. Excess DTT was added to initiate the electron transfer process and O_2consumption was measured overtime. Notably, rate of O_2 consumption was decreased in the presence of increasing amounts of Osm1/fumarate in comparison to O_2 alone. This suggests that Osm1/fumarate is able to compete with O_2 in accepting electrons from Erv2. In all, Osm1 is a peripheral protein of the ER and is able to accept electrons directly from Erv2.

Osm1 and Erv1 are partner proteins

Because Osm1 may accept electrons from Erv1, we investigated whether they might be partner proteins (Fig. 5A). The Erv1-His strain was used in which Erv1 contains a C-terminal His tag (Dabir et al., 2007). Mitochondria were purified, solubilized in 1 % digitonin, and subjected to pull-down experiments with Ni^{2+} agarose. Similar to cyt *c*, a subset of Osm1 co-purified with Erv1; in contrast, Osm1 did not co-purify with the untagged Erv1 (Fig. 5B). Thus, Osm1 and Erv1 form a complex in the IMS.

Erv1 transfers electrons to Osm1

Osm1 may accept electrons from Erv1. We used the in vitro reconstitution system with minimal components to test if Osm1 facilitated oxidation of Tim13 (Tienson et al., 2009). Tim13

oxidation was monitored over a 4-h time course by the addition of AMS followed by nonreducing SDS-PAGE and immunoblot analysis with anti-Tim13 antibodies (Fig. 6A). The alkylating agent 4-acetamido-4'-maleimidylstilbene-2,2'-disulfonic acid (AMS) binds to reduced cysteine residues and increases the molecular mass by 0.5 kDa. Reduced Tim13 acquired 4 AMS molecules, whereas the absence of AMS addition indicated that Tim13 was oxidized (Fig. 6A). In agreement with published studies (Tienson et al., 2009), excess Tim13 (15 μM) was oxidized over a 4-h time period in the presence of 1 μM Mia40 and 1 μM Erv1, with O_2 being used as a terminal electron acceptor. The addition of 1 μM Osm1 partially oxidized Tim13, but the inclusion of excess fumarate (20 μM) markedly increased the oxidation rate of Tim13 oxidation to 30 min, because Osm1 transfers electrons from fumarate to generate succinate. In a series of control reactions, the addition of Osm1, fumarate, and Osm1/fumarate to reduced Tim13 did not directly oxidize Tim13 (Fig. 6B). Increasing the concentration of Osm1 in the reconstitution assay from 1 to 2-4 μM correlated with a decrease in the rate of Tim13 oxidation to less than 30 min (Fig. 6B).

We also used the O_2 electrode to determine if Osm1/fumarate could effectively compete with O_2 during the oxidation of the nonphysiologic substrate DTT (Fig. S3), as was done previously to show that cyt *c*/Ccp1 was more efficient at accepting electrons from Erv1 than O_2 (Dabir et al., 2007). Subsequent additions of fumarate, Osm1, and Erv1 along with appropriate controls were added to a buffer that contained excess substrate DTT and reduction was measured by the consumption of O_2. As shown in Fig. S3A,D, the rate of O_2 consumption was decreased in the presence of Osm1/fumarate in comparison to O_2, indicating that Osm1 effectively competes with O_2 to accept electrons. Moreover, control reactions that lacked Erv1 but contained Osm1, fumarate, or Osm1/fumarate supported that Osm1 did not directly oxidize DTT and that Erv1 was required (Fig. S3B). Finally, in a comparison reaction with cyt *c*/Ccp1

addition, the decreased rate of O_2 consumption with cyt *c*/Ccp1was similar to that of Osm1/fumarate (Fig. S3C,D), confirming that Osm1 and cyt *c* are similarly efficient in accepting electrons from Erv1 in vitro. In addition to cyt *c,* Erv1 thus shuttles electrons to Osm1.

Osm1 and Cyt *c* are poised to accept electrons from Erv1

We propose that Erv1 is able to shuttle electrons to either Osm1 or cyt *c*. Thus, we compared Tim13 oxidation in the presence of cyt *c* vs. Osm1/fumarate (Fig. 7A). As shown previously, when the terminal electron acceptor was O_2, Tim13 essentially remained oxidized in the 30 min assay, instead requiring approximately 4 hours. However, Osm1/fumarate oxidized Tim13 more quickly than cyt *c*, suggesting both electron acceptors may work in vivo (Fig. 7A). Taken together, both cyt *c* and Osm1 are poised to accept electrons from Erv1 in the mitochondrial IMS. It was reported that Δ*cyc3erv1* failed to grow anaerobically(Dabir et al., 2007). Deletion of *cyt c* in our parental strain did not display marked growth defects in aerobic conditions (Fig. 7B). However, we observed a slight growth defect in Δ*cyc3* grown anaerobically in the absence of the mitochondrial genome (Fig. 7B). We then predicted that Osm1 mutant would display a synthetic lethality with cyt *c* mutant grown in anaerobic conditions. We crossed *Δosm1* and Δ*cyc3* and analyzed growth of the tetrads under aerobic vs. anaerobic conditions in the presence and absence of the mitochondrial genome (Fig. 7C). In aerobic and anaerobic conditions, all strains including the double mutant *Δosm1Δcyc3* grew (Fig. 7C). Taken together, using our parental strain, we were unable to observe marked growth defects in Δ*osm1Δcyc3* grown anaerobically suggesting the possibility of additional electron acceptors of Erv1 that has not been identified.

Osm1 and cyt *c* regulates the redox state of Mia40

Previously it has been shown that depletion of Erv1 activity leads to increased sensitivity to reducing agents such as DTT. Since Osm1 and cyt *c* are postulated to function downstream of Erv1 in anaerobic conditions, we tested DTT sensitivity in Δ*osm1,* Δ*cyc3* and Δ*osm1Δcyc3* strains in aerobic and anaerobic conditions. In aerobic conditions, we observed no changes either in the DTT sensitivity or in the sensitivity against oxidizing agents such as diamide or hydrogen peroxide in Δ*osm1,* Δ*cyc3* and Δ*osm1Δcyc3* strains (Fig. 8, Fig. S4). In anaerobic conditions, we also observed no changes in sensitivity against the oxidizing agents, diamide or hydrogen peroxide. In anaerobic conditions, while Δ*cyc3* didn't show no changes in its growth profile*,* Δ*osm1* and Δ*osm1Δcyc3* showed a marked increase in DTT-sensitivity (Fig. 8). The DTT sensitivity was analogous to our Erv1 mutant control harbouring a cysteine point-mutation at C30. Taken together, in contrast to cyt *c,* Osm1 has a greater influence in regulating the redox state of Erv1.

Coordinated regulation of terminal electron acceptors

In contrast to Frd1 with expression that is induced during anaerobiosis, Osm1 is constitutively expressed, which suggests that Osm1 may function under both aerobic and anaerobic conditions (Camarasa et al., 2007). Because cyt *c* and Osm1 both function as electron acceptors, we investigated the abundance of cyt *c* in *Δosm1* cells grown aerobically in rich glucose medium (YPD) at 25°C. Increasing amounts of mitochondrial proteins were separated by SDS-PAGE followed by immunoblot analysis with a variety of antibodies against mitochondrial proteins (Fig. 6A). The abundance of general marker proteins such as α-ketoglutarate dehydrogenase (KDH), Tim22, and Tim54 was not altered in cells deleted for *osm1*. In addition, steady state levels of Erv1, Tim9, and Tim13 were equal in the WT and

Δosm1 mitochondria. However, the abundance of cyt *c* was markedly increased in *Δosm1* mitochondria. Subsequently, we investigated the abundance of Osm1 in *Δcyc3* in cells grown aerobically in YPD at 25°C. While steady-state levels of Erv1, Tim9, and Tim13 were equal in WT and *Δcyc3* mitochondria, there was a marked increase in Osm1 steady-state levels. In addition, while steady-state levels of Tim9 and Tim13 were equal in both WT and *Δosm1Δcyc3* mitochondria,the steady-state level of Erv1 was markedly increased. Taken together, the expression of terminal electron acceptors seems to be coordinately regulated.

Discussion

Prokaryotic cells have a wide range of terminal electron acceptors for both aerobic and anaerobic conditions, enabling the cell to maintain oxidative folding in the periplasm across diverse environmental conditions (Mamathambika and Bardwell, 2008). Whereas electron acceptors have been identified for aerobic conditions in eukaryotes, questions still remain about strategies in the anaerobic state. Here we show that yeast have a new protein Osm1 that can fill this gap.

Osm1 is a potential terminal electron acceptor in the ER

Surprisingly, Osm1 has dual localization to the ER and the mitochondria. Whereas a large number of proteins show dual localization, most proteins localize to the mitochondria and cytosol or nucleus (Karniely and Pines, 2005). A few proteins have been identified that localize to both the ER and mitochondria including the tail-anchored protein cytochrome b_5 and cytochrome P4502B1, which has targeting sequences for both ER and mitochondria (Anandatheerthavarada et al., 1999; Hwang et al., 2004). General analysis of the N-terminal targeting region suggests that the N-terminal 32 amino acids function as a classical

mitochondrial targeting sequence that is cleaved upon import (Muratsubaki and Enomoto, 1998) and this sequence does directed DHFR to the mitochondria in vivo (Fig 2D). Amino acids 32-60 are rich in hydrophobic residues that may target the precursor to the ER (Walter and Johnson, 1994). Indeed, fusing amino acids 32-60 directed DHFR to both the mitochondria and ER (Fig. 2E). A competition between targeting factors as the nascent chain of Osm1 emerges from the ribosome may potentially direct Osm1 to different compartments (Raue et al., 2007); alternatively, ER vs. mitochondrial distribution could be regulated by other factors such as redox, stress, or nutritional status (Karniely and Pines, 2005).

In yeast, Osm1 in the ER may function as a terminal electron acceptor, especially in anaerobic conditions because the only well characterized acceptor is O_2 (Tu and Weissman, 2004). Electrons may be shuttled from Ero1 or the yeast specific sulfhydryl oxidase Erv2, which is a homolog of Erv1 (Sevier, 2012). Indeed, the O_2 assay shows that Erv1 is able to shuttle electrons directly to Osm1 (Fig. 3B). Having an anaerobic acceptor in yeast is important because the organism grows anaerobically. A fumarate reductase has not been identified for mammals. Potentially, an anaerobic acceptor is not required because cells are not typically anaerobic except in pathogenic conditions such as ischemia reperfusion (Blaisdell, 2002). However, human embryonic stem cells originate from the blastocyst inner cell mass (Thomson et al., 1998), which is in a hypoxic microenvironment estimated at 1.5 – 5.3% in the mammalian reproductive tract (Dunwoodie, 2009); thus, free O_2 may be limiting. As a result, mammals may have alternative oxidases, which is likely because ERO-1 deficient cells were surprisingly viable (Zito et al., 2010). In this case, proposed oxidases include vitamin K epoxide reductase, quiescin sulfhydryl oxidase, and/or peroxiredoxin IV (Mairet-Coello et al., 2004; Wajih et al., 2007; Zito et al., 2010) that, in addition to O_2, may shuttle electrons to potential anaerobic acceptors such as free flavins, which can be reduced in vitro, or other small molecules (Gross et al., 2006).

Osm1 is a terminal electron acceptor in the mitochondrial IMS

Osm1 is a soluble protein in the mitochondrial IMS and import is dependent upon the presence of a membrane potential. Like cyt *c*, a fraction of Osm1 assembles in a complex with Erv1 (Fig. 5). This is likely a transient interaction as electrons can be shuttled from Erv1 to Osm1 in vitro (Fig. 6). Because Osm1 is expressed in both aerobic and anaerobic conditions and lacks obvious growth defects (Fig. 1A), Osm1 likely functions in both aerobic and anaerobic conditions. A synthetic lethal interaction between *erv1-101* and *Δosm1* was observed in anaerobic conditions (Fig. 1B), and a similar synthetic lethality was reported with temperature-sensitive *erv1* mutants and cyt *c* (Allen et al., 2005; Dabir et al., 2007). It is difficult to interpret why Erv1 and cyt *c* showed synthetic lethality under anaerobic conditions as cyt *c* transfers electrons to the electron transport chain or Ccp1 and ultimately O_2 (Dabir et al., 2007); however, this may be caused by pleiotropic defects associated with the *erv1* mutants. Because Osm1 uses fumarate as an electron acceptor to generate succinate, it is poised to function anaerobically. Suprisingly, we did not observe obvious growth defects in *Δosm1Δcyc3* strains grown aerobically and anaerobically. However, we were able to observe a different phenotype amongst all the strains upon DTT treatment in anaerobic conditions. Whereas *Δcyc3* was slightly sensitive to DTT, *Δosm1* and *Δosm1cyc3* strains were extremely sensitive towards DTT (Fig. 8B). This phenotype was analogous to the C30S *erv1* mutant strain, which suggests that Osm1 has a greater control on the redox state of Erv1 in comparison to cyt *c*. In addition, yeast seemingly has a network to regulate expression of terminal electron acceptors because cyt *c* and Osm1 were upregulated in *Δosm1* and *Δcyc3* cells respectively (Fig. 9A,B).

Because Osm1 is absent in mammals, the presence of other anaerobic electron acceptors is an open question. In trypanosomes, a homologous fumarate reductase has been identified in

the glycosome, a peroxisomal-like organelle, which maintains glycosomal NAD^+/NADH balance (Besteiro et al., 2002). Again, mammals may not require an acceptor as cells are never truly anaerobic, but taking clues from the ER, other systems may also function. To this end, the peroxiredoxin family is large and peroxiredoxin 3 and 5 have been localized to the mitochondrial matrix (Cox et al., 2010). In addition, small molecules such as GSH/GSSG may also mediate disulfide bond formation in anaerobic conditions (Bien et al., 2010). As well as prokaryotes, yeast has diverse terminal electron acceptors in the IMS.

Materials and Methods

Cloning General cloning procedures were used in making the constructs. Osm1 with a C-terminal Myc tag was cloned into pRS425, using yeast genomic DNA isolated from GA74-6A strain as a template and using a 5' primer immediately upstream of the open reading frame of Osm1 and a 3' primer containing the Myc tag immediately downstream of the stop codon. Osm1 with a C-terminal His_9 tag was cloned into pRS426, using yeast genomic DNA as a template and by using a 5' primer that was immediately upstream of the open reading frame and a 3' primer containing the His tag, immediately downstream of the stop codon. Osm1-Myc and Osm1-His_6 were amplified by PCR and cloned into the BamHI and SalI sites of pRS425 and pRS426 respectively

For studies involving the expression and purification of the truncated version of recombinant OSM1(starting at amino acid 23), Osm1 was subcloned into pET28a vector (Novagen) using isolated Osm1-myc construct (QIAGEN) as a template and 5' primer and a 3' primer that was immediately downstream of the stop codon. Truncated Osm1 was amplified by PCR and cloned into the BamHI and SalI sites of pET28a.

The sequences of all constructs were verified by sequencing (Agencourt). Sequences of primers are available upon request.

Yeast Strains The parental *S. cerevisiae* yeast strain used in the study was GA74-6A and GA74-1A. To generate the yeast strain Δ*osm1*::*LEU2* in GA74-6A, we used the leucine cassette within pUG73 provided by Euroscarf (Frankfurt, Germany) (Gueldener, Heinisch, Koehler, Voss, & Hegemann, 2002). In brief, the cassette contained the LEU2 gene flanked by 45 bp of upstream and downstream OSM1 sequence. The linearized DNA was transformed into yeast GA74-6A via the LiCl transformation technique(Gietz, St Jean, Woods, & Schiestl, 1992) and grown in rich or

selective media. Δ*cyc31*::*URA3* was generated the same way as Δ*osm1*::*LEU2* except pUG72 containing the uracil cassette was used. To generate a yeast strain co-expressing Erv1-His_9 and Osm1-myc, Osm1-myc was subcloned into the BamHI and SalI sites of pRS426 and transformed into Erv1-His_6 yeast strain and grown in selective media. To see a list of strains used in this study, see Table 1.

Protein Expression and Purification Recombinant Mia40, Erv1, Erv2 and Osm1 were expressed and purified under native conditions as previously described(Dabir et al., 2007; Tienson et al., 2009). In brief, His_6Tim13, His_6Mia40, His_6Erv1, and His_6Osm1 was transformed into BL21-CodonPlus (DE3)-RIL *Escherichia coli (*Stratagene) and expressed via IPTG induction in 2YT medium(1.6% Tryptone, .5% Yeast Extract, .5% NaCl, and 10 mM Tris 7.4 for 4 hours at 30^{o}C. His_6Mia40, His_6Erv1, and His_6Osm1 were purified under native conditions using Ni2+-agarose (QIAGEN) according to manufacturers' instructions. The proteins were dialyzed in MPP buffer (20 mM Tris-HCl, pH 7.0, 150 mM KCl, and 1 mM EDTA) at 4^{o}C overnight. In addition, recombinant Tim13 was purified under denaturing conditions with 8 M Urea (QIAGEN) and reduced with 20 mM DTT as previously described(Tienson et al., 2009). For all recombinant proteins, protein concentration was measured by the Bradford method using bovine serum albumin as the standard. In addition, for Tim13 and Mia40, the protein concentrations were determined by their absorbance at 280 nm. The extinction coefficients for Tim13 and Mia40 were calculated to be .903 M^{-1} cm^{-1} and .9054 M^{-1} cm^{-1} respectively. For Erv1, the protein concentration was determined via FAD content. The extinction coefficients was calculated at 275 nm(72,684 M^{-1}cm-1), 374.5 nm (11,592 M^{-1} cm^{-1}), and 460 nm (12,600 $M^{-1}cm^{-1}$).

Yeast and bacterial strains, media Yeast strains were maintained in YPD medium (1% yeast extract, 2% bactopeptone, 2% glucose) or minimal SD medium (2% glucose, 0.67% yeast nitrogen base without amino acids) that was complemented when necessary. For growth in anaerobic conditions, yeast media was supplemented with Ergosterol (7.5 mg/l) and oleic acid (2.5 mg/l).

Culture conditions Yeast cells were pre-cultured in rich glucose (YPD) or ethanol-glycerol (YPEG) media for 24 h and cultures were inoculated at a density of 10^6 cells/ml. Aerobic cultures were grown in Erlenmeyer flasks filled to 20% of their volume, at 30°C with shaking (200 r.p.m.). For oxygen-depleted conditions, cultures were inoculated and grown in in bioreactors with a working volume of 400 ml, at 30°C with gentle continuous magnetic stirring. Under these conditions, traces of oxygen are present at the beginning of the culture. Anaerobiosis, was obtained, by bubbling nitrogen gas through the medium, for 30 min.

Tetrad Analysis The synthetic genetic array analysis was performed as previously described(Tong & Boone, 2006). Diploids were constructed by mating Δ*osm1*::*LEU2* strain to the temperature-sensitive *erv1-101* strain or Δ*cyc3*::*URA3* to Δ*osm1*::*LEU2* strain via patch mating. Mating proceeded for 4 hours at 30°C. Tetrads were formed by the sporulation of the diploids on minimal sporulation medium (.8% yeast extract, .3% peptone, 10% dextrose and 2% agar) for 4 days at 25°C. To prepare yeast tetrads for dissection, the tetrads were incubated in zymolase solution (1 M 2.4 M Sorbitol, 50 mM Tris-HCl pH 7.4 and 6 mg/mL Zymolyase-100T) for 10 minutes at 30°C and 20 µl of this solution was added to 80 µl of deionized water and placed on ice. Finally, the yeast suspension was plated on YPD plates and the tetrads were dissected via a dessecting light microscope and needle and the plates were incubated at 25°C for 2 days. Tetrad analysis was performed by replica pinning the plates on various selective

medium. The resulting tetrads were serially diluted by a factor of 3 onto rich glucose (YPD) medium and incubated in aerobic ($+O_2$) or anaerobic ($-O_2$) conditions via anaerobic chamber at 25°C for 4 days.

Subcellular Fractionation Subcellular fractionation was performed as previously described (Claypool, McCaffery, & Koehler, 2006). In brief, Osm1-myc yeast was grown at 30°C in rich lactate medium (1% yeast extract, 2% tryptone, 0.05% dextrose, and 2% lactic acid, 3.4 mM $CaCl_2$ $2H_2O$, 8.5 mM NaCl, 2.95 mM $MgCl_2$ $6H_20$, 7.35 mM KH_2PO_4, and 18.7 mM NH_4Cl) to an OD_{600} of ~1.5. Subcellular fractions were separated by differential centrifugation and protein amount in each fraction was calculated via the BCA assay (Pierce Chemical Co.). Subcellular fractionation was performed in duplicates from two separate batches of purified mitochondria.

Import Assay Mitochondria were purified from lactate-grown yeast cells and assayed for in vitro protein import as described(Curran et al., 2004). Proteins were synthesized by the TNT Quick Coupled Transcription/Translation kits (Promega) in the presence of [^{35}S] methionine and plasmids carrying the gene of interest. In addition, transcription of genes was initiated by the T7 promoter. The radiolabeled precursors were incubated with isolated mitochondria at the indicated time points in import buffer(.6 M Sorbitol, 150 mM KCl, 10 mM MgCl2, 2.5 mM EDTA, 2 mM ATP, 2 mM NADH, 20 mM K+-Hepes, pH 7.4) at 25°C. Where indicated, the potential across the mitochondrial inner membrane was dissipated with 5 mM FCCP. Non-imported radiolabeled protein was removed by treatment with 100 μg/ml trypsin for 15 minutes on ice and trypsin was inhibited with 250 μg/ml of soybean trypsin inhibitor. (Check calculations)

Submitochondrial localization Submitochondrial localization was performed as described previously(Claypool et al., 2006). For intact mitochondria, 300 μg of isolated mitochondria were incubated in 0.6 M sorbitol and 20 mM Hepes-KOH, pH 7.4. For osmotically shocked

mitochondria, 300 μg of isolated mitochondria were incubated in 0.03 M Sorbitol and 20 mM Hepes-KOH, pH 7.4 for 30 minutes on ice. As indicated, 20 μg/mL of Proteinase K and .1% Triton-X-100 were added. Trypsin was inhibited with 5 mM PMSF. Samples were centrifuged at 14,000 g for 10 minutes to separate pellet (P) and supernatant (S). The supernatants were precipitated with 20% (wt/vol) of TCA (trichloroacetic acid). Finally, the pellet and supernatant fractions were resuspended in equal volumes of thorner buffer (10% glycerol, 8 M urea, 5% (wt/vol) SDS, 40 mM Tris, pH 6.8, 4 mg/ml bromophenol blue, and 5% β-mercaptoethanol).

Carbonate Extraction Carbonate extraction was performed as described previously(Claypool et al., 2006). 200 μg of mitochondria were incubated in 200 μL of 0.1 M Na_2CO_3 at the indicated pH. Samples were centrifuged at 14,000 rpm for 5 minutes to separate the pellet (P) and supernatant (S). The supernatants were precipitated with 20% (wt/vol) TCA and the pellet and supernatant fractions were resuspended in equal volumes of thorner buffer.

Pulldown Assay Mitochondria were purified from the Erv1-His_6 strain and pull down experiments were performed as previously described (Dabir et al., 2007). In brief, 1 mg of isolated mitochondria were solubilized in 200 μL of 1% (wt/vol) digitonin buffer (20 mM Hepes-KOH, pH 7.4, 20 mM imidazole, 10% glycerol, 100 mM NaCl, 1 mM $CaCl_2$ and 1% (wt/vol) digitonin) supplemented with protease inhibitors (1 mM PMSF, 10 μM leupeptin, 2 μM pepstatin A, and 10 μM chymostatin). Samples were centrifuged at 14,000 rpm for 30 min at 4^{o}C to remove insoluble materials. Extracts were transferred to 700 μL of lysis buffer base supplemented with protease inhibitors and 50 μL of NiNTA resin (QIAGEN) and the beads were rotated for 3 hours at 4^{o}C. The sample was centrifuged at 2,000 rpm for 2 minutes at 4^{o}C to separate the supernatant (unbound) and beads(bound) . The supernantant fraction was precipitated with 20% (wt/vol) of TCA. The beads were washed twice for 10 minutes in wash buffer (20 mM Hepes-KOH, pH 7.4, 50 mM NaCl, 20 mM imidazole) + 0.1% digitonin. Finally,

the supernatant fraction was resuspended in 25 µL 0.6 NaOH +25 µL 2x reducing sample buffer. The bead fraction was resuspended in 50 µL 1x reducing sample buffer supplemented with 300 mM imidazole. Pull down experiments was performed in duplicates from two separate batches of purified mitochondria.

Reconstitution Studies In vitro reconstitution studies with recombinantly purified Tim13, Mia40 and Erv1 was performed as previously described(Tienson et al., 2009). Reduced Tim13 (15 µM), Erv1 (1 µM), Osm(1 µM) or (8µM) and fumarate (20µM) were mixed in MPP buffer(20 mM Tris-HCl, pH 7.0 150 mM KCl, and 1 mM EDTA) foat 25^{o}C. Length of incubation varied as indicated and the redox state of Tim13 was determined by thiol trapping via AMS. All proteins were resolved on 15% SDS-PAGE followed by immunoblot analysis with antibodies against Tim13.

Amplex Red Reconstitution StudiesH_2O_2 levels in the reconstitution assays were measured using the Amplex Red/horseradish peroxidase reaction mix (Invitrogen) as previously described(Tienson et al., 2009). In brief, 2 µM Mia40, 2 µM Erv1, 20 µM fumarate and 2 µM or 8 µM Osm1 were mixed in MPP buffer. 7.5 µM of reduced Tim13 was added to initiate the reaction which proceeded for 30 minutes at 25^{o}C. H_2O_2 levels were measured every minute for a total of 30 minutes by the FlexStation plate reader(Molecular Devices) and data was acquired by SoftMax Pro software(Molecular Devises). The Prism software was used for graphing and statistical analysis.

O_2 Consumption O_2 consumption assay was performed as previously described(Dabir et al., 2007). Reduction of O_2 by Erv1 or Erv2 was measured via Hansatech O_2 electrode. To initiate O_2 consumption, 2 µM of Erv1 or Erv2 was added to 1 ml of MPP buffer containing 2 mM DTT. In order to measure the competition between Osm1/fumarate and O_2 as Erv1's or Erv2's electron acceptor, 2 µM or 8 µM Osm1 and 10 µM fumarate were pre-equiblibrated with MPP buffer

containing DTT before addition of Erv1 or Erv2 in the O_2 electrode. As indicated, 2 μM BSA or 2 μM ccp1/cyt c were used as negative and positive controls respectively.

Steady-state levels 1 mg of isolated mitochondria was solubilized in 200 μL of 1% (wt/vol) digitonin buffer (20 mM Hepes-KOH, pH 7.4, 20 mM imidazole, 10% glycerol, 100 mM NaCl, 1 mM CaCl2 and 1% (wt/vol) digitonin) supplemented with protease inhibitors (1 mM PMSF, 10 μM leupeptin, 2 μM pepstatin A, and 10 μM chymostatin) for 1 hour at 4^{o}C. Samples were centrifuged at 14,000 rpm for 30 min at 4^{o}C to remove insoluble materials. 25 μg, 50 μg, and 100 μg of mitochondrial extracts were loaded and resolved on 12% or 15% SDS-PAGE followed by immunoblot analysis with the indicated antibodies.

Miscellaneous Mitochondrial proteins were analyzed by SDS-PAGE using a 12 or 15% polyacrylamide gel and a Tricine-based running buffer. Proteins were detected by immunoblotting using nitrocellulose membranes.

Figures and Tables

Table 1. Strains used in this study		
Strain	**Genotype**	**Source**
GA74-1A	**MATa** *his3-11,15 leu2 ura3 trp1 ade8 rho+ mit+*	(Koehler et al., 1998)
erv1-101	**MATα** *his3-11,15 leu2 ura3 trp1 ade8 erv1::HIS3 [perv1- 101:TRP1* CEN]	(Dabir et al., 2007)
Erv1-His	**MATα** *his3-11,15 leu2 ura3 trp1 ade8 erv1::HIS3 [pERV1- 10xHis:LEU2* 2μ]	(Dabir et al., 2007)
Erv1-His/Osm1-myc	**MATα** *his3-11,15 leu2 ura3 trp1 ade8 erv1::HIS3 [pERV1- 10xHis:LEU2*	(Neal et al., 2012)
GA74-1A.d	**MATa/α** *his3-11,15/his3-11,15 leu2/leu2 ura3/ura3 trp1/trp1 ade8/ade8*	(Koehler et al., 1998)
GA74-6A	**MATα** *his3-11,15 leu2 ura3 trp1 ade8 rho+ mit+*	(Koehler et al., 1998)
Osm1-myc	**MATα** *his3-11,15 leu2 ura3 trp1 ade8 [pOSM1-Myc:LEU2* 2μ]	(Neal et al., 2012)
Δ*osm1*	**MATa** *his3-11,15 leu2 ura3 trp1 ade8 osm1::LEU2*	(Neal et al., 2012)
Δ*cyc3*	**MATa** *his3-11,15 leu2 ura3 trp1 ade8 cyc3::URA3*	(Neal et al., 2012)
Δ*osm1cyc3*	**MATa** *his3-11,15 leu2 ura3 trp1 ade8 cyc3::URA3 osm1::LEU2*	(Neal et al., 2012)
erv1-101 / Δ*osm1*	**MATα** *his3-11,15 leu2 ura3 trp1 ade8 osm1::LEU2 erv1::HIS3 [perv1-101:TRP1* CEN]	(Neal et al., 2012)

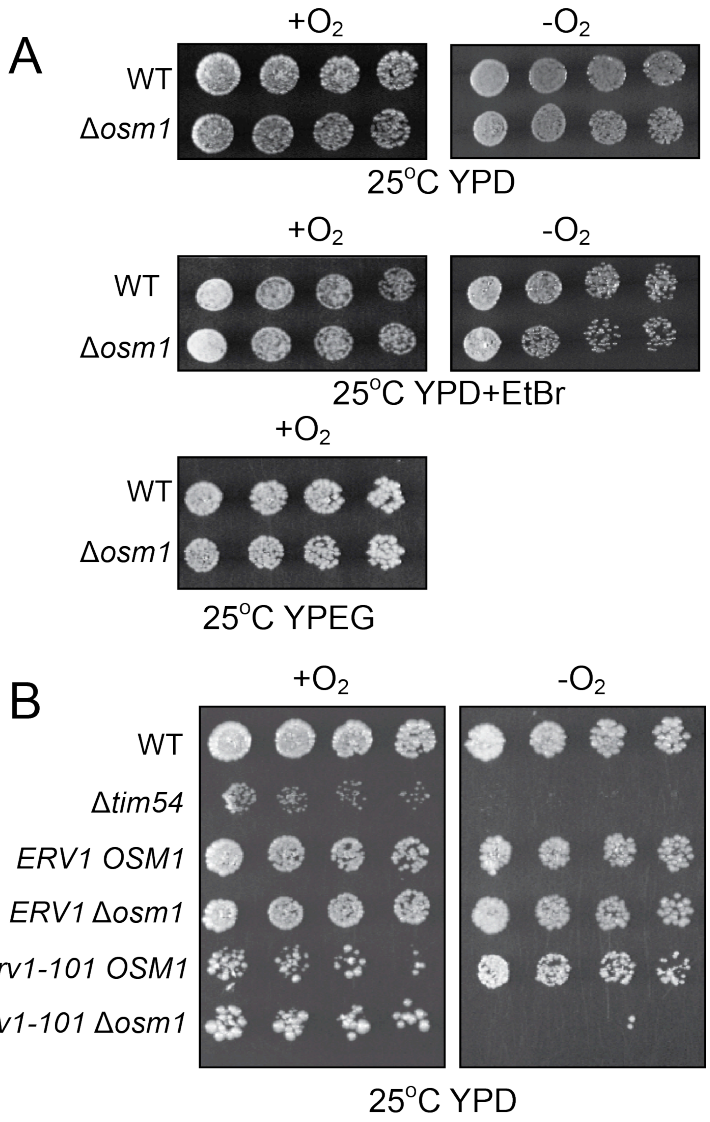

Figure 1. ***ERV1* and *OSM1* are synthetic lethal.** (A) Growth analysis of *Δosm1* in aerobic ($+O_2$) and anaerobic ($-O_2$) conditions on glucose (YPD) and ethanol/glycerol (YPEG) carbon sources. Ethidium bromide (EtBr) addition removed the mitochondrial DNA. (B) A cross of *erv1-101* with *Δosm1* was sporulated, and the resulting tetrads were serially diluted by a factor of 2 onto rich glucose media (YPD) and incubated in aerobic ($+O_2$) and anaerobic ($-O_2$) conditions. The parental strain (WT) and *tim54-1* mutant (petite negative) were included as controls. Plates were photographed after 3 days at 25°C.

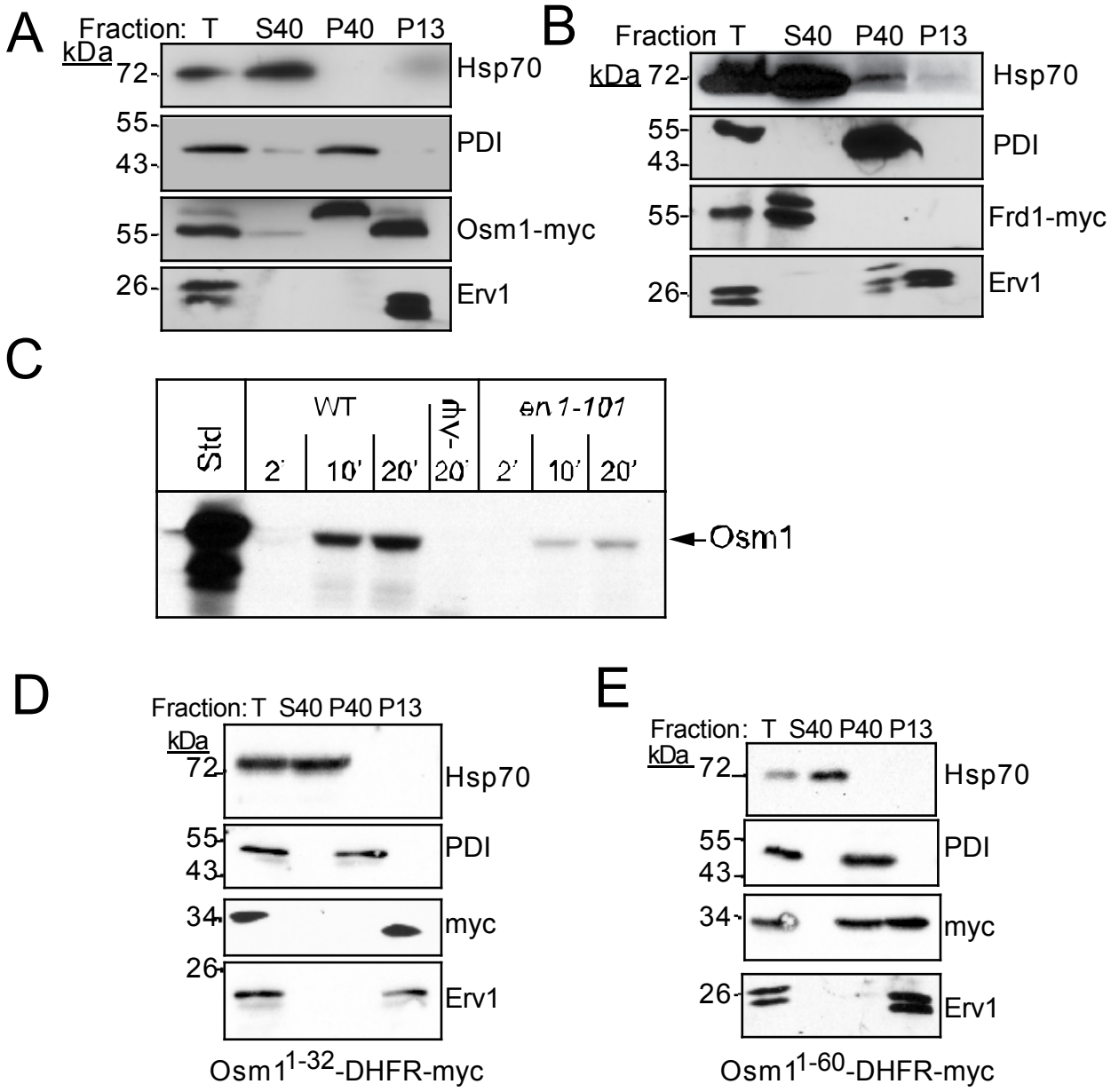

Figure 2. **Osm1 localizes to microsomes and mitochondria, whereas Frd1 resides in the cytosol.** (A) A yeast transformant expressing Osm1 with a C-terminal myc-tag was grown in YPEG at 30°C, converted to spheroplasts, and fractionated into a total homogenate (T), mitochondrial fraction (P13), microsome fraction (P40), and cytoplasm (S40). An equal amount of each fraction was analyzed by SDS-PAGE and immunoblotting with a monoclonal antibody

against the myc tag. As a control, antibodies against cytosolic Hsp70, PDI (microsomes), and Erv1 (mitochondria) were included. (B) As in 'A', but Frd1 was expressed with a myc tag. (C) Radiolabeled Osm1 was imported into WT and *erv1-101* mitochondria in the presence and absence of a membrane potential. Non-imported precursor was removed by protease treatment and the imported protein was analyzed by SDS-PAGE and autoradiography. (D) Construct $Osm1^{1-32}$-DHFR-myc was expressed in yeast and subcellular fractionation was performed as in 'A'. A myc monoclonal antibody was used to detect the fusion protein. (E) As in 'D' with construct $Osm1^{1-60}$-DHFR-myc.

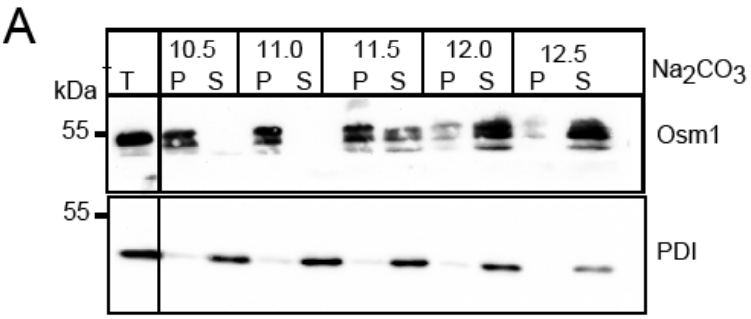

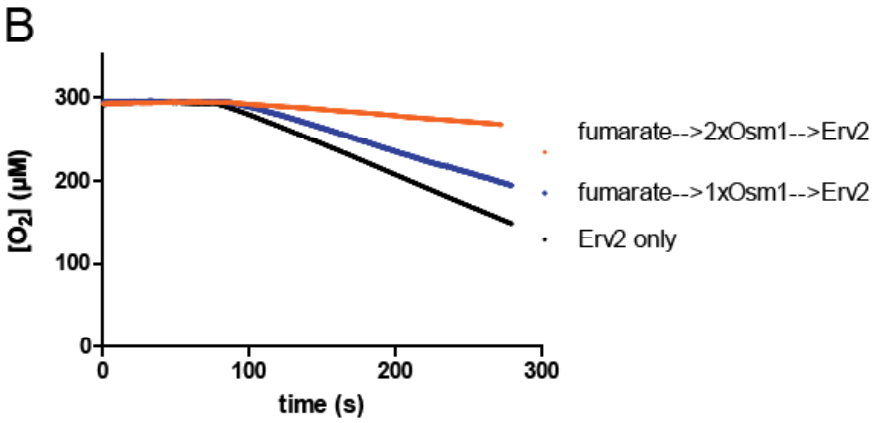

Substrates added	Rate of O_2 consumption
fumarate-->2xOsm1-->Erv2	-0.11 μM/sec ± 0.001
fumarate-->1xOsm1-->Erv2	-0.40 μM/sec± 0.002
Erv2 only	-0.58 μM/sec± 0.002

Figure 3. **Osm1 is a peripheral protein in the ER and transfers electrons to Erv2 in vitro** (A) Mitochondria were analyzed by alkali extraction (Na_2CO_3) with 0.1 M carbonate at the indicated pH values. Equal volumes of the pellet (P) and TCA-precipitated supernatant (S) fractions were resolved by SDS-PAGE and analyzed by immunoblotting. PDI, was used as a control that is a soluble protein. (A) O_2 consumption was measured with the O_2 electrode (Hansatech, chamber is 1 ml) with air-saturated buffer containing 2 mM DTT and Erv2. Additional reactions include the addition of 10 μM fumarate/2 μM Osm1 and 10 μM fumarate/4 μM Osm1.

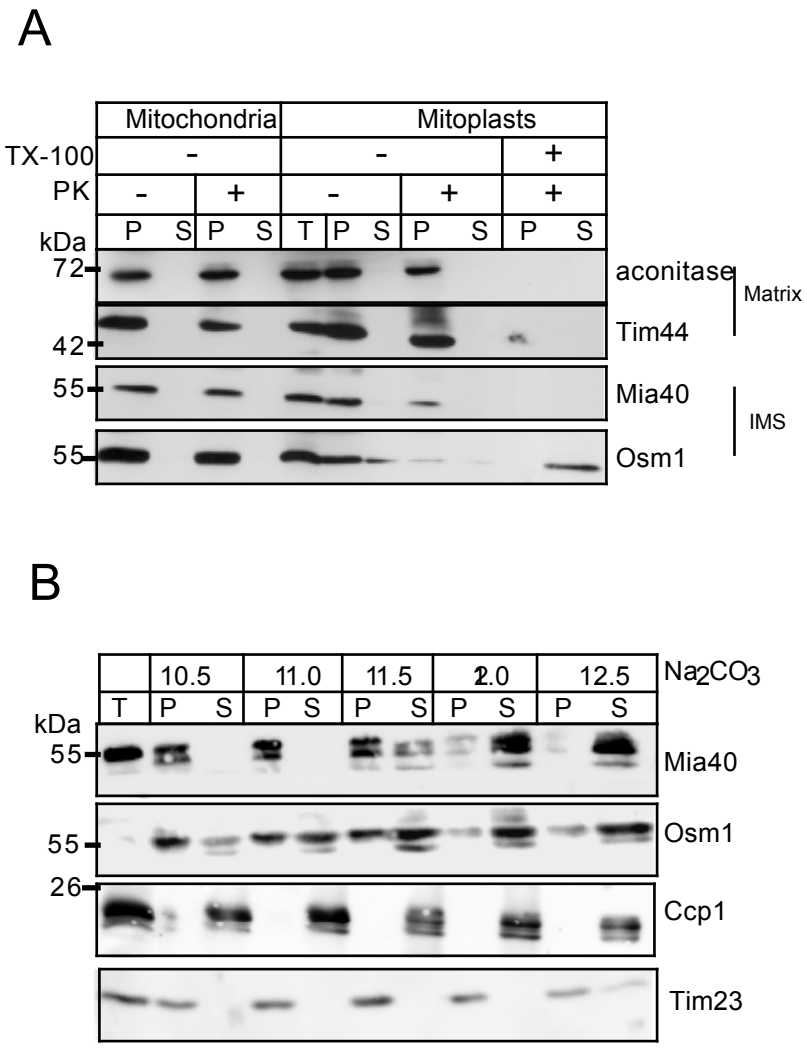

Figure 4. **Osm1 is a mitochondrial IMS resident.** (A) Sub-mitochondrial localization of Osm1. WT mitochondria were subjected to osmotic shock and the mitoplasts (P) were separated from the soluble IMS fraction (S) by centrifugation. Proteinase K (PK) addition verified localization to the IMS and detergent (TX-100) treatment was included as a control. Aconitase and Tim44, matrix markers; Mia40, IMS marker (B) Mitochondria were analyzed by alkali extraction (Na_2CO_3) with 0.1 M carbonate at the indicated pH values. Equal volumes of the pellet (P) and TCA-precipitated supernatant (S) fractions were resolved by SDS-PAGE and analyzed by immunoblotting. Tim23 and Mia40, controls that are integral membrane proteins.

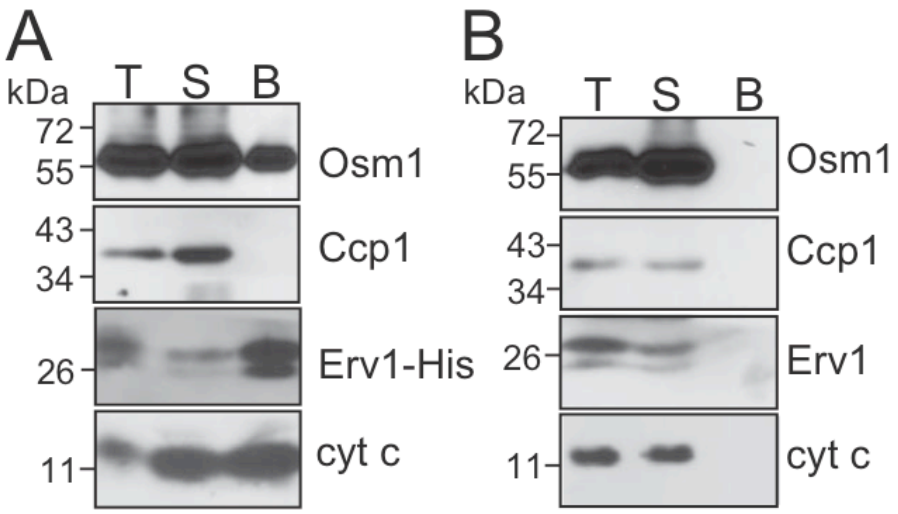

Figure 5. **Osm1 and Erv1 are partner proteins.** (A) Mitochondria from a strain expressing a C-terminal histidine-tagged Erv1 (Erv1-His) was solubilized in 1% digitonin. As a control, 100 µg of extract was withdrawn (T), and 500 µg lysate was incubated with Ni^{2+}-agarose beads. The beads were washed, and bound proteins (B) were eluted with SDS–PAGE sample buffer. To assess the effectiveness of binding, 100 µg of the unbound protein fraction (S) was also included. Samples were resolved by SDS-PAGE and analyzed by immunoblotting with specific antibodies against Osm1, Ccp1, Erv1, and cyt *c*. (B) Similar to A, except that WT mitochondria were utilized.

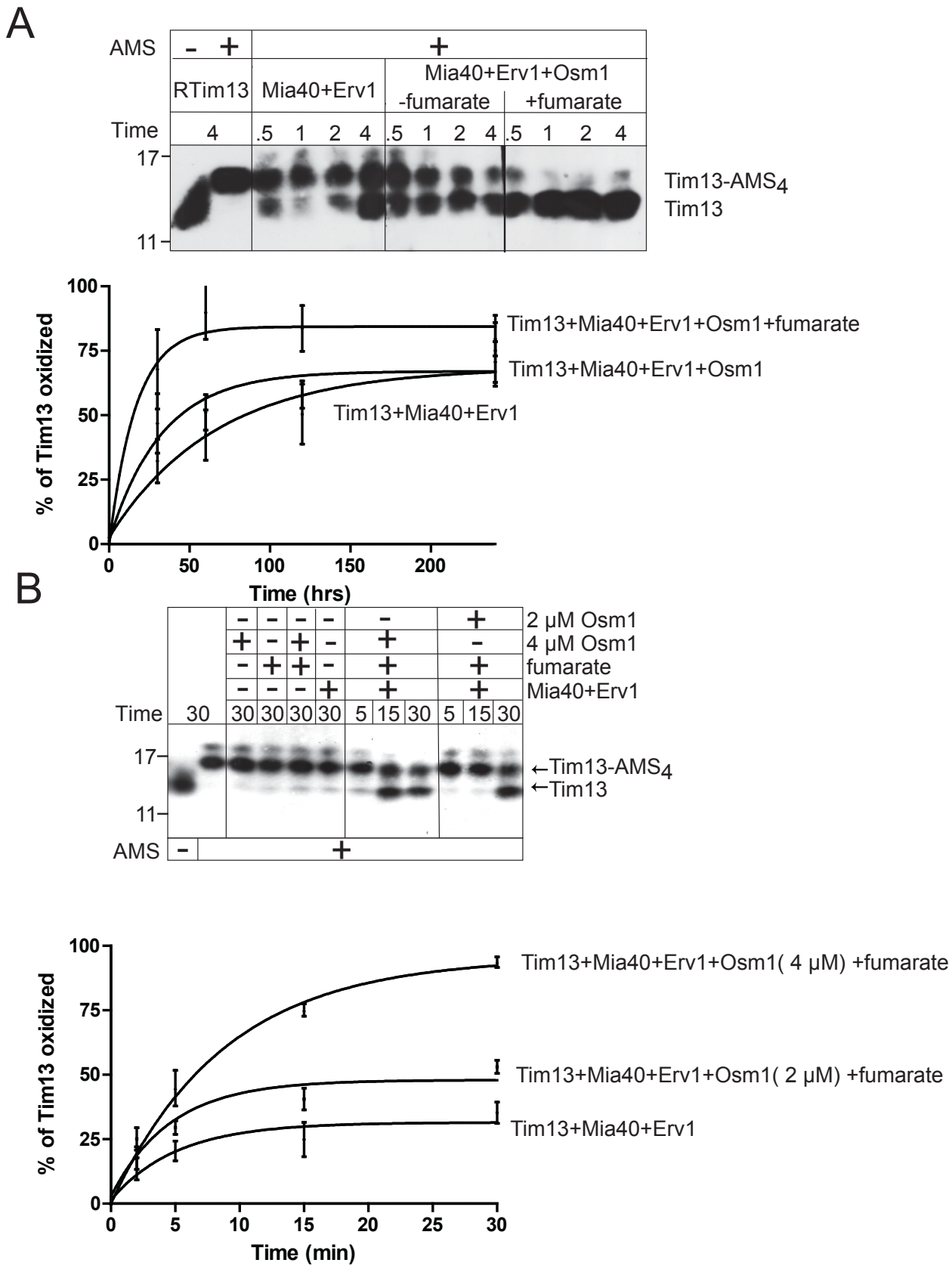
A
AMS
RTim13
Mia40+Erv1
Mia40+Erv1+Osm1
-fumarate
+fumarate
Time
17
11
Tim13-AMS4
Tim13
% of Tim13 oxidized
Time (hrs)
Tim13+Mia40+Erv1+Osm1+fumarate
Tim13+Mia40+Erv1+Osm1
Tim13+Mia40+Erv1
B
2 μM Osm1
4 μM Osm1
fumarate
Mia40+Erv1
←Tim13-AMS4
←Tim13
Time (min)
Tim13+Mia40+Erv1+Osm1(4 μM) +fumarate
Tim13+Mia40+Erv1+Osm1(2 μM) +fumarate
Tim13+Mia40+Erv1

Figure 6. **Osm1 increases the rate of Tim13 oxidation in vitro.** (A) Reduced Tim13 (15 μM) was incubated with combinations of Mia40 (1 μM), Erv1 (1 μM), Osm1 (1 μM) and fumarate (20 μM) in a time course assay up to 4 hrs as indicated. Aliquots were removed at the indicated times and free thiols were blocked with AMS addition. Oxidized and reduced (Tim13-AMS_4) Tim13 were detected by nonreducing SDS-PAGE followed by immunoblotting with antibodies against Tim13. (B) As indicated in (A) except different concentrations of Osm1 (2 and (4 μM) were used in the reconstitution and the time course was decreased to 60 min.

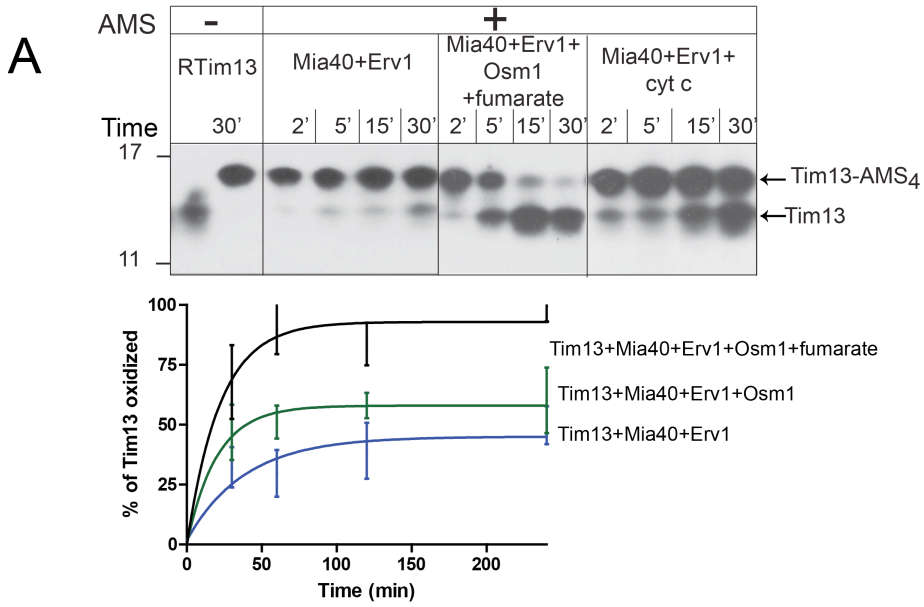
A
AMS
-
+
RTim13
Mia40+Erv1
Mia40+Erv1+ Osm1 +fumarate
Mia40+Erv1+ cyt c
Time
30'
2'
5'
15'
30'
17
11
Tim13-AMS4
Tim13
% of Tim13 oxidized
100
75
50
25
0
0
50
100
150
200
Time (min)
Tim13+Mia40+Erv1+Osm1+fumarate
Tim13+Mia40+Erv1+Osm1
Tim13+Mia40+Erv1

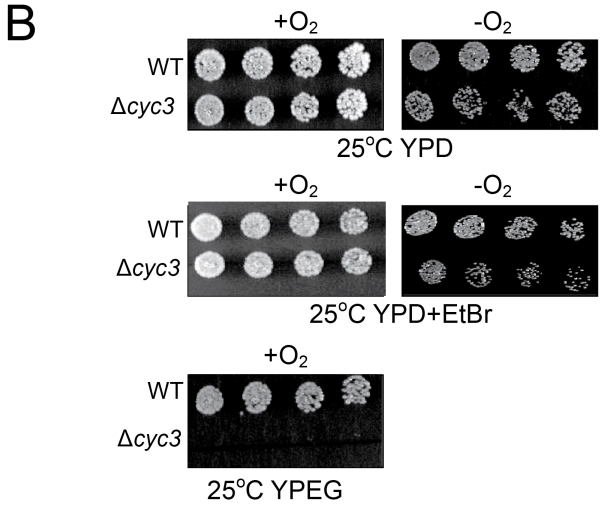
B
+O2
-O2
WT
Δcyc3
25°C YPD
25°C YPD+EtBr
25°C YPEG

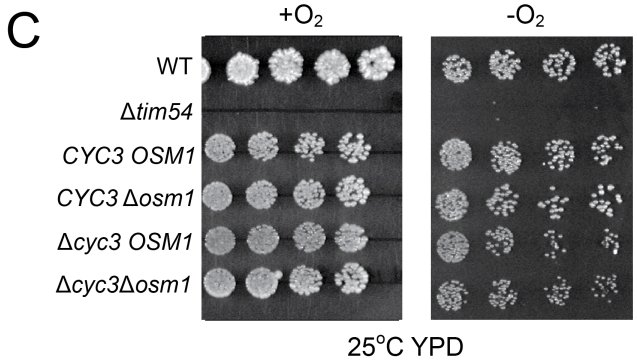
C
+O2
-O2
WT
Δtim54
CYC3 OSM1
CYC3 Δosm1
Δcyc3 OSM1
Δcyc3Δosm1
25°C YPD

Figure 7. **Osm1 and cyt *c* are poised to accept electrons from Erv1** (A) The reconstitution assay as in 'Fig. 5A' with an additional panel of cyt *c* (10 μM). The time course was decreased to 30 min. (B) Growth analysis of *Δcyc3* in aerobic ($+O_2$) and anaerobic ($-O_2$) conditions on glucose (YPD) and ethanol/glycerol (YPEG) carbon sources. Ethidium bromide (EtBr) addition removed the mitochondrial DNA. (B) A cross of *Δcyc3* with *Δosm1* was sporulated, and the resulting tetrads were serially diluted by a factor of 2 onto rich glucose media (YPD) and incubated in aerobic ($+O_2$) and anaerobic ($-O_2$) conditions. The parental strain (WT) and *tim54-1* mutant (petite negative) were included as controls. Plates were photographed after 3 days at 25°C.

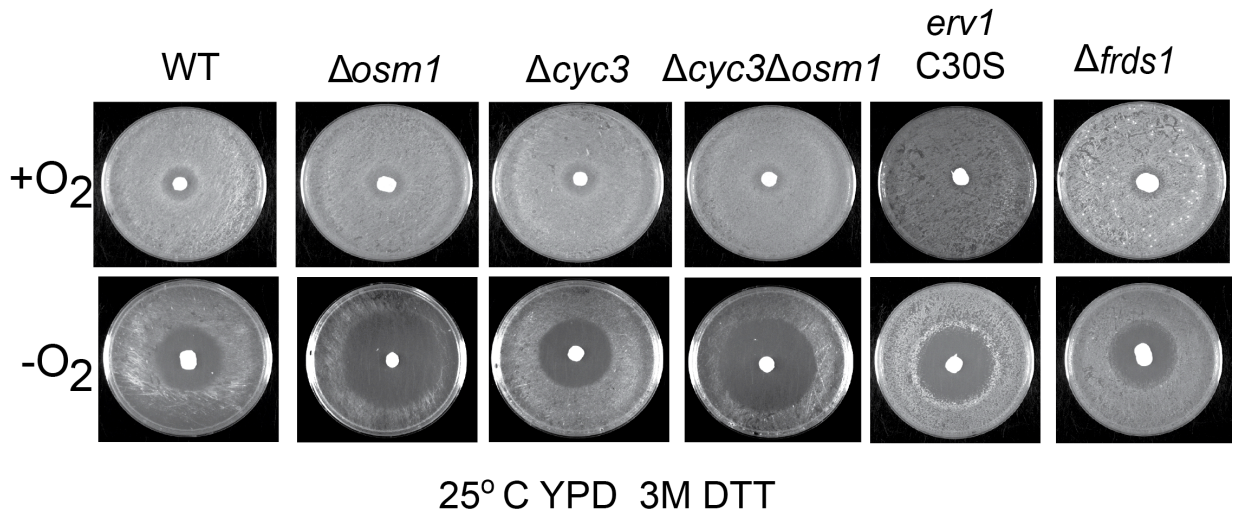

Figure 8. **Osm1 monitors the redox state of Erv1** Equal amount of cells from WT, Δ*osm1*, Δ*cyc3,* and Δ*osm1Δcyc3* were spread on YPD plates. Filter discs were placed in the middle of the plates and 10 µl of 3 M DTT were aliquoted directly onto the filter discs. The plates were grown at 25°C for 2 days.

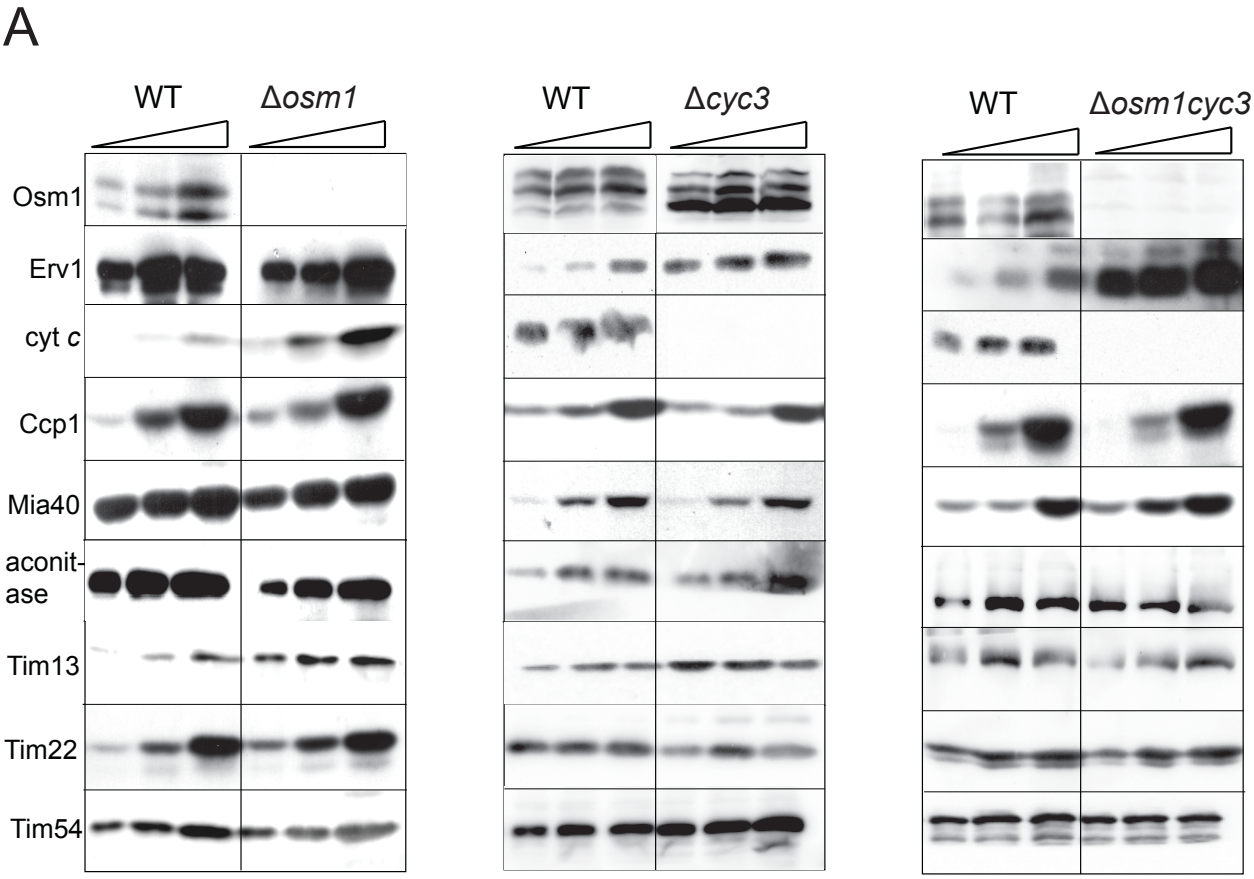

Figure 9. **Cooperation of terminal electron acceptors.** (A) Analysis of steady-state levels of mitochondrial proteins in the WT and *Δosm1* strains. Cells were grown aerobically in YPD at 25°C and protein levels were analyzed in isolated mitochondria. Antibodies against mitochondrial proteins α-ketoglutarate dehydrogenase (KDH), Tim54, Tim22, Osm1, Erv1, Tim9, Tim13, and cyt *c* were included. (B) As in 'Fig.9A' except steady-state levels of mitochondrial proteins were analyzed in WT and *Δcyc3* strains. (C) As in 'Fig. 9A' except steady-state levels of mitochondrial proteins were analyzed in WT and *Δcyc3osm1* strains.

Supplementary Figures

A

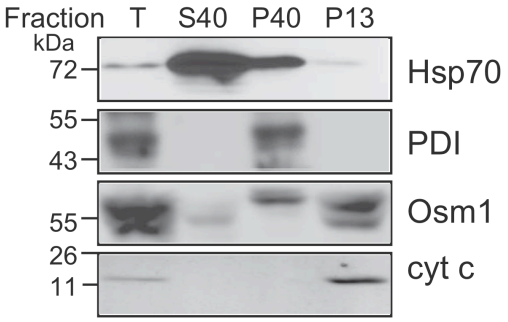

B

Presequence of Osm1

Osm1$^{1-32}$	MIRSVRRVFIYVSIFVLIIVLKRTLSGTDQTS
Osm1$^{1-60}$	MIRSVRRVFIYVSIFVLIIVLKRTLSGTDQTSMKQPVVVIGSGLAGLTTSNRLISKYRIPVVLLDKA

C Helical wheel of Osm1$^{1-32}$ Presequence

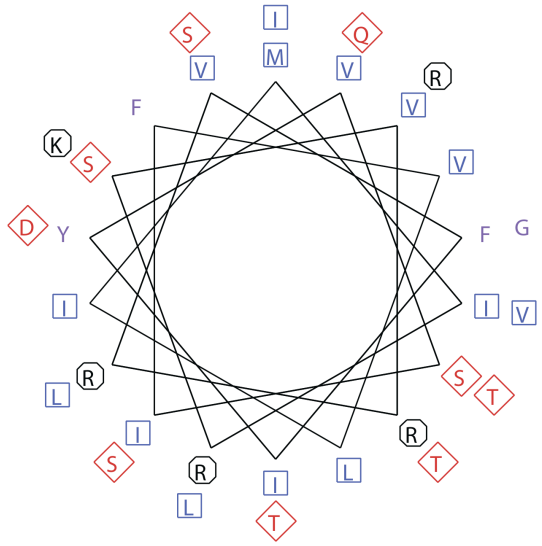

Figure 10 (S1). **Osm1 localizes to microsomes and the mitochondrial IMS.** (A) As in Fig. 2A except WT mitochondria were subjected to differential centrifugation. Samples were resolved on SDS-PAGE followed by immunoblot analysis with polycolonal antibody against Osm1. (B) Analysis of the N-terminal region of Osm1. Residues 1-32 (highlighted in red) contain a typical N-terminal targeting sequence and region 32-60 contains region rich in hydrophobic amino acids (underlined in black) that may function as an ER targeting sequence. (C) Analysis of the N-terminal 32 amino acids of Osm1 on a helical wheel (Mount, 2004). Positive, black; polar/negative, red; hydrophobic, blue.

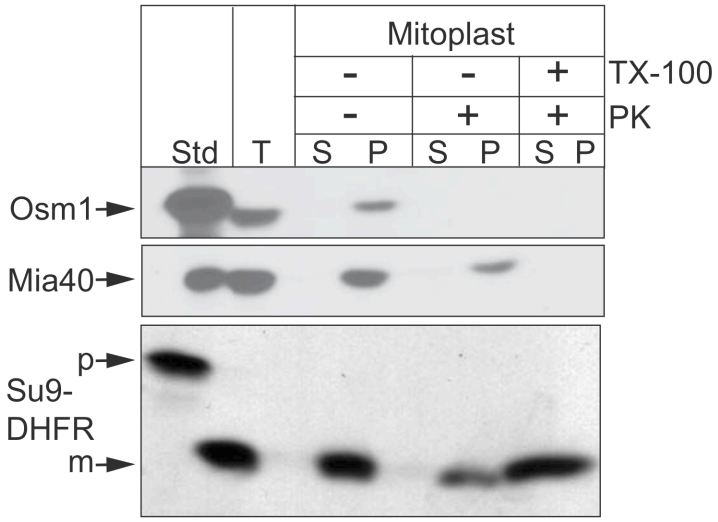

Figure 11 (S2). **Imported Osm1 localizes to the IMS.** As in Fig. 3A, radiolabeled Osm1 was imported into mitochondria followed by osmotic shock treatment to generate mitoplasts. Import controls include Mia40 (IMS) and Su9-DHFR (matrix).

A

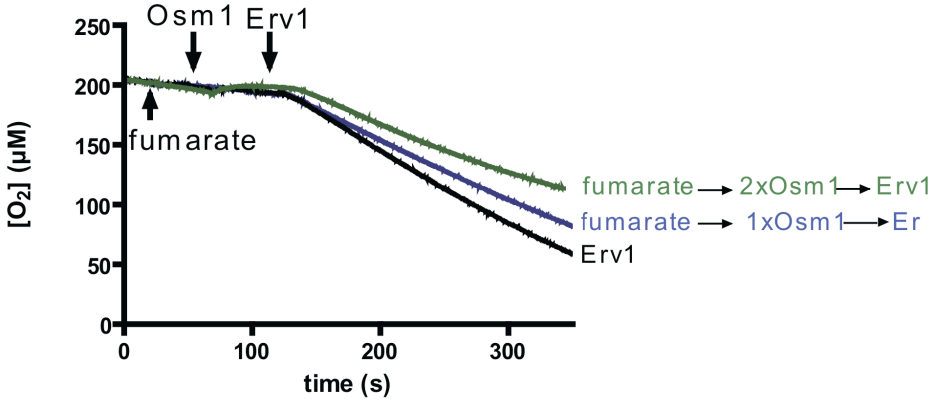

B

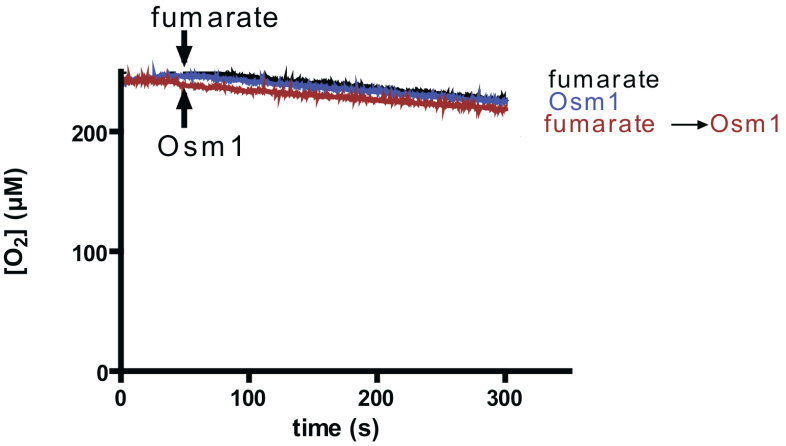

C

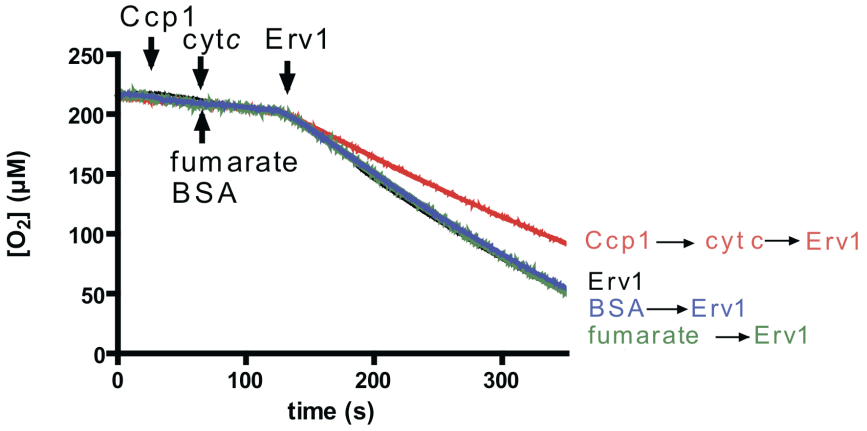

D

Substrates Added	Rate of O_2 consumption
Erv1	-.47 µM/sec ± .001
fumarate→ 1xOsm1→ Erv1	-.35 µM/sec ± .002
fumarate→ 2xOsm1→ Erv1	-.29 µM/sec ± .001
Ccp1→ cyt c → Erv1	-.33 µM/sec ± .002

Figure 12 (S3). **Osm1/fumarate competes with O_2 in the oxidation of the nonphysiologic substrate DTT.** (A) O_2 consumption was with with the O_2 electrode (Hansatech, chamber is 1 ml) with air-saturated buffer containing 2 mM DTT and Erv1. Additional reactions include the addition of 10 μM fumarate/2 μM Osm1 and 10 μM fumarate/ 4 μM Osm1. (B) As in (A), a control experiment was performed with the addition of fumarate (10 μM), Osm1 (4 μM), or fumarate (10 μM)→ Osm1 (4 μM). (C) As in (A), except that several proteins were added successively in the following order Ccp1 (20 μM)→ cyt *c* (20 μM)→Erv1 (2 μM), fumarate (10 μM)→Erv1 (2 μM), BSA (2 μM)→Erv1 (2 μM) and Erv1 alone (2 μM). O2 consumption was observed upon Erv1 addition. (D) Summary of the rate of O_2 consumption from 'A' and 'C' in reactions where O_2 was consumed.

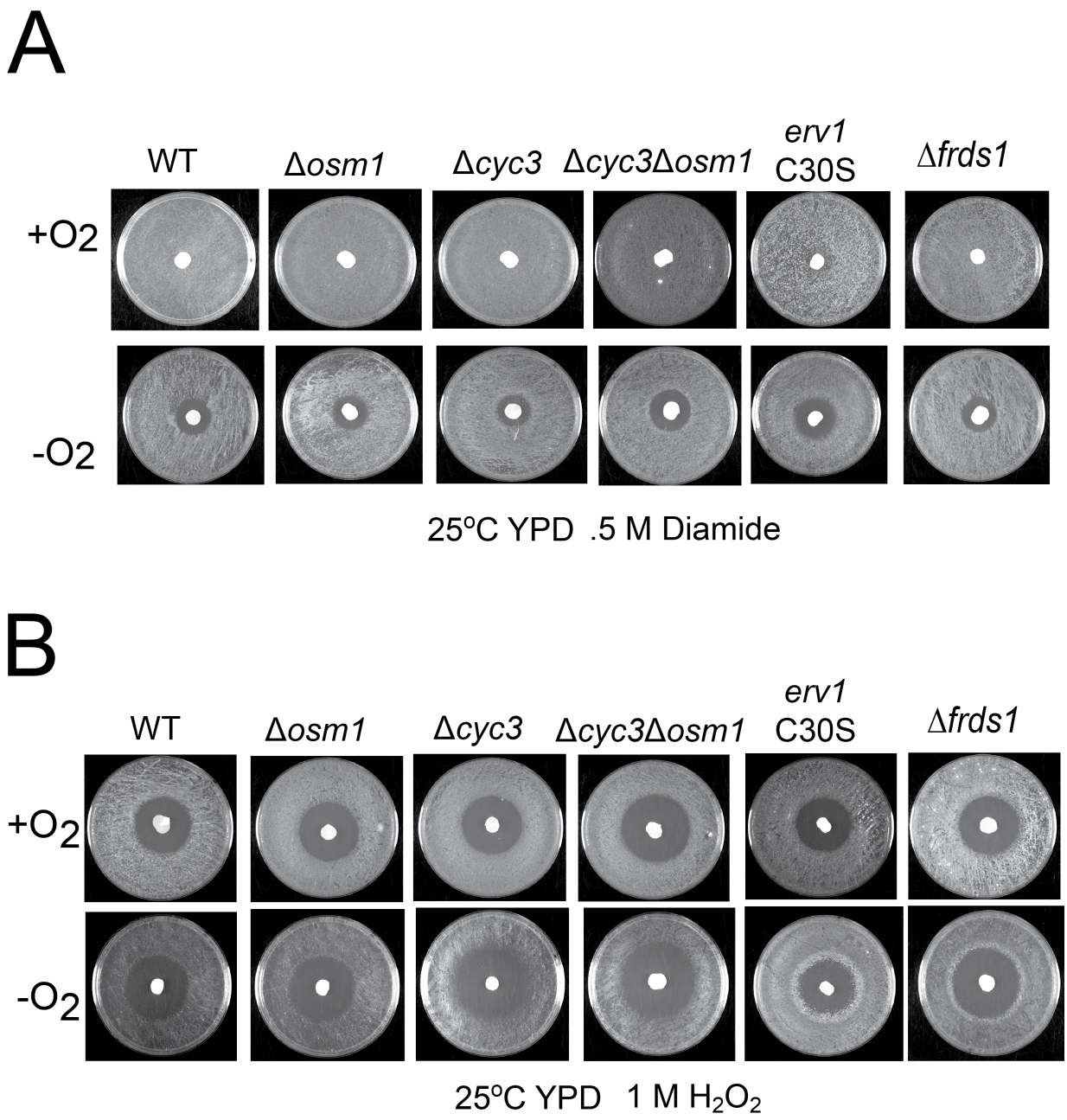

Figure 13 (S4). **There are no changes in diamide and H_2O_2 sensitivity in Δ*osm1*, Δ*cyc3,* and Δ*osm1cyc3* strains** (A) Equal amount of cells from WT, Δ*osm1*, Δ*cyc3,* and Δ*osm1*Δ*cyc3* were spread on YPD plates. Filter discs were placed in the middle of the plates and 10 µl of 500 mM diamide were aliquoted directly onto the filter discs. The plates were grown at 25°C for 2 days. (B) Same as (A), except 10 M H_2O_2 was soaked in the filter discs.

References

Allen, S., V. Balabanidou, D.P. Sideris, T. Lisowsky, and K. Tokatlidis. 2005. Erv1 mediates the Mia40-dependent protein import pathway and provides a functional link to the respiratory chain by shuttling electrons to cytochrome *c*. *J. Mol. Biol*. 353:937-944.

Anandatheerthavarada, H.K., G. Biswas, J. Mullick, N.B. Sepuri, L. Otvos, D. Pain, and N.G. Avadhani. 1999. Dual targeting of cytochrome P4502B1 to endoplasmic reticulum and mitochondria involves a novel signal activation by cyclic AMP-dependent phosphorylation at ser128. *EMBO J*. 18:5494-5504.

Arikawa, Y., K. Enomoto, H. Muratsubaki, and M. Okazaki. 1998. Soluble fumarate reductase isoenzymes from Saccharomyces cerevisiae are required for anaerobic growth. *FEMS Microbiol. Lett*. 165:111-116.

Bader, M., W. Muse, D.P. Ballou, C. Gassner, and J.C. Bardwell. 1999. Oxidative protein folding is driven by the electron transport system. *Cell*. 98:217-227.

Becher, D., J. Kricke, G. Stein, and T. Lisowsky. 1999. A mutant for the yeast scERV1 gene displays a new defect in mitochondrial morphology and distribution. *Yeast*. 15:1171-1181.

Besteiro, S., M. Biran, N. Biteau, V. Coustou, T. Baltz, P. Canioni, and F. Bringaud. 2002. Succinate secreted by Trypanosoma brucei is produced by a novel and unique glycosomal enzyme, NADH-dependent fumarate reductase. *J. Biol. Chem*. 277:38001-38012.

Bien, M., S. Longen, N. Wagener, I. Chwalla, J.M. Herrmann, and J. Riemer. 2010. Mitochondrial disulfide bond formation is driven by intersubunit electron transfer in Erv1 and proofread by glutathione. *Mol. Cell*. 37:516-528.

Bihlmaier, K., N. Mesecke, N. Terziyska, M. Bien, K. Hell, and J.M. Herrmann. 2007. The disulfide relay system of mitochondria is connected to the respiratory chain. *J. Cell Biol*. 179:389-395.

Blaisdell, F.W. 2002. The pathophysiology of skeletal muscle ischemia and the reperfusion syndrome: a review. *Cardiovasc. Surg*. 10:620-630.

Camarasa, C., V. Faucet, and S. Dequin. 2007. Role in anaerobiosis of the isoenzymes for Saccharomyces cerevisiae fumarate reductase encoded by OSM1 and FRDS1. *Yeast*. 24:391-401.

Chacinska, A., S. Pfannschmidt, N. Wiedemann, V. Kozjak, L.K. Sanjuan Szklarz, A. Schulze-Specking, K.N. Truscott, B. Guiard, C. Meisinger, and N. Pfanner. 2004. Essential role of Mia40 in import and assembly of mitochondrial intermembrane space proteins. *EMBO J.* 23:3735-3746.

Costanzo, M., A. Baryshnikova, J. Bellay, Y. Kim, E.D. Spear, C.S. Sevier, H. Ding, J.L. Koh, K. Toufighi, S. Mostafavi, J. Prinz, R.P. St Onge, B. VanderSluis, T. Makhnevych, F.J. Vizeacoumar, S. Alizadeh, S. Bahr, R.L. Brost, Y. Chen, M. Cokol, R. Deshpande, Z. Li, Z.Y. Lin, W. Liang, M. Marback, J. Paw, B.J. San Luis, E. Shuteriqi, A.H. Tong, N. van Dyk, I.M. Wallace, J.A. Whitney, M.T. Weirauch, G. Zhong, H. Zhu, W.A. Houry, M. Brudno, S. Ragibizadeh, B. Papp, C. Pal, F.P. Roth, G. Giaever, C. Nislow, O.G. Troyanskaya, H. Bussey, G.D. Bader, A.C. Gingras, Q.D. Morris, P.M. Kim, C.A. Kaiser, C.L. Myers, B.J. Andrews, and C. Boone. 2010. The genetic landscape of a cell. *Science*. 327:425-431.

Cox, A.G., A.V. Peskin, L.N. Paton, C.C. Winterbourn, and M.B. Hampton. 2010. Correction to Redox Potential and Peroxide Reactivity of Human Peroxiredoxin 3. *Biochemistry*.

Dabir, D.V., E.P. Leverich, S.K. Kim, F.D. Tsai, M. Hirasawa, D.B. Knaff, and C.M. Koehler. 2007. A role for cytochrome c and cytochrome c peroxidase in electron shuttling from Erv1. *EMBO J*. 26:4801-4811.

Depuydt, M., J. Messens, and J.F. Collet. 2011. How proteins form disulfide bonds. *Antioxid. Redox Signal*. 15:49-66.

Dunwoodie, S.L. 2009. The role of hypoxia in development of the Mammalian embryo. *Dev. Cell*. 17:755-773.

Dutton, R.J., D. Boyd, M. Berkmen, and J. Beckwith. 2008. Bacterial species exhibit diversity in their mechanisms and capacity for protein disulfide bond formation. *Proc. Natl. Acad. Sci. U. S. A*. 105:11933-11938.

Enomoto, K., Y. Arikawa, and H. Muratsubaki. 2002. Physiological role of soluble fumarate reductase in redox balancing during anaerobiosis in Saccharomyces cerevisiae. *FEMS Microbiol. Lett*. 215:103-108.

Fujiki, Y., A.L. Hubbard, S. Fowler, and P.B. Lazarow. 1982. Isolation of intracellular membranes by means of sodium carbonate treatment: application to endoplasmic reticulum. *J. Cell Biol*. 93:97-102.

Gabriel, K., D. Milenkovic, A. Chacinska, J. Muller, B. Guiard, N. Pfanner, and C. Meisinger. 2007. Novel mitochondrial intermembrane space proteins as substrates of the MIA import pathway. *J. Mol. Biol*. 365:612-620.

Gerber, J., U. Muhlenhoff, G. Hofhaus, R. Lill, and T. Lisowsky. 2001. Yeast ERV2p is the first microsomal FAD-linked sulfhydryl oxidase of the Erv1p/Alrp protein family. *J. Biol. Chem*. 276:23486-23491.

Glick, B.S., and L.A. Pon. 1995. Isolation of highly purified mitochondria from Saccharomyces cerevisiae. *Methods Enzymol*. 260:213-223.

Gross, E., C.S. Sevier, N. Heldman, E. Vitu, M. Bentzur, C.A. Kaiser, C. Thorpe, and D. Fass. 2006. Generating disulfides enzymatically: reaction products and electron acceptors of the endoplasmic reticulum thiol oxidase Ero1p. *Proc. Natl. Acad. Sci. U. S. A*. 103:299-304.

Grumbt, B., V. Stroobant, N. Terziyska, L. Israel, and K. Hell. 2007. Functional characterization of Mia40p, the central component of the disulfide relay system of the mitochondrial intermembrane space. *J. Biol. Chem*. 282:37461-37470.

Guthrie, C., and G.R. Fink. 1991. Guide to yeast genetics and molecular biology. *Methods Enzymol*. 194:1-863.

Herrmann, J.M., and J. Riemer. 2012. Mitochondrial Disulfide Relay: Redox-regulated Protein Import into the Intermembrane Space. *J. Biol. Chem*. 287:4426-4433.

Hwang, D.K., S.M. Claypool, D. Leuenberger, H.L. Tienson, and C.M. Koehler. 2007. Tim54p connects inner membrane assembly and proteolytic pathways in the mitochondrion. *J. Cell Biol*. 178:1161-1175.

Hwang, Y.T., S.M. Pelitire, M.P. Henderson, D.W. Andrews, J.M. Dyer, and R.T. Mullen. 2004. Novel targeting signals mediate the sorting of different isoforms of the tail-anchored membrane protein cytochrome b5 to either endoplasmic reticulum or mitochondria. *Plant Cell*. 16:3002-3019.

Karniely, S., and O. Pines. 2005. Single translation--dual destination: mechanisms of dual protein targeting in eukaryotes. *EMBO Rep*. 6:420-425.

Katzen, F., and J. Beckwith. 2000. Transmembrane electron transfer by the membrane protein DsbD occurs via a disulfide bond cascade. *Cell*. 103:769-779.

Koehler, C.M., and H.L. Tienson. 2009. Redox regulation of protein folding in the mitochondrial intermembrane space. *Biochim. Biophys. Acta*. 1793:139-145.

Longen, S., M. Bien, K. Bihlmaier, C. Kloeppel, F. Kauff, M. Hammermeister, B. Westermann, J.M. Herrmann, and J. Riemer. 2009. Systematic analysis of the twin cx(9)c protein family. *J. Mol. Biol*. 393:356-368.

Mairet-Coello, G., A. Tury, A. Esnard-Feve, D. Fellmann, P.Y. Risold, and B. Griffond. 2004. FAD-linked sulfhydryl oxidase QSOX: topographic, cellular, and subcellular immunolocalization in adult rat central nervous system. *J. Comp. Neurol*. 473:334-363.

Mamathambika, B.S., and J.C. Bardwell. 2008. Disulfide-linked protein folding pathways. *Annu. Rev. Cell Dev. Biol*. 24:211-235.

Mesecke, N., N. Terziyska, C. Kozany, F. Baumann, W. Neupert, K. Hell, and J.M. Herrmann. 2005. A disulfide relay system in the intermembrane space of mitochondria that mediates protein import. *Cell*. 121:1059-1069.

Messens, J., J.F. Collet, K. Van Belle, E. Brosens, R. Loris, and L. Wyns. 2007. The oxidase DsbA folds a protein with a nonconsecutive disulfide. *J. Biol. Chem*. 282:31302-31307.

Muratsubaki, H., and K. Enomoto. 1998. One of the fumarate reductase isoenzymes from Saccharomyces cerevisiae is encoded by the OSM1 gene. *Arch. Biochem. Biophys*. 352:175-181.

Naoe, M., Y. Ohwa, D. Ishikawa, C. Ohshima, S.I. Nishikawa, H. Yamamoto, and T. Endo. 2004. Identification of Tim40 that mediates protein sorting to the mitochondrial intermembrane space. *J. Biol. Chem.* 279:47815-47821.

Ohtsu, I., N. Wiriyathanawudhiwong, S. Morigasaki, T. Nakatani, H. Kadokura, and H. Takagi. 2010. The L-cysteine/L-cystine shuttle system provides reducing equivalents to the periplasm in Escherichia coli. *J. Biol. Chem*. 285:17479-17487.

Omura, T. 1998. Mitochondria-targeting sequence, a multi-role sorting sequence recognized at all steps of protein import into mitochondria. *J. Biochem*. 123:1010-1016.

Raue, U., S. Oellerer, and S. Rospert. 2007. Association of protein biogenesis factors at the yeast ribosomal tunnel exit is affected by the translational status and nascent polypeptide sequence. *J Biol. Chem*. 282:7809-7816.

Rietsch, A., D. Belin, N. Martin, and J. Beckwith. 1996. An in vivo pathway for disulfide bond isomerization in Escherichia coli. *Proc.Natl. Acad. Sci. U. S. A*. 93:13048-13053.

Sevier, C.S. 2012. Erv2 and quiescin sulfhydryl oxidases: Erv-domain enzymes associated with the secretory pathway. *Antioxid. Redox Signal*. 16:800-808.

Sevier, C.S., J.W. Cuozzo, A. Vala, F. Aslund, and C.A. Kaiser. 2001. A flavoprotein oxidase defines a new endoplasmic reticulum pathway for biosynthetic disulphide bond formation. *Nat. Cell Biol*. 3:874-882.

Sevier, C.S., and C.A. Kaiser. 2006. Conservation and diversity of the cellular disulfide bond formation pathways. *Antioxid. Redox. Signal*. 8:797-811.

Sevier, C.S., H.J. Qu, N. Heldman, E. Gross, D. Fass, and C.A. Kaiser. 2007. Modulation of cellular disulfide-bond formation and the ER redox environment by feedback-regulation of Ero1. *Cell*. 129:333-344.

Stojanovski, D., D. Milenkovic, J.M. Muller, K. Gabriel, A. Schulze-Specking, M.J. Baker, M.T. Ryan, B. Guiard, N. Pfanner, and A. Chacinska. 2008. Mitochondrial protein import: precursor oxidation in a ternary complex with disulfide carrier and sulfhydryl oxidase. *J. Cell Biol*. 183:195-202.

Takahashi, Y.H., K. Inaba, and K. Ito. 2004. Characterization of the menaquinone-dependent disulfide bond formation pathway of Escherichia coli. *J. Biol. Chem*. 279:47057-47065.

Thomson, J.A., J. Itskovitz-Eldor, S.S. Shapiro, M.A. Waknitz, J.J. Swiergiel, V.S. Marshall, and J.M. Jones. 1998. Embryonic stem cell lines derived from human blastocysts. *Science*. 282:1145-1147.

Tienson, H.L., D.V. Dabir, S.E. Neal, R. Loo, S.A. Hasson, P. Boontheung, S.K. Kim, J.A. Loo, and C.M. Koehler. 2009. Reconstitution of the Mia40-Erv1 oxidative folding pathway for the small tim proteins. *Mol. Biol. Cell*. 20:3481-3490.

Tu, B.P., S.C. Ho-Schleyer, K.J. Travers, and J.S. Weissman. 2000. Biochemical basis of oxidative protein folding in the endoplasmic reticulum. *Science*. 290:1571-1574.

Tu, B.P., and J.S. Weissman. 2004. Oxidative protein folding in eukaryotes: mechanisms and consequences. *J. Cell Biol.* 164:341-346.

Wajih, N., S.M. Hutson, and R. Wallin. 2007. Disulfide-dependent protein folding is linked to operation of the vitamin K cycle in the endoplasmic reticulum. A protein disulfide isomerase-VKORC1 redox enzyme complex appears to be responsible for vitamin K1 2,3-epoxide reduction. *J. Biol. Chem*. 282:2626-2635.

Walter, P., and A.E. Johnson. 1994. Signal sequence recognition and protein targeting to the endoplasmic reticulum membrane. *Annu. Rev. Cell Biol*. 10:87-119.

Zito, E., E.P. Melo, Y. Yang, A. Wahlander, T.A. Neubert, and D. Ron. 2010. Oxidative protein folding by an endoplasmic reticulum-localized peroxiredoxin. *Mol. Cell*. 40:787-797.

Chapter 4: Synthetic Genetic Array Screen of Hot13 and Osm1

Abstract

Genetic analysis is a powerful way for assessing gene function in vivo, identifying new components in specific pathways and ordering gene products within a pathway (Hartman et al., 2001). Herein, I employed a high throughput method, which will be used to determine the genetic network involved with Hot13 and Osm1. Specifically, a Synthetic Genetic Array (SGA) screen was carried out by crossing the query strains, either Δ*osm1* or Δ*hot13*, to an ordered array of approximately 5,000 viable gene deletion mutants (representing ~80%) of all yeast genes). In all, this screen enabled us to globally analyze the genetic networks associated with either Hot13 or Osm1.

Introduction

Osm1's role in the Mia40-Erv1 import pathway

Given that Osm1 is localized to mitochondria, we considered a potential role as a terminal electron acceptor for Erv1, playing a crucial role in anaerobic conditions. Osm1 showed dual localization to microsomes and the mitochondrial IMS. Moreover, Osm1 accepted electrons from Erv1 using in vitro reconstitution assays in which reduced Tim13 was oxidized. Both Osm1 and cyt *c* functioned equally well in accepting electrons from Erv1 and cyt *c*

expression was induced in cells lacking *osm1*. Thus, Osm1 is postulated to be a new terminal electron acceptor that may be coordinately regulated with cyt *c*.

We used the SGA screen in order to identify additional pathways that Osm1 may function in. Given that it is also localized in the ER and has a physiological role in maintaining the redox balance via oxidation of NADH and $FADH_2$ within mitochondria, SGA will allow us to assess the global network of genetic interactions associated with Osm1 (Camarasa et al., 2007).

Hot13's role in Mitochondrial IMS

The main function of the Translocase of the Inner Membrane (TIM) 22 pathway is to import and insert nuclear-encoded membrane proteins to the mitochondrial inner membrane. The membrane proteins imported via the Tim22 import pathway are known as the mitochondrial carrier family, which includes Tim22, Tim23 and the ATP/ADP carrier (Koehler, 2000)(Paschen and Neupert). The Tim22 import machinery is a 300-kDa complex consisting of the pore-forming subunit Tim22, the accessory protein Tim18 and Tim54, which stabilizes the import machinery. Also, there is a fraction of small Tims; Tim9, Tim10 and Tim12 which functions in the insertion of substrates through the Tim22 translocon (Pfanner and Geissler, 2001). Once substrates pass through the Translocon of the Outer Membrane (TOM) complex, the hydrophobic carrier proteins are chaperoned through the aqueous environment of the mitochondrial IMS by two different 70-kDa-chaperone complexes: Tim9-Tim10 and Tim8-Tim13 complex. More specifically, the small Tim proteins bind to the hydrophobic domains within the substrates and chaperone them to the 300-kDa complex (Curran et al., 2002b; a). The substrate is subsequently transferred to the Tim22 translocon machinery and inserted into the membrane.

The small Tim proteins contain the "twin CX_3C" motif. Also, small Tim proteins form juxtapositional intramolecular disulfide bonds, which are inserted by the Mia40-Erv1 oxidative folding pathway (Koehler et al., 1999). The intramolecular disulfide bonds within the small Tim proteins are required for assembly into a functional 70-kDa chaperone-like complex to allow for import via the Tim22 import pathway (Curran et al., 2002b; a).

To date, the events by which the small Tim proteins bind and release substrates are not understood. Thus, our laboratory identified a 13 kDa soluble intermembrane space protein, Helper of Small Tims (Hot13). Hot13 is a zinc-binding protein, which contains 9 cysteine residues that are highly conserved from yeast to humans (Curran et al., 2004). There are several evidence suggesting a role of Hot13 in the assembly of the small Tim complexes. For example, *in organello* import studies showed that Tim13 was crosslinked to Hot13. Interestingly, the steady-state levels and assembly of small Tim proteins were compromised in yeast strains lacking Hot13. We were able to observe an arrest of the ADP/ATP carrier to the Tim9-Tim10 complex by treatment with oxidizing agents. With subsequent treatment with reductant, the intermediate was no longer arrested and the substrate was released and inserted to the inner membrane by the Tim22 translocon. Thus, by adapting this experiment, the AAC import is markedly decreased by treatment with oxidizing agent in Δ*hot13* mitochondria and that the defects of AAC import was rescued with overexpression of Hot13 (Curran et al., 2004). Taken together, these studies suggest a role of Hot13 in the assembly and recycling of the small Tim complexes.

Recent studies proposed a different role for Hot13 in modulating the redox state of Mia40. More specifically, Hot13 was suggested to maintain Mia40 in a zinc-free state, which facilitates Erv1 oxidation of Mia40. Reimer et al. provided *in vivo* and *in vitro* evidence that

Hot13 improves the efficiency of Erv1-dependent oxidation of Mia40 (Mesecke et al., 2008). Also, the import of Mia40-dependent substrates is decreased in yeast mitochondria lacking Hot13. Finally, there is in vitro evidence that zinc chelators functionally replace Hot13(Mesecke et al., 2008). In all, these studies suggest that Hot13 is able to facilitate Erv1-dependent oxidation of Mia40 by keeping Mia40 in a zinc-free state.

Both studies suggest contradictory roles for Hot13. Thus, it is advantageous to use a genetics approach for determining Hot13's function in the IMS. Herein, we performed an unbiased genetic approach, the SGA screen, in order to determine the genetic interactions associated with Hot13. Determining the large-scale genetic interactions of Hot13 will give us further insight into the various pathways Hot13 functions in.

Overview of the Synthetic Genetic Array Screen

Synthetic genetic interactions are usually identified when a second-site mutation or increased gene dosage suppresses or enhances the original mutant phenotype. This type of genetic screening approach has been used extensively in yeast, worms, flies, mice, and other model organisms. In particular, a genetic interaction termed "synthetic lethality" occurs when the combination of two viable mutations results in a lethal phenotype (Kaelin, 2005). When two genes show a synthetic lethal interaction, it often reflects that the gene products impinge on the same essential function, such that one pathway functionally compensates for, or buffers, the defects in the other (Hartman et al., 2001). Thus, large-scale mapping of genetic interactions provides a global view of functional relationships between genes.

SGA screen allows you to systematically construct double mutations(Tong et al., 2001). A MATa yeast strain carrying a query mutation linked to a dominant selectable marker, is crossed to an ordered array of MATa viable deletion mutants (xxxD), each carrying a gene

deletion mutation linked to a kanamycin-resistance marker kanMX that confers resistance to the antibiotic geneticin (G418) (Fig. 2). Growth of resultant zygotes is selected on medium containing drop-out media selecting for your query mutation and geneticin. The heterozygous diploids are transferred to medium with reduced levels of carbon and nitrogen to induce sporulation and the formation of haploid meiotic spore progeny. Spores are transferred to synthetic medium lacking histidine and containing canavanine and thialysine. This allows for selective germination of MATa meiotic progeny because only these cells express the MFA1pr-HIS3 reporter and carry the can1D and lyp1D markers. The MATa meiotic progeny are then transferred to medium that contains G418, which selects for growth of meiotic progeny that carries the gene deletion mutation (xxxD::kanR). Finally, the MATa meiotic progeny are transferred to medium, which then selects for growth of double mutant (hot13::URA3 or osm1::LEU2 xxxD::kanR) (Hin et al., 2005).

Results

We screened a Δ*hot13* query strain against an array of 4,848 different viable deletion strains. For high-throughput automated screening, we designed a robotic system for manipulation of high-density yeast arrays. To ensure reproducibility within a screen and to facilitate visual scoring, we performed 3 independent screens in duplicates. We scored 82 potential synthetic lethal/sick interactions. At the current stage of development, SGA analysis yields a substantial number of false-positives; however, these can be reduced by repeated screening. To group the identified genes by function, we assembled a list of their cellular roles as defined by the Gene Ontology Database. The *HOT13* interactions were highly enriched for genes with roles in mitochondrial and cytoplasmic translation (15.8% and 21.95% respectively). Pathways critical

for the fitness of Δ*hot13* cells were revealed by multiple interactions with subsets of genes involved in mitochondrial function which includes aerobic respiration (*RMD9, PET10, PET309, SLS1, PPA2, MCT1*), mitochondrial DNA maintenance (*UGO1, MRPL8, MGM101, MGM1*), and mitochondrial fusion (*FZO1, UGO1, MGM1)*(Table1).

We subsequently screened a Δ*osm1* query strain against an array of 4,848 different viable deletion strains. We scored 81 potential synthetic lethal/sick interactions. The *OSM1* interactions were highly enriched for genes with roles in mitochondrial aerobic respiration, which included *QCR9*, *CYT1*, *QCR2*, *COX7*, *COX10*, and *CEM1*. Additional pathways critical for the fitness of Δ*osm1* cells were revealed by multiple interactions with subsets of genes involved in purine base biosynthesis (*DAL7, AMD1*) and cellular copper ion homeostasis (*YLR126C, CUP9*) (Table 2).

Discussion

As expected, the putative genetic interactions of Hot13 pointed to a connection between Hot13 and mitochondrial biogenesis. For example, majority of negative interactions were observed with genes encoding components of the mitochondrial translation machinery and the electron transport chain. Although we did not find obvious genetic interactions with genes encoding components of the Mia40-Erv1 and Tim22 import pathway, strong genetic interactions were observed in genes encoding several components responsible for mitochondrial fusion: *FZO1, UGO1 AND MGM1*. Interestingly, Mgm1 is an IMS protein containing 7 cysteines and functions in fusion of the mitochondrial inner membrane (Meglei and McQuibban, 2009)(DeVay et al., 2009). A recent report suggested that a population of Mgm1 oligomerizes via intermolecular disulfide bond formation. It is possible that the assembly of Mgm1 is redox-regulated by Hot13. There was also a strong synthetic growth defect observed with Δ*crd1* which

is a gene encoding a component of the cardiolipin biosynthetic pathway, which is important for inner membrane integrity and organization. Studies by Devay et al., show a requirement for cardiolipin in the assembly of Mgm1on the mitochondrial inner membrane which may explain the synthetic growth defect observed between Δ*hot13* and Δ*crd1* (DeVay et al., 2009). Finally, genetic interactions were observed in a gene encoding the catalytic subunit of the inner membrane m-AAA-protease, *YME1*, which functions in protein quality control of the inner membrane (Graef et al., 2007). Together, these observations suggest that Hot13 possibly functions in the same pathway as mitochondrial inner membrane fusion by regulating the assembly of Mgm1.

SGA screen with Δ*osm1* yielded genetic interactions enriched with genes encoding components of Complex III and IV of the electron transport chain. This observation is most likely a result of the electron transport chain functioning downstream of Osm1in the Mia40-Erv1 import pathway. Notably, a genetic interaction was seen with *CYT1*, a gene encoding cyt *c1*. Indeed, the same genetic interaction was reported between Δ*osm1* and Δ*cyt1* (Costanzo et al., 2010).

SGA screens consisting of pairwise measurement of growth defects in double mutant cells provide a useful strategy for comprehensively exploring gene function. SGA revealed an unprecedented level of information regarding to the function of Hot13 that has not been identified recently. Future works include the verification of the putative interactions found for Osm1 and Hot13. This will be done in an independent experiment of tetrad analysis with Δ*osm1* or Δ*hot13* and a subset of gene mutants found from the SGA screen.

Materials and Methods

Construction of Query Strains: PCR-Mediated Gene Deletion

1. Two gene-deletion primers were synthesized, each containing 45 bp of sequence at 5' end that is specific to the region upstream or downstream of either Osm1 or Hot13 and 21 bp of sequence at the 3' end that is specific to the Ura or Leu cassette.
2. The Ura or Leu cassette flanked with 45bp target sequences is amplified from pUG72 or pUG73 with the gene-deletion primers designed in step 1.
3. The PCR produce is transfored into the SGA starting strain, Y7092 and the transformants selected on the appropriate drop-out media. Finally, correct targeting of the deletion cassette was verified by PCR.

Media and stock solutions

1. **G418** (Geneticin, Invitrogen): Dissolve in water at 200 mg/mL, filter sterilize, and store in aliquots at 4^{o}C.
2. **Canavanine** (L-canavine sulfate salt, Sigma): Dissolve in water at 100 mg/mL, filter sterilize, and store in aliquots at 4^{o}C.
3. **Thialysine** (S-(2-aminoethyl)-L-cysteine hydrochloride, Sigma): Dissolve in water at 100 mg/mL, filter sterilize, and store in aliquots at 4^{o}C.
4. **Amino-acids supplement powder mixture for synthetic media (complete):** Contains 3 g adenine (Sigma), 2 g uracil (ICN), 2 g inositol, 0.2 g para-aminobenzoic acid (Acros Organics), 2 g alanine, 2 g arginine, 2 g asparagines, 2 g aspartic acid, 2 g cysteine, 2 g glutamic acid, 2 g glutamine, 2 g glycine, 2 g histidine, 2 g isoleucine, 10 g leucine, 2 g

lysine, 2 g methionine, 2 g phenylalanine, 2 g proline, 2 g serine, 2 g threonine, 2 g tryptophan, 2 g tyrosine, 2 g valine (Fisher). Drop-out (DO) powder mixture is a combination of the above ingredients minus the appropriate supplement. 2 g of the DO powder mixture is used per 1 liter of medium.

5. **Amino-acids supplement for sporulation medium**: Contains 2 g histidine, 10 g leucine, 2 g lysine, 2 g uracil; 0.1 g of the amino-acid supplements posder mixture is used per liter of sporulation medium.
6. **B-glucuronidase** (Sigma): Prepare 0.5% solution in water and store at 4^{o}C.
7. **Glucose (Dextrose):** Prepare 40% solution, autoclave and store at room temperature.
8. **YEPD**: Add 120 mg adenine (Sigma), 10 g yeast extract, 20 g peptone, 20 g bacto agar (BD Difco) to 900 mL water in a 2 L flask. After autoclaving, add 50 mL of 40% glucose solution, mix thoroughly, cool to ~65^{o}C and pour into QTrays.
9. **YEPD + G418**: cool YEPD medium to ~65^{o}C, add 1 mL of G418 (final concentration 200 mg/L), mix thoroughly and pour into QTrays.
10. **SD/MSG-Ura+G418**: Add 1.7 g yeast nitrogen base w/o amino acids, 1 g MSG (L-glutamic acid sodium salt hydrate, Sigma), 2 g amino-acids supplement poswer mixture (DO-Ura), 100 mL water in a 250 mL flask. Add 20 g bacto agar to 800 mL water in a 2 L flask. Autoclave separately. Combine autoclaved solutions, add 100 mL of 20% glucose solution, cool medium to ~65^{o}C, add 1 mL G418 stock solutions, mix thoroughly and pour into QTrays.
11. **SD/MSG-Leu+G418**: Add 1.7 g yeast nitrogen base w/o amino acids, 1 g MSG (L-glutamic acid sodium salt hydrate, Sigma), 2 g amino-acids supplement poswer mixture (DO-Leu), 100 mL water in a 250 mL flask. Add 20 g bacto agar to 800 mL water in a 2

L flask. Autoclave separately. Combine autoclaved solutions, add 100 mL of 20% glucose solution, cool medium to ~65°C, add 1 mL G418 stock solutions, mix thoroughly and pour into QTrays.

12. **Enriched sporulation**: Add 10 g potassium acetate (Fisher), 1 g yeast extract, 0.5 g glucose, 0.1 g amino-acids supplement powder mixture for sporulation, 20 g bacto agar to 1 L water in a 2 L flask. After autoclaving, cool medium to ~65°C, add 250 µL of G418 stock solution (final concentration 50 mg/L), mix thoroughly and pour into QTrays.
13. **SD – His/Arg/Lys + canavanine/thialysine**: Add 1.7 g yeast nitrogen base w/o amino acids, 1 g MSG, 2 g amino-acid supplement powder mixture (DO-His/Arg/Lys), 100 mL water in a 250 mL flask. Add 20 g bacto agar to 200 mL water in a 2 L flask. Autoclave separately. Combine autoclaved solutions, add 100 mL 20% glucose solution, cool medium to ~65°C, add 0.5 ml canavanine and 0.5 mL thialysine stock solutions, mix thoroughly and pour into QTrays.
14. **SD/MSG-His/Arg/Lys+canavnanine/thialysine+G418**: Add 1.7 g yeast nitrogen base w/o amino acids, 1 g MSG, 2 g amino-acid supplement powder mixture (DO-His/Arg/Lys), 100 mL water in a 250 mL flask. Add 20 g bacto agar to 200 mL water in a 2 L flask. Autoclave separately. Combine autoclaved solutions, add 100 mL 20% glucose solution, cool medium to ~65°C, add 0.5 ml canavanine, 0.5 mL thialysine and 1 mL G418 stock solutions, mix thoroughly and pour plates.
15. **SD/MSG-His/Arg/Lys/Ura+canavanine/thialysine+G418**: Add 1.7 g yeast nitrogen base w/o amino acids, 1 g MSG, 2 g amino-acids supplement powder mixture (DO-His/Arg/Lys/Ura), 100 mL water in a 250 mL flask. Add 20 g bacto agar to 800 mL water in a 2 L flask. Autoclave separately. Combine autoclaved solutions, add 100 mL

20% glcose, cool medium to ~65°C, add 0.5 mL canavanine, 0.5 mL thialysine and 1 mL G418 stock solutions, mix thoroughly and pour into QTrays.

16. **SD/MSG-His/Arg/Lys/Leu+canavanine/thialysine+G418**: Add 1.7 g yeast nitrogen base w/o amino acids, 1 g MSG, 2 g amino-acids supplement powder mixture (DO-His/Arg/Lys/Leu), 100 mL water in a 250 mL flask. Add 20 g bacto agar to 800 mL water in a 2 L flask. Autoclave separately. Combine autoclaved solutions, add 100 mL 20% glcose, cool medium to ~65°C, add 0.5 mL canavanine, 0.5 mL thialysine and 1 mL G418 stock solutions, mix thoroughly and pour into QTrays.

Plates and accessories

1. Aluminum sealing tape is used for resealing the 384-well plates that contain the frozen stocks of yeast deletion strains.
2. QTrays (Nunc) are used for SGA analysis.

Robotic Pinning Systems

1. Qbot, (Genetix, Boston, MA).

SGA Analysis

1. Preparing query strain in 384-well plate: A frozen strock of Mat α hot13::URA3 or osm1::LEU2 was streaked onto YEPD agar plate and incubated overnight at 30°C. The next day, 100 mL of YEPD was inoculated from the freshly streaked plate and the culture was grown overnight at 30°C. In the biosafety hood, 65 μL of yeast cells were dispensed into two 384-well plates (Nunc) via a multidrop.
2. Replica Gridding query strains onto QTrays: Query strains from 384-well plates were pinned onto a YEPD QTray. The cells were grown at 30 °C for two days.

3. Preparation of the Deletion Mutant Array (DMA): The foil coverings from the 384-well frozen stock of the yeast deletion library was peeled off and thawed on a flat surface. The plates were gently shaken and the library stock was replicated directly onto YEPD+G418 agar QTrays via the Qbot. The frozen yeast deletion stock was resealed with fresh aluminum sealing tap and returned to -80^{o}C. The cells were grown at 30 ^{o}C for two days.

Mating the Query Strain with the DMA:

1. The query strain was pinned onto a fresh YEPD plate. The DMA was subsequently pinned on top of the query cells and the mating plates were incubated at 30 ^{o}C for 1 day.

MATa/α Diploid Selection and Sporulation

1. The resulting *MAT*a/α zygotes were pinned onto SD/MSG-Ura+G418 or SD/MSG-Leu+G418 QTrays (for Hot13 and Osm1 respectively) and the diploid-selection plates were incubated at 30 ^{o}C for 1 day. Subsequently, the diploid cells were pinned onto enriched sporulation medium and the QTrays were incubated at 22 ^{o}C for 5 days.

*MAT*a *Meiotic Progeny Selection*

1. Spores were pinned onto SD-His/Arg/Lys+canavanine,thialysine plates and the haploid-selection plates were incubated at 30 ^{o}C for 2 days. The *MAT*a meiotic progeny were pinned onto SD-His/Arg/Lys+canavanine, thialysine QTrays for a second round of haploid selection and the QTrays were incubated at 30 ^{o}C for 1 day.

*MAT*a-*kanR Meiotic Progeny Selection*

1. The *Mat*a meiotic progeny were pinned onto (SD/MSG)-His/Arg/Lys+canavanine/thialysine/G418 QTrays and the Qtrays were incubated at 30 ^{o}C for 2 days.

*MAT*a-*kanR-Ura or MAT*a-*kanR-Leu Meiotic Progeny Selection*

1. The *Mat*a meiotic progeny was pinned onto (SD/MSG) His/Arg/Lys/Ura+canavanine/thialysine/G418 or (SD/MSG)-His/Arg/Lys/Leu+canavanine/thialysine/G418 QTrays for Hot and Osm1 respectively and the QTrays were incubated at 30^{o}C for 2 days.

Image capturing and measurement of colony sizes

In brief, image capturing and colony measurements were performed as previously described (Collins et al., 2006). In brief, after each selection, pictures of each QTray were taken using a set-up consisting of a KAISER RS 1 camera stand and a digital camera with Illumination from two Testrite 16-24 Light Boxes). The final colony images were typically around 500 pixels. Colonies were measured as described in (Collins et al., 2006) using an executable JAVA program, HT Colony Grid Analyzer.

Scoring Putative interactions

SGA score was determined based on the Matlab alogorithm as previously described previously(Baryshnikova et al., 2010b). In brief, colony size was based on a multiplicative combination of double mutant fitness, time, and experimental factors. Specifically, for a double mutant with deletions of genes iand j, colony area C_{ij} can be expressed as:

$$C_{ij} = \alpha * f_{ij} * t * s_{ij} * e \qquad \text{Eq. 1}$$

where f_{ij} is the fitness of the double mutant, t is time, s_{ij} is the combination of all systematic factors, α is a constant scale factor, and e is log-normally distributed error. In addition, double mutant fitness f_{ij} can be expressed as $f_{ij} = f_i f_j + \varepsilon_{ij}$, where f_i and f_j are the single mutant fitness measures, and ε_{ij} is the genetic interaction between genes i and j.

Tables and Figures

Table 1. Putative genetic interactions with HOT13

Mitochondrial Translation	Cytoplasmic Translation	Mitochondrial dynamics
MRPL37	RPS9B	FZO1
MRPL27	RPL21	UGO1
MRP10	AMTF2	MGM1
RSM25	MRPL7	
MRPL7	MRPL8	
MRPL8	MRPL49	
MRPL49	RSM7	
RSM7	CTK1	
SLS1	RPS0B	
MSK1	SLS1	
MSE1	HCR1	
UF1	HER2	
MRPL40	MSK1	
	MSE1	
	RPS7A	
	TUF1	
	MSY1	
	MRPL40	
Aerobic respiration	**AMP biosynthetic process**	**tRNA biosynthesis**
RMD9	ADO1	ARC1
PET10	APT1	MSK1
PET309		MSE1
SLS1		MSY1
PPA2		
MCT1		
pyrimidine base biosynthesis	**Mitochondrial DNA maintenance**	**Intraluminal vesicle formation**
URA1	UGO1	DID4
URA5	MRPL8	VPS20
	MGM101	
	MGM1	
double-strand break repair		
RSC2		
FYV6		
RAD50		

Putative interactions were categorized by the FunSpec program (http://funspec.med.utoronto.ca/) functionally annotated by the GO database

Table 2. Putative genetic interactions with OSM1

Aerobic respiration	Purine Base Biosynthesis	Cellular Copper Ion Homeostasis
QCR9	DAL7	YLR126C
CYT1	AMD1	CUP9
QCR2		
COX7		
COX10		
CEM1		

Putative interactions were categorized by the FunSpec (http://funspec.medutoronto.ca/) and functionally annotated by the GO database.

Table 3. Strains used in this study

Yeast Mata Collection
Yeast Mata (plates 1-51)
Yeast Mata (plates 72-73)
Yeast Mata (plates 74-75)
Yeast Parental Strain BY4730
MATa leu2Δ0 met15Δ0 ura3Δ0
Yeast Parental Strain BY4741
MATa his3Δ1 leu2Δ0 met15Δ0 ura3Δ0
Y7092 starter strain:
can1delta::STE2pr-Sp_his5 lyp1delta
his3delta1 leu2delta0 ura3delta0 met15delta0
hot13::URA can1delta::STE2pr-Sp_his5 lyp1delta
his3delta1 leu2delta0 ura3delta0 met15delta0
osm1::LEU can1delta::STE2pr-Sp_his5 lyp1delta
his3delta1 leu2delta0 ura3delta0 met15delta0

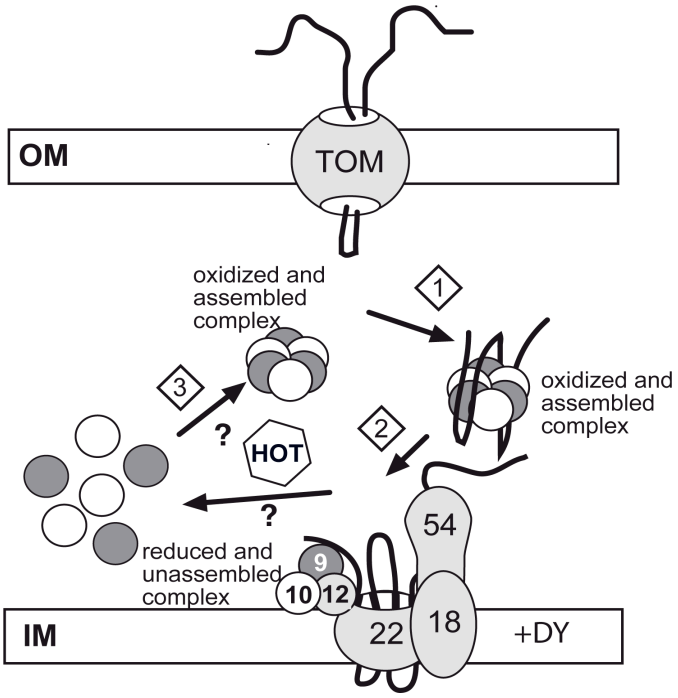

Figure 1. **The role of Hot13 in the Tim22 import pathway**. Hot13 is a peripheral inner membrane protein in the IMS. Newly imported Tim proteins assemble into soluble 70-kDa complexes in the IMS. After crossing the TOM complex, the inner membrane substrates are escorted across the IMS to the TIM22 membrane complex. Under oxidizing condition, the substrates remain bound to the small Tim complex. Subsequent treatment with reductant results in release of the substrate from the small Tim complex and insertion into the inner membrane. Hot13 is proposed to facilitate in the release of substrate from the small Tim complex and potential recycling of the small Tim complex for another round of import.(Koehler and Tienson, 2009)

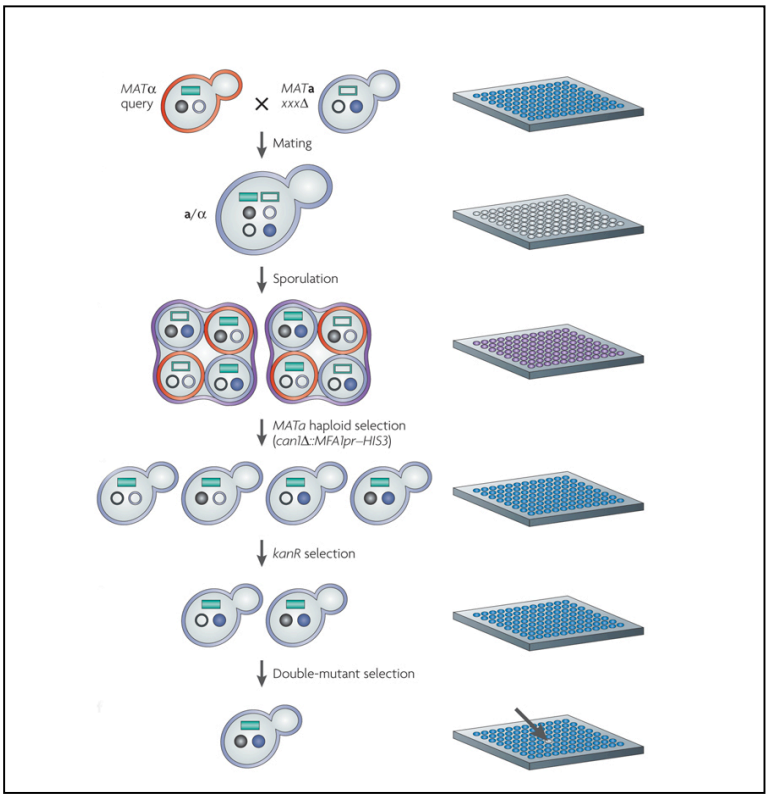

Figure 2. **SGA methodology** (*a*) A *MATα* strain carries a query mutation linked to a dominant selectable marker. This query strain is crossed to an ordered array of *MATa* deletion mutants (*xxxΔ*). (*b*) The resulting heterozygous diploids are transferred to a medium with reduced carbon and nitrogen to induce sporulation and form haploid meiotic spore progeny. (*c*) Spores are transferred to a synthetic medium that lacks histidine, which allows selective germination of *MATa* meiotic progeny owing to expression of the SGA reporter, *can1Δ::STE2pr–Sp_his5*. To improve this selection, canavanine and thialysine, which select *can1Δ* and *lyp1Δ* while killing *CAN1* and *LYP1* cells, respectively, are included in the selection medium. (*d*) The *MATa* meiotic progeny are transferred to a medium, which selects for the double mutants. Modified from (Baryshnikova et al., 2010a).

Appendix A

Putative gene interactions with Hot13

ORF	Common Name	Function	SGA score	P-value
FRE6	YLL051C	Putative ferric reductase with similarity to Fre2p	-0.355	1.266E-08
PDR17	YNL264C	Phosphatidylinositol transfer protein (PITP)	-0.304	0.00055
MSY1	YPL097W	Mitochondrial tyrosyl-tRNA synthetase	-0.301	0.001161
FZO1	YBR179C	Mitofusin	-0.282	0.02987
MRPL40	YPL173W	Mitochondrial ribosomal protein of the large subunit	-0.271	4.994E-06
NPL3	YDR432W	RNA-binding protein that promotes elongation, regulates termination,	-0.244	2.364E-09
SWC5	YBR231C	Protein of unknown function	-0.242	0.00002812
MRPL37	YBR268W	Mitochondrial ribosomal protein of the large subunit	-0.236	0.0002311
GLY1	YEL046C	Threonine aldolase	-0.236	0.0002311
SSE1	YPL106C	ATPase that is a component of the Hsp90 chaperone complex	-0.219	0.001477
GEP4	YHR100C	Mitochondrial phosphatidylglycerophosphatase (PGP phosphatase)	-0.2	0.006155
GND1	YHR183W	6-phosphogluconate dehydrogenase (decarboxylating)	-0.195	0.00009071
SLS1	YLR139C	Mitochondrial membrane protein	-0.195	0.00009071
SWI6	YLR182W	Transcription cofactor	-0.195	0.004669
CYT2	YKL087C	Cytochrome c1 heme lyase	-0.195	0.00009071
BUD2	YKL092C	GTPase activating factor for Rsr1p/Bud1p	-0.195	0.00009071
TUF1	YOR187W	Mitochondrial translation elongation factor Tu	-0.195	0.004669
DID4	YKL002W	Class E Vps protein of the ESCRT-III complex	-0.194	0.01216
MGM1	YOR211C	Mitochondrial GTPase	-0.194	0.01216
PCP1	YGR101W	Mitochondrial serine protease	-0.193	0.004947
SRB5	YGR104C	Subunit of the RNA polymerase II mediator complex	-0.193	0.004947
MCT1	YOR221C	Predicted malonyl-CoA:ACP transferase	-0.188	0.03684
MET7	YOR241W	Folylpolyglutamate synthetase	-0.188	0.03684
RSC2	YLR357W	Component of the RSC chromatin remodeling complex	-0.186	0.03095
ATP12	YJL180C	Assembly factor for the F1 sector of mitochondrial F1F0 ATP synthase	-0.186	0.03095
RAI1	YGL246C	Decapping endonuclease for mRNAs with unmethylated 7-mG cap structures	-0.18	0.01973
RSM24	YDR175C	Mitochondrial ribosomal protein of the small subunit	-0.18	2.116E-12
COQ4	YDR204W	Protein with a role in ubiquinone (Coenzyme Q) biosynthesis	-0.17	0.04667
UME6	YDR207C	Key transcriptional regulator of early meiotic genes	-0.168	0.03658
BRO1	YPL084W	Cytoplasmic class E vacuolar protein sorting (VPS) factor	-0.168	0.03658
MRPL7	YDR237W	Mitochondrial ribosomal protein of the large subunit	-0.162	2.519E-08
RIM8	YGL046W	Protein involved in proteolytic activation of Rim101p	-0.157	0.02665
RAD6	YGL058W	Ubiquitin-conjugating enzyme (E2)	-0.151	0.03232
URA1	YKL216W	Dihydroorotate dehydrogenase	-0.151	0.03232
UTH1	YKR042W	Mitochondrial outer membrane and cell wall localized SUN family member	-0.151	0.03232
VPS20	YMR077C	Myristoylated subunit of ESCRTIII	-0.151	0.03232
LOC1	YFR001W	Nuclear protein involved in asymmetric localization of ASH1 mRNA	-0.149	0.03082
RAD50	YNL250W	Subunit of MRX complex	-0.149	0.03082
ZAP1	YJL056C	Zinc-regulated transcription factor	-0.146	0.0475
RPS7A	YOR096W	Protein component of the small (40S) ribosomal subunit	-0.146	8.622E-06
URA5	YML106W	Major orotate phosphoribosyltransferase (OPRTase) isozyme	-0.146	0.0475
ADO1	YJR105W	Adenosine kinase	-0.145	0.03852
MRPL49	YJL096W	Mitochondrial ribosomal protein of the large subunit	-0.143	0.03423
MRPL8	YJL063C	Mitochondrial ribosomal protein of the large subunit	-0.143	0.02623
RSM7	YJR113C	Mitochondrial ribosomal protein of the small subunit	-0.143	0.02623

ORF	Common I	Function	SGA score	P-value
MGM101	YJR144W	Protein with a role in mitochondrial DNA recombinational repair	-0.141	0.04201
HIT1	YJR055W	Protein of unknown function	-0.137	0.007782
MRPL27	YBR282W	MRPL27	-0.136	9.97E-09
VPS53	YJL029C	Component of the GARP (Golgi-associated retrograde protein) complex	-0.127	0.001132
KCS1	YDR017C	Inositol hexakisphosphate and inositol heptakisphosphate kinase	-0.127	0.001132
RPS9B	YBR189W	Protein component of the small (40S) ribosomal subunit	-0.127	0.02543
CSG2	YBR036C	Endoplasmic reticulum membrane protein	-0.126	0.03545
DBF2	YGR092W	Ser/Thr kinase involved in transcription and stress response	-0.124	0.03574
TRK1	YJL129C	Component of the Trk1p-Trk2p potassium transport system	-0.123	0.01051
CTK1	YKL139W	Catalytic (alpha) subunit of C-terminal domain kinase I (CTDK-I)	-0.123	0.01051
FYV6	YNL133C	Protein of unknown function	-0.121	0.03352
MSK1	YNL073W	Mitochondrial lysine-tRNA synthetase	-0.116	0.002337
ATP1	YBL099W	Alpha subunit of the F1 sector of mitochondrial F1F0 ATP synthase	-0.115	0.04542
PET10	YKR046C	Protein of unknown function that co-purifies with lipid particles	-0.11	0.04901
BUD23	YCR047C	Methyltransferase	-0.108	0.03761
RPL21A	YBR191W	Protein component of the large (60S) ribosomal subunit	-0.108	0.000171
ADA2	YDR448W	Transcription coactivator	-0.105	0.01643
HCR1	YLR192C	eIF3j component of translation initiation factor 3 (eIF3)	-0.104	0.01578
YLR358C	YLR358C	Protein of unknown function	-0.102	0.03431
UGO1	YDR470C	Outer membrane component of the mitochondrial fusion machinery	-0.102	0.03728
APT1	YML022W	Adenine phosphoribosyltransferase	-0.099	0.04411
GPM2	YDL021W	Homolog of Gpm1p phosphoglycerate mutase	-0.099	0.04411
PUF6	YDR496C	Pumilio-homology domain protein that binds the 3' UTR of ASH1 mRNA	-0.099	0.04462
YME1	YPR024W	Catalytic subunit of the mitochondrial i-AAA protease complex	-0.099	0.000407
MTF2	YDL044C	Mitochondrial protein that interacts with mitochondrial RNA polymerase	-0.097	6.48E-05
MRP10	YDL045W-	Mitochondrial ribosomal protein of the small subunit	-0.096	0.01154
YJR003C	YJR003C	Putative protein of unknown function	-0.096	0.01154
ARC1	YGL105W	Protein that binds tRNA and methionyl- and glutamyl-tRNA synthetases	-0.095	0.002104
RMD9	YGL107C	Mitochondrial protein required for respiratory growth	-0.095	0.01552
AAT2	YLR027C	Cytosolic aspartate aminotransferase	-0.087	0.03091
RPS0B	YLR048W	Protein component of the small (40S) ribosomal subunit	-0.085	0.04241
PET309	YLR067C	Specific translational activator for the COX1 mRNA	-0.084	0.002729
PPA2	YMR267W	Mitochondrial inorganic pyrophosphatase	-0.084	0.002729
MSE1	YOL033W	Mitochondrial glutamyl-tRNA synthetase	-0.083	0.04155
HER2	YMR293C	Subunit of the trimeric GatFAB AmidoTransferase(AdT) complex	-0.082	0.01208
MIP1	YOR330C	Mitochondrial DNA polymerase	-0.082	0.01208

Appendix B

Putative gene interactions with Osm1

ORF	Common Name	Function	SGA score	P-value
YML018C	YML018C	Putative protein of unknown function	-0.355	1.266E-08
CSG2	YBR036C	Endoplasmic reticulum membrane proteins	-0.323	0.01143
AMD1	YML035C	AMP deaminase	-0.304	0.00055
PML39	YML107C	Protein required for nuclear retention of unspliced pre-mRNAs	-0.301	0.001161
GTR1	YML121W	Cytoplasmic GTP binding protein and negative regulator of the Ran/Tc4 GTPase cycle	-0.282	0.02987
RCO1	YMR075W	Essential subunit of the histone deacetylase Rpd3S complex	-0.271	4.994E-06
STP4	YDL048C	Protein containing a Kruppel-type zinc-finger domain	-0.263	1.909E-12
SNZ1	YMR096W	Protein involved in vitamin B6 biosynthesis	-0.244	2.364E-09
YDL094C	YDL094C	Dubious open reading frame unlikely to encode a protein	-0.242	7.32E-09
PKR1	YMR123W	V-ATPase assembly factor	-0.242	0.00002812
YMR160W	YMR160W	Putative protein of unknown function	-0.236	0.0002311
MLH1	YMR167W	Protein required for mismatch repair	-0.236	0.0002311
RAD14	YMR201C	Protein that recognizes and binds damaged DNA during nucleotide excision repair	-0.219	0.001477
LDB17	YDL146W	Protein of unknown function	-0.211	0.002622
COX7	YMR256C	Subunit VII of cytochrome c oxidase	-0.202	0.02253
NIS1	YNL078W	Protein localized in the bud neck at G2/M phase	-0.2	0.006155
NST1	YNL091W	Protein of unknown function	-0.195	0.00009071
CPT1	YNL130C	Cholinephosphotransferase	-0.195	0.00009071
ARE2	YNR019W	Acyl-CoA:sterol acyltransferase	-0.195	0.004669
AGA1	YNR044W	Anchorage subunit of a-agglutinin of a-cells	-0.194	0.01216
PHO80	YOL001W	Cyclin, negatively regulates phosphate metabolism	-0.193	0.004947
SPE2	YOL052C	S-adenosylmethionine decarboxylase	-0.188	0.03684
APM4	YOL062C	Mu2-like subunit of the clathrin associated protein complex	-0.186	0.03095
YDL187C	YDL187C	Dubious ORF unlikely to encode a functional protein	-0.185	0.01958
GCS1	YDL226C	ADP-ribosylation factor GTPase activating protein	-0.183	7.193E-17
CYT1	YOR065W	Cytochrome c1, component of the mitochondrial respiratory chain	-0.18	2.116E-12
SHE4	YOR035C	Involved in endocytosis, polarization of the actin cytoskeleton, and asymmetric mRN	-0.18	0.01973
TPS2	YDR074W	Phosphatase subunit of the trehalose-6-phosphate synthase/phosphatase complex	-0.172	0.004453
BUD21	YOR078W	Component of small ribosomal subunit (SSU)	-0.17	0.04667
RFM1	YOR279C	Involved in telomere maintenance	-0.168	0.03658
FRT1	YOR324C	Tail-anchored, endoplasmic reticulum membrane protein	-0.168	0.03658
PPH3	YDR075W	phosphatase complex containing Psy2p and the regulatory subunit Psy4p	-0.167	0.003886
MGR2	YPL098C	Protein required for growth of cells lacking the mitochondrial genome	-0.162	2.519E-08
SWF1	YDR126W	Palmitoyltransferase that acts on the SNAREs	-0.162	0.0001218
YDR134C	YDR134C	Hypothetical protein	-0.157	0.00187
YPL162C	YPL162C	Putative protein of unknown function	-0.157	0.02665
FCY21	YER060W	Putative purine-cytosine permease	-0.152	3.272E-33
PAD1	YDR538W	Phenylacrylic acid decarboxylase	-0.152	0.0001569
CEM1	YER061C	Mitochondrial beta-keto-acyl synthase	-0.151	0.003131
COX10	YPL172C	Heme A:farnesyltransferase	-0.151	0.03232
CUP9	YPL177C	Homeodomain-containing transcriptional repressor of PTR2,	-0.151	0.03232
MRN1	YPL184C	RNA-binding protein	-0.149	0.03082
QCR2	YPR191W	Subunit 2 of the ubiquinol cytochrome-c reductase complex	-0.146	8.622E-06
YPL205C	YPL205C	Hypothetical protein	-0.146	0.0475
RPL24A	YGL031C	Ribosomal protein L30 of the large (60S) ribosomal subunit	-0.145	1.444E-50
YER181C	YER181C	Dubious open reading frame unlikely to encode a protein	-0.145	1.876E-11
SKI8	YGL213C	Ski complex component and WD-repeat protein	-0.144	0.004359
SLX9	YGR081C	Protein required for pre-rRNA processing	-0.141	0.00002414
CLB6	YGR109C	B-type cyclin involved in DNA replication during S phase	-0.133	3.134E-11
MEP1	YGR121C	Ammonium permease	-0.133	0.02541
QCR9	YGR183C	Subunit 9 of the ubiquinol cytochrome-c reductase complex	-0.132	1.808E-22
ELP2	YGR200C	Subunit of Elongator complex	-0.129	2.26E-53
YGR237C	YGR237C	Putative protein of unknown function	-0.129	5.411E-08
PHB2	YGR231C	Subunit of the prohibitin complex (Phb1p-Phb2p)	-0.129	0.00005307
HGH1	YGR187C	Nonessential protein of unknown function	-0.129	0.004199
FMP43	YGR243W	Putative protein of unknown function	-0.127	0.0001184
RNH70	YGR276C	3'-5' exoribonuclease	-0.126	2.262E-16
PTC7	YHR076W	Mitochondrially localized type 2C protein phosphatase	-0.126	0.02897
SEE1	YIL064W	Protein with a role in intracellular transport;	-0.125	0

ORF	Common Name	Function	SGA score	P-value
YIL108W	YIL108W	Putative metalloprotease	-0.119	0.0116
DAL7	YIR031C	Malate synthase	-0.118	1.665E-07
QDR1	YIL120W	Multidrug transporter of the major facilitator superfamily	-0.118	0.01053
SNX4	YJL036W	Sorting nexin	-0.116	0.00132
TAX4	YJL083W	regulates phosphatidylinositol 4,5-bisphosphate levels and autophagy	-0.116	0.003684
ERM6	YJR054W	Vacuolar protein of unknown function; potential Cdc28p substrate	-0.115	5.372E-06
JJJ2	YJL162C	Protein of unknown function	-0.115	0.00133
RPA34	YJL148W	RNA polymerase I subunit A34.5	-0.115	0.03959
MEH1	YKR007W	Component of the EGO complex, regulates microautophagy	-0.114	0.0004473
LDB18	YLL049W	Protein of unknown function	-0.113	8.267E-24
YPS1	YLR120C	Aspartic protease	-0.113	0.007385
YLR143W	YLR143W	Putative protein of unknown function	-0.108	0.002467
YLR126C	YLR126C	Putative protein of unknown function	-0.108	0.01272
STM1	YLR150W	Protein required for optimal translation under nutrient stress;	-0.106	6.974E-17
PUS5	YLR165C	Pseudouridine synthase	-0.106	0.004971
RSA3	YLR221C	role in ribosomal maturation	-0.105	0.03481
YPT7	YML001W	GTPase	-0.104	1.915E-08
CDC73	YLR418C	Constituent of Paf1 complex with RNA polymerase II	-0.104	0.0005743
YLR415C	YLR415C	Putative protein of unknown function	-0.104	0.01537
PPZ1	YML016C	Serine/threonine protein phosphatase Z	-0.103	1.554E-06
PSP2	YML017W	Asn rich cytoplasmic protein that contains RGG motifs	-0.103	0.001136

References

Baryshnikova, A., M. Costanzo, Y. Kim, H. Ding, J. Koh, K. Toufighi, J.-Y. Youn, J. Ou, B.-J. San Luis, S. Bandyopadhyay, M. Hibbs, D. Hess, A.-C. Gingras, G.D. Bader, O.G. Troyanskaya, G.W. Brown, B. Andrews, C. Boone, and C.L. Myers. 2010. Quantitative analysis of fitness and genetic interactions in yeast on a genome scale. *Nature methods*. 7:1017-24.

Camarasa, C., V. Faucet, and S. Dequin. 2007. Role in anaerobiosis of the isoenzymes for Saccharomyces cerevisiae fumarate reductase encoded by OSM1 and FRDS1. *Yeast*. 391-401.

Collins, S.R., M. Schuldiner, N.J. Krogan, and J.S. Weissman. 2006. A strategy for extracting and analyzing large-scale quantitative epistatic interaction data. *Genome biology*. 7:R63.

Costanzo, M., A. Baryshnikova, J. Bellay, Y. Kim, E.D. Spear, C.S. Sevier, H. Ding, J.L.Y. Koh, K. Toufighi, S. Mostafavi, J. Prinz, R.P. St Onge, B. VanderSluis, T. Makhnevych, F.J. Vizeacoumar, S. Alizadeh, S. Bahr, R.L. Brost, Y. Chen, M. Cokol, R. Deshpande, Z. Li, Z.-Y. Lin, W. Liang, M. Marback, J. Paw, B.-J. San Luis, E. Shuteriqi, A.H.Y. Tong, N. van Dyk, I.M. Wallace, J.A. Whitney, M.T. Weirauch, G. Zhong, H. Zhu, W.A. Houry, M. Brudno, S. Ragibizadeh, B. Papp, C. Pál, F.P. Roth, G. Giaever, C. Nislow, O.G. Troyanskaya, H. Bussey, G.D. Bader, A.-C. Gingras, Q.D. Morris, P.M. Kim, C.A. Kaiser, C.L. Myers, B.J. Andrews, and C. Boone. 2010. The genetic landscape of a cell. *Science (New York, N.Y.)*. 327:425-31.

Curran, S.P., D. Leuenberger, E.P. Leverich, D.K. Hwang, K.N. Beverly, and C.M. Koehler. 2004. The role of Hot13p and redox chemistry in the mitochondrial TIM22 import pathway. *The Journal of biological chemistry*. 279:43744-51.

Curran, S.P., D. Leuenberger, W. Oppliger, and C.M. Koehler. 2002a. The Tim9p-Tim10p complex binds to the transmembrane domains of the ADP/ATP carrier. *The EMBO journal*. 21:942-53.

Curran, S.P., D. Leuenberger, E. Schmidt, and C.M. Koehler. 2002b. The role of the Tim8p-Tim13p complex in a conserved import pathway for mitochondrial polytopic inner membrane proteins. *The Journal of cell biology*. 158:1017-27.

DeVay, R.M., L. Dominguez-Ramirez, L.L. Lackner, S. Hoppins, H. Stahlberg, and J. Nunnari. 2009. Coassembly of Mgm1 isoforms requires cardiolipin and mediates mitochondrial inner membrane fusion. *The Journal of cell biology*. 186:793-803.

Graef, M., G. Seewald, and T. Langer. 2007. Substrate recognition by AAA+ ATPases: distinct substrate binding modes in ATP-dependent protease Yme1 of the mitochondrial intermembrane space. *Molecular and cellular biology*. 27:2476-85.

Hartman, J.L., B. Garvik, and L. Hartwell. 2001. Principles for the buffering of genetic variation. *Science (New York, N.Y.)*. 291:1001-4.

Hin, A., Y. Tong, and C. Boone. 2005. 16 High-Throughput Strain Construction and Systematic Synthetic Lethal Screening in Saccharomyces cerevisiae. *Methods*.

Kaelin, W.G. 2005. The concept of synthetic lethality in the context of anticancer therapy. *Nature reviews. Cancer*. 5:689-98.

Koehler, C.M. 2000. Protein translocation pathways of the mitochondrion. *FEBS letters*. 476:27-31.

Koehler, C.M., S. Merchant, and G. Schatz. 1999. How membrane proteins travel across the mitochondrial intermembrane space. *Trends in biochemical sciences*. 24:428-32.

Meglei, G., and G.A. McQuibban. 2009. The dynamin-related protein Mgm1p assembles into oligomers and hydrolyzes GTP to function in mitochondrial membrane fusion. *Biochemistry*. 48:1774-84.

Mesecke, N., K. Bihlmaier, B. Grumbt, S. Longen, N. Terziyska, K. Hell, and J.M. Herrmann. 2008. The zinc-binding protein Hot13 promotes oxidation of the mitochondrial import receptor Mia40. *EMBO reports*. 9:1107-1113.

Paschen, S.A., and W. Neupert. Protein import into mitochondria. *IUBMB life*. 52:101-12.

Pfanner, N., and A. Geissler. 2001. Versatility of the mitochondrial protein import machinery. *Nature reviews. Molecular cell biology*. 2:339-49.

Tong, A.H., M. Evangelista, A.B. Parsons, H. Xu, G.D. Bader, N. Pagé, M. Robinson, S. Raghibizadeh, C.W. Hogue, H. Bussey, B. Andrews, M. Tyers, and C. Boone. 2001. Systematic genetic analysis with ordered arrays of yeast deletion mutants. *Science (New York, N.Y.)*. 294:2364-8.